

UNIVERSITY OF CALIFORNIA, SANTA BARBARA

**The Harmonic Pattern Function:  
A Mathematical Model Integrating Synthesis of  
Sound and Graphical Patterns**

A Dissertation submitted in partial satisfaction of the  
requirements for the degree Doctor of Philosophy  
in Media Arts and Technology

by

Lance Jonathan Putnam

Committee in charge:  
Professor JoAnn Kuchera-Morin, Chair  
Professor Marcos Novak  
Professor Curtis Roads

March 2012

The Dissertation of Lance Jonathan Putnam is approved.

---

Professor Marcos Novak

---

Professor Curtis Roads

---

Professor JoAnn Kuchera-Morin, Committee Chair

December 2011

The Harmonic Pattern Function:  
A Mathematical Model Integrating Synthesis of Sound and Graphical Patterns

Copyright © 2012

by

Lance Jonathan Putnam

To the makers of patterns ...

## Acknowledgements

First and foremost, I would like to thank my family for their support and patience. I thank my committee members for teaching me to think in ways I never thought imaginable. Most importantly, I thank Dr. JoAnn Kuchera-Morin for her lasting support and cultivation of media research at the intersection of art, science, and engineering. I thank Dr. Curtis Roads for his insightful feedback and support of this work. I thank Dr. Marcos Novak for his Transvergence series that foster holistic thinking across modalities and time. The MAT community has been incredibly inspiring. I especially thank Dan Overholt, Graham Wakefield, and Haru Ji for all of the thought-provoking conversations and support over the years. I thank Stephen Pope for his continual support and feedback during the writing process, Adriano Abbado for his audiovisual art course, John Whitney Jr. for the exclusive screenings of his films and those of John Whitney Sr., Dr. Mihai Putinar for help with complex analysis, Dr. Julius O. Smith for his review input, and finally, Dr. Matthew Turk, George Legrady, and Marko Peljhan for their support and input over the years. I thank Wesley Smith and Pablo Colapinto for all things geometry and Dr. Matt Wright for helpful input concerning both content and editing. Lastly, I express much gratitude to NSF for their support through the IGERT in Interactive Digital Multimedia and EAGER programs. Much of this work would not have been possible without it.

# Curriculum Vitae of Lance Jonathan Putnam

December 2011

## EDUCATION

---

Ph.D., Media Arts and Technology, December 2011

University of California, Santa Barbara

Dissertation: The Harmonic Pattern Function: A Mathematical Model Integrating Synthesis of Sound and Graphical Patterns

Committee: JoAnn Kuchera-Morin (chair), Marcos Novak, Curtis Roads

M.A., Electronic Music and Sound Design, 2005

University of California, Santa Barbara

Thesis: Transfer: An Interactive Program for Real-Time Spectral Transformations and Visualization

Committee: JoAnn Kuchera-Morin (chair), Stephen Pope, Curtis Roads

B.S., Electrical and Computer Engineering, 2002

University of Wisconsin, Madison

## RESEARCH EXPERIENCE

---

February 2009 - Present: Graduate Student Researcher in multimedia signal processing software infrastructure, AlloSphere Research Facility, University of California, Santa Barbara. PI: JoAnn Kuchera-Morin.

September 2008 - February 2009: Graduate Student Researcher under NSF CreativeIT grant "Artistic Group Performance as a Model for Novel Collaborative Multimodal Human-Computer Interfaces", Media Arts and Technology Program, University of California, Santa Barbara. PIs: JoAnn Kuchera-Morin, Tobias Hollerer.

September 2006 - June 2008: Graduate Student Researcher under NSF IGERT Interactive Digital Multimedia grant, University of California, Santa Barbara. Investigated untethered, multimodal interactive musical performance systems culminating in performance of *timeandagain* at Eastman Computer Music Center 25th Anniversary Series. PI: JoAnn Kuchera-Morin.

## TEACHING EXPERIENCE

---

2010: Co-instructor, MAT 594P: Composing Media Pieces for the AlloSphere  
Taught six sessions on sound synthesis and GUI design in C++. University of California, Santa Barbara

2010: Instructor, AlloSphere Summer Workshops Led three full-day workshops on sound synthesis and GUI design in C++. University of California, Santa Barbara

2008: Instructor, "Audiovisual Programming in C++" workshop, September 1-2  
Medialogy, Aalborg University, Denmark

2004 - 2005: Teaching Assistant, MAT 240: Digital Audio Programming Series  
University of California, Santa Barbara

## PUBLICATIONS

---

Putnam, L., Wakefield, G., Ji, H., Adderton, D., Alper, B., and Kuchera-Morin, J. (2010). Beautiful Visualization: Looking at Data through the Eyes of Experts, chapter Immersed in Unfolding Complex Systems. O'Reilly Media.

Putnam, L. (2005). "Transfer: An interactive program for real-time spectral transformations and visualization." Master of Arts Project Thesis, Media Arts and Technology, UC Santa Barbara.

Overholt, D., Thompson, J., Putnam, L., Bell, B., Kleban, J., Sturm, B., and Kuchera-Morin, J. (2009). Toward a general purpose interface for interactive musical performance using multimodal detection. *Computer Music Journal*, 33(4):69–82.

Pope, S., Amatriain, X., Putnam, L., Castellanos, J., Avery, R. (2006). "Metamodels and design patterns in CSL4." Proceedings of the 2006 International Computer Music Conference, New Orleans, LA.

## PRESENTATIONS

---

Putnam, L. (2011). "S Phase and Wrapture: Sonic Spacetime Structures." Presented at Polytopes: The Architecture of Soundscapes, February 23, Southern California Institute of Architecture (SCI-Arc), Los Angeles, California.

Putnam, L. (2009). "Voyages Through Absolute Landscapes." Presented at Machine Dreams International Generative Art Exhibition and Symposium: Computer-Created, Computer Creator Session, Media Space at Soongsil University, June 20, Seoul, South Korea.

Adderton, D., Kuchera-Morin, J., Putnam, L. (2008). "Experiencing the Quantum Realm: Visualizing and Sonifying the Bloch Sphere and Time-dependent Schrödinger Equation." Presented at Kavli Institute for Theoretical Physics Colloquium, December 3, UC Santa Barbara.

Putnam, L. (2007). "Generalizing Time and Frequency Intervals: Towards a More Unified Model of Sound Processing." Presented at the 2007 Watson Emerging Leaders in Multimedia Workshop, October 11, Hawthorne, New York.

Ji, H., Overholt, D., Putnam, L., Wakefield, G. (2006). "Towards the Allosphere: Intensive Art, Immersive Worlds." Presented at UC DARNet Grad Res Info/Xchge, April 28, UC Los Angeles.

#### HONORS AND AWARDS

---

2007: Selected as one of eight student presenters at the 2007 IBM Emerging Leaders in Multimedia Workshop

2006 - 2008: NSF IGERT Interactive Digital Multimedia Traineeship

1999 - 2000: AIESEC Internship Exchange, Utrecht, Netherlands

1997 - 2001: Dean's List, 7 semesters, University of Wisconsin, Madison

1995: Eagle Scout



# Abstract

The Harmonic Pattern Function:

A Mathematical Model Integrating Synthesis of Sound and Graphical Patterns

by

Lance Jonathan Putnam

The current landscape of parametric techniques for synthesis of digital sound waveforms and graphical curves and shapes is vast, but is largely an incongruous mixture of closed and highly specialized mathematical equations. While much of this can be attributed to the independent development of synthesis techniques within each field, upon closer examination it is clear that there exist common mathematical bases between the modalities. By pulling back into a broader mathematical context, it is possible to develop a language of unified audio/visual synthesis principles so that many of the existing paradigms, regardless of modality, can be understood from a single vantage point.

This dissertation defends the thesis that a large portion of known sound and graphical synthesis techniques can be unified through a rational function of inverse discrete Fourier transforms and that symmetry, invariance under transformation, plays an important role in understanding the patterns that it produces. We call this newly proposed audio/visual synthesis model the *harmonic pattern function*. A survey of a wide assortment of historic mechanical and electronic devices and computational systems used for generating sonic and visual patterns in art and science reveals that their underlying mathematical descriptions are special cases of

this new synthesis function.

The contributions of this dissertation include the introduction of a simple mathematical function, the harmonic pattern function, capable of generating a wide assortment of both known and previously unknown patterns useful for sound and/or visual synthesis, a simplified notation for specifying the complex sinusoids composing such patterns, and a thorough analysis of general themes and specific instances of patterns producible from the harmonic pattern function.

# Contents

<b>1</b>	<b>Introduction</b>	<b>1</b>
1.1	Data and Process in Multimedia . . . . .	2
1.2	Problem Statement . . . . .	3
1.3	Outline of Dissertation . . . . .	4
<b>2</b>	<b>Background on Harmonic Pattern Synthesis</b>	<b>5</b>
2.1	Mechanical and Electronic Devices . . . . .	5
2.1.1	Oscillating Devices . . . . .	6
2.1.2	Gear Systems . . . . .	12
2.1.3	Oscillography . . . . .	21
2.2	Digital Systems . . . . .	26
2.2.1	Early Sound Synthesis Languages . . . . .	26
2.2.2	Sound Synthesis From Series Formulae . . . . .	29
2.2.3	Early Vector Graphics Languages . . . . .	31
2.2.4	Turtle Graphics . . . . .	33
2.2.5	Parametric Equations . . . . .	37
2.2.6	Graphical Shapes From Fourier Series . . . . .	42
2.2.7	Graphical Shapes From Sound . . . . .	45
2.2.8	Digital Harmony . . . . .	47
2.3	Mathematical Abstractions . . . . .	50
2.3.1	Epicyclic Curves . . . . .	50
2.3.2	Fourier Series . . . . .	54
2.3.3	The Transfer Function . . . . .	57
2.4	Symmetry and Its Importance in Mathematics, Science, and Art . . . . .	60
<b>3</b>	<b>Conceptual Framework</b>	<b>64</b>
3.1	Conventions . . . . .	65
3.1.1	General Terminology . . . . .	65
3.1.2	Mathematical Symbols . . . . .	66
3.1.3	Graphical Representations . . . . .	66
3.2	The Harmonic Pattern Function . . . . .	68
3.3	The Role of Symmetry . . . . .	71
3.4	Methodology . . . . .	75

<b>4</b>	<b>Generalizations of Harmonic Patterns</b>	<b>78</b>
4.1	Frequency-domain Transformations . . . . .	79
4.1.1	Amplitude Transformations . . . . .	80
4.1.2	Phase Transformations . . . . .	81
4.1.3	Frequency Transformations . . . . .	84
4.1.4	Frequency and Phase Negation . . . . .	87
4.2	Planar Symmetry of Curves . . . . .	88
4.2.1	Cyclic Symmetry . . . . .	90
4.2.2	Dihedral Symmetry . . . . .	91
4.3	Regular (Star) Polygon Patterns . . . . .	93
4.4	Interpolation Patterns . . . . .	94
4.5	Unit Circle Patterns . . . . .	96
4.6	Inversion-symmetric Patterns . . . . .	99
<b>5</b>	<b>Taxonomy of Harmonic Patterns</b>	<b>102</b>
5.1	Order 1 . . . . .	104
5.1.1	Constant . . . . .	104
5.1.2	Regular Polygon . . . . .	105
5.1.3	Regular Star Polygon . . . . .	107
5.1.4	Interleaved Harmonic . . . . .	110
5.1.5	Simple Motion . . . . .	112
5.2	Order 2 . . . . .	114
5.2.1	Eccentric Polygon . . . . .	115
5.2.2	Ellipse . . . . .	120
5.2.3	Rose Curve . . . . .	122
5.2.4	Cuspoid . . . . .	130
5.2.5	Smooth Star Polygon . . . . .	131
5.2.6	Low $N$ Rose Curve . . . . .	134
5.2.7	Star . . . . .	135
5.2.8	Polygon Star Wrapping . . . . .	136
5.2.9	Interleaved Bicircloid . . . . .	139
5.2.10	Simple Beat . . . . .	146
5.2.11	Archimedes' Spiral . . . . .	147
5.2.12	Inverse Beat . . . . .	149
5.2.13	Hyperbolic Spiral . . . . .	150
5.2.14	Trochoid . . . . .	151
5.2.15	Standing Waves . . . . .	151
5.2.16	Inverse Bicircloid . . . . .	153
5.2.17	Volute Curve . . . . .	158
5.3	Order 3 . . . . .	159
5.3.1	Eccentric Tusi Couple . . . . .	160
5.3.2	Botanic Curve . . . . .	160

5.3.3	Petal Curve . . . . .	161
5.3.4	Double Rose Curve . . . . .	162
5.3.5	Fanned Rose . . . . .	163
5.3.6	Envelope Bicircloid . . . . .	165
5.3.7	Conic Sections . . . . .	166
5.3.8	Double-sided Spectral Exponential . . . . .	170
5.3.9	Moving Bicircloid . . . . .	171
5.3.10	Circle Cuspoid . . . . .	172
5.3.11	Circle Chain . . . . .	173
5.4	Higher Order . . . . .	175
5.4.1	Rectangular Hyperbola . . . . .	175
5.4.2	Bowditch Curves . . . . .	176
5.4.3	Comb Filters . . . . .	180
5.4.4	Truncated Spectral Exponential . . . . .	183
5.4.5	Fourier Polygons . . . . .	184
<b>6</b>	<b>Future Research Directions</b>	<b>195</b>
6.1	Three-dimensional Patterns . . . . .	195
6.2	Self-similar Patterns . . . . .	198
6.3	Level Set Patterns . . . . .	200
<b>7</b>	<b>Conclusion</b>	<b>202</b>

# List of Figures

2.1.1	Thomas Young’s illustrations of the transverse orbits of a single point on vibrating string [133]. Fig. 44. Various orbits of a musical chord. Fig. 45. Forms from sound produced by means of a bow. Fig. 46. Epitrochoidal curves formed by combining simple vibrations. . . . .	7
2.1.2	Nathaniel Bowditch’s illustrations of various pendulum orbits. . . . .	9
2.1.3	Charles Wheatstone’s illustrations of his Kaleidophone instrument and some of the curves it produces [123]. . . . .	10
2.1.4	First known direct transcriptions of sound from Édouard-Léon Scott de Martinville’s phonautograph. The images are from his 1857 manuscript “Principes de Phonautographie” showing (a) speech, (b) a guitar, and (c) various trochoidal patterns. . . . .	12
2.1.5	John Baptist Suardi’s geometric pen [4] (left) and John Holt Ibbetson’s geometric chuck [11] (right). . . . .	14
2.1.6	Patterns produced by the five major ornamental lathe apparatus—eccentric chuck, ellipse chuck, ellipse-cutting instrument, rose-cutting instrument, and geometric chuck (left to right) [77]. . . . .	14
2.1.7	Centric, ciscentric, and transcentric figures (left to right). . . . .	17
2.1.8	Elphinstone’s turning patterns. From left to right, Turk’s-head surrounded with basket-work, shell, star, waved ellipse, and a double counting. . . . .	17
2.1.9	Figures displaying the diversity of curves possible from compound circular motion of two geometric chucks. . . . .	18
2.1.10	The four basic looping patterns of a single geometric chuck as described by Thomas Sebastian Bazley [11] are (a) consecutive/internal, (b) consecutive/external, (c) circulating/internal, and (d) circulating/external. . . . .	18
2.1.11	Examples of unicursal figures displaying what Bazley termed “symmetrical overlap”. . . . .	19
2.1.12	Some of Ben Laposky’s <i>Oscillon</i> series of photographs. Images © 1952-1960, Sanford Museum, Cherokee, Iowa. . . . .	22
2.1.13	Images of Alexandre Vitkine’s oscilloscope work. . . . .	24
2.2.1	Path taken by a turtle following the <code>drawSquare</code> function. . . . .	35

2.2.2	The recursive application of any (a) turtle drawing routine has (b) the skeletal structure of a regular star polygon. . . . .	35
2.2.3	Turtle reference frame in $\mathbf{R}^2$ and $\mathbf{R}^3$ . . . . .	36
2.2.4	Turtle on $\mathbf{S}^2$ . . . . .	37
2.2.5	Superformula shapes. The symmetry parameter $m$ is 1, 2, 3, 4, and 9 going from the left column to the right column. The top row shows inscribed shapes using the parameters $a = b = n_1 = n_2 = n_3 = 1$ . The middle row show circumscribed shapes using the parameters $a = b = n_2 = n_3 = 1$ and $n_1 = -1$ . The bottom shows lobed shapes made using the parameters $a = b = 1$ , $n_2 = n_3 = 8$ , and $n_1 = -1$ . . . . .	41
2.2.6	Partials sums of the Fourier series of a pentagon given by Eq. 2.2.9 for $n = 5$ and $a = 1$ . The number of harmonic components in each figure (pictured left to right) is 3, 5, 7, and 33. . . . .	43
2.2.7	The basis functions (complex sinusoids) of an 8-point discrete Fourier transform form polygons in the complex plane if we connect successive samples with lines. The complex sinusoids are ordered by increasing harmonic number from (a) 0 to (h) 7. Figure reprinted from Glassner [35], © 1999 IEEE. . . . .	43
2.2.8	Shapes produced from Fourier descriptors (a) $A_1 = 3.83171$ , (b) $A_1 = 7.01559$ , (c) $A_4 = 3.0, \alpha_4 = \pi/2, A_8 = 2.0, \alpha_8 = 3\pi/2$ , (d) $A_5 = 4.0$ . Images reprinted from Zahn and Roskies [134], © 1972 IEEE. . . . .	45
2.4.1	A piece of ochre carved with abstract patterns dated back to 77,000 B.C. From Henshilwood et al. (2002). Emergence of modern human behavior: Middle stone age engravings from South Africa. (Science, 295:1278–1280. Reprinted with permission from AAAS.) . . . . .	61
3.1.1	Various graphical plots used to display a one-dimensional complex sequence. All plots show the same sequence $\alpha_n = \{1\} + \{20\}$ with $N = 400$ . . . . .	67
3.3.1	Two different models of spatiotemporal patterns. The top figure is the discontinuous model where the pattern has separate space and time components. The bottom figure is the continuous model where patterns run smoothly across space and time. . . . .	73
3.3.2	Three types of flow patterns in continuous pattern model: under-shooting (top), overshooting (middle), and coinciding (bottom). . . . .	74
3.3.3	Band-limited waveform constructed through destructive interference of complex exponentials in the frequency domain. . . . .	75

3.4.1	<i>Spool</i> screenshot. On the leftmost side are synthesis controls for setting harmonics of the harmonic pattern function and other synthesis parameters. To the right of the synthesis controls is a grid of graphs showing the resulting complex sequence in both the position domain and frequency domain on the complex plane and its polar and Cartesian projections. . . . .	77
4.1.1	Effect of a phase rotation transformation on $x_n = \{1\} + \{2\} + \{3\}$ . Red and black designate the start and end of the sequence, respectively. . . . .	83
4.1.2	Effect of a phase shift transformation on $x_n = \{1\} + \{2\} + \{3\}$ . Red and black designate the start and end of the sequence, respectively.	83
4.1.3	Frequency shifting by varying amounts. A frequency shift causes the curve to wind more, but leaves the magnitude invariant as shown by magnitude/phase plots in the top row. . . . .	85
4.1.4	Frequency shifting by fractional amounts $\delta = 0, \frac{1}{4}, \frac{2}{4}, \frac{3}{4}, 1$ (left to right). . . . .	86
4.1.5	Comparison between sequence and curve plots of frequency negation of $\alpha_n = \{1, 0.1\} + \{2\} + \{-1\}$ . Frequency negation reverses the position-domain sequence. . . . .	87
4.2.1	Two curves with the same continuous symmetries, but differing discrete symmetries. The dashed boxes show a $16\times$ magnification at the origin. . . . .	89
4.4.1	An interpolation pattern with different types of interpolating polynomials. The constant, linear, and quadratic interpolation patterns are obtained from successive integrations of the delta interpolation pattern. . . . .	95
5.1.1	Regular polygons constructed from $\alpha_n = \{1\}$ for (a-e) $N = 2, 3, \dots, 6$ and (f) $N = 60$ . . . . .	105
5.1.2	Negating frequency results in an opposite winding direction. Shown for (a) $\alpha_n = \{1\}$ and (b) $\alpha_n = \{-1\}$ . . . . .	106
5.1.3	Regular star polygons produced from $\alpha_n = \{\ell\}$ for $N = 7$ and $\ell = 1, 2, \dots, 6$ (left to right). . . . .	107
5.1.4	Densest $N = 360$ star polygon at $1\times$ magnification (top-left), $64\times$ magnification (top-right) and $1024\times$ magnification (bottom).	108
5.1.5	Component and raster plots of complex sinusoids for $N = 100^2$ and $\ell = 0, 1, 2, 3$ (a-d). Raster plots reveal approximate plane waves in the $+y$ direction. . . . .	109
5.1.6	Raster plots displaying how one-dimensional complex sinusoids can approximate plane waves. The plots show various harmonic numbers, $\ell$ , for $M = 100$ . . . . .	110



5.1.7	A single harmonic producing a rotating triangle. Figure (a) shows the entire space-time shape specified by $\alpha_n = \{41\}$ with $N = 120$ and (b-d) show a succession of length 12 subsequences. . . . .	112
5.1.8	Top row, left to right: The first four elements of $\{41\}$ , $\{40\}$ , and $\{39\}$ with $N = 120$ . Bottom row, left to right: The first twelve elements of $\{41\}$ , $\{40\}$ , and $\{39\}$ with $N = 120$ . . . . .	113
5.2.1	Ordinary cycloids produced through discrete integration of eccentric polygons. . . . .	116
5.2.2	Moving regular polygons for $N = 24$ , $a = 0.02$ , and $m = 12, 8, 6, 4, 3$ (left to right). . . . .	117
5.2.3	Progression from static polygon (top) to cycloid (bottom). The velocity parameter $a$ is varied from from 0 to 1 in increments of 0.1 (top to bottom). . . . .	117
5.2.4	Examples of moving star polygon patterns with $N = 240$ . . . . .	118
5.2.5	Ellipses resulting from $b = -0.97, -0.5, 0, 0.5, 0.97$ (left to right). . . . .	121
5.2.6	Inverse ellipse curves for $b = \frac{1}{10}, \frac{1}{6}, \frac{2}{5}, \frac{4}{5}$ (left to right). . . . .	121
5.2.7	Roses with (a) inward and (b) outward pointing petals. . . . .	123
5.2.8	Outward looping roses with the three different petal intersection conditions: (a) non-touching, (b) touching, and (c) intersecting. . . . .	124
5.2.9	Visualization of similar roses. Columns are $k \in [-200, 200]$ going left to right and rows are $m \in [1, 300]$ going top to bottom. Red indicates outward roses while cyan indicates inward roses. The lighter colors indicate the conjugates (reverse windings) of the darker colors. . . . .	126
5.2.10	Comparison of raster plot (left) and curve plot (middle) with phase plot (right) of the complex sequence $\alpha_n = \{k\} + \{k + 5\}$ . . . . .	129
5.2.11	Spoke shapes given by $\alpha_n = \{1\} + \{\frac{N}{2} + 1\}$ . . . . .	134
5.2.12	A sampling of low $N$ rose curves. The leftmost column displays the continuous rose curve shape ( $N \rightarrow \infty$ ). The numbers under each figure are $N, \phi$ . . . . .	135
5.2.13	Star shapes given by $\alpha_n = \{1\} + b\{\frac{N}{2} + 1\}$ for $N = 12$ and $b = 0, \frac{1}{3}, \frac{2}{3}, 1$ (a-d). The shapes progress from a regular polygon to a spoke. . . . .	136
5.2.14	Connecting star points with a triangle strip creates (a) an annulus ( $b < 1$ ) or (b) a disc ( $b = 1$ ). . . . .	136
5.2.15	A 120-gon progressively split into two 60-gons by variation of parameters $a$ and $b$ of $\alpha_n = a\{1\} + b\{\frac{120}{2}\}$ . The top figures show the vertices and the bottom figures show the edges. . . . .	140
5.2.16	Equiamplitude ( $a = b$ ) interleaved eccentric polygons (a) $\alpha_n = \{1\} + \{\frac{120}{3}\}$ , (b) $\alpha_n = \{1\} + \{\frac{120}{4}\}$ , (c) $\alpha_n = \{1\} + \{\frac{120}{5}\}$ . The top figures show the vertices and the bottom figures show the edges. . . . .	141

5.2.17	Interleaved 30-gons constructed from $\alpha_n = \{1\} + b \left\{ \frac{60}{2} + 1 \right\}$ : (a) regular 60-gon, (b) and (c) star figures, and (d) spoke. . . . .	142
5.2.18	Interleaved ellipses given by $\alpha_n = \{1\} + b \left\{ \frac{60}{2} - 1 \right\}$ for increasing $b$ . 143	
5.2.19	Interleaved bicircloids given by $\alpha_n = \{1\} + b \left\{ \frac{120}{2} - 2 \right\}$ and various $b$ . 144	
5.2.20	Some patterns produced from subsequences of interleaved bicircloids. 145	
5.2.21	Anatomy of a rising beat $\alpha_n = \frac{1}{2}(\{10\} - \{9\})$ . Figure (a) shows the entire beat while (b) and (c) show the first and second half-sequences, respectively. . . . .	147
5.2.22	Linear spirals with $k = 1, 2, 3, 4$ winding(s) (left to right). The parameters are $N = 16000, M = 160$ . . . . .	147
5.2.23	John Whitney's example of a radial differential motion pattern. 148	
5.2.24	Regular polygon linear spirals with $m = 3, 4, 5, 6$ polygon vertices (left to right) and $k = 4$ windings. . . . .	148
5.2.25	Extrapolation of triangular linear spiral approximation to (a), (b) half and (c) full sequences. The curve begins as a triangular spiral and evolves into three intersecting circles. The curve is given by $\alpha_n = i(\left\{ \frac{N}{3} \right\} - \left\{ \frac{N}{3} + 1 \right\})$ . . . . .	149
5.2.26	Anatomy of an inverse rising beat $\alpha_n = \frac{1}{2}(\{10\} - \{9\})$ . Figure (a) shows the entire beat while (b) and (c) show the first and second half-sequences, respectively. . . . .	150
5.2.27	Hyperbolic spirals with $m = 1, 2, 3, 4$ winding(s) (left to right). . . . .	150
5.2.28	Illustration of standing wave given by space-time curve $\alpha_n = \{11\} + \{13\}$ where $N_t = 12$ . . . . .	153
5.2.29	Smooth saw ( $m = 1$ ) and square ( $m = 2$ ) waveforms along higher symmetry extrapolations ( $m = 3, 4$ ). . . . .	157
5.2.30	Various volute curves. . . . .	158
5.2.31	Volute curves with linear middle segment. The parameter $b$ is $\frac{m}{m+1}$ . 159	
5.3.1	Integrated eccentric Tusi couples with $\phi = 0, m = 1$ (left) and $m = 5$ (right). . . . .	160
5.3.2	Botanic curves with $m = 1$ and $a = \frac{1}{4}, a = \frac{1}{2}$ (eccentric cardioid), and $a = 1$ (limaçon trisectrix) shown left to right. . . . .	161
5.3.3	Petal curves with $m = 1, 2, 3, 4, 5, 6$ (left to right). . . . .	162
5.3.4	Magnitude/phase plots of petal curves for $m = 1, 2, 3$ (left to right). 162	
5.3.5	Double rose curves with $\ell = 1$ and $m = 1, 2, 3, 4, 5, 6$ (top row, left to right). Once-integrated curves are displayed in the bottom row. . . . .	163
5.3.6	Fanned rose curves for $\phi = 0, m = 1, 2, 3, 4, 5$ (top row, left to right) and $\phi = \frac{1}{2}, m = 1, 2, 3, 4, 5$ (bottom row, left to right). . . . .	164
5.3.7	Envelope bicircloids given by $p = 1, q = \frac{1}{2}, m = 20\frac{1}{2}, b = 1, \frac{1}{2}, \frac{1}{4}$ (left to right). . . . .	166
5.3.8	Conic sections circle, ellipse, parabola, and hyperbola. . . . .	167

5.3.9	Circle cuspidals. The rows are different base cuspid curves, a cardioid, a nephroid, and a deltoid going top to bottom, and the columns are circular curves with different amplitudes. . . . .	173
5.3.10	Circle chain curves. The symmetry parameter $m$ ranges from 2 to 6 going left to right. The top row curves have $\ell = 0$ and the bottom row curves have $\ell = -1$ . . . . .	174
5.3.11	Details at center of circle chain curves for $m = 5$ and $\ell = 0$ (left) and $\ell = -1$ (right). The curves are skewed slightly to make the path more visible. . . . .	174
5.3.12	A circle chain curve is a special case of a moving cardioid curve.	175
5.4.1	Rectangular hyperbola (left) and its inverse curve, the lemniscate of Bernoulli (right). . . . .	176
5.4.2	The larger curve on the left is the entire curve plot of $\text{Re}\{9\} + \text{Im}\{10\}$ . The grid of curves on the right shows 9 successive subsequences of the entire curve, in order, going from top to bottom, then left to right. . . . .	178
5.4.3	Crosshatched disc patterns for $\ell = 1, \frac{N}{4} + 1, \frac{N}{2} + 1$ (left to right). $N = 120$ . . . . .	179
5.4.4	Curve plots of (a) delta ( $p = 0$ ), (b) constant ( $p = 1$ ), (c) linear ( $p = 2$ ), and (d) quadratic ( $p = 3$ ) Fourier 3-gons made with 8 harmonics and $N = 90$ points. . . . .	186
5.4.5	Real and imaginary projections of Fourier polygons with (a) $p = 0$ and (b) $p = -2$ . Vertical lines show sample boundaries. . . . .	188
5.4.6	Real and imaginary projections of Fourier polygons with $p = 1$ . Figure (a) is a constant polygon with $m = 5$ and (b) is the same curve rotated by $-\pi/5$ . Vertical lines show sample boundaries.	190
5.4.7	Raster plots of frequency-scaled Fourier polygons by the amounts $s = 0, M, M + 1, M - 1$ (left to right) where $M = \sqrt{N}$ , $m = 5$ , $\ell = 1$ , and $p = 1$ . . . . .	192

## List of Tables

2.1	A selection of Perigal's "Spiroeid" curves some of which are well-known including Freeth's nephroid (top left), an ellipse envelope (top center), the lemniscate of Geronno (top right), and the right parabola (center right). . . . .	16
2.2	Rigge's six classes of harmonic curves. . . . .	20

2.3	The complete set of MUSIC V unit-generators. . . . .	28
2.4	Equations for the circle, ellipse, and superellipse . . . . .	39
2.5	Special superellipse shapes based on the implicit equation $\left \frac{x}{a}\right ^n + \left \frac{y}{b}\right ^n = 1$ . The gridlines are positioned at integer multiples of $\frac{1}{4}$ . . . . .	39
2.6	Graphical scale of discrete rose curves . . . . .	49
2.7	The various types of epicyclic roulette curves. . . . .	52
2.9	Fourier series of some simple functions. . . . .	56
3.1	Listing of terminology . . . . .	65
3.2	Listing of mathematical symbols . . . . .	66
4.1	Frequency-domain transformations . . . . .	79
4.2	Comparison of phase rotation and shift transformations of $x_n = \{1\} + \{2\} + \{3\}$ . The plots show $n$ (the domain) increasing in the $+x$ -direction, magnitude along the $+y$ -direction, and phase as hue. . . . .	82
4.3	Conjugation and reversal transformations. A $+$ indicates the identity operation (no negation) while a $-$ indicates a negation operation. . . . .	88
4.4	Types of interpolation functions . . . . .	95
5.1	Unique harmonic pattern function formulae up to order 4. . . . .	103
5.2	Singly-wound rose curves from one to eight petals that are unique up to similarity. The curves are given by $\alpha_n = \{k\} + \{k + m\}$ . The solid line running through the table demarcates where the patterns reverse sequence. . . . .	125
5.3	Complex plane wave superpositions derived from $\alpha_n = \{k\} + \{k + m\}$ , $N = 100^2$ . The solid line running through the table demarcates where the patterns reverse sequence. . . . .	127
5.4	Low-frequency, non-similar cuspsoids given by $\alpha_n = i \int \{\ell\} + \{\ell + m\}$ . . . . .	131
5.5	Low-frequency, non-similar smooth star polygons given by $\alpha_n = \frac{1}{\ell^2} \{\ell\} + \frac{1}{(\ell+m)^2} \{\ell + m\}$ . . . . .	133
5.6	Polygon star wrappings. The numbers under each figure are the harmonic amplitudes $a, b$ . . . . .	138
5.7	Inverse Rose Curves . . . . .	154
5.8	Inverse botanic curves for various $m$ and $b$ . When $m = 1$ , the curves are conic sections. . . . .	168
5.9	Integrations of an inverse botanic curve with $b = 0.9999$ , $N = 60$ , and $m = 3$ . . . . .	169
5.10	Integrations of an inverse botanic curve with $b = 0.9999$ , $N = 60$ , and $m = 4$ . . . . .	169
5.11	Integrations of an inverse botanic curve with $b = 0.9999$ , $N = 60$ , and $m = 5$ . . . . .	170

5.12	Well-known algebraic curves that are also Bowditch curves. On the top row going left to right are the Chebyshev polynomials of degree 1 (a line), degree 2 (a parabola), degree 3, and degree 4. On the bottom row going left to right are an ellipse, lemniscate of Geronno, saddlebag, and Tschirnhausen cubic. . . . .	177
5.13	Parametric descriptions of comb filters. . . . .	181
5.14	Magnitude/phase frequency responses of the general comb filter types. Frequencies run from 0 on the left to $N - 1$ on the right. The height of the graph is $ z $ while the hue corresponds to $\arg z$ where $0, \frac{1}{3}2\pi, \frac{2}{3}2\pi \rightarrow$ red, green, blue. . . . .	182
5.15	Regular polygon families constructed from $\alpha = \sum_{k=1(m),  k  < 4m} \{k\} / k^p$ .	189
5.16	Raster plots of $\alpha_n = \sum_{k=1(m),  k  < 8m} \{k\} / k^p$ . For $p = 1$ , $\alpha_n$ is multiplied by the phase correction factor $e^{-i\pi/m}$ . . . . .	191

# 1. Introduction

---

To date, there is no formal mathematical framework that explicitly addresses the simultaneous generation of both visual and sonic patterns in the context of digital arts. Artists and researchers working with digital media must often construct multimodal systems and artworks by combining a variety of seemingly independent techniques from sound synthesis and computer graphics or rely on purely data-based representations, such as sound files and raster- or vector-based images. This fragmentation and independence of modalities not only creates a technical burden complicating systems design, but can force media artists, designers, and researchers into creating works that are a patchwork of modality-specific techniques and data, rather than a cohesive product stemming from a unified set of principles.

In recent years, the combination of computers and discrete mathematics led to the development of digital signal processing (DSP). A digital signal is any variable quantity that is measured at regular intervals in space or time and at discrete levels of intensity. The ability to convert physical media, namely sound and light, into digital signals and back has opened up new possibilities for storing, synthesizing, transforming, transcoding, and transmitting multiple media types from within a single system. “Multimedia” is the term given to this notion of combining one or more medium of expression or communication [79].

## 1.1 Data and Process in Multimedia

In light of these recent developments, multimedia has still not come to fruition as a medium with its own set of inherent qualities. Our current use of multimedia can be criticized on two grounds: 1) it is often a combination of single modalities rather than a true integration [48] and 2) it is overly data-centric rather than process-centric [15]. Combining several media does not lead to multimedia [48]. In *Hamlet on the Holodeck*, Janet Murray calls early multimedia artworks “scrapbook multimedia” referring to the fact that they were often nothing more than digital amalgamations of prior media types, such as photographs, text, film, and sound recordings [73]. The reason, she argues, is that multimedia was (and most likely still is) going through an initial derivative stage before its intrinsic properties are uncovered and developed. Digital signals are reservoirs of possible patterns because, in theory, they can represent any sound, image, or video sequence numerically. However, a digital signal is not a description of a process. Something else is required to fill this role—a language for generating patterns. The computer opens up a large space of possibilities for art, but it is only useful with a repertoire of image- or sound-generating functions [91]. The first languages for generating computer graphics and sound were developed in the 1960s and consisted of a small set of primitives that could be combined to construct more complex forms. Max Mathews’ *MUSIC 1-5* series of acoustic compilers defined a small set of unit generators—simple oscillators, filters, and random number generators—that could be connected together in a modular fashion to create more complex instruments [63]. Georg Nees’ *G1*, *G2*, and *G3* series of graphics languages consisted of various pen commands for drawing lines and a random number generator [75]. Mathews’ and Nees’ early computer languages provided a way to generate sound timbres and

visual shapes, respectively, however, they were not truly multimodal.

## 1.2 Problem Statement

At the moment, there are a wide variety of techniques for synthesizing sonic and graphical patterns in the digital arts. What is currently missing in the audio/visual domain is a simple and coherent mathematical construct specifically oriented towards the simultaneous synthesis of sound and graphics. The problem is eloquently stated by John Whitney [127]: “Technical innovation is thus providing the means to begin a fine art for eye and ear. Regrettably, the formal idea of such an extraordinary art remains obscure and is still poorly defined.” Also, as stated by Jaimes et al [47], “Without theoretical frameworks for integrating multiple sensors and media, we are likely to continue working on each modality separately and ignoring the integration problem, which should be at core of multimedia research.” Such attempts at audio/visual integration should not happen after the fact in the data, but before in the process.

While some research has been done to correlate audio and visual data in the areas of visual music [126, 6], two-dimensional sound visualization and transformation [83], and image sonification [132, 131, 20], there is still lack of a simple, well-defined mathematical framework that relates audio and visual patterns from first principles rather than through extraneous mappings or extrinsic synchronization. Composer Adriano Abbado notes that the correspondence between timbre and shape should form the basis of any audio/visual language [2, 1].

Although the standard definition of multimedia addresses the notion of a medium having more than one perceptual mode of experience, it does not specifically define deeper unifying processes tying together different media types. Central to



understanding process-centric multimedia, we consider the complex sinusoid (or harmonic) as an atomic unit of digital sound and graphical patterns. Harmonics, being the dual frequency-domain representation of the samples and pixels of digital media, permit a different view of data as a combination of simple motions. The advantage of seeing data from the frequency domain is that it informs us about its process of creation rather than just stating its final form in the time and/or position domains.

### **1.3 Outline of Dissertation**

This dissertation continues with a historical background of mechanical, electronic, and digital systems using harmonics as a basis for audio/visual synthesis. Following this, in Chapter 3, the conceptual framework is presented which 1) introduces the harmonic pattern function, a mathematical model tying together prior work on harmonic pattern generation, 2) describes the role of symmetry in understanding how the harmonic pattern function operates, and 3) outlines the methodology used in this dissertation. In Chapter 4, generalizations of the harmonic pattern function are given and in Chapter 5 specific instances of sound waveforms along with graphical curves and raster plots are categorized according to the number of harmonics comprising the pattern. Finally, before concluding, Chapter 6 discusses some possible directions for future research.

## 2. Background on Harmonic Pattern Synthesis

---

### 2.1 Mechanical and Electronic Devices

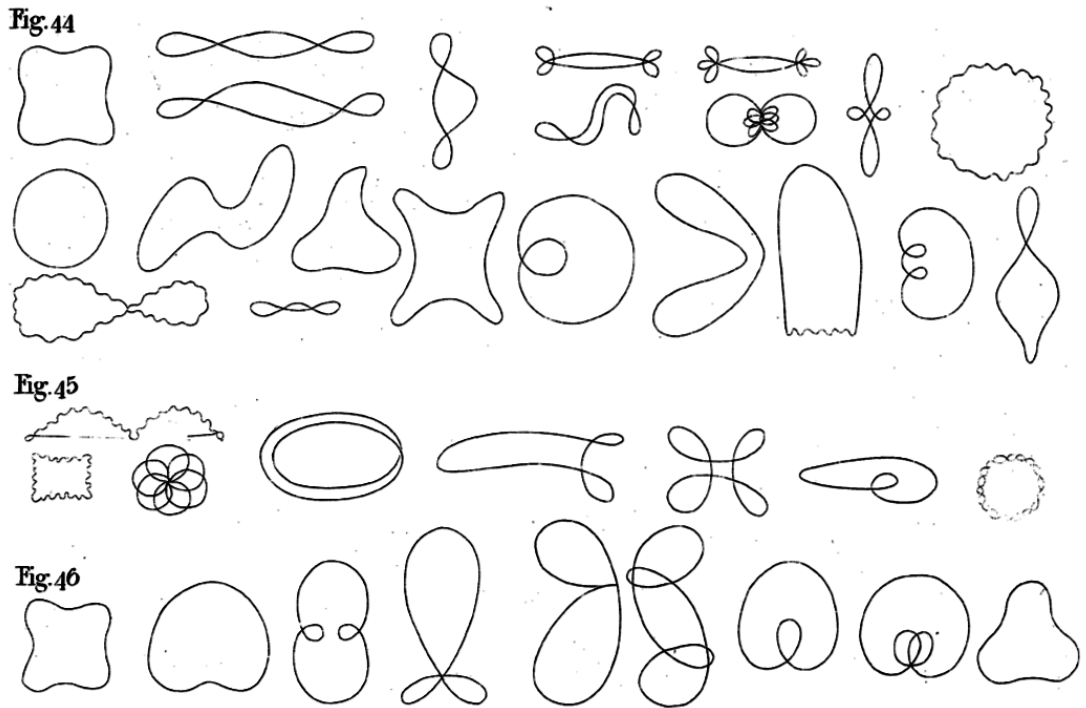
There is a long and diverse lineage of mechanical devices constructed in order to visualize sound and produce forms from simple and compound harmonic motion [7, 82, 124, 125, 8]. The principle operating components of these mechanical devices are vibrating diaphragms, rods, and strings, oscillating pendulums, and systems of rotating gears. Many of the devices were constructed in order to study and/or demonstrate simple types of motion occurring in nature, while others were made directly for producing complex patterns for artistic purposes or simply as a “philosophical toy.” The attraction of these devices is their ability to produce a seemingly endless variety of patterns from simple operating principles. In the electronic era, oscillography opened up new possibilities for creation of harmonic patterns. While the earlier mechanical devices can only produce relatively simple harmonic motions, electrical signals are capable of encoding any type of waveform shape.

### 2.1.1 Oscillating Devices

The study of forms produced by means of controlled sound vibrations is called *cymatics*. The process involves taking a finely granulated or fluid-like substance and placing it on a vibrating surface where it then produces patterns corresponding to the resonant modes of the surface. In the 15th century, Leonardo da Vinci noticed that by striking a wooden table covered with a thin layer of dust, various shapes would form displaying the nodal (motionless) regions of the vibration. In 1787, Ernst Chladni published *Entdeckungen über die Theorie des Klanges* (*Discoveries in the Theory of Sound*) describing a method for visualizing the nodal regions of vibrating surfaces using sand. Chladni used a bow to strum the surface under investigation until a resonant frequency was reached causing patterns corresponding to normal modes to emerge in the sand. Even with a single driving frequency, complex patterns could be made as a result of the nodes formed from the geometry of the vibrating surface. Chladni's work was later expanded upon using more plate shapes with mathematical descriptions of the resulting patterns [111] and more precise and varied vibrating mechanisms [50]. Margaret Watts Hughes' "voice-figures" are some of the most remarkably organic cymatic patterns ever produced [43]. While cymatic patterns are certainly a type of sound visualization, they are by no means a direct structure-preserving translation of the original sound waves. They are not holistic visualizations since it is only the nodal or anti-nodal regions of the waveform that are observed. Also, like many other mechanical devices, the shapes of the resultant patterns depend in complex ways on the physical and geometric nature of the vibrating media that are used for observation.

In 1800, Thomas Young published the first known illustrations of the transverse

motion of a vibrating string [133]. His experimental setup was comprised of a light-reflecting silver wire wound around the lowest-pitched string of a piano. When the string was plucked, the transverse orbit of the silver wire could be observed as a “line of light” owing to the human perceptual phenomenon of persistence of vision. Young made several illustrations of the string orbits (Fig. 2.1.1) exemplifying the great diversity of harmonic patterns possible.



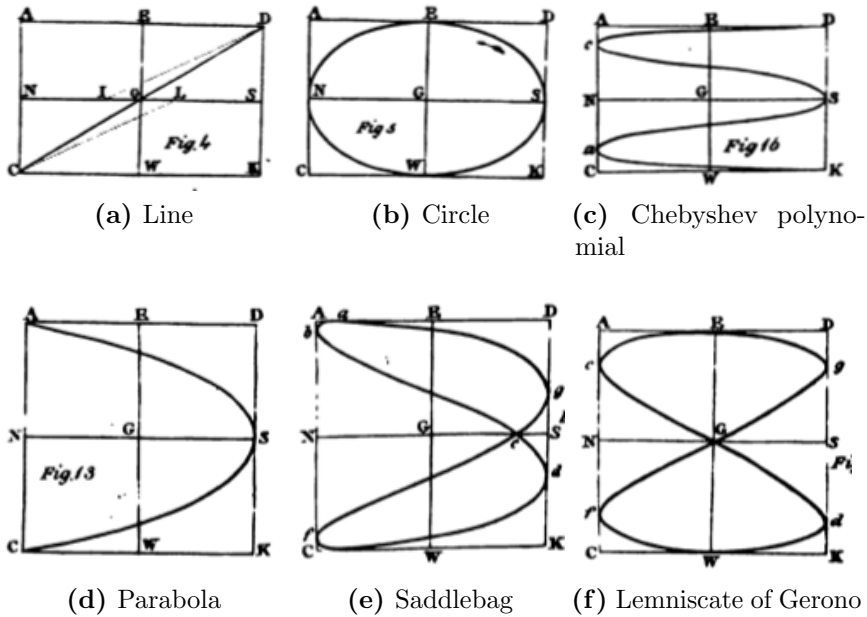
**Figure 2.1.1:** Thomas Young’s illustrations of the transverse orbits of a single point on vibrating string [133]. Fig. 44. Various orbits of a musical chord. Fig. 45. Forms from sound produced by means of a bow. Fig. 46. Epitrochoidal curves formed by combining simple vibrations.

In 1815, Nathaniel Bowditch made the first known illustrations of the periodic motion of a two-dimensional pendulum [16]. Though not a direct visualization of sound, this experiment set an important precedent for developments later in the century. The pendulum experiment Bowditch performed was suggested by James

Dean as a way to study the apparent motion of the earth from the moon [21]. The parametric equation Bowditch gives for the orbits traced out by a pendulum suspended from two points (for small variations) is

$$\begin{aligned}x &= b \cos(at + c) \\y &= b' \cos(a't)\end{aligned}$$

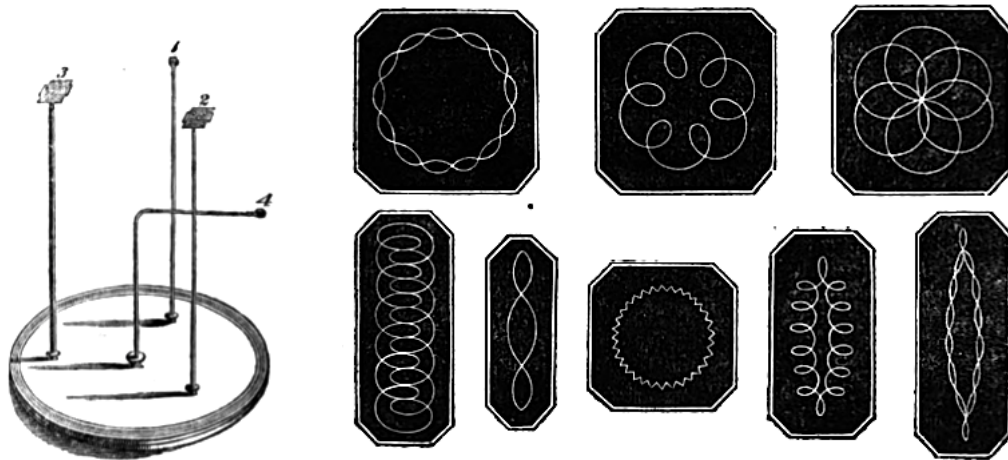
where  $x$  and  $y$  give the position of the pendulum,  $t$  is time,  $b$  and  $b'$  are the oscillation amplitudes,  $a$  and  $a'$  are the oscillation frequencies, and  $c$  is a phase shift that depends on the initial pendulum position. Each dimension oscillates independently allowing a large variety of curves to be produced. Bowditch curves subsume many types of well-known curves including circles, line segments, ellipses, parabolas, the lemniscate of Geronno, the Tschirnhausen cubic, and Chebyshev polynomials [65]. As one conclusion to his work, Bowditch noted [16] "... the method of finding these curves is very easy from what is here taught, and there appears to be such an endless variety, that it would be useless to attempt to note them." Some illustrations Bowditch made of these curves are shown in Fig. 2.1.2.



**Figure 2.1.2:** Nathaniel Bowditch's illustrations of various pendulum orbits.

In 1827, Charles Wheatstone, performed several experiments in visualizing the sonic vibrations of metal rods. He constructed an apparatus called the Kaleidophone or Phonic Kaleidoscope (named after David Brewster's Kaleidoscope), that consisted of an assortment of steel rods which at one end were perpendicularly fixed to a board and on the other end had a spherical silvered-glass bead attached [123]. The bead, by absorbing and reflecting incident light, allowed the orbit of the rod tip to be seen as a "continuous line of light" in a manner similar to Young's experiments with vibrating strings. Wheatstone made several important observations about the curves produced from his apparatus: 1) the extent of spatial motion is smaller for higher frequencies, 2) damped vibrations create spiral forms, 3) the number of indentations in a figure composed from two frequencies is related to the difference of the frequencies, 4) multiple points vibrating in unison trace out solid looking figures, and 5) images vibrated as a whole can appear duplicated at points where the motion of the orbit is retarded. While Wheatstone's

illustrations of the orbits (Fig. 2.1.3) appear closed and stationary, in a recent reconstruction of his experiments [107] it was observed that the figures actually rotate in space due to the fact that the rod vibrational modes have inharmonic frequencies  $f_0, 6.267f_0, 17.55f_0, 34.29f_0$ , etc. where  $f_0$  is the fundamental frequency. Kaleidophone curves (as drawn by Wheatstone) closely resemble those produced from a vibrating string, as observed by Thomas Young in 1800. This indicates that similar natural laws of harmonic motions describe the dynamics of what appear to be completely different physical systems.



**Figure 2.1.3:** Charles Wheatstone’s illustrations of his Kaleidophone instrument and some of the curves it produces [123].

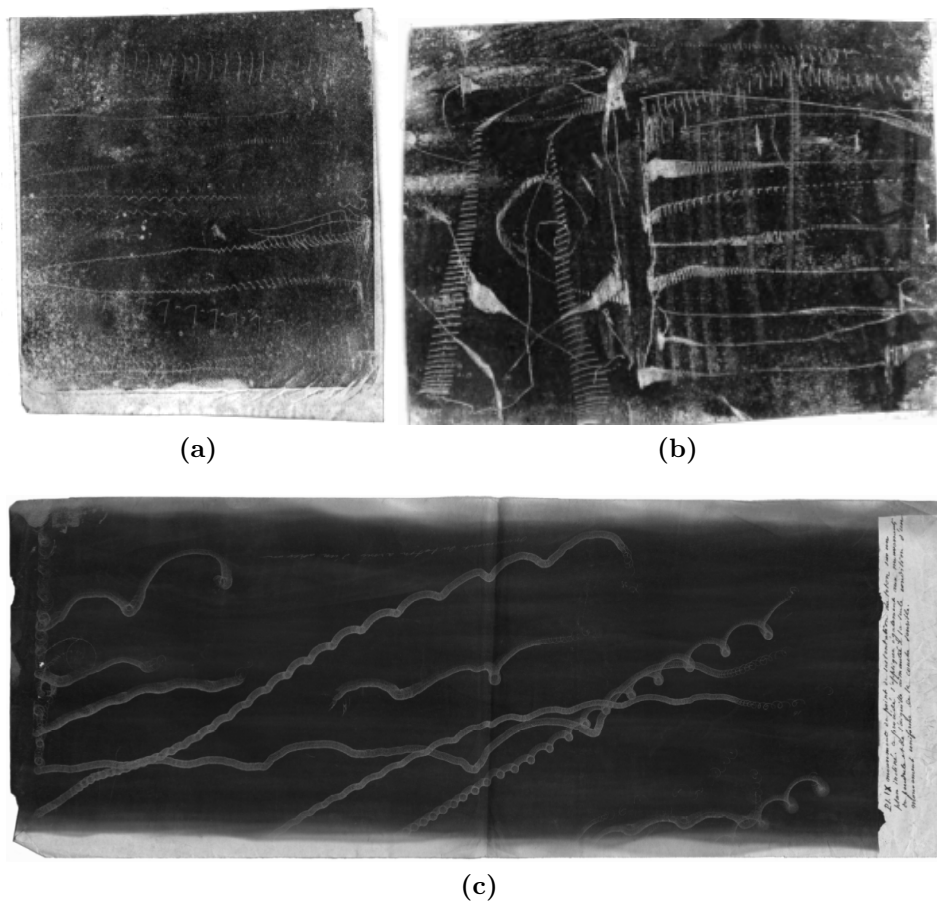
In 1855, Jules Antoine Lissajous built a device in order to visualize acoustic vibrations [60]. His system consisted of two tuning forks with attached mirrors positioned at right angles to one another. Light reflected from the mirrors would trace out curves on a screen that could be studied to determine the frequency relationships between the two tuning forks. For simple sinusoidal waves, the frequency ratio between the tuning fork vibrations can be deduced by counting the number of extrema along the boundary of each dimension of the figure. Like earlier devices, Lissajous’ apparatus took advantage of reflected light and persistence of

vision to see the path of the tuning forks' combined vibration.

The harmonograph is an instrument that traces out the path of a swinging pendulum in two dimensions. The curves produced by a harmonograph are similar to Bowditch curves (being essentially the same device), but due to friction, the markings decay towards the central equilibrium point of the pendulum. The swinging of the pendulum is due to an oscillation between the system's kinetic energy (maximum at center) and potential energy (maximum at edge). The first harmonograph was constructed by Blackburn in 1844 using a pendulum suspended from two points that traced patterns in sand [37, 124]. In 1871, Hubert Airy made an account of a naturally occurring harmonograph, a vibrating twig of an acacia tree [5]. Airy was able to trace the motions by attaching a small pencil to the twig (replaced by a thicker hazel stem, for technical reasons) and holding a piece of paper in contact with the pencil. In 1874, S. C. Tisley built the harmonograph in its "present" form using two independently swinging pendulums [37].

In 1856, Édouard-Léon Scott de Martinville patented the *phonograph*, a general sound transcribing device modeled after the human ear [27]. The device consists of a horn, acting as a conduit for sound waves, at the end of which is a diaphragm with a small stylus attached at a  $90^\circ$  angle. The stylus traces out the vibrations of the incoming sound onto a piece of paper wrapped around a rotating cylinder. This device is important because it allowed for the first time arbitrarily complex sounds to be transcribed in a one-to-one fashion with very few artifacts. Certain tracings produced by the phonograph demonstrate a direct connection between sound waveforms and trochoidal curves (Fig. 2.1.4).





**Figure 2.1.4:** First known direct transcriptions of sound from Édouard-Léon Scott de Martinville’s phonograph. The images are from his 1857 manuscript “Principes de Phonautographie” showing (a) speech, (b) a guitar, and (c) various trochoidal patterns.

## 2.1.2 Gear Systems

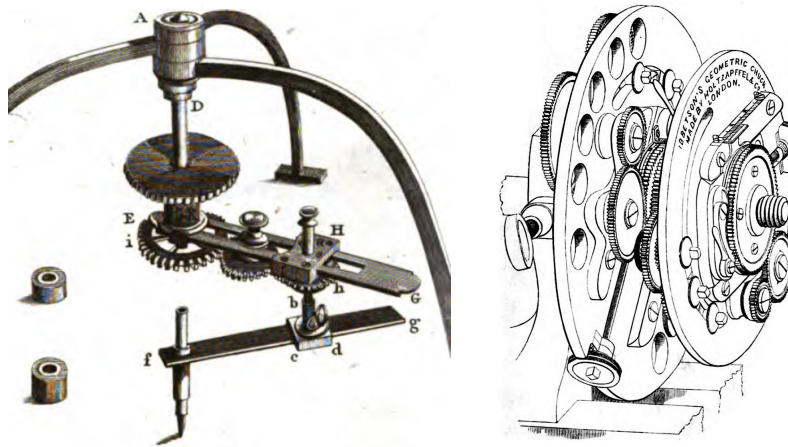
While many types of curves and patterns can be produced by oscillating mechanical devices, they have several disadvantages. First of all, unless continually excited, they will naturally evolve towards a motionless equilibrium due to friction. In general, the faster the vibrations, the quicker the curves decay. While the harmonograph specifically depends on this natural damping to create complicated curves, in most other cases it would be desirable to have control over the damping or even

eliminate it completely so that closed or sustained patterns can be constructed. A second disadvantage is that when an oscillating device has two or more independent dimensions of motion, the figures tend to drift, morphing from one shape to another, due to lack of frequency synchronization. Third, certain non-linearities in the physical medium (e.g., a rod or a pendulum) create complicated inharmonic vibration patterns making it difficult to control the stability of forms over time.

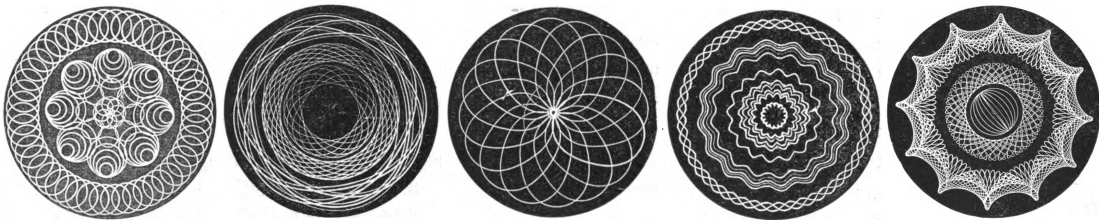
Gear systems, being more geometrically rigid, grant more precise control over production of curves. These devices operate through the principle of compound harmonic motion which is mathematically equivalent to the notion of deferents and epicycles used to model planetary motions in antiquity. Each gear rotates at a uniform rate and typically has another independently rotating gear attached rigidly to it. A stylus is attached to the last gear of the series for etching or drawing the resulting compound motion. It is interesting to note that the innate complexity of compound harmonic motions is both the cause of their highly successful application in the (ornamental) arts and the reason for their failure as scientific theory which seeks the simplest explanations of natural phenomena. In fact, the term “epicycles-on-epicycles” is now used as a general indicator of pseudoscientific theories.

There is a long history of using “turning” lathes to create ornamental patterns and designs dating back to the 15th century [42, 25]. Ornamental turning lathes are used in a variety of applications ranging from watch decorations to candlestick holders to anti-counterfeiting patterns for bank notes. A turning lathe operates by rotating an object that is in contact with a fixed cutting tool or by holding the carved object fixed while moving the cutting tool. The geometric pen is a drawing machine invented by John Baptist Suardi in 1750 that draws figures based on the compound motion of two circles [102, 12, 4, 125]. The geometric chuck,

invented by John Holt Ibbetson in 1827, is a special type of lathe based on the principle of a geometric pen [45, 77]. As stated by Ibbetson [46], the “power of The Geometric Chuck consists in its capability of combining all its powers and every kind of work it can accomplish, into one pattern, in any order of arrangement the workman pleases.” Representative patterns produced by various chucks are shown in Fig. 2.1.6.



**Figure 2.1.5:** John Baptist Suardi’s geometric pen [4] (left) and John Holt Ibbetson’s geometric chuck [11] (right).

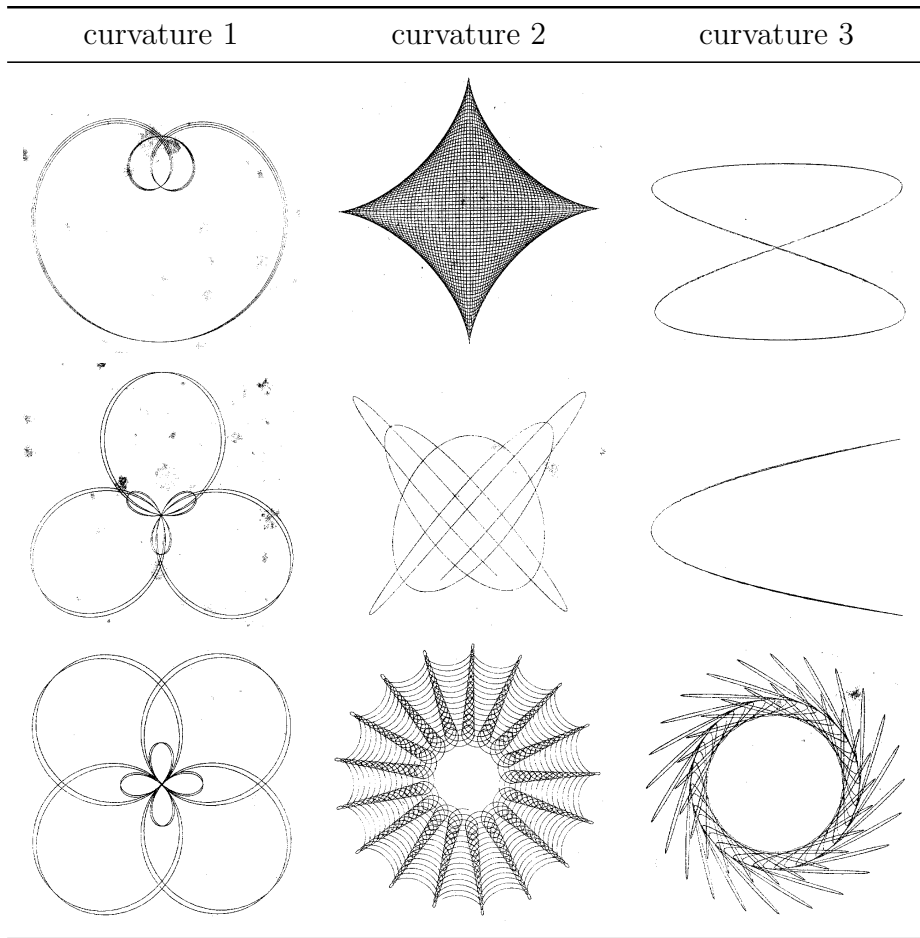


**Figure 2.1.6:** Patterns produced by the five major ornamental lathe apparatus—eccentric chuck, ellipse chuck, ellipse-cutting instrument, rose-cutting instrument, and geometric chuck (left to right) [77].

One of the earliest accounts of the mathematical details underlying chuck patterns is John Holt Ibbetson’s *Specimens In Eccentric Turning* published in 1800 [44]. For the first time, the *compound eccentric chuck* is introduced which is

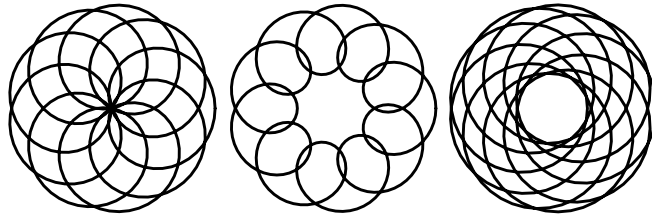
“capable of delineating and recording the path of [Geometric Pen] curves, by means of dots and circles.” The compound eccentric chuck operates under the principle of two compound circular motions. Ibbetson observes that inward and outward loops are related to whether the circular motions are in the same or contrary directions, respectively. He also notes that the cyclical symmetry of the resulting curves is a direct consequence of the ratio of the angular velocities of the two gears.

In 1838, Henry Perigal published *Experimental Researches in Kinematics* with illustrations of several curves produced using a geometric chuck using up to four compound harmonic motions [40]. The so-called “kinematic curves” produced from the chuck are “Curves that result from Motion . . .” and “. . . in contradistinction to Algebraic Curves representing the Geometric Loci of Equations; which express the limits of extension or magnitude, not the path of motion; defining a boundary line, not describing an orbit . . .” He calls the particular instances of kinematic curves “spiroeids,” “periodic Curves which progress in coils or circumvolutions.” In later writings, he uses the term “bicircloid” to describe curves made from two compound harmonic motions [81]. All bicircloids lie within an annulus where the outer radius is the apocenter and the inner radius is the pericenter [81]. Table 2.1 displays spiroeids of different curvature, where the curvature is the number of compound harmonic motions that are combined with a “right-lined” motion. It is worth noting that Perigal’s mechanical tracings of Bowditch curves, classified as spiroeids having a curvature of three, predate Lissajous’ publication of the same curves in 1855 [60].



**Table 2.1:** A selection of Perigal’s “Spiroeid” curves some of which are well-known including Freeth’s nephroid (top left), an ellipse envelope (top center), the lemniscate of Geronio (top right), and the right parabola (center right).

Extending the work of Perigal, W. Henry Northcott introduced several new ways of classifying geometric chuck patterns [77]. The terms circloid, bicircloid, tricircloid, etc. refer to patterns constructed from one, two, three, and so on, simple harmonic motions. Centric patterns have all loops passing through the center, ciscentric patterns have all loops wholly on one side of the center and transcentric patterns have all loops circumscribing the center (Fig. 2.1.7).



**Figure 2.1.7:** Centric, ciscentric, and transcentric figures (left to right).

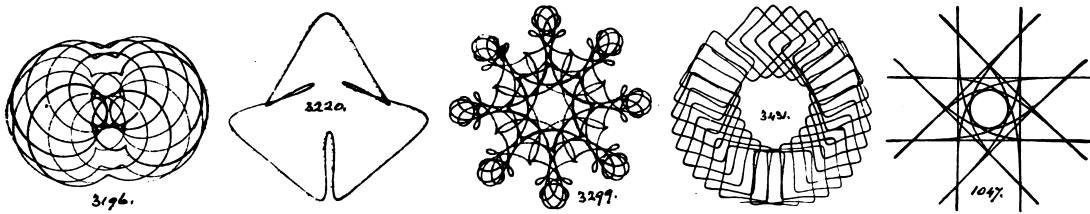
In 1872, Sir Howard Warburton Elphinstone published a pattern design book for the lathe with both illustrations and mathematical equations describing the patterns [26]. One of his unifying principles is the use of the mathematical concept of envelopes—secondary curves or surfaces tangent to a family of curves in close proximity. Fig. 2.1.8 shows illustrations of several of the general pattern types he identified, all of which make use of envelopes of circles. In addition to pointing out the aesthetic potency of envelopes, he also makes the valuation “it will generally be found that the beauty of the pattern is much enhanced by causing the circles to touch each other exactly ...”



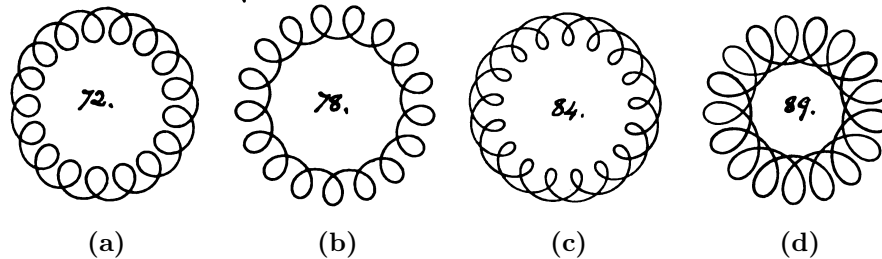
**Figure 2.1.8:** Elphinstone’s turning patterns. From left to right, Turk’s-head surrounded with basket-work, shell, star, waved ellipse, and a double counting.

An extensive catalog of geometric chuck patterns is Thomas Sebastian Bazley’s *Index to the Geometric Chuck* published in 1875 which includes 3,500 figures with parametric descriptions [11]. Fig. 2.1.9 shows some figures from the catalog that demonstrate the versatility of the geometric chuck. Bazley distinguishes both between “consecutive” and “circulating” loops and “internal” and “external” loops

(Fig. 2.1.10). A consecutive loop results when the gear velocities are in a simple integer relationship  $1 : n$  where  $n$  is an integer greater than 0. A circulating loop results when the gear velocities are in a rational relationship  $n : m$  where  $n$  and  $m$  are both integers greater than 1. The difference between internal and external loops results from whether the gears turn in the same or opposite direction, respectively.



**Figure 2.1.9:** Figures displaying the diversity of curves possible from compound circular motion of two geometric chucks.



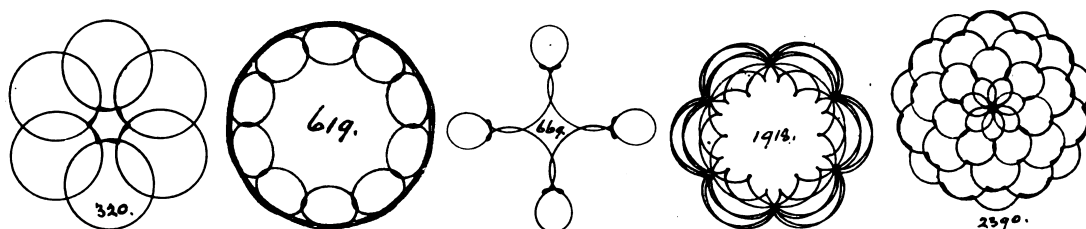
**Figure 2.1.10:** The four basic looping patterns of a single geometric chuck as described by Thomas Sebastian Bazley [11] are (a) consecutive/internal, (b) consecutive/external, (c) circulating/internal, and (d) circulating/external.

Bazley, speaking of the symmetrical qualities of more complex forms produced by compound circular motions, made an important observation about a rather curious phenomenon:

The curve, it will be remembered, is single and continuous, and, for a considerable part of its course, the several portions of which it is (so far) composed appear discordant, and to have no prospect of

forming a harmonious whole. But as the delineation proceeds, the irregular convolutions of the curve recur at such intervals as to overlap symmetrically, or to adopt such positions with reference to one another as to render the effect both complete and ornamental.

Figures displaying this overlapping symmetry are shown in Fig. 2.1.11. Bazley did not analyze this phenomenon to find any patterns in the numerical relationships that generate these types of shapes. He did, however, observe that for a single geometric chuck (two compound circular motions) when the gear amplitudes are inversely proportional to their angular velocities, then cusped forms emerge. Similarly, when the gear amplitudes are proportional to the squared inverse of their angular velocities, then rectilinear figures are produced.



**Figure 2.1.11:** Examples of unicursal figures displaying what Bazley termed “symmetrical overlap”.

One last observation of Bazley that is worth mentioning is his assessment of the aesthetic qualities of the figures:

It may be well, however, to bear in mind that consecutive loops are less susceptible of varied results than circulating, and internal loops less satisfactory than external.

While many other gear-based machines were constructed to draw or etch curves (see, for example [125]), the *Creighton Compound Harmonic Motion Machine*



designed by William Francis Rigge in 1915 is arguably the most complex and versatile of them all capable of drawing 7,618,782,498 distinct patterns [87]. Rigge describes his invention as such:

The Creighton machine will in principle draw any form of harmonic curve, for the reason that the number of its sections and the ratios of its gears may be made almost anything. It is the first machine, as far as is known, to use many components in series in both X and Y on a stationary and on a rotating disk, and on a moving ribbon.

Rigge defines a “harmonic curve” as “a planar curve parameterized independently along its basis axes as Fourier series.” Harmonic curves are classified into six curve types—sine, rectangular, rectangular-polar, sine-polar, rectangular-sine, and stereoscopic. Table 2.2 describes these six curve types.

Harmonic curve	Description
Sine	Pen moves in harmonic motion along Y while paper moves linearly along X
Rectangular	Pen moves in harmonic motion parallel to both its axes (e.g., Bowditch curve, line, ellipse, circle, parabola)
Rectangular-polar	Pen moves in rectangular curve while paper rotates (e.g., epicycloid, hypocycloid)
Sine-polar	Pen moves along one axis while paper rotates (e.g., rosette, spiral of Archimedes, envelope rosette)
Rectangular-sine	Pen moves in rectangular curve while paper drawn linearly along one axis (e.g., cycloid, progressive ellipse/line)
Stereoscopic	Two plane curves with a slight change in phase of one or more components

**Table 2.2:** Rigge’s six classes of harmonic curves.

It should be noted that the stereoscopic phasing effect did not originate with

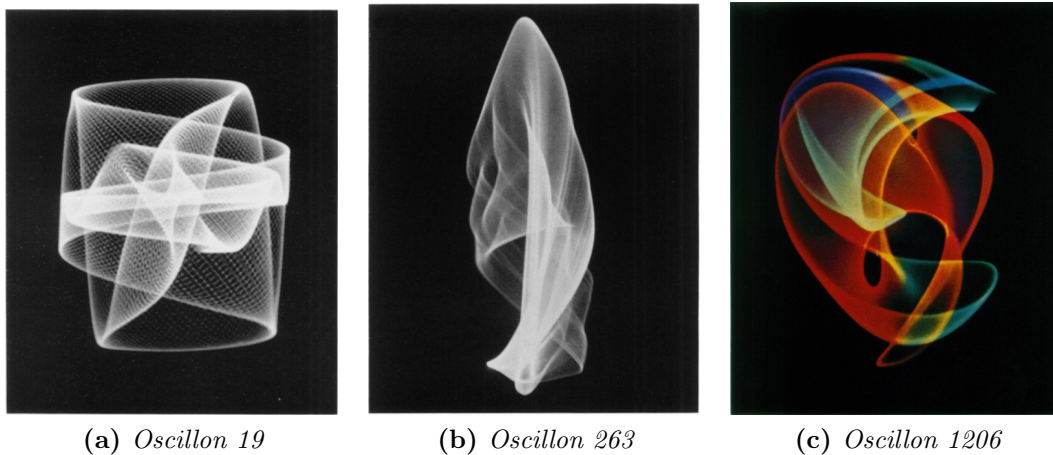
Rigge. Earlier accounts of this effect were given by S. C. Tisley in 1878 [124], Charles Slichter in 1896 [96], and Charles E. Benham in 1909 [37].

### 2.1.3 Oscillography

In the early 1950s, *oscillography* arose as a fertile new medium with the capability to produce multifarious curvilinear light forms through electronic means [29]. The art of oscillography uses waveforms produced from various electronic (audio) signal generators to directly control the two-dimensional path of a laser or oscilloscope electron beam. While many works helped establish oscillography as an expressive artistic medium (for example, *Around is Around* (Norman McClaren, 1950), *Divertissement Rococo* (Hy Hirsh, 1951), *Abstronic* (Mary Ellen Bute, 1954) [72], *Magnet TV* (Nam June Paik, 1965), and *Chromophonie* (Alexandre Vitkine, 1967)), very little has been written about the medium on a more analytical or mathematical level.

Ben Laposky thoroughly explored the artistic potential of oscillography, exhibiting thousands of images of his work around the world and publishing several articles on his theories and techniques (see [54, 55, 56]). His work is recognized as being the first major initiative in generating graphics by means of electronic machines [29]. He described his creations as *Oscillons*, “images in light composed of waveforms as they appear on the screen of a cathode ray oscilloscope” (Fig. 2.1.12). While much oscillographic art tends to be monochromatic, Laposky utilized spinning color wheels to give his Oscillon curves varying gradients (Fig. 2.1.12c). Laposky made two observations about the relationship between the sound waveforms and light images that are worth noting. First, high frequencies produce more solid appearing sheets and forms [55]. This is due to the fact that higher-frequency

components in a waveform will create more vibratory motion in the same interval of time. Second, he states [55] (regarding the forms) “Some have mathematical precision, others are free-flowing in their curvatures and symmetries.” This distinction largely stems from the ability to move continuously between simple waveforms with few harmonics (Fig. 2.1.12a) and more complex waveforms with many harmonics (Fig. 2.1.12b). Laposky notes that the use of electronics allows a wider variety of forms than are possible through mechanical devices, such as pendulums [55]. This, again, can be attributed to the increased control over the harmonic content of the driving waveforms.



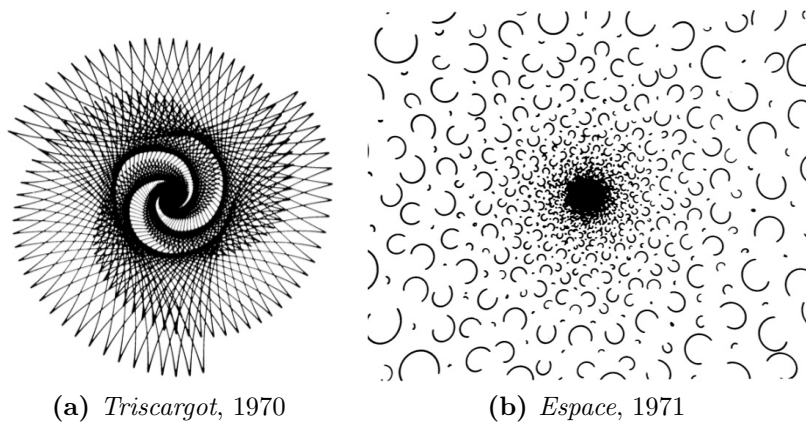
**Figure 2.1.12:** Some of Ben Laposky’s *Oscillon* series of photographs. Images © 1952-1960, Sanford Museum, Cherokee, Iowa.

Herbert Franke also made use of the oscilloscope as an artistic medium around the same time as Laposky. In his description [29] of the forms produced “These configurations are not usually produced as still pictures but as events; the graphic is a phase picture of such an event.” In other words, the figures on the oscilloscope display the accumulation of the temporal motion through space of the electron beam. This is the same notion as the “line of light” produced by vibrating mechanical devices as articulated earlier by Young, Wheatstone, and Lissajous. The advantage

of the cathode ray tube over the earlier mechanical devices is that the phosphor screen extends the time over which events can be captured, thus allowing otherwise fleeting events to be observed.

Alexandre Vitkine analyzed in more mathematical detail the relationships between the waveforms and visual results in his oscilloscope art [110]. In his work *Triscargot* (Fig. 2.1.13a), he constructs a slowly rotating triangle by adding together two quadrature signals at 100 Hz and 51 Hz. (In signal processing, a quadrature signal is a two-component signal comprised of a sine and cosine.) While never stated explicitly, we can assume the refresh rate of the television he was using to produce his forms was 50 Hz, a common frequency used for household alternating current. With this in mind, a 100 Hz waveform will complete exactly two cycles per display refresh and appear stable on the screen. The slow movement of the form was the result of an additional 1 Hz added to a 50 Hz frequency. This detuning reveals an important relationship between the spatial stability and temporal motion of a waveform displayed on an oscilloscope or similar device. If the waveform period is an exact integer multiple of the display's period, then the figure will appear static, otherwise, the figure will appear in motion. The further away from integer multiples, the more animated the figure will be. In his work *Espace* (Fig. 2.1.13b), Vitkine employs several other mathematical relationships to obtain specific visual results. Initially, two signals, one with low frequency and high amplitude (signal A) and the other with high frequency and low amplitude (signal B), are combined. The two signals alone draw only circles, but when combined show an emergent hypocycloid structure breaking the symmetry of the original forms. Next, signal C at 0.4 times the frequency of A modulates B changing the diameter of the smaller circles. Signal D slowly decreases and is multiplied by A and B to create an inward falling spiral. Finally, a periodic digital signal with  $3/4$

the frequency of B abruptly switches the signal on and off to produce a sequence of isolated curls. This technique of mixing digital signals with analog signals is important since it allows spatially separated objects to be produced from the same signal. A very similar technique was developed by Wheatstone to produce multiple images, but instead of superposing a digital signal, he superposed a more rapid vibration, effectively interleaving the image into multiple points in space.



**Figure 2.1.13:** Images of Alexandre Vitkine’s oscilloscope work.

Oscillography introduced a new level of complexity to artificially-generated patterns brought forth through the use of controlled electronic signals. The use of more complex waveforms—those having a rich set of harmonics—led to more complex and organic patterns. In addition, it was discovered that certain qualities of the patterns depended in precise ways on the harmonic content of the signals used. For example, sinusoidal waveforms produce rounded patterns and stepped waveforms produce independent visual components.

## Conclusion

While the mechanical devices mentioned can produce a wide variety of forms through simple means, their patterns are easily recognized due to the use of a limited number of harmonics; a fact that can be attributed to the difficulty in constructing such machines. Creating more complex patterns required more complex machines. In addition, one has limited control over the rate at which patterns are produced. Oscillating devices that react to vibrations produce curves that are often fleeting due to friction and inharmonicity of the system. Other devices, such as pendulums and gear systems, can require an extended amount of time to create a pattern of sufficient complexity (although in some sense, this can be considered an asset).

Oscillography subsumed many of the capabilities of its mechanical predecessors with the additional benefits of producing patterns more rapidly and with more mathematical generality. However, like its mechanical predecessors, recreating the same patterns on an oscilloscope was not always possible due to the inherent non-linearities and other complexities of the electronic circuitry involved.

As harmonic pattern producing devices progressed from simple oscillating devices, to mechanical gears systems, to electronic oscillography, the degree of mathematical abstraction underlying the systems increased along with the ability to control their parameters. In this way, the machines came closer to the ideal of a *universal* pattern generator. As the next step in this evolution, computers and digital systems brought forth a way to realize even more abstract mathematical constructs leading to almost entirely open-ended systems.

## 2.2 Digital Systems

Computers bring forth the ability to work directly with discrete mathematics thereby offering a much higher degree of numerical control than possible with either mechanical or electronic devices. This additional precision permits mathematical structures to be represented and transformed in a more exact manner. Another important trait unique to computers is their ability to store, recall, and process information with unprecedented speed and precision. With this comes the ability to convert signals of sounds and images between analog and digital forms and perform *digital signal processing*. The ability to generate or process an abstract signal that can later be converted to sound or graphics opens up the possibility of developing a unified audio/visual synthesis language. While many possible languages could be proposed, it is likely that one based on harmonic superposition will prove fruitful due to its past success within the gamut of mechanical and electronic devices discussed above and its position as a fundamental principle of modern digital systems. This goal of this section is to highlight developments in audio, visual and combined audio/visual digital systems pertaining to the construction of patterns through harmonics.

### 2.2.1 Early Sound Synthesis Languages

In the field of computer music, many synthesis techniques have been developed in order to produce sounds entirely abstract in character or that emulate acoustic instruments. The major techniques are discussed comprehensively [88, 24, 68] and surveyed [70] elsewhere. Generally speaking, the primary goal in sound synthesis is to generate sounds with a quality that match the richness and subtlety of naturally occurring sounds. Sound synthesis techniques are based almost entirely

on the manipulation of real-valued signals through mathematical models and signal networks. Three of the major synthesis paradigms are additive synthesis, subtractive synthesis, and what could most generally be called mapping synthesis. Additive synthesis is algorithmically the simplest involving the summation of two or more (periodic) waveforms to create a more complex waveform. Subtractive synthesis involves filtering the spectral content of a richly harmonic source waveform to produce a new timbre. Mapping synthesis is related to the mathematical operation of function composition—mapping the output of one function into the input of a second function to produce a new function. In sound synthesis parlance, mapping synthesis involves either passing a waveform through a mathematical function (e.g., waveshaping and amplitude modulation) or using a waveform to control the phase or frequency of another oscillator (e.g., wavetable synthesis and phase/frequency modulation).

In the early 1960s, Max Mathews created an *acoustic compiler* that allowed one to program a computer to generate musical sounds [64]. This first compiler evolved into a series of programs called MUSIC I-V that provided mechanisms for synthesizing sounds and sequencing them into musical passages. From Mathews' perspective, creating sounds on a computer is best accomplished in a manner in between specifying each individual sample and triggering recorded sounds with note numbers [63]. His idea was to use encapsulated functions called *unit-generators*, a concept influenced by the signal data flow model used in analog circuit design. The power of unit-generators is less about their individual functions, but their ability to be used as nodes in a signal flow graph allowing a variety of custom *instruments* to be constructed. MUSIC I included only four types of unit generators: G1, a digital-to-analog output unit, G2, a periodic function generator, G3, G4, and G5, adders, and RAND, a random signal generator. MUSIC V, the last compiler of



the series, only added a few more unit generators to the initial set including FLT, a two-pole band-pass filter, ENV, a three-segment envelope generator, and various generators for constructing stored functions. The entire MUSIC V unit generator set is listed in Table 2.3.

Unit Generator	Description
AD2	Two-input adder
AD2	Three-input adder
AD4	Four-input adder
MLT	Two-input multiplier
OSC	Periodic function generator
RAN	Low-pass random function generator
ENV	Three-segment envelope generator
FLT	Two-pole band-pass filter
GEN1	Creates stored function from line segments
GEN2	Creates stored function from a sum of sinusoids
GEN3	Creates stored function from a list of relative amplitudes
OUT	Outputs samples to digital-to-analog convertor

**Table 2.3:** The complete set of MUSIC V unit-generators.

MUSIC V contained the minimal components for executing additive, subtractive, and mapping synthesis. The MUSIC V language was so successful, that practically all synthesis languages made after it followed its same design (thus are deemed *MUSIC N* languages [62]). Aside from the unit-generator concept, the reason MUSIC V was an effective synthesis language was that it was based largely on simple, yet powerful time-tested mathematical concepts, algebra and mapping, applied to sound waveforms.

## 2.2.2 Sound Synthesis From Series Formulae

One of the oldest forms of sound synthesis is additive synthesis, the direct summation of multiple base waveforms, usually pure tones, in order to create a more complex waveform. While the mathematical idea of additive synthesis can be traced to the work of Fourier in 1878 [28], musically, it dates back as far as 200 B.C. with the invention of the Hydraulis organ by Ctesibius of Alexandria. While conceptually simple, the central problems with additive synthesis techniques are the sheer number of parameters that must be specified to create sounds of sufficient richness and the mechanical or computational complexity required for adding together hundreds of sine waves each possibly having its own independent amplitude and/or frequency envelope.

Discrete summation formula (DSF) synthesis [69] is an efficient method of producing many harmonics in mathematically precise ways using very few oscillators. A DSF is a rational function of a small number of harmonics that generates a particular class of trigonometric series of either an infinite or variable number of harmonics. The simplest DSF produces a spectrum with harmonic magnitudes obeying an infinite geometric progression (Eq. 2.2.1) [24]. By adding an additional harmonic to the numerator, it is possible to realize frequency shifts (Eq. 2.2.2) [69]. A more complicated type of DSF permits control over the highest harmonic present in the spectrum (Eq. 2.2.3) [69]. By setting  $a = 1$  and  $\beta = \pi/2$  in Eq. 2.2.3 and simplifying, one obtains a DSF for a band-limited impulse train (BLIT) (Eq. 2.2.4) [129, 24]. Through additional integration and addition of BLITs, band-limited saw, square, pulse, and triangle waves can be constructed [100]. There are also compact

DSFs for direct synthesis of odd harmonic series (Eq. 2.2.5 and Eq. 2.2.6) [51].

$$\sum_{k=1}^{\infty} a^{k-1} \sin(k\theta) = \frac{\sin \theta}{1 + a^2 - 2a \cos \theta} \quad (2.2.1)$$

$$\sum_{k=0}^{\infty} a^k \sin(k\theta + \beta) = \frac{\sin \beta - a \sin(\beta - \theta)}{1 + a^2 - 2a \cos \theta} \quad (2.2.2)$$

$$\sum_{k=0}^N a^k \sin(k\theta + \beta) = \frac{\sin \beta - a \sin(\beta - \theta) - a^{N+1} [\sin((N+1)\theta + \beta) - a \sin(N\theta + \beta)]}{1 + a^2 - 2a \cos \theta} \quad (2.2.3)$$

$$\frac{1}{N} \sum_{k=1}^N \cos(k\theta) = \frac{1}{2N} \left( \frac{\sin[(2N+1)(\theta/2)]}{\sin(\theta/2)} - 1 \right) \quad (2.2.4)$$

$$\sum_{k=1}^N \cos(2k-1)\theta = \frac{\sin 2N\theta}{2 \sin \theta} \quad (2.2.5)$$

$$\sum_{k=1}^N \sin(2k-1)\theta = \frac{\sin^2 N\theta}{\sin \theta} \quad (2.2.6)$$

The infinite harmonic DSF can be written more compactly as a rational function of complex sinusoids (Eq. 2.2.7) [76]. In this form, the DSF produces two waveforms whose corresponding harmonics differ in phase by  $90^\circ$ . By substituting  $e^{i\theta} = \cos \theta + i \sin \theta$  into Eq. 2.2.7 and “simplifying” (Eq. 2.2.8), we see that its imaginary component is identical to Eq. 2.2.1.

$$\sum_{k=1}^{\infty} a^{k-1} e^{ik\theta} = \frac{e^{i\theta}}{1 - ae^{i\theta}} \quad (2.2.7)$$

$$= \frac{(\cos \theta - a) + i \sin \theta}{1 + a^2 - 2a \cos \theta} \quad (2.2.8)$$

It is also possible to write the finite harmonic DSF in terms a complex rational function using the closed-form expression of a geometric series [100].

$$\sum_{k=0}^{N-1} a^k e^{ik\theta} = \frac{1 - (ae^{i\theta})^N}{1 - ae^{i\theta}}$$

The advantage of formulating DSFs in terms of complex numbers is not only that they become more compact and simpler to analyze, but also that any of them can be frequency shifted by a simple multiplication with a complex sinusoid. In fact, representing any sound through complex numbers permits ideal (single-sideband) frequency shifting to become an basic type of sound transformation. This is in opposition to sounds represented as real numbers, where frequency shifting can only be approximated with a Hilbert filter or a combination of amplitude modulation and high-order filtering [14]. By developing a slightly more abstract notion of sound as a complex-valued signal, then we obtain not only a more powerful and self-consistent framework for processing sound, but also a more powerful geometric representation that can be used directly for visual synthesis.

### 2.2.3 Early Vector Graphics Languages

Many of the early computer graphics languages were based on the notion of a programmable pen that could be moved from one point to another and raised and lowered in relation to a drawing canvas. This approach, from a more mathematical perspective, is known as vector graphics. The earliest programming language developed for computer graphics was a set of drawing functions built directly in ALGOL by Georg Nees called G1, G2, and G3 [75]. The first iteration, G1, provided only four main commands: OPEN, CLOSE, LEER (blank), and LINE. The function OPEN(A, B) opened a local coordinate system at global coordinates

(A, B) while CLOSE would close the active local coordinate system. The function LEER(U, V) moved the pen to point (U, V) without drawing while LINE(U, V) drew a line from the current pen location to point (U, V). The second iteration, G2, added several random number generators, Jn, where ‘n’ indicated the generator ID. The generators operated through the simple recursive equation  $x_{n+1} = cx_n \bmod 128$  producing a pseudo-random sequence of integers in the interval  $[0, 128)$ . The last iteration in the series, G3, added the functions ZIRK (circle), REC (rectangle), and SCHWARM (swarm). ZIRC(M, N, R, P, Q) drew a circle of radius R centered at (M, N) starting at the the point (P, Q) lying on the circle. REC(D, E, F, G, S) drew a rectangle enclosed by the abscissas D and E and ordinates F and G. SCHWARM(D, E, F, G, U, V, N, P) was a function permitting a single figure to be drawn many times with variations in size and position. The argument P is the drawing routine defining the figure and N is the number of times it is called. The arguments D, E, F, and G define an enclosing frame (similar to REC) and U and V specify a scaling interval. SCHWARM is an early example of how symmetry is used in computer graphics to construct more complex scenes by duplicating objects in space.

While many of the early computer graphics systems were based strongly on mathematical constructs, later systems began to incorporate more interactive control leading to “paint systems” where graphical elements could be drawn directly to computer memory (i.e., the screen) [22, 103, 104]. Modern computer graphics systems generally combine programmatic and interactive control. Another conceptual thread in early computer graphics related to the notion of a programmable pen is *turtle graphics*. Turtle graphics continues to evolve in the domains of logic and mathematics and thus plays a more direct role in defining a common language between sound and graphics. Turtle geometry provides a concrete mechanism for

generating sequences of points or discrete curves therefore uniting the synthesis of visual patterns and sound waveforms.

### 2.2.4 Turtle Graphics

Turtle graphics is based on the notion of a drawing agent that, at the simplest level, can be commanded to move forward, rotate, and raise or lower its pen. The original idea of the turtle came largely from the work of William Grey Walter in the early 1950s who built simple robot vehicles equipped with various sensors in order to autonomously navigate their environment [112, 113, 31]. Since the robots would often bump into obstacles, they were built with a protective “shell” resembling that of a turtle. In the 1960s, Seymour Papert added turtle graphics to the Logo programming language which was based on William Grey Walter’s robots but now equipped with a retractable pen that could draw its path on the screen [3].

The four basic turtle commands (move, rotate, raise/lower pen) in conjunction with a programming language that permits procedures and iteration, allows complex forms to be generated from simple algorithms. The uniqueness of turtle geometry over other geometric systems, such as Cartesian or polar coordinates, lies in the fact that it is *intrinsic* (properties do not depend on external frame of reference) rather than *extrinsic* (properties depend on a fixed frame of reference) [3]. A square, for example, can be described intrinsically as a series of relative motion commands as

```
void drawSquare() {  
    forward(1); right(90);  
    forward(1); right(90);
```

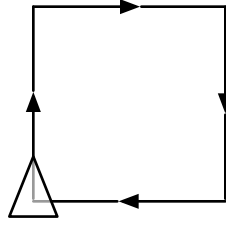
```
forward(1); right(90);  
forward(1); right(90);  
}
```

or extrinsically as a series of absolute coordinate settings as

```
void drawSquare() {  
    position(0,0);  
    position(0,1);  
    position(1,1);  
    position(1,0);  
    position(0,0);  
}
```

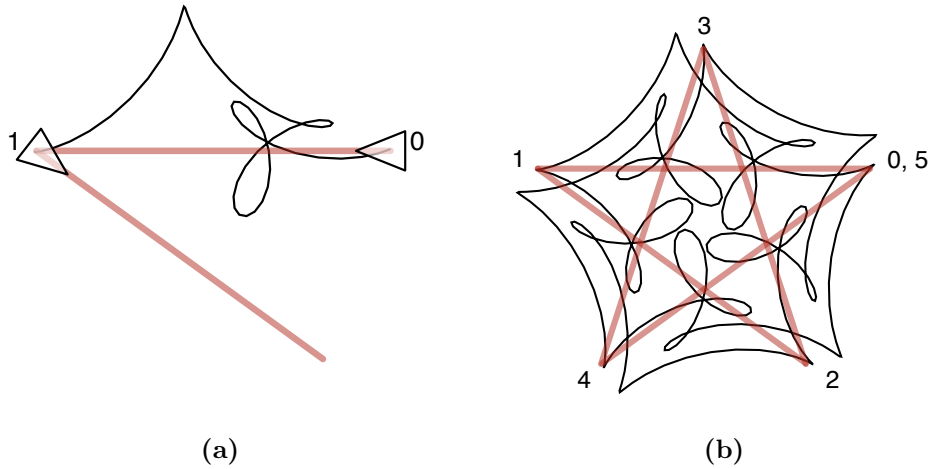
Intrinsic geometry depends on having an object that can remember its state. Each time the turtle is commanded to move forward or turn it is relative to its current position and orientation. In this way, the turtle's path is an accumulation of angular and linear differential quantities. Extrinsic geometry, on the other hand, is a memoryless description of shape. A shape is described in terms of absolute coordinates of some global space. Both intrinsic and extrinsic turtle routines can be viewed in terms of complex numbers. An intrinsic turtle routine is the integration of a sequence of complex numbers given in polar form. An extrinsic turtle routine is simply a sequence of complex numbers in Cartesian form.

An important insight of turtle graphics is that any recursive composition of drawing routines has the underlying structure of a regular star polygon [3]. All drawing routines can be thought of as black-box algorithms that ignore the actual path the turtle takes and simply change its position and orientation (Fig. 2.2.2a).



**Figure 2.2.1:** Path taken by a turtle following the `drawSquare` function.

If the same drawing routine is applied recursively, then the result is a (part of a) regular star polygon with some arbitrary path connecting the vertices (Fig. 2.2.2b).



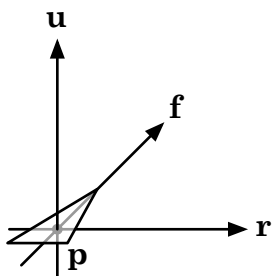
**Figure 2.2.2:** The recursive application of any (a) turtle drawing routine has (b) the skeletal structure of a regular star polygon.

Turtle geometry was originally devised in two-dimensional Euclidean space, but has been extended to three-dimensional Euclidean space,  $\mathbf{R}^3$ , and the surface of a sphere,  $\mathbf{S}^2$  [3]. An essential component of a three-dimensional turtle is an orthonormal reference frame. The operations of motion are rotations around and translations along the axes of the reference frame.

A reference frame in  $\mathbf{R}$  is comprised of three unit vectors  $\mathbf{f}$ ,  $\mathbf{u}$ , and  $\mathbf{r}$  that specify the relative forward, up, and right directions, respectively, of the turtle in absolute coordinates. An  $\mathbf{R}^2$  turtle is a special case of an  $\mathbf{R}^3$  turtle restricted to



rotations around its up vector and translations along its forward and right vectors.



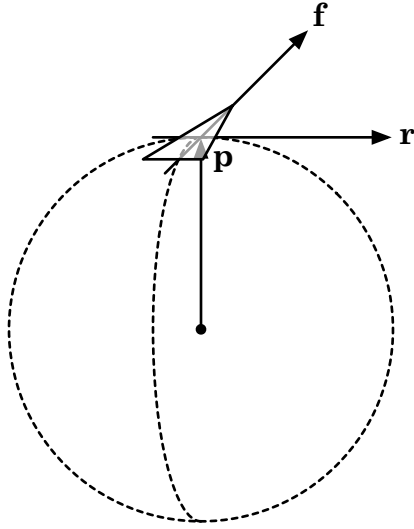
**Figure 2.2.3:** Turtle reference frame in  $\mathbf{R}^2$  and  $\mathbf{R}^3$ .

Forward movement and rotations in  $\mathbf{R}^3$  are accomplished with the functions

$$\begin{aligned}
 \textit{forward}(d) &= \mathbf{p} + d\mathbf{f} \\
 \textit{yaw}(a) &= \begin{cases} \mathbf{r}' = \cos(a)\mathbf{r} + \sin(a)\mathbf{f} \\ \mathbf{f}' = \cos(a)\mathbf{f} - \sin(a)\mathbf{r} \end{cases} \\
 \textit{pitch}(a) &= \begin{cases} \mathbf{f}' = \cos(a)\mathbf{f} + \sin(a)\mathbf{u} \\ \mathbf{u}' = \cos(a)\mathbf{u} - \sin(a)\mathbf{f} \end{cases} \\
 \textit{roll}(a) &= \begin{cases} \mathbf{u}' = \cos(a)\mathbf{u} + \sin(a)\mathbf{r} \\ \mathbf{r}' = \cos(a)\mathbf{r} - \sin(a)\mathbf{u} \end{cases}
 \end{aligned}$$

where  $d$  is the amount to translate forward and  $a$  is the turn amount in radians.

Turtle motions on the surface of a sphere are conceptually similar to those on a two-dimensional plane (move forward, rotate left/right), however, the underlying mathematics are quite different since the space is curved rather than flat. A spherical turtle has a set of three orthonormal vectors  $\mathbf{p}$ ,  $\mathbf{f}$ , and  $\mathbf{r}$  that represent its position and its forward and right directions, respectively.



**Figure 2.2.4:** Turtle on  $S^2$ .

The equations of motion of a spherical turtle are

$$\begin{aligned} \textit{forward}(a) &= \begin{cases} \mathbf{p}' = \cos(a)\mathbf{p} + \sin(a)\mathbf{f} \\ \mathbf{f}' = \cos(a)\mathbf{f} - \sin(a)\mathbf{p} \end{cases} \\ \textit{right}(a) &= \begin{cases} \mathbf{f}' = \cos(a)\mathbf{f} + \sin(a)\mathbf{r} \\ \mathbf{r}' = \cos(a)\mathbf{r} - \sin(a)\mathbf{f} \end{cases} \end{aligned}$$

where  $a$  is the turn amount in radians. An  $S^2$  turtle is a special case of an  $\mathbf{R}^3$  turtle that is restricted to rotations around the right and up vectors and whose position is its up vector.

### 2.2.5 Parametric Equations

A parametric equation defines a function using a specific set of parameters. They provide an economical means for describing higher-dimensional shapes using less dimensions and allow one to control a shape's global properties [10, 30, 49]. Parametric equations can be used to generate Cartesian coordinates of curves and

surfaces. For example, a helix can be defined in terms of one parameter,  $t$ , using the parametric equation

$$helix(t) = \begin{cases} x(t) = \cos(bt) \\ y(t) = \sin(bt) \\ z(t) = t \end{cases} \quad t \in [0, 2\pi) .$$

A spherical surface can be defined using two parameters,  $u$  and  $v$ , with the equation

$$sphere(u, v) = \begin{cases} x(u, v) = \sin(v) \cos(u) \\ y(u, v) = \sin(v) \sin(u) \\ z(u, v) = \cos(v) \end{cases} \quad u, v \in [0, 2\pi) .$$

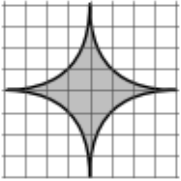
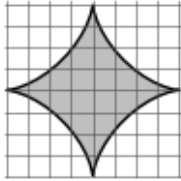
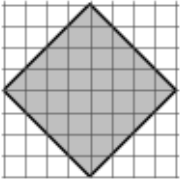
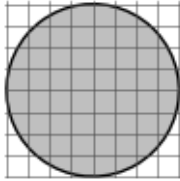
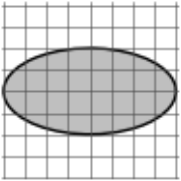
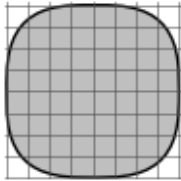
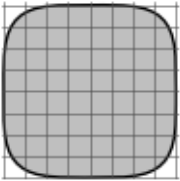
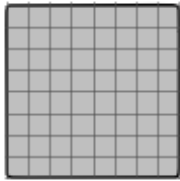
The general category of *supershapes* involve mapping trigonometric functions onto coordinates in Cartesian or spherical space. Supershapes are described either implicitly as an algebraic equation or explicitly as a set of parametric equations.

A superellipse or Lamé curve is a generalization of an ellipse formulated by Gabriel Lamé in 1818 [98]. Its mathematical description is an implicit function with a parameter  $n$  that controls its curvature and parameters  $a$  and  $b$  that control its scaling factors in the  $x$  and  $y$  directions, respectively. The superellipse is derived from a series of generalizations of the implicit equation of a circle (Table 2.4).

Table 2.5 shows a selection of other shapes that the superellipse subsumes.

Name	Implicit Equation
Circle	$ x ^2 +  y ^2 = 1$
Ellipse	$ \frac{x}{a} ^2 +  \frac{y}{b} ^2 = 1$
Superellipse	$ \frac{x}{a} ^n +  \frac{y}{b} ^n = 1$

**Table 2.4:** Equations for the circle, ellipse, and superellipse

			
parabolic diamond $n = \frac{1}{2}, a = b$	astroid $n = \frac{2}{3}, a = b$	diamond $n = 1, a = b$	circle $n = 2, a = b$
			
ellipse $n = 2, a \neq b$	witch of Agnesi $n = 3, a = b$	“squiracle” $n = 4, a \neq b$	square $n = \infty, a = b$

**Table 2.5:** Special superellipse shapes based on the implicit equation  $|\frac{x}{a}|^n + |\frac{y}{b}|^n = 1$ . The gridlines are positioned at integer multiples of  $\frac{1}{4}$ .

The superellipse can also be described parametrically as

$$x(\theta) = a \operatorname{sgn}(\cos \theta) |\cos \theta|^{2/n}$$

$$y(\theta) = b \operatorname{sgn}(\sin \theta) |\sin \theta|^{2/n}$$

revealing its close relationship to trigonometric functions:

The shapes derived from the superellipse formula suffer from one major shortcoming—they can only express a limited range of symmetry groups,  $D_2$ ,  $D_4$ ,  $D_\infty$ , and  $C_\infty$ . Any shape constructed through the additive mixture or Cartesian product

of superellipses will reflect these symmetry limitations.

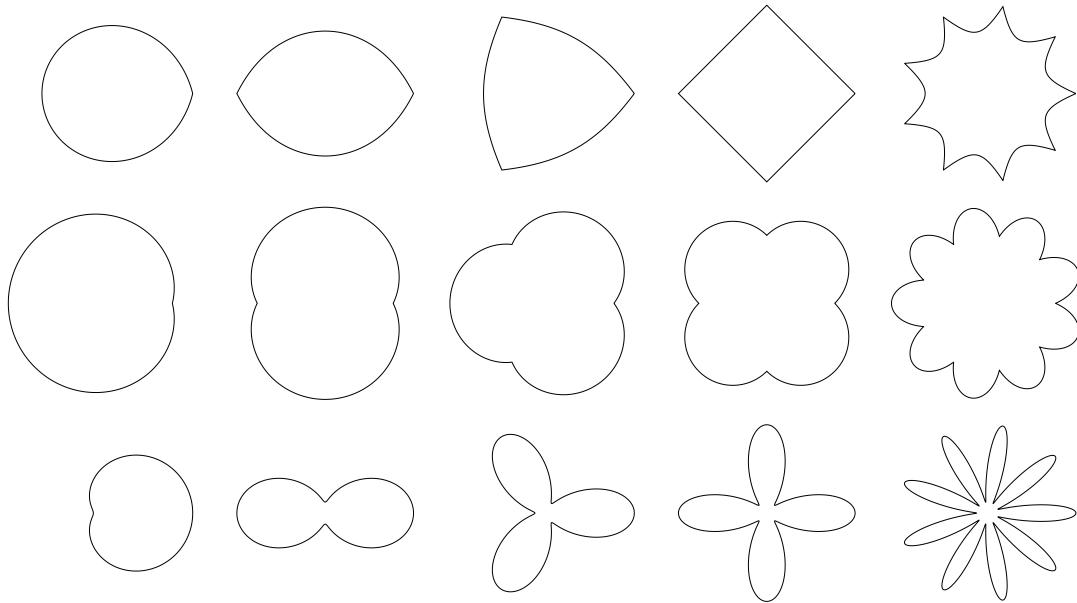
Johan Gielis' *Superformula* further generalizes the superellipse to express all cyclic and dihedral symmetry groups [33]. It can produce a wide variety of shapes that resemble plant stem cross-sections, diatoms, starfish, shells, flowers, and abstract geometric shapes [32]. Gielis points out several advantages of the Superformula over other techniques:

- describes a wide variety of geometrical shapes found in nature and culture through one simple expression
- precisely represents symmetry and individual characteristics of shapes
- permits easy calculation of associated measurements such as perimeter, curvature, and area
- allows natural variation in shapes
- derived from existing basic mathematics

The Superformula equation is given in polar coordinates as

$$r = \left( \left| \frac{1}{a} \cos \left( \frac{m}{4} \phi \right) \right|^{n_2} + \left| \frac{1}{b} \sin \left( \frac{m}{4} \phi \right) \right|^{n_3} \right)^{-\frac{1}{n_1}}.$$

The Superformula's use of polar coordinates rather than Cartesian coordinates is key to its ability to generate curves with arbitrary cyclical symmetry. The variable  $m$  determines the cyclical symmetry of the shape. The values  $n_2$  and  $n_3$  determine whether the shape inscribes ( $|n_d| < 2$ ) or circumscribes ( $|n_d| > 2$ ) the unit circle. Other parameters control the sharpness of corners and straightness of sides. A selection of Superformula shapes are presented in Fig. 2.2.5.



**Figure 2.2.5:** Superformula shapes. The symmetry parameter  $m$  is 1, 2, 3, 4, and 9 going from the left column to the right column. The top row shows inscribed shapes using the parameters  $a = b = n_1 = n_2 = n_3 = 1$ . The middle row show circumscribed shapes using the parameters  $a = b = n_2 = n_3 = 1$  and  $n_1 = -1$ . The bottom shows lobed shapes made using the parameters  $a = b = 1$ ,  $n_2 = n_3 = 8$ , and  $n_1 = -1$ .

Gielis discusses several ways in which the Superformula can be extended to construct more complex shapes [33]. First of all, the Superformula equation can be multiplied by another function  $f(\phi)$  to form the Generalized Superellipse Equation. The function  $f(\phi)$  is a general function that provides further control over the shape’s form. If  $f(\phi) = 1 + g(\phi)$ , then the Superformula base curve can be modulated by the function  $g(\phi)$ . Logarithmic and Archimedean spiral shapes can be constructed by using  $f(\phi) = e^{-c\phi}$  and  $f(\phi) = \max(1 - c\phi, 0)$ , respectively. A second method is to apply polynomial functions of the angle  $\phi$  to the variables. This allows the rotational symmetry of the shapes to be broken. Finally, Superformula shapes can be combined with others through addition and multiplication and Boolean operations. The shapes generated by the Superformula can be interpreted as “atomic” shapes from which more complex and higher-dimensional forms can be

constructed [32]. In a very simple manner, shapes can be summed together similar to the way that Fourier series are used to construct arbitrary functions from a summation of simpler sinusoidal functions.

In summary, mathematically described supershapes have the ability to express a wide range of forms and symmetry groups through very few parameters. Forms constructed through implicit equations in Cartesian coordinates have limited degrees of symmetry. To alleviate this problem, polar coordinates can be used instead. However, the deeper problem with parametric equations is that they are too specialized algorithmically resulting in a limited range of forms for any given equation. This often results in a number of different parametric equations needing to be used in order to obtain a sufficient variety of distinct shapes. It would be desirable to work with a mathematical construct that is more complete in the sense that it permits a wide variety of different forms and a fluid continuum between them. Synthesis techniques based entirely on Fourier series offer one possible solution.

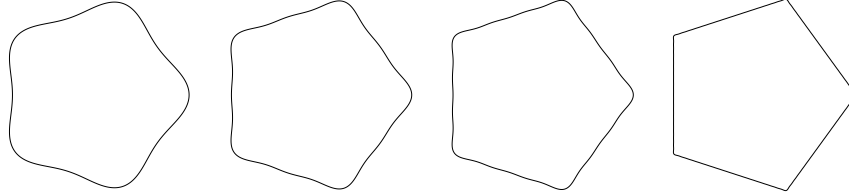
### 2.2.6 Graphical Shapes From Fourier Series

Just as a sum of sine waves can describe a sound waveform, complex Fourier series can be used to describe two-dimensional curves directly as a continuous path or as a discrete sequence of vertices. Regular star  $n$ -gons with Schläfli symbol  $\{n/a\}$  have a very simple Fourier series representation given by

$$f_n(t) = \sum_k \frac{1}{k^2} e^{ikt} \tag{2.2.9}$$

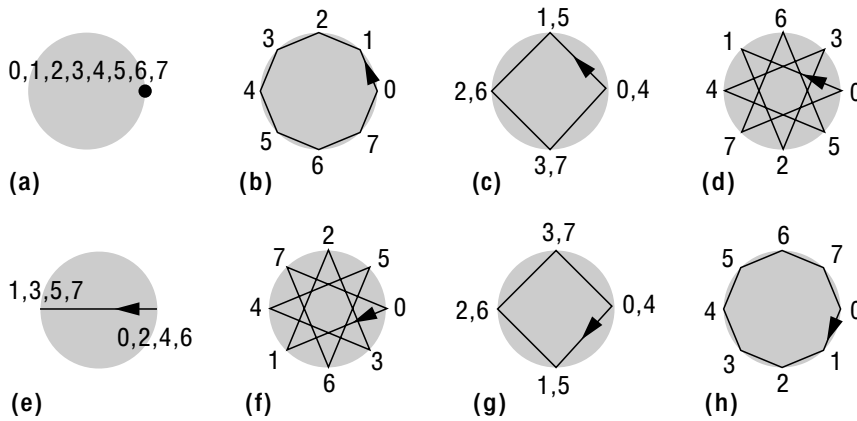
where  $k = -\infty, \dots, a - 2n, a - n, a, a + n, a + 2n, \dots, \infty$  [89]. Eq. 2.2.9 describes a regular star  $n$ -gon as a set of linear functions rather than a sequence of vertices.

This means that each side of the polygon has a constant speed. The sharpness of the corners increases as more harmonic components are used (Fig. 2.2.6).



**Figure 2.2.6:** Partial sums of the Fourier series of a pentagon given by Eq. 2.2.9 for  $n = 5$  and  $a = 1$ . The number of harmonic components in each figure (pictured left to right) is 3, 5, 7, and 33.

The basis functions of the discrete Fourier transform form the vertices of regular polygons in the complex plane and as a consequence of this, any  $N$ -sided polygon may be described as a weighted sum of  $N$  regular polygons (some of which are degenerate) [35]. The basis functions of an 8-point discrete Fourier transform are shown in Fig. 2.2.7.



**Figure 2.2.7:** The basis functions (complex sinusoids) of an 8-point discrete Fourier transform form polygons in the complex plane if we connect successive samples with lines. The complex sinusoids are ordered by increasing harmonic number from (a) 0 to (h) 7. Figure reprinted from Glassner [35], © 1999 IEEE.

Two-dimensional curves can also be described with Fourier series in a somewhat less direct manner. In pattern recognition, Fourier descriptors, the Fourier

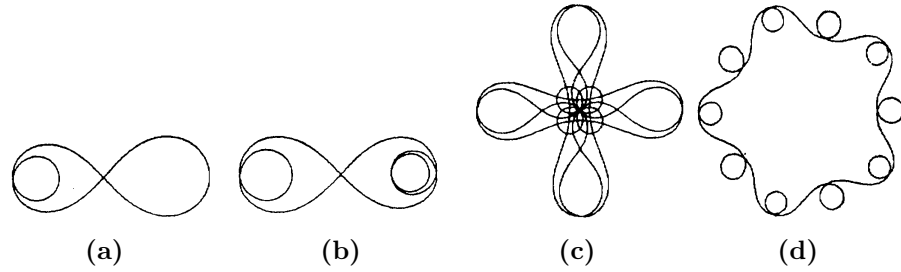


components of a planar curve’s tangent angle as a function of arc length [19], are commonly used to analyze the outlines of shapes. Synthesizing a curve from its Fourier descriptors can be accomplished through a sequence of move/turn turtle commands (2.2.4) where the move amount is a constant and the turn amount is determined by the sequence of tangent angles reconstructed from the Fourier descriptors. Zahn and Roskies discuss several mathematical relationships between a curve’s Fourier descriptors and its geometry, including its rotational symmetry and closure [134]. The mathematical equation for curve reconstruction from Fourier descriptors is given as

$$\phi^*(t) = \mu_0 + \sum_{k=1}^{\infty} A_k \cos(kt - \alpha_k)$$

where  $\phi^*(t)$  is the normalized cumulative angle function with domain  $t \in [0, 2\pi]$  and  $A_k$  and  $\alpha_k$  are the harmonic amplitude and phase of the  $k^{th}$  Fourier descriptor. A curve has  $n$ -fold rotational symmetry only when the  $(nk)^{th}$  coefficients have non-zero amplitude where  $k = 0$  is a circle. Zahn and Roskies also show that fairly complex curves can be generated from only a few Fourier descriptors (Fig. 2.2.8) [134]. A major disadvantage of using Fourier descriptors for shape synthesis is that rotationally asymmetric curves have rather complicated closing criteria based on Bessel functions leading to use of non-intuitive values of the amplitude parameter,  $A_k$  (Fig. 2.2.8a and Fig. 2.2.8b).

Harmonograms [17] are produced using the same equation given by Zahn and Roskies, however, the Fourier descriptors used to generate curves are given as compact *formal descriptors*—an ASCII string, a harmonic spacing amount, and a global scaling factor. Each character in the string corresponds to an amplitude value of a Fourier descriptor. Undersampling is used as an additional control over



**Figure 2.2.8:** Shapes produced from Fourier descriptors (a)  $A_1 = 3.83171$ , (b)  $A_1 = 7.01559$ , (c)  $A_4 = 3.0, \alpha_4 = \pi/2, A_8 = 2.0, \alpha_8 = 3\pi/2$ , (d)  $A_5 = 4.0$ . Images reprinted from Zahn and Roskies [134], © 1972 IEEE.

the complexity of the curve.

## 2.2.7 Graphical Shapes From Sound

Another approach to shape synthesis is to use digital sound synthesis techniques to produce signals acting as sequences of points. The points can then be plotted directly or connected with lines or surfaces to make geometric forms in space. This general procedure is simply a discrete version of oscillography and thus follows many of the same principles.

One method is to take an audio signal and plot it against delayed versions of itself. Monro and Pressing have examined the use of the mathematical technique of *embedding* to visualize sounds [67]. Embedding works by taking a one-dimensional sequence and forming a new sequence of  $m$ -tuples whose components are  $m$  evenly-delayed (lagged) versions of the original sequence. Monro and Pressing analyze properties of two-dimensional embedded signals from several common types of sounds. White noise results in a uniformly filled square plot and Gaussian noise gives a plot with circular symmetry. For periodic signals, a lag of one-fourth the period creates the most well-distributed plots. A triangle wave produces a square and a square wave creates four points on the vertices of a square. A single harmonic

will produce circles, ellipses, and lines depending on the lag time, as has been noted many times before by others. A signal comprised of the first and  $n^{\text{th}}$  harmonics creates either exact or skewed symmetric figures when the lag time is an integer multiple of  $1/(n \pm 1)$  times the fundamental period. Monro and Pressing also point out that all embedded signals share an important mathematical property given by Takens' embedding theorem. This theorem states that specific properties of an  $M$ -dimensional signal, such as its complexity, may be determined by embedding any one dimension of the signal at most  $2M + 1$  times. This can be interpreted to mean that certain global properties of dynamic systems are encoded in each independent dimension. Embedding has also been utilized to visualize the effects of products of amplitude- and frequency-modulated signals [92, 94, 93].

Andrew Glassner developed a model for synthesizing three-dimensional shapes based on the operating principles of analog modular sound synthesizers [34]. Rather than a flow of voltages, the fundamental data unit is a 3-vector of real numbers that can represent a 3D point, 3D vector, or a color. Glassner outlines three main design principles for the data flow system, 1) a small number of versatile modules are provided, 2) each module has parametric controls, and 3) only one type of data is passed between modules. The third principle is especially important since it means that there are no restrictions on how information can be processed by networks of modules. While this system is interesting from the point of view of being a sonically-inspired approach to visual synthesis, it is not clear if it can also be used for sound synthesis.

## 2.2.8 Digital Harmony

Digital harmony is a compositional method conceived by John Whitney in the 1940s that aimed to combine audio and visual synthesis through a common grammar based on musical harmony [127, 126]. Central to digital harmony is the technique of *differential dynamics*, where the position of each element in a composition moves at an integer multiple of a particular base rate. Because of the harmonic relationships, at specific points in time patterns will form and then dissipate. The parameters of differential action are  $TD$ , the rate of angular or x-direction movement,  $RD$ , the rate of radial or y-direction movement, and  $ZD$ , the rate of z-direction movement. The parameters  $TD$  and  $RD$  thus can describe motions in either a polar or Cartesian coordinate system. Whitney makes extensive use of a mathematical curve called a *rose curve* which is given in polar coordinates as

$$r = \sin\left(\frac{n}{m}\theta\right)$$

where  $n, m \in \mathbf{Z}$ ,  $|m| > 0$ , and  $\theta \in [0 \dots 2m\pi]$  to guarantee that the curve is closed.

Whitney uses a discrete rose curve

$$r_n = \sin\left(\frac{RD}{TD + 1} \frac{2\pi n}{N}\right)$$

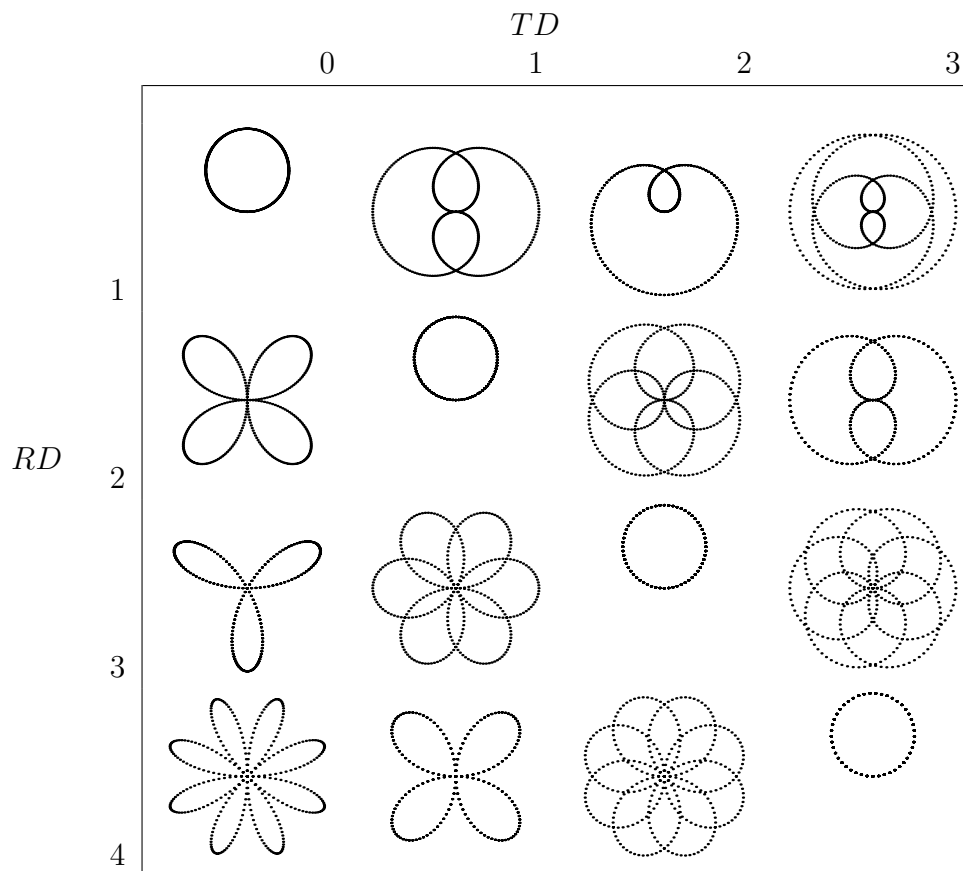
where  $n$  is the  $n^{th}$  point in the sequence and  $N$  is the total number of points.

Whitney discusses the notion of graphical scales which are formed as the matrix of all integer-valued combinations of  $RD$  and  $TD$ . Table 2.6 shows a 4x4 “graphical scale” of discrete rose curves. The graphical scales are a harmonic subset of the planar continuum which consists of all real-valued combinations of  $RD$  and  $TD$ . Integer values of  $RD$  and  $TD$  demarcate stable points in the field of all possible

forms. From Whitney's illustrations [126] it is clear that the stable points are closed curves, while the so-called tensive points are open curves with free endpoints. To get from one form to another, Whitney interpolates the differential parameters from one state to another. As he notes, this results in a complicated sequence of shapes:

The continuum is stepless until the selection of a frequency value is made. Once made, a string of consequences follows automatically: the entire family of intervals related to the first selection falls into place. One can deduce from this the status before and after the first choice. Out of the void, so to speak, a complete tensional hierarchy of structural elements is given substantiality by the one singular decision.

The "tensional hierarchy" is a result of complicated integer relationships between the differential amounts  $TD + 1$  and  $RD$ . Whenever the differentials have a common multiple the form will degenerate into an "overwound" form described by the lowest possible ratio of integers. The set of all non-degenerate rose curves are those where the two differentials are coprime (having no common multiple).



**Table 2.6:** Graphical scale of discrete rose curves

While Whitney did not apply his theory of differential dynamics beyond visual motion, Bill Alves has continued in this direction with his work *Hiway 70*, in which a Just intonation soundtrack and visual composition of rose patterns correspond through the same frequency ratios and modulations [6].

## Conclusion

With the advent of computers came the ability to directly synthesize sound and graphical patterns using digital signal processing and other forms of discrete mathematics. Patterns could be constructed with more precision and control than with mechanical and electronic devices. However, throughout this evolution the

development of techniques for audio and visual synthesis remained largely separate disciplines. It could be argued that if the audio and visual domains were considered together from the start, a reasonable idea considering the generality of the computer as a data processor, we might have a stronger mathematical foundation for describing multimedia. In the next section, we present the mathematical abstractions that thread through the previous work in harmonic pattern generation for sound and graphics.

## 2.3 Mathematical Abstractions

With the advent of the computer and digital techniques for synthesis of both sound and graphics, one can extract their various underlying mathematical principles and begin to define a new language that unites visual and audio domains. As evidenced above, there is a long history of successful application of trigonometric functions towards the construction of complex curvilinear visual patterns and audio waveforms. Common amongst these systems is the observation that the addition of more harmonics directly lead to an increased complexity and variety of results. In this section, we present a progression of mathematical abstractions from the rose curve to the transfer function that explicitly tie together the harmonic audio/visual synthesis techniques described above.

### 2.3.1 Epicyclic Curves

Plane curves exist in a variety of types each with their own intrinsic mathematical properties and construction methods [61, 130, 57]. A large number of planar curves can be classified as *roulette curves*, tertiary curves produced by the path (or locus) of a point, the *generator*, attached to a *rolling curve* as it rolls without slipping

along a *fixed curve* [61]. A particularly well-studied subset of roulette curves are the *epicyclic curves* [84], those curves having a rolling curve a circle and a fixed curve a line or a circle.

There are myriad terms used to describe epicyclic curves both with regards to the specific type of fixed curve and the location of the generator as well as certain generalizations. Table 2.7 presents the most common terms in present use. One exception is the general class of curves generated by a circle rolling on a circle for which no modern equivalent could be found. This type of curve takes the name spiroeid [40], bicircloid [81], cyclic-harmonic curve [71], and rosette [86]. For reasons of historical precedence and descriptiveness, we will use the term bicircloid. A description of each curve in Table 2.7 can be constructed by inserting the column headings into the following template:

A(n) *{name}* is the locus of a point attached rigidly *{point location}*  
the circumference of a circle rolling without slipping *{rolling location}*  
a fixed *{fixed curve}*.



fixed curve	rolling location	point location	name
line or circle	along	normal to	epicyclic curve
line	along	normal to	trochoid
		on	cycloid
		inside	curtate cycloid
		outside	prolate cycloid
circle	along	normal to	bicircloid
	inside	normal to	hypotrochoid
		on	hypocycloid
	outside	normal to	epitrochoid
		on	epicycloid

**Table 2.7:** The various types of epicyclic roulette curves.

The cycloid was discovered in the early 16th century by mathematician Charles Bouvelles. In 1659, Christian Huygens discovered that the cycloid is an isochrone, the curve along which a particle always has the same descent time, regardless of its starting position [9]. In 1696, Johann Bernoulli discovered that the inverted cycloid is a brachistochrone, the curve along which a free-sliding particle descends the fastest [9]. The parametric equation of a cycloid is

$$x = a\theta - b \sin(\theta)$$

$$y = a - b \cos(\theta)$$

The standard parameterization of one cycle of a cycloid on the Argand plane is

$$f(\theta) = a\theta + ai + (c - ai)e^{i\theta}$$

where  $a \in \mathbf{R}$ ,  $c \in \mathbf{C}$ , and  $\theta \in [0, 2\pi]$  [90]. In this standard view, a cycloid is

superposition of a linear motion  $a\theta + ai$  and circular (harmonic) motion  $e^{i\theta(c-ai)}$ .

A *rhodonea* or *rose curve*, studied by Guido Grandi in 1728 [38, 99], is a specific type of bicircloid where the tracing point is positioned on the rolling circle so that it passes through the center of the fixed circle. It is defined in polar form as

$$r = \cos(k\theta)$$

in Cartesian parametric form as

$$\begin{aligned} x &= \cos(\theta) \cos(k\theta) \\ y &= \sin(\theta) \cos(k\theta) \end{aligned} \tag{2.3.1}$$

and in complex parametric form as

$$\begin{aligned} f(\theta) &= \frac{1}{2}(e^{i(1-k)\theta} + e^{i(1+k)\theta}) \\ &= e^{i\theta} \operatorname{Re}(e^{ik\theta}) \end{aligned}$$

where  $\theta \in [0, 2\pi]$  and  $k \in \mathbf{N}$  determines the number of petals.

A bicircloid generalizes the rose curve as well as all other circle-on-circle curves including the hypotrochoid, hypocycloid, epitrochoid, and hypotrochoid. If integrated, the bicircloid also describes all the epicyclic curves given in Table 2.7. The bicircloid is described in complex form as

$$f(\theta) = be^{im\theta} + ce^{in\theta}$$

where  $m, n \in \mathbf{Z}$ ,  $b, c \in \mathbf{C}$ , and  $\theta \in [0, 2\pi]$ . This is clearly a sum of two complex sinusoids; a special case of a complex Fourier series.

While roulette curves account for many different types of curves, they are defined in terms of curves already given (the rolling and fixed curves) leading to the problem of how to generate these initial curves. Epicyclic curves solve this problem by having simple, compact parameterizations, but unfortunately exhibit a relatively limited range of possible patterns. Seeing as how epicyclic curves are constructed from a sum of two independent sinusoidal components, it is natural to extend their range of expression by including more harmonics thus adopting a more general framework of construction based on Fourier series.

### 2.3.2 Fourier Series

A Fourier series is an analytical description of a function in terms of a sum of harmonically-related sinusoidal functions. It is given by

$$f(x) = \sum_{k=0}^{\infty} a_k \cos(kx) + b_k \sin(kx)$$

where  $f(x)$  is a real-valued function and  $a_k$  and  $b_k$  are scalars. Fourier series were suggested by Jean Baptiste Joseph Fourier in 1822 as a more general form of representing heat flow than the prevailing methods at the time using partial differential equations [28]. In essence, his theory provided a more numerically precise way of describing the temporal evolution of heat within an arbitrary system. Even though Fourier specifically addressed propagation of heat, he was well aware that his theorems would apply to the analysis of more general dynamic systems and mathematical functions:


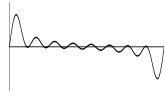

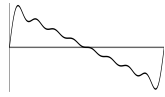
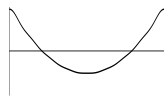
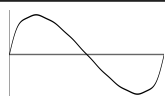


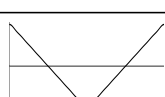

The analytical equations, unknown to the ancient geometers, which Descartes was the first to introduce into the study of curves and surfaces, are not restricted to the properties of figures, and to those properties

which are the object of rational mechanics; they extend to all general phenomena. There cannot be a language more universal and more simple, more free from errors and from obscurities, that is to say more worthy to express the invariable relations of natural things.

The central tenet of his theory is that any function can be decomposed into a sum of sinusoidal functions. He used this notion to describe the movement of heat in a ring, sphere, cylinder, rectangular prism, and cube. It is conceivable that Fourier's insight was influenced by a Pythagorean point of view:

The problems of the theory of heat present so many examples of the simple and constant dispositions which spring from the general laws of nature; and if the order which is established in these phenomena could be grasped by our senses, it would produce in us an impression comparable to the sensation of musical sound.

Fourier showed that geometric waveforms, such as a square or sawtooth, have very simple analytical representations as a sum of sinusoids. In his words, "The series formed of sines or cosines of multiple arcs are therefore adapted to represent, between definite limits, all possible functions, and the ordinates of lines or surfaces whose form is discontinuous." Table 2.9 enumerates some of the trigonometric series of functions given by Fourier [28] and fills in missing series using basic calculus of trigonometric functions. In an effort to simplify the equations, the original series given by Fourier have been slightly adapted to eliminate phase shifts around the origin. The modified series follow the simple pattern of cosine series having their maximum value at  $x = 0$  and sine series being zero with positive slope at  $x = 0$ .

name	graph	ideal function	Fourier series
impulse		$\begin{cases} 1 & x = 0 \\ 0 & x \neq 0 \end{cases}$	$\frac{1}{K} \sum_{k=1}^K \cos kx$
cotangent		$\frac{1}{K} \cot \frac{x}{2}$	$\frac{1}{K} \sum_{k=1}^K \sin kx$
log sine		$-\ln \left  2 \sin \frac{x}{2} \right $	$\sum_{k=1(1), k>0} \frac{\cos kx}{k}$
saw		$\text{saw}(x) = \frac{-x}{\pi} \bmod 2 - 1$	$\frac{2}{\pi} \sum_{k=1(1), k>0} \frac{\sin kx}{k}$
parabolic		$\frac{3}{2} \left( \text{saw}(x)^2 - \frac{1}{3} \right)$	$\frac{6}{\pi^2} \sum_{k=1(1), k>0} \frac{\cos kx}{k^2}$
smooth saw		$\int -\ln \left  2 \sin \frac{x}{2} \right $	$\sum_{k=1(1), k>0} \frac{\sin kx}{k^2}$
log cotangent		$\frac{1}{2} \ln \left  \cot \frac{x}{2} \right $	$\sum_{k=1(2), k>0} \frac{\cos kx}{k}$
square		$\text{sgn}(\text{saw}(x))$	$\frac{4}{\pi} \sum_{k=1(2), k>0} \frac{\sin kx}{k}$
triangle		$2  \text{saw}(x)  - 1$	$\frac{8}{\pi^2} \sum_{k=1(2), k>0} \frac{\cos kx}{k^2}$
smooth square		$\int \frac{1}{2} \ln \left  \cot \frac{x}{2} \right $	$\sum_{k=1(2), k>0} \frac{\sin kx}{k^2}$

**Table 2.9:** Fourier series of some simple functions.

A Fourier series can be written in a more general form as a sum of complex exponentials

$$f(\theta) = \sum_{k=-\infty}^{\infty} c_k e^{ik\theta} \quad (2.3.2)$$

where  $e^{ik\theta} = \cos(k\theta) + i \sin(k\theta)$  according to the Euler's formula. Real-valued Fourier series can be obtained from a complex Fourier series as its real and imaginary components.

While in theory it is possible to construct any function with a Fourier series, in practice, it is not feasible to evaluate an infinite (or large finite) number of harmonics in order to produce a curve of substantial complexity. What would be desirable is a way to efficiently produce sets of harmonics in a highly controllable fashion. The transfer function, a ratio of complex Fourier series, offers one possible solution.

### 2.3.3 The Transfer Function

In digital signal processing, a standard signal for analyzing linear time-invariant (LTI) systems is a complex exponential given by

$$x[n] = z_0 z_1^n$$

where  $z_0$  and  $z_1$  are complex numbers representing its *complex amplitude* and *complex frequency*, respectively. A complex exponential is written in polar form as

$$x[n] = A_0 e^{i\theta_0} (A_1 e^{i\theta_1})^n$$

where  $A_0 = |z_0|$  is the *amplitude*,  $\theta_0 = \arg(z_0)$  is the *phase*, and  $\theta_1 = \arg(z_1)$  is the *frequency*. When  $|z_1| < 1$ , we get a *decaying complex exponential* and when  $|z_1| > 1$ , we get a *growing complex exponential*. For the special case  $|z_1| = 1$ , we obtain a *complex sinusoid* [97].

The discrete Fourier transform (DFT),  $\mathcal{F}$ , of a signal  $x$  of length  $N$  is given by

$$\mathcal{F}(x[n]) = X[k] = \frac{1}{N} \sum_{n=0}^{N-1} x[n] e^{-i2\pi kn/N}$$

and the inverse discrete Fourier transform (IDFT),  $\mathcal{F}^{-1}$ , by

$$\mathcal{F}^{-1}(X[k]) = x[n] = \sum_{k=0}^{N-1} X[k] e^{i2\pi kn/N}$$

where  $x$  is a position- or time-domain sequence,  $X$  is a frequency-domain sequence,  $N$  is the total period in samples,  $n$  is a position-domain index,  $k$  is a frequency-domain index, and the summation terms are harmonically-related complex sinusoids.

A transfer function,  $H(z)$ , is a complex rational function that describes the frequency response of a difference equation. It maps a complex input representing the frequency of a unit magnitude complex sinusoid to a complex output representing the complex sinusoid's change in phase and amplitude.

Transfer functions are used to analyze systems given by a linear constant-coefficient difference equation (LCCD). An LCCD specifies how to produce the next element of a sequence out of a linear combination of its next and previous inputs and outputs. In its most general form, it is given by

$$\sum_k b_k y[n+k] = \sum_k a_k x[n+k]$$

where  $x$  is the input sequence,  $y$  is the output sequence,  $b_k$  and  $a_k$  are complex coefficients,  $n$  is the sample index, and  $k$  is a sample delay ( $k \leq 0$ ) or sample advance ( $k > 0$ ). A difference equation is *causal* if it depends only on its previous inputs and outputs. These are commonly used for unidirectional signals, such as real-time audio or other types of temporal data. A difference equation is *acausal* if it depends on both its next and previous inputs and/or outputs. These are generally used for processing bidirectional signals, such as images, volume data, or other types of spatial data.

Obtaining a transfer function from an LCCD is accomplished by determining the effect of the system on the complex frequency,  $z_1$ , of a complex exponential. If  $x$  and  $y$  are both taken to be complex exponentials, then we can use the  $z$ -transform to substitute  $X(z)z^k$  for  $x[n+k]$  (likewise for  $y$ ). Performing this substitution into the LCCD equation and solving for  $Y(z)/X(z) = H(z)$  we get

$$H(z) = \frac{Y(z)}{X(z)} = \frac{\sum a_k z^k}{\sum b_k z^k} \quad (2.3.3)$$

It can be seen from Eq. 2.3.3 that the transfer function is simply a rational function of complex power series. When  $|z| = 1$ , the power series are isomorphic to the DFT.

## Conclusion

With the transfer function, we have finally arrived at an equation that can begin to unify pattern synthesis both within and across the audio and visual domains. All of the pattern synthesis devices and techniques described up to this point, from string vibrations to the geometric chuck to modern digital signal processing, have

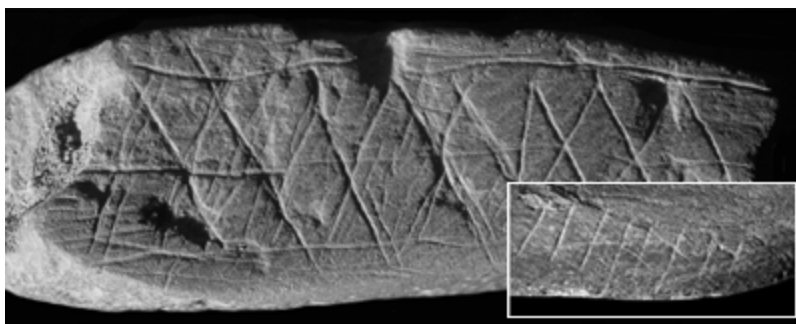


Eq. 2.3.3 as an underlying model. While it is useful to have a single equation that describes so many different phenomena, what is more important is how to use it and furthermore, how to do so in an economical fashion. To help provide some guidance in this direction, the modern notion of symmetry may provide some important clues.

## 2.4 Symmetry and Its Importance in Mathematics, Science, and Art

Symmetry is an important integrating factor in its application in mathematics, science and art. Throughout history, the definition of symmetry as a balance of equivalent parts to make a whole has remained consistent. In the early 19th century, its definition become more formalized and generalized as a result of the development of group theory in mathematics.

The history of symmetry begins in the prehistoric era where excavated art from the period signifies mankind's first recognition and understanding of regularity in nature. At the Blombos Caves in Western Cape, South Africa, several pieces of ochre were found with engraved cross-hatched patterns [41]. Fig. 2.4.1 shows one of the discovered artifacts. The artifacts have been dated back to 77,000 B.C. making them the earliest known evidence of abstract art and human understanding of pattern.



**Figure 2.4.1:** A piece of ochre carved with abstract patterns dated back to 77,000 B.C. From Henshilwood et al. (2002). Emergence of modern human behavior: Middle stone age engravings from South Africa. (*Science*, 295:1278–1280. Reprinted with permission from AAAS.)

The Pythagoreans were the first to use the term symmetry to refer to the harmonization of different elements into a unitary whole. To them, *symmetria* was visible beauty and *harmonia* was audible beauty [105]. Although there is no direct translation of symmetry from its Greek roots, it can be used to describe harmony, rhythm, balance, equipoise, stability, good proportions, and evenness of structure [13]. The Romans also adopted the Greek notion of symmetry, most notably the architect Vitruvius who wrote in his *De Architectura* “Symmetry results from proportion; proportion is the commensuration of the various constituent parts with the whole.” After the Renaissance, a more precise definition of symmetry developed based on an equivalence and interchangeability of parts making a whole. This eventually led to a more general definition of symmetry as invariance under transformation [122].

Beginning in the 1830s, symmetry developed a more scientific definition originating in the mathematical notion of a *group*. A group is a set of transformations that is closed under an operation that is associative, admits a unit element and inverse elements [52]. Group theory arose in the attempts to find general solutions to quintic and higher degree polynomials. In 1832, French mathematician Évariste

Galois showed that the quintic equation cannot be solved using usual algebraic operations and radicals. He was able to do this by showing how equations can be broken down into more fundamental subgroups of permutations. Symmetry played a significant role in this development. In 1884, German mathematician Felix Klein demonstrated how to solve the quintic equation using a symmetry group isomorphic to an icosahedron.

In physics, symmetry is extended from the form of objects to include the laws governing the dynamics of objects. The harmonic oscillator is one such symmetry of physical laws. It turns up as a solution to many problems in dynamics because its general form, an exponentially decaying sinusoid, is invariant under differentiation and integration. As another example of symmetry in physics, Galilean invariance says that the fundamental laws of physics are the same in all inertial frames. In this case, the laws exhibit a type of compact translational symmetry in space and time. Einstein's special theory of relativity also has strong ties to symmetry through the geometry of space-time. Hermann Minkowski framed special relativity in Minkowski space which forms a group of symmetry transformations. From this connection, it became clear that physical laws could be deduced from symmetry requirements. Minkowski's interpretation of Einstein's laws of special relativity made, for the first time, symmetry considerations an important prerequisite in formulating physical laws [135].

Along with symmetry come some natural complementary concepts. The most obvious of these, *asymmetry*, designates lack of symmetry. *Dissymmetry* can mean asymmetry or, more specifically, the condition of an object not being superimposable on its mirror image [121]. *Antisymmetry* describes a situation where a symmetry operation is accompanied by a property that turns into its opposite [39]. *Dissymmetrization* is the process of composing a system that has less sym-

metry than its parts. *Symmetrization* is the opposite process whereby a system is composed that has more symmetry than its parts [95]. *Symmetry breaking* occurs when there is a reduction in the number of symmetry operations leaving something unchanged. In physics, symmetry breaking can occur in one of two ways: explicit or spontaneous. A system is said to exhibit *explicit symmetry breaking* if there are intrinsic asymmetries in its dynamical laws [135]. On the other hand, *spontaneous symmetry breaking* occurs when a physical system does not exhibit all the symmetries of the laws by which it is governed [120]. A simple example of a system exhibiting spontaneous symmetry breaking is the dropping of a marble into a punted wine bottle. The marble will eventually come to rest on one side of the bottle even though the shape of the bottle (assumed to be perfectly symmetric) does not bias motion in any one particular direction [135].

### 3. Conceptual Framework

---

What the background has shown us is the great diversity of visual and sonic patterns possible through simple compositions of harmonics. From superpositions of just a few harmonics, we already obtain a bewildering array of patterns applicable to both sound and graphics. The question that naturally arises is how we can make sense of this vast space of possibilities to serve both artistic and scientific inquiry. With clear underlying principles at hand, one can explore the space of patterns more effectively shortening the path between intention and outcome. This dissertation proposes to advance our understanding of harmonic spatiotemporal patterns through a simple, unified mathematical construct with the capacity to compactly describe such patterns. The main thesis is:

*A large variety of waveforms, shapes, and patterns for sound and graphical synthesis are direct mappings of a one-dimensional rational function of inverse discrete Fourier transforms, hereby called the harmonic pattern function, with parameters compactly described in terms of symmetry principles.*

The term *harmonic pattern function* is used to refer to a complex-valued rational function of two inverse discrete Fourier transforms. While similar in form to a transfer function, the harmonic pattern function differs in that its domain is discrete-space and/or -time rather than continuous-frequency. It produces a

sequence of complex numbers which can be mapped in various ways to construct graphical patterns or directly converted to a sound waveform by taking its real or imaginary component.

## 3.1 Conventions

The following subsections present the terminological, mathematical, and graphical conventions used throughout the document.

### 3.1.1 General Terminology

Term	Description
codomain	the set of all possible outputs of a function
complex sequence	a sequence of complex numbers
complex sinusoid	a periodic complex sequence whose real and imaginary components are sinusoids with equal frequency and amplitude, but phases differing by $\pi/2$
domain	the set of all possible inputs of a function
eccentric	(a curve) not centered at the origin
harmonic	a complex sinusoid
sequence	an ordered multiset (a set where a member may have multiple instances)
speed (of a curve)	a measure proportional to the distance between sample points of a curve

**Table 3.1:** Listing of terminology

### 3.1.2 Mathematical Symbols

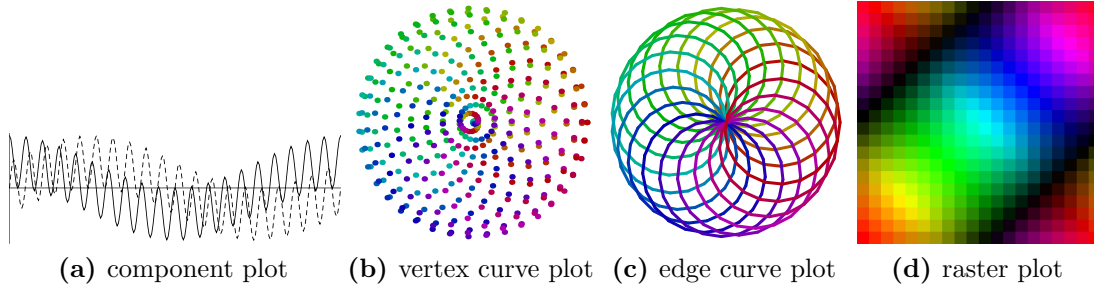
Symbol	Description
$z = a + ib$	complex number or sample
$\bar{z} = a - ib$	complex conjugate
$\mathcal{F}$	discrete Fourier transform
$\mathcal{F}^{-1}$	inverse discrete Fourier transform
$x = \mathcal{F}^{-1}(X)$	position-domain sequence
$X = \mathcal{F}(x)$	frequency-domain sequence
$N \in \mathbf{N}$	size of $x$ and $X$ , in samples
$k \in [0, N)$	frequency-domain sample index
$n \in [0, N)$	position-domain sample index
$\theta_i$	$i^{\text{th}}$ sample phase, in radians
$A_i$	$i^{\text{th}}$ sample amplitude

**Table 3.2:** Listing of mathematical symbols

### 3.1.3 Graphical Representations

Throughout this document, several different types of graphical plots will be utilized to represent one-dimensional complex sequences (Fig. 3.1.1). A *component plot* displays the values of the real and imaginary components along the  $y$  axis and the sequence index along the  $x$  axis (Fig. 3.1.1a). A *curve plot* is a direct mapping of the complex numbers' real and imaginary components to  $x$  and  $y$  Cartesian coordinates, respectively. This type of plot is known as an *Argand plot* in complex analysis. We refer to the points as *vertices* and the lines between successive points as *edges* after the same terminology used in graph theory [36, 109]. A *vertex curve plot* displays only the vertices and is used to illustrate unordered relationships between points (Fig. 3.1.1b). An *edge curve plot* displays lines between successive

points in the sequence and is used whenever ordered relationships are important (Fig. 3.1.1c). The hue of each point along the curve correlates to its position in the sequence, the first point being red, the next point going towards orange, and the last point being violet. More precisely, the angle of the hue of the  $n^{\text{th}}$  point in a sequence of  $N$  points is  $\frac{n}{N} \cdot 360^\circ$ . A *raster plot* displays a raster scan [66] of the complex sequence on an  $\sqrt{N} \times \sqrt{N}$  grid (Fig. 3.1.1d). Scanning starts at the bottom-left corner and moves in the positive  $x$  direction incrementing in the positive  $y$  direction and jumping back to the left edge whenever the right edge is reached. The raster grid is thus topologically equivalent to the surface of a torus. The hue and value components of each cell directly correspond to the phase and magnitude, respectively, of the complex number.



**Figure 3.1.1:** Various graphical plots used to display a one-dimensional complex sequence. All plots show the same sequence  $\alpha_n = \{1\} + \{20\}$  with  $N = 400$ .

The figures displayed on the curve plot are normalized so that for any point along the curve given by the complex number  $z$ ,  $|z| \leq 1$ . When presenting shape equations, the normalization factor will be omitted for clarity. The normalization factor is computed directly from the complex sequence as  $1/\max(|\alpha_0|, |\alpha_1|, \dots, |\alpha_{N-1}|)$  so as to make the figure lie within the unit circle.



## 3.2 The Harmonic Pattern Function

The harmonic pattern function,  $\alpha_n$ , is a newly proposed mathematical generating function formally defined as a rational function of two inverse discrete Fourier transforms. It provides a means for producing complex-valued sequences that can be directly mapped into graphical curve and image patterns, sound waveforms, and other types of spatiotemporal trajectories (such as the path of a spatial audio source). The general equation of the harmonic pattern function is

$$\alpha_n = \frac{x_n}{y_n} = \frac{\sum_{k=0}^{N-1} X_k e^{i2\pi kn/N}}{\sum_{k=0}^{N-1} Y_k e^{i2\pi kn/N}} \quad (3.2.1)$$

where  $\alpha_n$ ,  $x_n$ ,  $y_n$ , are complex time- and/or position-domain sequences,  $X_k$  and  $Y_k$  are the  $k^{\text{th}}$  elements of complex frequency-domain sequences, and  $N$  is length of all sequences. Since the harmonic pattern function is often used with a sparse set of parameters, we adopt the following shorthand notations for the complex sinusoid terms to assist in reducing clutter

$$\begin{aligned} |X_k| \cdot \{k, \arg(X_k)/2\pi\} &:= X_k e^{i2\pi kn/N} \\ A \cdot \{k\} &:= A e^{i2\pi kn/N} \quad \text{where } A \in \mathbf{R} \\ \{k\} &:= e^{i2\pi kn/N} \end{aligned}$$

where  $e^{i2\pi n/N}$  is a discrete complex sinusoid sequence of length  $N$  indexed by  $n$ . The value of  $N$  will typically accompany a harmonic pattern function although, not strictly so such as the case when  $N \rightarrow \infty$ . Arithmetic of complex sinusoids in the abbreviated form follow the same mathematical rules as before. Addition and

multiplication are written as

$$A\{a, \theta\} + B\{b, \phi\}$$

and

$$A\{a, \theta\}B\{b, \phi\},$$

respectively. Multiplication and inversion of complex sinusoids have the reduced forms

$$\begin{aligned} A\{a, \theta\} \times B\{b, \phi\} &= AB\{a + b, \theta + \phi\} \\ \frac{1}{A\{a, \theta\}} &= \frac{1}{A}\{-a, -\theta\}, \end{aligned}$$

respectively. Multiplication is associative and is distributive across addition. The real and imaginary components of a complex sinusoid  $A\{a, \theta\}$  are specified as

$$A \operatorname{Re}\{a, \theta\}$$

and

$$A \operatorname{Im}\{a, \theta\}.$$

Any curve given in polar coordinates as a function of trigonometric functions has an equivalent harmonic pattern function. If a curve's polar equation is  $r = f(\theta)$ , then its equivalent harmonic pattern function is  $\alpha_n = f(2\pi n/N) \cdot \{1\}$  with  $\theta \rightarrow 2\pi n/N$ . For example, a quadrifolium with the polar equation

$$r = 2 \cos(2\theta)$$

has the harmonic pattern function

$$\begin{aligned}
 \alpha_n &= 2 \cos(2 \cdot 2\pi n/N) \cdot \{1\} \\
 &= 2 \frac{\{-2\} + \{2\}}{2} \{1\} \\
 &= \{-1\} + \{3\}.
 \end{aligned}$$

Implementation of the harmonic pattern function on a computer is straightforward, but not without a few less obvious considerations that are now discussed. There are two principle methods for computing  $\alpha_n$ , the first in the frequency domain and the second in the time domain. For the frequency-domain approach,  $\alpha_n$  is computed by performing two inverse discrete Fourier transforms, storing the quotient into a table, and then accessing the table. While the cost of computing the table samples is at best on the order of  $O(2N \log_2 N)$  using the FFT, once computed, the table can be efficiently accessed in  $O(1)$  time for any particular sample  $n$ . For the time-domain approach,  $\alpha_n$  is computed directly for all  $k$ , but only at a particular  $n$ . In this way, Eq. 3.2.1 is treated like a complex function of a real variable  $n$ . Considering the task of generating the sequence  $\alpha_0, \alpha_1, \dots, \alpha_{N-1}$ , the frequency-domain approach has complexity  $O(2N \log_2 N + N)$  while the time-domain method has complexity  $O(2N^2)$ . However, if we assume there are only  $m$  non-zero complex sinusoids, then the time-domain complexity becomes  $O(mN)$ . Thus, for  $m \lesssim 2 \log_2 N$ , direct computation in the time-domain is both faster and better amortized over time than in the frequency-domain. For these reasons, in addition to simplicity of implementation, the time-domain approach is better if only a small number of complex sinusoidal components are used.

A final implementation consideration is the efficient evaluation of  $e^{i\theta}$ . Direct evaluation using language-provided trigonometric functions can be prohibitively

expensive as two calls to  $\cos$  and  $\sin$  are required per complex sinusoid. A table lookup procedure can replace the two trigonometric calls with a single array access, permitting more speed but at the price of less precision. Fortunately, the geometric properties of complex numbers provide an efficient way for substantially improving the precision of table lookups. The trick [108] is to perform a double lookup from two tables of size  $\sqrt{N}$  where a coarse table stores the complex sinusoid  $e^{i2\pi n/\sqrt{N}}$  and a fine table stores the complex arc  $e^{i2\pi n/N}$  for  $n \in [0, \sqrt{N})$ . The tables can be combined through a single complex multiplication into an “product” table containing a full-precision complex sinusoid  $e^{i2\pi n/N}$ . Even with two moderately sized tables of  $\sqrt{N} = 4096$ , we can obtain an effective resolution of  $N = 16,777,216$ . For audio synthesis, this translates to a full-precision sine wave with a period of approximately 6 minutes at a sample rate of 44.1 kHz.

### 3.3 The Role of Symmetry

The role of symmetry in this thesis is not to aid in categorization of patterns already generated, but to help in understanding and describing the processes underlying the generation of patterns. The three main functions of symmetry considered are

1. *Symmetries in the frequency domain have corresponding symmetries in the time domain.* The frequencies, phases, and amplitudes of the harmonics comprising a pattern have a direct consequence on the formal symmetries of the composed pattern.
2. *All spatiotemporal patterns stem from a one-dimensional sequence.* The structure of the one-dimensional sequence remains invariant under mappings to sonic and graphical patterns such as curves, images, and sound waveforms.

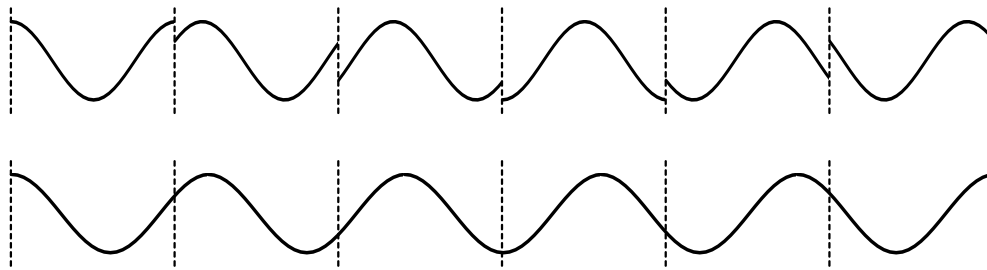
For example, generated curves are unicursal; they can be drawn in a single movement.

3. *Near or perfect symmetries lead to near or perfect reinforcements and cancellations.* For example, patterns exhibiting envelopes are comprised of nearly symmetric components and perfect symmetry can eliminate infinities.

Symmetries between harmonics in the frequency domain determine, to a large part, symmetries of synthesized forms in the position or time domain. There are particular symmetry relationships between the frequency-domain and position-domain representations of patterns. When visualizing curves on the complex plane, it has been found that frequency is directly related to cyclic symmetry and phase is related to dihedral symmetry. In addition, multiple similar objects in space are made by superposing low-amplitude, low-frequency harmonics with high-frequency, high-amplitude harmonics.

Another important conceptual standpoint will be to suppose that all patterns produced by the harmonic pattern function occupy a single space-time block. The patterns are always closed since they are produced from periodic functions, however, these patterns experienced as incomplete subsequences give no indication of the finished product [87]. In one interpretation, these patterns are derived from a single pattern existing as a pre-established spatiotemporal structure. The space-time is considered to be a type of Euclidean space-time [80] where the time dimension is viewed as nothing more than an extra spatial dimension. From this perspective, time experienced is a linear movement through regular spatial slices of a holistic space-time block. Each moment in time is one of the spatial slices. In what could be called the “film-strip” convention of space-time, a series of spatial “images” are viewed individually in rapid succession to give the (illusory) sensation of time.

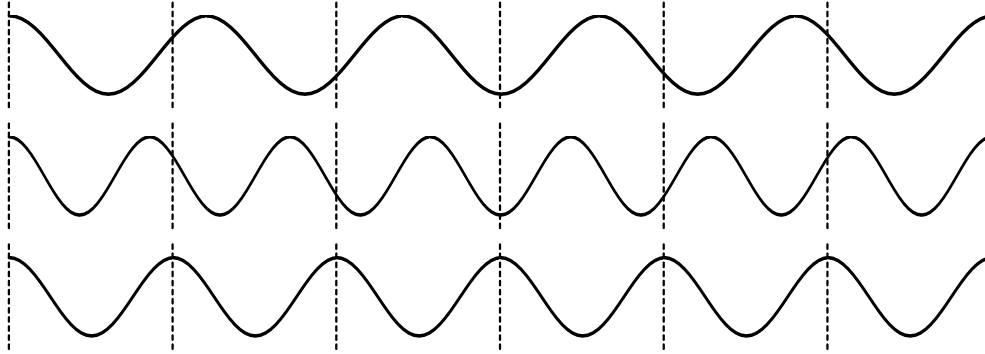
What leads to a coherent spatiotemporal experience (or at least one familiar to us in the physical world we perceive) is that the images vary gradually from one frame to the next. While the space-time being proposed here is similar to the film-strip convention, it differs in that it makes a stronger assertion about how spatial structures and their evolution over time are related. Fig. 3.3.1 illustrates the difference between a continuous and discontinuous spatiotemporal pattern model of a traveling sinusoidal wave. The top figure shows the discontinuous model where the pattern taken as a single curve running from left to right is comprised of multiple segments periodic through space within each time-frame, but discontinuous at the frame boundaries. Each point within each time-frame “ticks” independently of the others, albeit all at the same frequency in this particular example. If the frames were shown in rapid succession, it would appear as though the wave was traveling to the right. In contrast, the bottom figure shows the continuous model which is distinguished by the fact that there is only one continuous curve flowing across the entire length of the film. If these cells were shown individually in rapid succession, they would also show a wave moving to the right.



**Figure 3.3.1:** Two different models of spatiotemporal patterns. The top figure is the discontinuous model where the pattern has separate space and time components. The bottom figure is the continuous model where patterns run smoothly across space and time.

With continuous space-time patterns, there naturally arise different ways that a pattern exhibiting simple motion can “flow” through space-time. If the

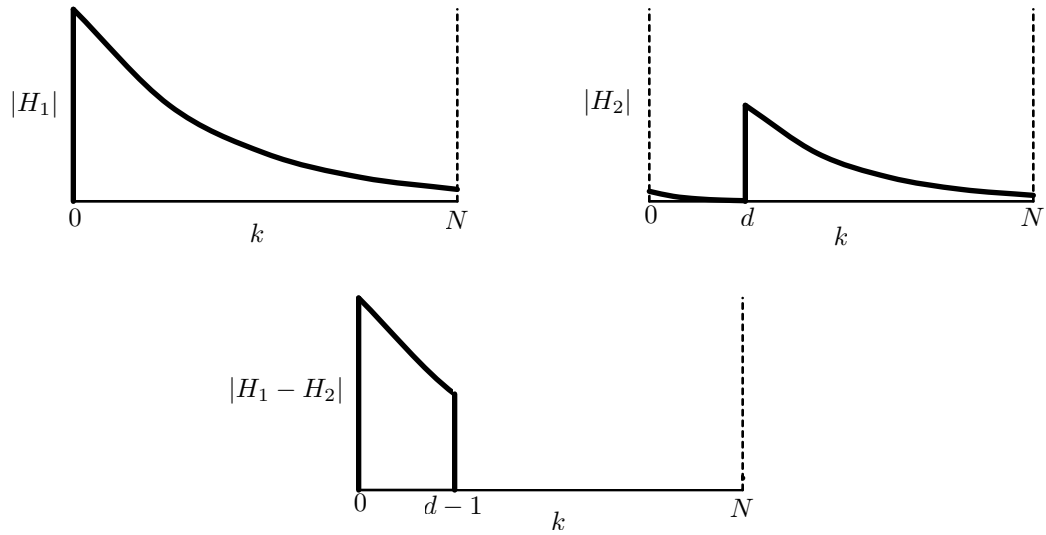
pattern comes short of closing on itself within one time-frame, then it *undershoots*. Conversely, if the pattern runs past perfect closure, then it *overshoots*. When it closes perfectly on itself within the time-frame, then it is *coincident*. Fig. 3.3.2 compares the three different flow types. Both undershooting and overshooting patterns exhibit motion, whereas a coincident pattern is static.



**Figure 3.3.2:** Three types of flow patterns in continuous pattern model: undershooting (top), overshooting (middle), and coinciding (bottom).

Another important role of symmetry, especially for sound synthesis, is that it permits interference of waveforms in precise ways. When two antisymmetric complex sequences are summed together, they cancel each other out. In particular, complex exponentials have a unique symmetrical form that allows them to perfectly interfere with one another. In this way, band-limited waveforms with an arbitrary number of harmonics can be constructed through destructive interference of waveforms with infinite harmonics. Fig. 3.3.3 illustrates the basic process. Two sequences,  $h_1[n] = \frac{1}{1-b\{1\}}$  and  $h_2[n] = \frac{b^d\{d\}}{1-b\{1\}}$ , with respective spectra  $H_1[k] = \sum_{m=0}^{\infty} b^{k+mN}$  and  $H_2[k] = \sum_{m=0}^{\infty} b^{[(k-d) \bmod N]+d+mN}$  are subtracted from one another resulting in a spectrum that is truncated above the  $(d-1)^{th}$  harmonic.

This perfect cancellation between the spectra is made possible by two factors—ideal frequency shifting and self-similarity. The ability to perfectly frequency



**Figure 3.3.3:** Band-limited waveform constructed through destructive interference of complex exponentials in the frequency domain.

shift the waveform is due to the fact that it is composed of complex numbers rather than real numbers. This eliminates the need for a Hilbert transform filter to approximate a  $90^\circ$  phase-shifted signal [14, 114] and instead only requires multiplying the input signal by a complex exponential with its frequency set to the desired shift in frequency. The self-similar nature of the spectrum (a decaying complex exponential) means that its general shape is invariant under amplitude scaling and, most importantly, under shifts in frequency.

### 3.4 Methodology

The contribution of this research is to codify a canonical set of audio/visual forms constructed from a sparse set of complex sinusoids used in the harmonic pattern function. This is seen as a necessary preliminary step towards understanding the composition of more complex patterns. The second contribution is in providing a precise numerical way for describing symmetry and asymmetry of sequences

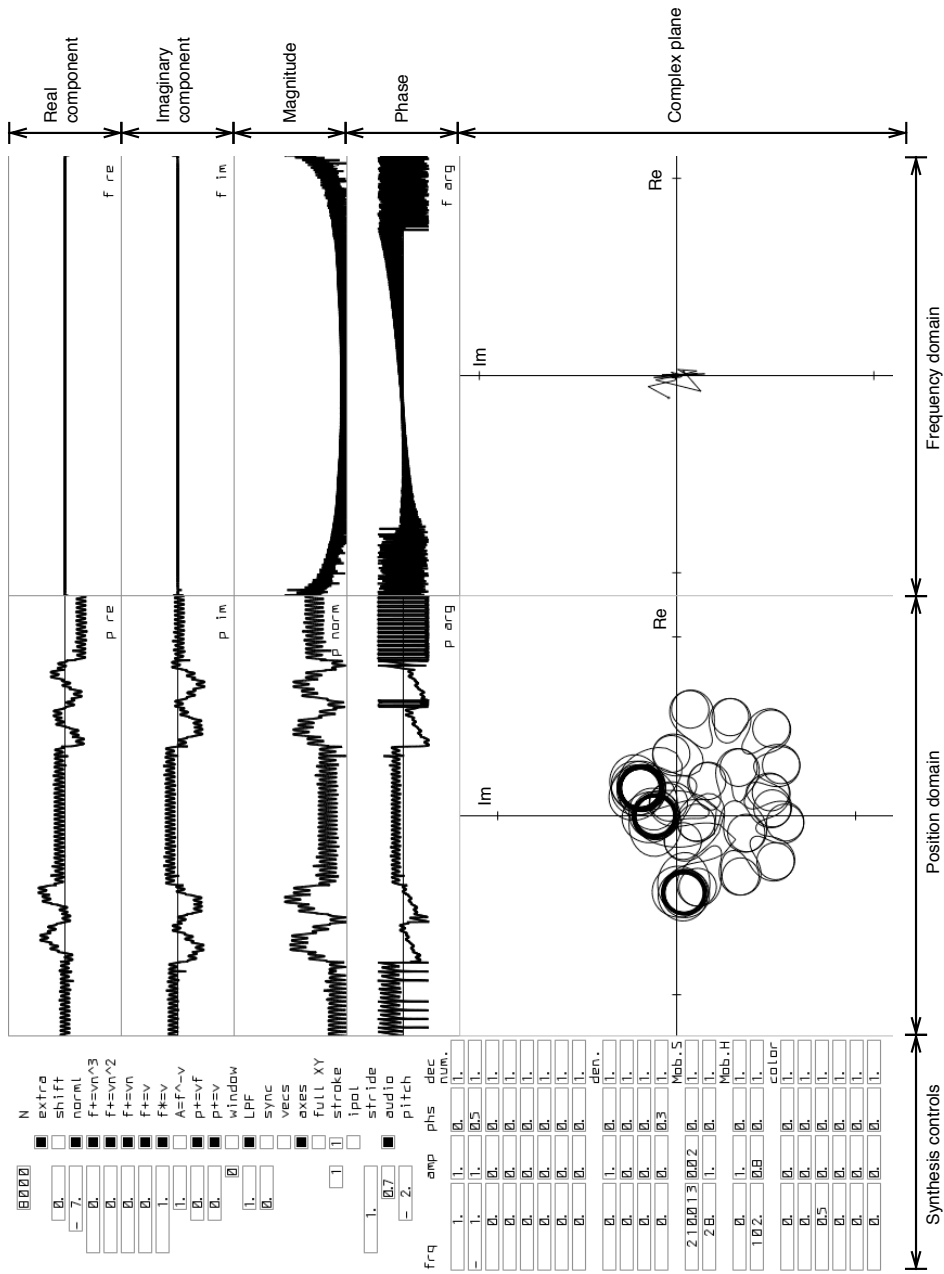


from the perspective of the frequency domain. Current theories of symmetry [18, 95, 59, 58], as they relate to form, do not make an explicit connection to the frequency domain nor address how to compose symmetries into particular patterns that can be used for audio/visual synthesis.

On the basis of the harmonic pattern function, the complex sequences produced thereof, and the conceptual framework as defined above, the following items are investigated:

1. Classification of sound waveforms and geometric shapes produced by:
  - (a) single complex sinusoids
  - (b) low-order superpositions of (a)
  - (c) rational functions of (b)
  - (d) integration of (b) and (c)
2. Correlation between frequency, amplitude, and phase parameters and formal qualities of patterns
3. Basic principles of combined spatiotemporal patterns stemming from single one-dimensional complex sequences

Investigations were conducted using a custom-made real-time, interactive program called *Spool* (Fig. 3.4.1). *Spool* provides an interface for parametric construction of curves based on the harmonic pattern function with direct audio/visual feedback. It serves as a general tool for exploring sonic and multiple visual representations of the harmonic pattern function in parallel. By taking such a tautological approach to rendering these sonic and graphical forms, patterns that may be perceived differently can be related through a common mathematical basis.



**Figure 3.4.1:** *Spool* screenshot. On the leftmost side are synthesis controls for setting harmonics of the harmonic pattern function and other synthesis parameters. To the right of the synthesis controls is a grid of graphs showing the resulting complex sequence in both the position domain and frequency domain on the complex plane and its polar and Cartesian projections.

# 4. Generalizations of Harmonic Patterns

---

The goal of this chapter is to present general mathematical rules and formal themes that apply across a wide range of harmonic patterns. By examining quantitative and qualitative aspects together, we can predict the appearance and behavior of patterns from their mathematical description and vice versa. The most general transformations to harmonic patterns are modifications to the amplitudes, phases, and frequencies of harmonic components. For the most part, these transformations vary one or more aspects of the pattern while leaving others unchanged. Formal generalizations are primarily concerned with the outward appearance of patterns and are almost always associated with numerical descriptions.

The mathematical and formal characteristics of patterns are discussed from the perspective of symmetry—invariance under transformation. There are two main reasons for this. First, by clearly defining the symmetries of patterns, we automatically obtain an understanding of the complementary concept of asymmetry. This is a logical way to proceed as symmetric patterns take up a much smaller portion of the entire space of possible patterns. Furthermore, since the parameter space of patterns we are considering is connected, it is entirely possible to generate gradations between symmetry and asymmetry. This is important since some of the

most interesting patterns are near-symmetric or pseudo-symmetric. The second reason for considering symmetry is rather simple—it provides an effective means for describing and categorizing patterns.

## 4.1 Frequency-domain Transformations

A frequency-domain transformation is an operation on the complex amplitudes and/or indices of frequency-domain samples. For every frequency-domain transformation there is a corresponding position-domain transformation.

Transformation	Frequency Domain	Position Domain	Result
integration	$X_k \frac{1}{ik}$	$\int x_n$	indefinite integral
differentiation	$X_k ik$	$\frac{d}{dn} x_n$	derivative
phase rotation	$X_k e^{i\phi}$	$x_n e^{i\phi}$	rotate samples
phase shift	$X_k e^{ik\phi}$	$x_{n+\frac{\phi}{2\pi}N}$	shift position
phase negation	$\bar{X}_k$	$\bar{x}_{N-n}$	conjugate and reverse
frequency shift	$X_{k+\delta}$	$x_n e^{i2\pi\delta n/N}$	
frequency scale	$X_{\frac{k}{m}}$	$x_{mn \bmod N}$	shift pitch
frequency negation	$X_{N-k}$	$x_{N-n}$	reverse sequence

**Table 4.1:** Frequency-domain transformations

In the following subsections, the aforementioned transformations are discussed in more detail. Wherever it is deemed necessary, visual examples of the transformations are supplied.

### 4.1.1 Amplitude Transformations

An amplitude transformation changes the amplitudes of the harmonics comprising a complex sequence while leaving phases and frequencies invariant. The simplest amplitude transformation is amplitude scaling which is associative across the frequency and position domains. Two less trivial amplitude transformations are integration and differentiation. The effect of these is to apply a power law to the amplitudes of each harmonic where the exponent is proportional to the (integer) harmonic number. The phases are also modified, but by a uniform amount which can easily be corrected for if necessary. Considering the fact that integration and differentiation are distributive across harmonics, they can be understood fully by their operation on a single complex exponential. Differentiation of a complex exponential is defined by

$$\frac{d}{dt}e^{ikt} = ik e^{ikt} \quad (4.1.1)$$

and integration as

$$\int e^{ikt} = -i\frac{1}{k}e^{ikt} + C. \quad (4.1.2)$$

where  $C$  is an arbitrary constant. The effect of integrating or differentiating a complex sequence is thus to scale the amplitude of each of its constituent complex exponentials in inverse or direct proportion, respectively, to their frequency and apply a global phase rotation (discussed below). Integration and differentiation can be generalized into the single operation

$$\frac{d^p}{dt^p}e^{ikt} = (ik)^p e^{ikt} \quad (4.1.3)$$

where  $p > 0$  is the  $p^{th}$  derivative and  $p < 0$  is the  $p^{th}$  integral.

### 4.1.2 Phase Transformations

Phase transformations change the phases of the harmonics comprising a complex sequence. There are two main phase transformations that leave some aspect of a complex sequence,  $x_n$ , invariant. The primary distinction between the phase transformations is whether they operate in a *local* or *global* fashion on the sequence while leaving invariant its *global* or *local* properties, respectively. The first transformation, a *phase rotation*, adds a constant phase amount  $\phi$  to each harmonic comprising  $x_n$ . The operation is described by

$$h_{rotate,\phi}(X_k) = X_k e^{i\phi} \quad (4.1.4)$$

where each complex amplitude  $X_k$  is multiplied by  $e^{i\phi}$ . Due to the linearity property of the Fourier transform, this operation is equivalent to

$$x'_n = x_n e^{i\phi} \quad (4.1.5)$$

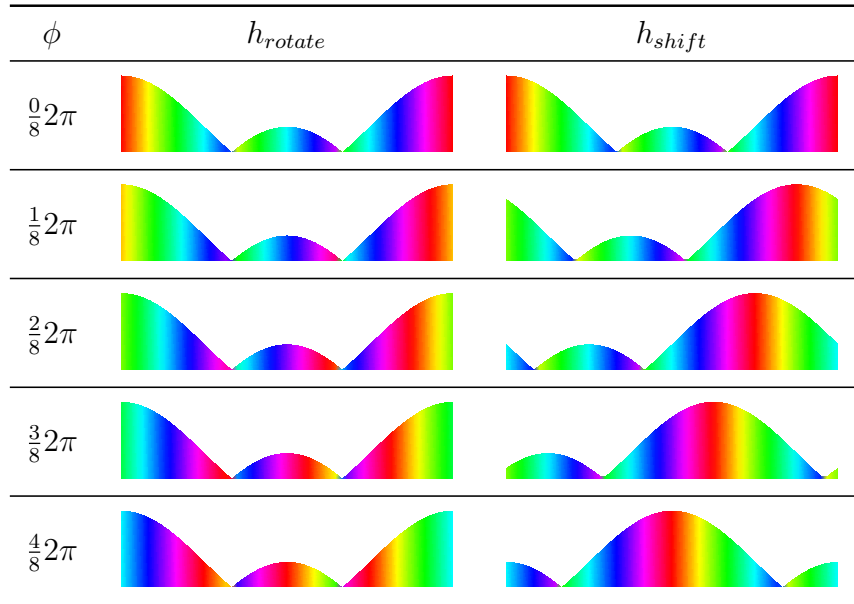
where  $x'_n$  is the transformed sequence. The effect of this transformation is visualized in the left column of Table 4.2 for various values of  $\phi$ . It is evident that as  $\phi$  varies, there is only a change in the *local* phase of the sequence while its *global* magnitude remains invariant. The second type of phase transformation, a *phase shift* or *position shift*, adds the phase amount  $k\phi$  to each harmonic  $k$  comprising  $x_n$ . The transformation is described by

$$h_{shift,\phi}(X_k) = X_k e^{ik\phi} \quad (4.1.6)$$

where  $X_k$  is the complex amplitude of the  $k^{th}$  harmonic of  $x_n$ . In the position domain, the transformation is given by

$$x'_n = x_{n + \frac{\phi}{2\pi}N}$$

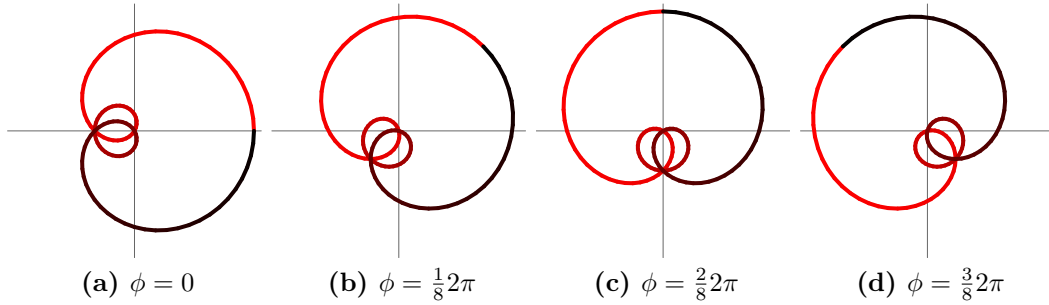
which simply shifts the position of all samples. The effect of this transformation is visualized in the right column of Table 4.2 for various values of  $\phi$ . Now we see that the effect of varying  $\phi$  is to shift (or rotate) the sequence along the domain; a consequence of the shift theorem of the Fourier transform [78]. It is evident that the transformation changes the *global* magnitude of the sequence (via shifting) while leaving its *local* phase invariant.



**Table 4.2:** Comparison of phase rotation and shift transformations of  $x_n = \{1\} + \{2\} + \{3\}$ . The plots show  $n$  (the domain) increasing in the  $+x$ -direction, magnitude along the  $+y$ -direction, and phase as hue.

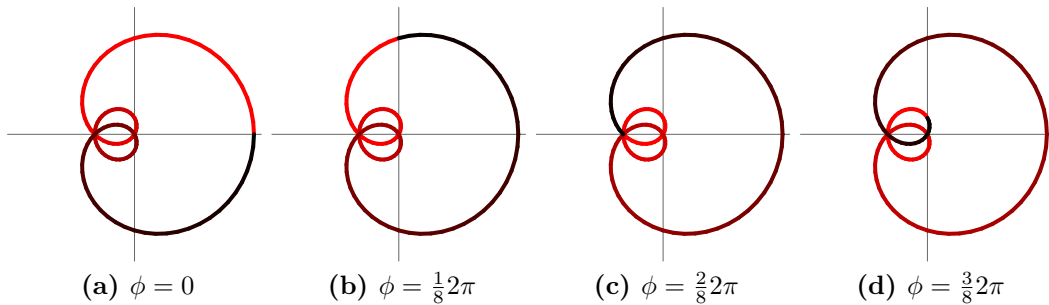
We now look at the effect of these two phase transformations (Eq. 4.1.4 and Eq. 4.1.6) on a curve plot of  $x_n$ . The effect of a phase rotation is visualized as a

curve plot in Fig. 4.1.1. It is clearly evident that this transformation results in a *global* rotation of the figure around the origin by  $\phi$  while leaving its *local* phase (starting point) invariant.



**Figure 4.1.1:** Effect of a phase rotation transformation on  $x_n = \{1\} + \{2\} + \{3\}$ . Red and black designate the start and end of the sequence, respectively.

The effect of a phase shift is visualized as a curve plot in Fig. 4.1.2. It is evident that this transformation realizes a *local* phase shift by  $\phi$  while leaving the *global* orientation of the figure invariant.



**Figure 4.1.2:** Effect of a phase shift transformation on  $x_n = \{1\} + \{2\} + \{3\}$ . Red and black designate the start and end of the sequence, respectively.

By looking at the two phase transformations on both the complex magnitude/phase and curve plots of  $x_n$ , it is clear that what one defines as a global or local property depends on the type of plotting method. With a magnitude/phase plot, the domain is identified as global while the codomain is identified as local.



Conversely, with a curve plot, the domain is identified as local while the codomain is identified as global. The reason for this is that when we construct a curve plot of  $x_n$ , we are mapping its codomain  $\mathbf{C}$  onto a new domain,  $\mathbf{R}^2$  (the Argand plane), as a displacement.

The last type of phase transformation considered is a *phase negation* where the phases of all frequency-domain samples are multiplied by  $-1$ . This transformation is given by

$$h_{neg}(X_k) = \bar{X}_k$$

where  $X_k = A_k e^{i\theta_k}$  and  $\bar{X}_k = A_k e^{i(-\theta_k)}$ . Phase negation is the same operation as taking the complex conjugate of the frequency samples. A phase negation reverses and conjugates the position-domain sequence described by the operation

$$x'_n = \bar{x}_{N-n}.$$

The effect of phase negation on a curve plot is to reflect the figure around the real axis while leaving the winding direction invariant.

### 4.1.3 Frequency Transformations

Frequency transformations are operations that change the frequencies of the harmonics comprising a complex sequence. Three frequency transformations will be discussed—frequency shift, frequency scale, and frequency negation.

A *frequency shift* is defined by

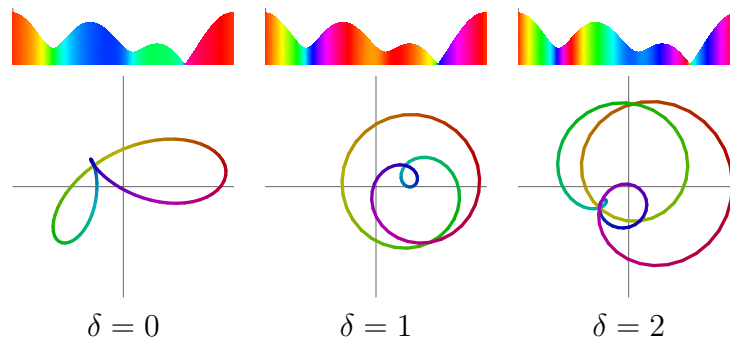
$$f_{shift,\delta}(X_k) = X_{k+\delta}$$

where  $\delta$  is a constant added to the frequency of each harmonic. As this operation

is simply to shift all samples in the frequency domain by a constant amount, it can also be performed by multiplying  $x_n$  by a complex sinusoid

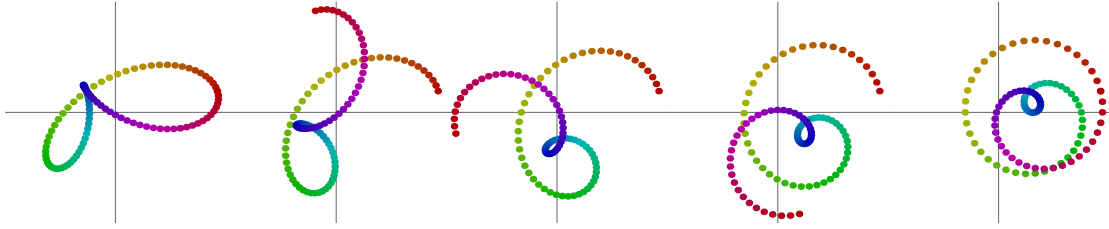
$$x'_n = x_n e^{i2\pi\delta n/N}.$$

The effect of frequency shifting on the magnitude/phase plot is to rotate the *local* phases by a linearly increasing amount while leaving the *global* magnitude invariant. Fig. 4.1.3 shows the results of frequency addition on  $x_n$  using magnitude/phase and curve plots.



**Figure 4.1.3:** Frequency shifting by varying amounts. A frequency shift causes the curve to wind more, but leaves the magnitude invariant as shown by magnitude/phase plots in the top row.

To make more clear how frequency shifting transforms the points in the sequence  $x_n$  we can look at a succession of fractional values of the addition amount  $\delta$  going from 0 to 1 using a vertex curve plot (Fig. 4.1.4). As the sample number increases, its rotational “velocity” increases proportionally. The first point ( $n = 0$ ) remains stationary while the last point ( $n = N - 1$ ) completes one full cycle. All other points move by the fractional amount  $n/N$  of a complete cycle.



**Figure 4.1.4:** Frequency shifting by fractional amounts  $\delta = 0, \frac{1}{4}, \frac{2}{4}, \frac{3}{4}, 1$  (left to right).

A *frequency scale* transformation is defined by

$$f_{scale,m}(X_k) = X_{\frac{k}{m}}$$

for  $\frac{k}{m} \in \mathbf{Z}$  and  $k \in [0, N)$ . Frequency scaling can be performed directly in the position domain through the corresponding operation

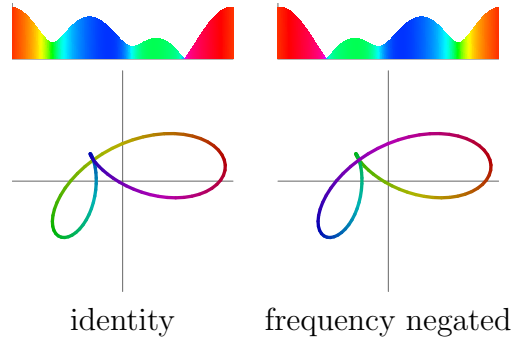
$$x'_n = x_{mn \bmod N} \tag{4.1.7}$$

which, unlike its frequency-domain counterpart, is well-defined for  $m = 0$ . Frequency scaling is analogous to performing an integer-valued pitch shift on a waveform. For example, the basis functions of the DFT are the set of  $x_n = e^{i2\pi n/N}$  pitch-shifted for all possible  $m$ . What is clear from Eq. 4.1.7 is that frequency multiplication leaves the values of position-domain samples unchanged while changing their order. To ensure that the mapping is injective (each index is mapped to a unique output) and thus there are no degenerate patterns  $m$  and  $N$  must be coprime. If  $N$  is made prime, then  $m$  can be varied freely and the mapping is always injective. Conversely, if  $N$  is a highly composite number, then a large amount of degenerate or exactly repeating patterns are produced.

A *frequency negation* is defined by

$$f_{neg}(X_k) = X_{N-k}$$

where  $k \in [0, N)$ . The effect of this transformation is to reverse both the position- and frequency-domain sequences. The curve plot of a frequency negated sequence is congruent to the original, but is drawn in the opposite direction.



**Figure 4.1.5:** Comparison between sequence and curve plots of frequency negation of  $\alpha_n = \{1, 0.1\} + \{2\} + \{-1\}$ . Frequency negation reverses the position-domain sequence.

#### 4.1.4 Frequency and Phase Negation

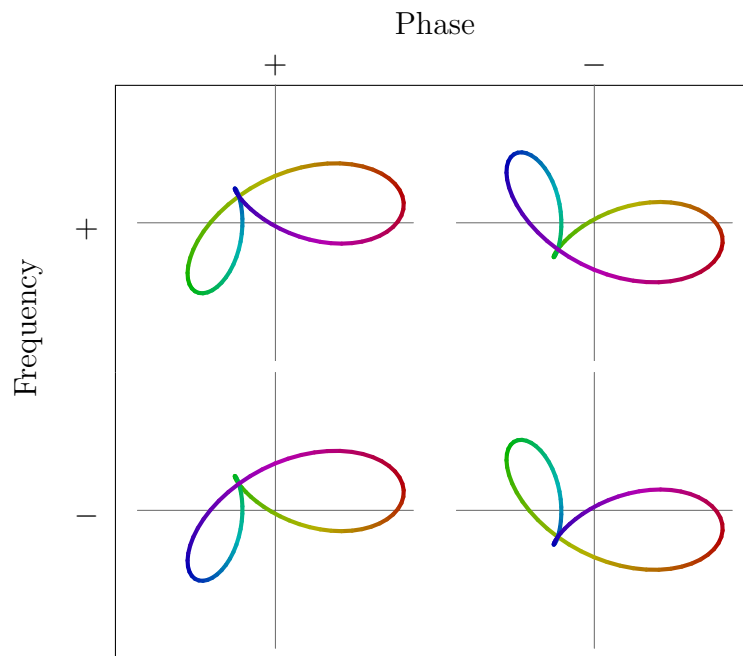
By combining a frequency and phase negation, we can effect a complex conjugation on the position-domain sequence. In the frequency domain, this transformation is

$$f_{neg}(h_{neg}(X_k)) = \bar{X}_{N-k}.$$

The combined effect in the position domain is

$$\begin{aligned} x'_n &= \bar{x}_{N-(N-n)} \\ &= \bar{x}_n \end{aligned}$$

which is clearly a complex conjugation of each position-domain sample. Since both the phase and frequency negation reverse the position-domain sequence they cancel one another out leaving the sequence order invariant. The only effect remaining is the complex conjugation due to the phase negation. Since  $|z| = |\bar{z}|$ , this transformation leaves the magnitudes of the position-domain sequence invariant. The individual and combined effects of frequency and phase negations are shown in Table 4.3.

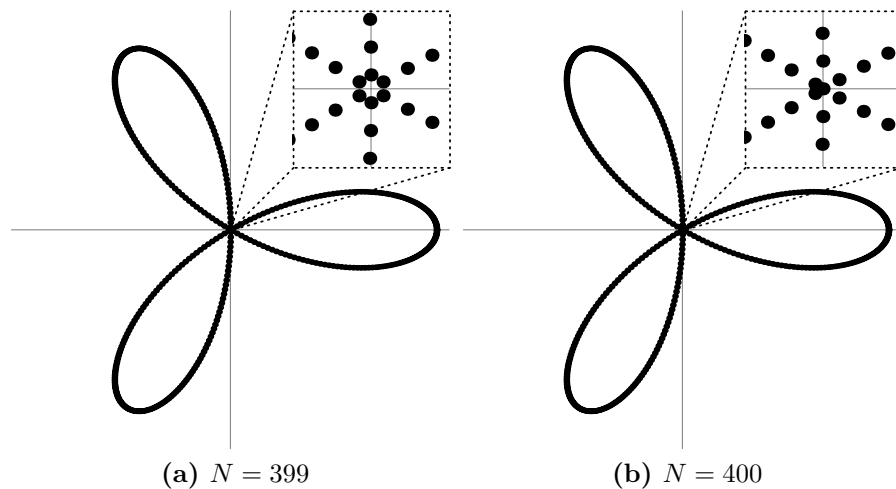


**Table 4.3:** Conjugation and reversal transformations. A + indicates the identity operation (no negation) while a - indicates a negation operation.

## 4.2 Planar Symmetry of Curves

Because we are working with discrete sequences of samples, we need to be precise in how we describe the symmetries of the resultant patterns. In theory, all symmetries should be formulated exactly in terms of the samples comprising the sequence under consideration. However, in practice, it can often times be more informative

to consider symmetries in a continuous sense—that is, on a more macroscopic scale—when the number of samples is effectively infinite. Fig. 4.2.1 illustrates how two curves having the same shape and symmetry “in the large” can have entirely different symmetry properties “in the small.” The curves shown in Fig. 4.2.1a and Fig. 4.2.1b are both trefoil curves, but have a number of points that differ by 1,  $N = 399$  and  $N = 400$  respectively. On a macroscopic scale, both shapes appear to have 3-fold cyclic ( $C_3$ ) and 3-fold dihedral ( $D_3$ ) symmetry. We can rotate the shape in increments of  $120^\circ$  or reflect it around the axes through the center of the lobes and it will remain unchanged. However, if we zoom in on the origin we see a different pattern of points for each curve. The curve with  $N = 399$  remains consistent with its apparent continuous symmetries ( $C_3$  and  $D_3$ ), however, the curve with  $N = 400$  is revealed to be a part of the less symmetric groups  $C_1$  and  $D_1$ .



**Figure 4.2.1:** Two curves with the same continuous symmetries, but differing discrete symmetries. The dashed boxes show a  $16\times$  magnification at the origin.

We define a *continuous symmetry* as a symmetry of an idealized pattern having an infinite number of points and a *discrete symmetry* as a symmetry of a pattern

with a finite number of points. The conventions are adopted from the notion of continuous and finite groups in group theory.

### 4.2.1 Cyclic Symmetry

A curve with continuous cyclic symmetry of degree  $m$  around the origin ( $C_m$ ) has non-zero amplitudes at harmonics

$$\begin{aligned} k &= \ell + lm \\ &= \dots, \ell - 2m, \ell - m, \ell, \ell + m, \ell + 2m, \dots \end{aligned} \quad (4.2.1)$$

where  $|m| \leq \frac{N}{2}$ ,  $0 < |\ell| < m$ ,  $l \in \mathbf{Z}$ , and the quantities  $\ell$  and  $\ell + m$  are coprime. For discrete cyclic symmetry, there is the additional condition  $N/m \in \mathbf{N}$ . A simple proof of this result follows.

We first observe that in general any curve with  $C_m$  symmetry must remain invariant when rotated about the origin by angles of  $\ell \frac{2\pi}{m}$  where  $\ell \in \mathbf{Z}$ . To check if the curve plot of a complex sequence  $x_n$  has  $C_m$  symmetry it is not enough to simply rotate the curve and check for equivalency since the starting position of the curve will also rotate. To counteract the change in starting position of the curve due to rotation, we need to shift the starting position back without rotating the curve. A slightly different, but equivalent observation is that for every shift in starting position of the curve by  $\frac{N}{m}$  there is a corresponding rotation by  $-\ell \frac{2\pi}{m} + 2\pi l$  for all  $l \in \mathbf{Z}$  that leaves the curve's sequence invariant. This symmetry transformation is stated formally as

$$\begin{aligned} X_k &= X_k e^{ik2\pi/m} e^{-i2\pi(\ell/m+l)} \\ &= X_k e^{i2\pi(k/m-\ell/m+l)} \end{aligned}$$

and gives the conditions for a curve plot of  $x_n$  to have  $C_m$  symmetry. The values of  $k$  that satisfy this condition are

$$\begin{aligned} 0 &= \frac{k}{m} - \frac{\ell}{m} + l \\ 0 &= k - \ell + lm \\ k &= \ell + lm. \end{aligned}$$

The general harmonic pattern function that will always produce curves with at most  $C_m$  symmetry is

$$\alpha_n = \sum_{k=\ell(m)} A_k \{k, \theta_k\} \quad (4.2.2)$$

where  $\ell(m) = \dots, \ell - 2m, \ell - m, \ell, \ell + m, \ell + 2m, \dots$  and  $|k| < N/2$ .

### 4.2.2 Dihedral Symmetry

A curve with dihedral symmetry  $D_m$  has  $C_m$  symmetry and harmonic phases

$$\theta_k = \phi + \pi l$$

where  $\phi$  is an arbitrary rotation constant and  $l \in \mathbf{Z}$ . This is readily shown by first recognizing that a curve having both  $C_m$  and  $D_1$  symmetries will have  $D_m$  symmetry. It is then enough to find the conditions for a curve sequence having  $D_1$  symmetry. The condition for  $D_1$  symmetry is that the complex sequence must equal itself with phases negated so that

$$\sum A_k e^{i(\theta_k - \phi)} e^{ik2\pi n/N} = \sum A_k e^{-i(\theta_k - \phi)} e^{ik2\pi n/N}$$



where  $\phi$  rotates the curve to make its symmetry axis coincide with the real axis. From this it is evident that

$$\begin{aligned}\theta_k - \phi &= -\theta_k + \phi + 2\pi l \\ 2\theta_k &= 2\phi + 2\pi l \\ \theta_k &= \phi + \pi l\end{aligned}$$

where  $l \in \mathbf{Z}$ . The general harmonic pattern function that will always produce curves with at most  $D_m$  symmetry is

$$\alpha_n = \sum_{k=\ell(m)} A_k \{k, \phi + \pi l\} \quad (4.2.3)$$

where  $\ell(m) = \dots, \ell - 2m, \ell - m, \ell, \ell + m, \ell + 2m, \dots$ ,  $l \in \mathbf{Z}$ , and  $|k| < N/2$ . Comparing Eq. 4.2.3 with Eq. 4.2.2 it is apparent that what distinguishes a dihedral-symmetric curve from a cyclic-symmetric curve is a rigid constraint on the possible harmonic phases. The phases across all harmonics must be equal to the same amount plus an integer multiple of  $\pi$ . Adding an odd integer multiple of  $\pi$  to a phase is the same as negating the amplitude. Therefore, another way of interpreting the constraint is that all harmonics must have the same phase with the amplitude being any positive or negative real value. This means that the dihedral symmetry of a curve is preserved under negation of harmonic amplitudes.

### 4.3 Regular (Star) Polygon Patterns

If we rewrite Eq. 4.2.2 above in the equivalent form

$$\alpha_n = \{\ell\} \sum_{k=0(1)} A_k \{mk, \theta_k\} \quad (4.3.1)$$

where  $|k| \leq \frac{N}{2m}$ , it becomes evident that all curves with cyclic symmetry are derived by scaling and shifting the spectrum of a curve having all harmonics up to the  $(\frac{N}{2m})^{th}$  harmonic. The scaling amount  $m$  determines the degree of cyclic symmetry of the curve, while the shifting amount  $\ell$  determines its winding pattern. The variable  $\ell$  distinguishes between three different types of curve patterns:

$$\left\{ \begin{array}{ll} \ell = 0 & \text{static-period curves} \\ |\ell| = 1 & \text{consecutive-period curves} \\ |\ell| > 1 & \text{circulating-period curves} \end{array} \right.$$

When  $\ell = 0$ , the curve is comprised of  $m$  cycles through the base curve resulting from  $m = 1$ . When  $|\ell| = 1$ , the resulting curve is comprised of a single motif repeating every  $2\pi/m$  radians in a cyclically symmetric fashion thus aligned to the vertices of a regular polygon. Likewise, when  $|\ell| > 1$ , the motif repeats itself every  $2\pi\ell/m$  radians coinciding with a regular star polygon pattern.

When  $\ell = 1$ ,  $A_k = A_{-k}$ , and  $\theta_k = \theta_{-k}$ , Eq. 4.3.1 simplifies to

$$\alpha_n = \{1\} \sum_{k=0(1)} A_k \cdot 2 \operatorname{Re}\{mk, \theta_k\} \quad (4.3.2)$$

which is equivalent to the polar equation

$$r = 2 \sum_{k=0(1)} A_k \cos[2\pi(mk\phi + \theta_k)]$$

for  $\phi = 0, \frac{1}{N}, \frac{2}{N}, \dots, \frac{N-1}{N}$ . Eq. 4.3.2 is thus the general harmonic pattern function that describes all polar curves constructed from Fourier series.

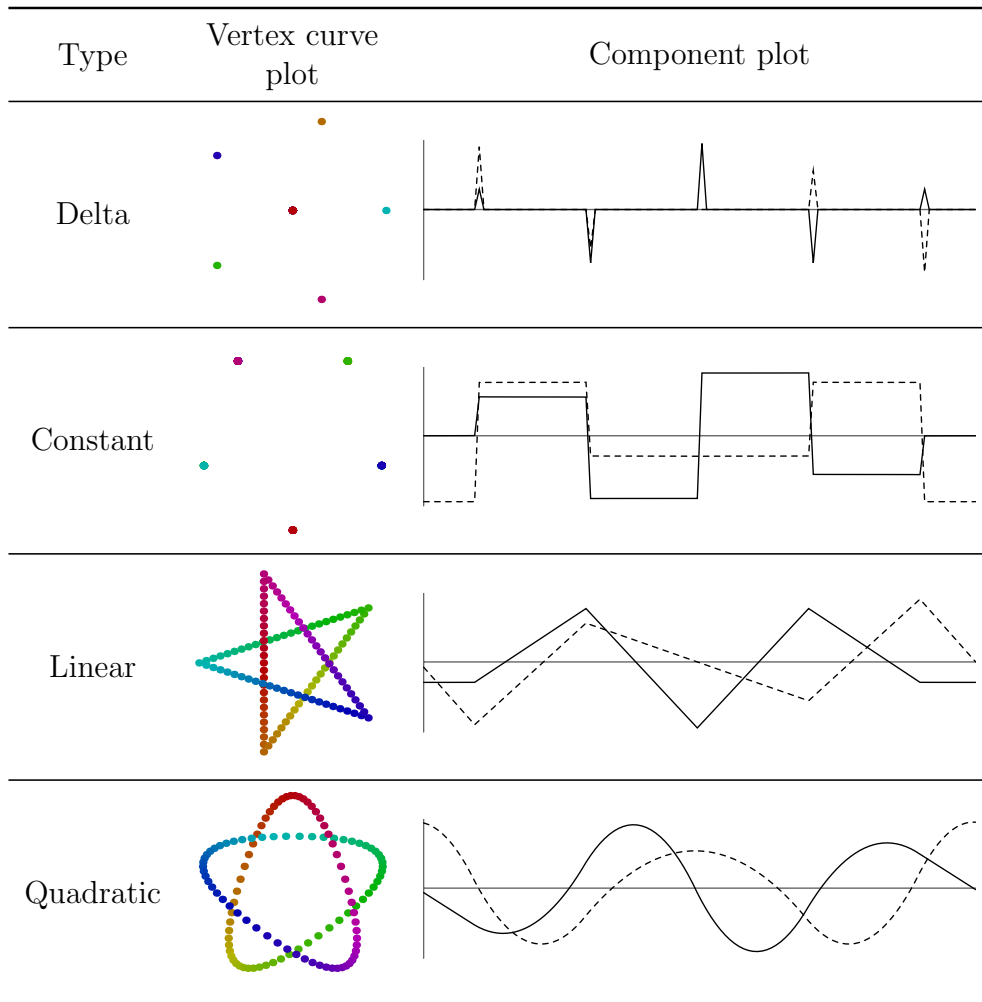
## 4.4 Interpolation Patterns

An *interpolation pattern* is a pattern that is either comprised of or approximates a relatively small sequence of “key” points connected by a polynomial function. Interpolation patterns help explain certain attributes of planar curves, such as cusps, jumps, and rectilinear sections. They also help in distinguishing between various waveforms such as impulse, saw, and triangle waves.

Interpolation patterns are characterized by the degree of their interpolating polynomial. Table 4.4 lists several interpolating polynomial types by their name and mathematical function. Moving between the different types of interpolation patterns is accomplished through integration (increasing polynomial degree) or differentiation (decreasing polynomial degree). An example interpolation pattern showing delta, constant, linear, and quadratic interpolating polynomials is shown in Fig. 4.4.1.

Type	Polynomial
Delta	0
Constant	$C_0$
Linear	$C_1x + C_0$
Quadratic	$C_2x^2 + C_1x + C_0$

**Table 4.4:** Types of interpolation functions



**Figure 4.4.1:** An interpolation pattern with different types of interpolating polynomials. The constant, linear, and quadratic interpolation patterns are obtained from successive integrations of the delta interpolation pattern.

Calculus of complex sequences are key to understanding certain features of

planar curves that arise often, such as cusps and rectilinear sections. Taking a dynamical perspective, we define the complex sequences  $x_t''$ ,  $x_t'$ , and  $x_t$  as the acceleration, velocity, and position of a particle from time  $t = 0$  to  $t = N - 1$  where  $x_t'' = \frac{d}{dt}x_t'$  and  $x_t' = \frac{d}{dt}x_t$ . In the first case, we consider some  $t$  where  $x_t' = 0$ , that is, the particle's velocity curve crosses through the origin of the complex plane. Integrating  $x_t'$  once, we obtain  $x_t = C$  where  $C$  is a constant. This constant indicates that the position of the particle remains invariant over time. A cusp on a curve, therefore, is a place where the first derivative is zero. In the second case, we consider what happens when at some time  $t$ ,  $x_t'' = (0, 0)$ , i.e., the particle's acceleration curve crosses the origin. Integrating  $x_t''$  twice, we obtain  $x_t = Dt + C$  where  $D$  and  $C$  are arbitrary constants. Therefore, when the particle's acceleration goes to zero, its position becomes a linear function of time. To summarize, wherever the first derivative of a curve goes to zero, a cusp is formed and wherever the second derivative of a curve goes to zero, a lineal region exists. Generalizing this further, wherever the  $n^{\text{th}}$  derivative of a curve goes to zero, it becomes a polynomial of degree  $n - 1$  in that region.

## 4.5 Unit Circle Patterns

A large assortment of patterns can be classified as *unit circle patterns*—patterns comprised of points lying on the unit circle. Given a complex sequence  $x$ , this requires  $|x_n| = 1$  for all  $n \in [0, N)$ . It must be noted that unit circle patterns are the position-domain analog of the all-pass class of frequency responses used in filter design. The underlying mathematical principle is a function that operates only on the phase component (argument) of a complex number leaving its magnitude invariant thus having the general form  $Ae^{jf(\theta)}$ . The importance of this symmetry

with regards to synthesizing audio/visual patterns is significant. It means we can derive a parameter space that is guaranteed to generate well-behaved patterns. For audio synthesis, this means that (real) waveforms will always have an amplitude less than or equal to 1 (because the complex waveform always has a magnitude of 1) making automatic gain control or normalization unnecessary. In terms of visual patterns, it means that all patterns are guaranteed to lie within a well-defined region, a unit disc. Unit circle patterns remain on the unit circle under inversion, phase shifting and negating, and frequency shifting, scaling, and negating.

A general harmonic pattern function that results in a unit circle pattern is given by

$$\alpha_n = \frac{\sum_{k=0}^M A_k \{k, \theta_k\}}{\sum_{k=0}^M A_{M-k} \{k, -\theta_{M-k}\}}. \quad (4.5.1)$$

The main operating principle is division of a complex sequence by itself having undergone a magnitude-preserving phase transformation. Each element of the quotient sequence will then have a magnitude of 1, but non-trivial phase. This is due to the simple fact that if  $|x_n| = |y_n|$  then  $\frac{|x_n|}{|y_n|} = 1$ . We will now show that Eq. 4.5.1 is derived from a series of magnitude preserving frequency-domain transformations. If the numerator frequency samples are given by  $X_k$  then the denominator is the result of a magnitude-preserving phase transformation on  $X_k$  given by  $Y_k = g(X_k)$ . It will be shown that  $g(X_k)$  is a combination of a phase negation, frequency negation, and frequency shift. Expanding  $g(X_k)$  as a series of

transformations we obtain

$$\begin{aligned}
Y_k = g(X_k) &= f_{shift, M-N}(f_{neg}(h_{neg}(X_k))) \\
&= f_{shift, M-N}(f_{neg}(\bar{X}_k)) \\
&= f_{shift, M-N}(\bar{X}_{N-k}) \\
&= \bar{X}_{(N-k)+(M-N)}
\end{aligned}$$

where the frequency shift amount is  $M - N$  or just  $M$ . This simplifies further to

$$Y_k = \bar{X}_{M-k}. \quad (4.5.2)$$

If we limit the interval of non-zero amplitude  $X_k$  to  $0 \leq k \leq M$ , then  $Y_k$  fall into the interval  $M \leq M - k \leq 0$  which is equivalent to  $0 \leq k \leq M$ . The harmonic pattern function can be written as

$$\alpha_n = \frac{\sum_{k=0}^M X_k e^{i2\pi kn/N}}{\sum_{k=0}^M \bar{X}_{M-k} e^{i2\pi kn/N}}$$

or in parametric form as

$$\alpha_n = \frac{\sum_{k=0}^M A_k \{k, \theta_k\}}{\sum_{k=0}^M A_{M-k} \{k, -\theta_{M-k}\}}$$

which is Eq. 4.5.1. Eq. 4.5.2 can also be performed directly in the position domain using the corresponding transformation

$$y_n = \bar{x}_n e^{i2\pi nM/N}$$

where  $M$  is now interpreted to be the highest non-zero amplitude harmonic present

in  $x_n$ . Eq. 4.5.1 can be computed efficiently in the position domain using the formula

$$\begin{aligned}\alpha_n &= \frac{x_n}{\bar{x}_n e^{i2\pi nM/N}} \\ &= \frac{x_n}{\bar{x}_n} e^{-i2\pi nM/N}.\end{aligned}\tag{4.5.3}$$

The advantage of the position-domain approach is that it can be applied to any complex sequence without needing to know its frequency-domain parameterization. To further understand its effect on  $x_n$ , we substitute  $x_n = A_n e^{i\theta_n}$  into Eq. 4.5.3 obtaining

$$\begin{aligned}\alpha_n &= \frac{A_n e^{i\theta_n}}{A_n e^{-i\theta_n}} e^{-i2\pi nM/N} \\ &= e^{i2\theta_n} e^{-i2\pi nM/N}.\end{aligned}$$

This makes it clear that for each  $x_n$  its magnitude is normalized to 1 and its phase angle is doubled. Since the amplitudes of each component drop out, any sequences that are same up to some global scaling factor produce the same unit circle pattern.

## 4.6 Inversion-symmetric Patterns

Inversion-symmetric patterns remain invariant under complex inversion up to a reversal and shift in position. An important characteristic of these patterns is that they exhibit symmetry around the equator of the Riemann sphere under stereographic projection. Inversion-symmetric patterns remain inversion symmetric under inversion, phase shifting and negating, and frequency shifting, scaling, and negating.



Inversion-symmetric patterns are given by

$$\alpha_n = \frac{\sum_{k=0}^M A_k \{k, \theta_k\}}{\sum_{k=0}^M e^{ik\phi} A_{M-k} \{k, \theta_{M-k}\}}$$

which is similar to the formula for a unit circle pattern (Eq. 4.5.1) except for lack of phase negation and the  $e^{ik\phi}$  (position-shifting) factor in the denominator. The variable  $\phi$  can be freely adjusted. For the special case of  $\phi = 0$ , a unit circle pattern results. The effect of the  $e^{ik\phi}$  term is to shift the position-domain sequence by  $\frac{\phi}{2\pi}N$  indices; possibly a non-integer amount. Like unit circle patterns, inversion-symmetric patterns can be generated directly in the position domain given a complex sequence  $x_n$ , but with the restriction that  $\frac{\phi}{2\pi}N \in \mathbf{Z}$ . We can write the denominator,  $Y_k$ , as a transformation of the numerator,  $X_k$ , as

$$Y_k = e^{ik\phi} X_{M-k}$$

which in the position domain translates to the transformation

$$y_n = x_{\frac{\phi}{2\pi}N-n} e^{i2\pi nM/N}.$$

An inversion-symmetric pattern can thus be generated entirely in the position domain given an arbitrary complex sequence  $x_n$  through the transformation

$$\begin{aligned} \alpha_n &= \frac{x_n}{y_n} \\ &= \frac{x_n}{x_{\frac{\phi}{2\pi}N-n}} e^{-i2\pi nM/N} \end{aligned} \tag{4.6.1}$$

where  $\frac{\phi}{2\pi}N \in \mathbf{Z}$ . We will now show that inverting inversion-symmetric sequences effects a reversal and shift in the position domain. If we substitute  $x_n = A_n e^{i\theta_n}$

and  $m = \frac{\phi}{2\pi}N$  into Eq. 4.6.1, we obtain

$$\begin{aligned}\alpha_n &= \frac{A_n e^{i\theta_n}}{A_{m-n} e^{i\theta_{m-n}}} \\ &= \frac{A_n}{A_{m-n}} e^{i(\theta_n - \theta_{m-n})}\end{aligned}\tag{4.6.2}$$

Under inversion this becomes

$$(\alpha_n)^{-1} = \frac{A_{m-n}}{A_n} e^{-i(\theta_n - \theta_{m-n})}.$$

If we now reverse the position-domain sequence (negating all index subscripts)

$$(\alpha_{-n})^{-1} = \frac{A_{n-m}}{A_{-n}} e^{-i(\theta_{-n} - \theta_{n-m})}$$

and shift it by  $m$  (adding  $m$  to all index subscripts)

$$\begin{aligned}(\alpha_{m-n})^{-1} &= \frac{A_n}{A_{m-n}} e^{-i(\theta_{m-n} - \theta_n)} \\ &= \frac{A_n}{A_{m-n}} e^{i(\theta_n - \theta_{m-n})}\end{aligned}$$

we arrive back at Eq. 4.6.2. Thus, an inversion-symmetric sequence under inversion is reversed and shifted by  $\frac{\phi}{2\pi}N$  samples in the position domain.

# 5. Taxonomy of Harmonic Patterns

---

The purpose of this section is to identify and analyze the various types of patterns that can be produced from the most basic configurations of harmonics in the harmonic pattern function. Many well-studied planar curves can be derived exactly or closely approximated by the harmonic pattern function without any modification. The patterns are discussed in increasing number of harmonics since new general characteristics and expressions of patterns tend to emerge as harmonics are added. Furthermore, complex patterns built from many harmonics can often be understood in terms of compositions of simpler patterns with fewer harmonics.

For each additional degree of harmonics, the following points will be discussed:

- emergent qualities not present or apparent with fewer harmonics
- connections to archetypical sonic and graphical shapes
- when possible, how new patterns are comprised of subpatterns
- when possible, how new patterns subsume or resemble previously discussed patterns

We will define the order of an harmonic pattern function as the sum of harmonic components in the numerator and denominator in reduced fraction form excluding

any constants alone in either the numerator or denominator. One desirable consequence of defining the order of a harmonic pattern function in this way is that its inverse is of the same order. The reduced fraction form of a harmonic pattern function is the equivalent formula with harmonic numbers reduced until there is at least one constant term,  $\{0\}$ , in either the numerator or denominator. The possible harmonic pattern function formulae up to order 4 are given in Table 5.1.

Order	Harmonic pattern function
1	$A_1\{k, \theta_1\}$
2	$A_1\{k_1, \theta_1\} + A_2\{k_2, \theta_2\}$
2	$\frac{1}{A_1\{k_1, \theta_1\} + A_2\{k_2, \theta_2\}}$
3	$A_1\{k_1, \theta_1\} + A_2\{k_2, \theta_2\} + A_3\{k_3, \theta_3\}$
3	$\frac{1}{A_1\{k_1, \theta_1\} + A_2\{k_2, \theta_2\} + A_3\{k_3, \theta_3\}}$
4	$A_1\{k_1, \theta_1\} + A_2\{k_2, \theta_2\} + A_3\{k_3, \theta_3\} + A_4\{k_4, \theta_4\}$
4	$\frac{1}{A_1\{k_1, \theta_1\} + A_2\{k_2, \theta_2\} + A_3\{k_3, \theta_3\} + A_4\{k_4, \theta_4\}}$
4	$\frac{1 + A_1\{k_1, \theta_1\}}{A_2\{k_2, \theta_2\} + A_3\{k_3, \theta_3\}}$

**Table 5.1:** Unique harmonic pattern function formulae up to order 4.

## 5.1 Order 1

The two defining characteristics of single harmonic patterns are constant magnitude and constant linear change in phase. The elements of a sequence form a cyclic group and, therefore, all generated curves exhibit dihedral symmetry. Some fundamental visual representations include point, circle, line, helix, toroidal helix, regular polygon and star polygon, zigzag, and plane wave. Sonically, a single harmonic is a pure tone that can be either audible or non-audible. Non-audible harmonics, either having too low of an amplitude or lying outside the audible range of hearing, can still be perceptually relevant as modulation effects, such as two slowly beating harmonics.

Patterns produced from one harmonic have the general harmonic pattern function

$$\alpha_n = A\{\ell, \theta\}$$

where  $\ell$  is the frequency-shifting amount,  $a$  is the amplitude, and  $\theta$  is the phase angle. Since  $A$  and  $\theta$  act as similarity transformations (a scaling and rotation, respectively), we need only consider  $\alpha_n = \{\ell\}$  to describe all unique shapes.

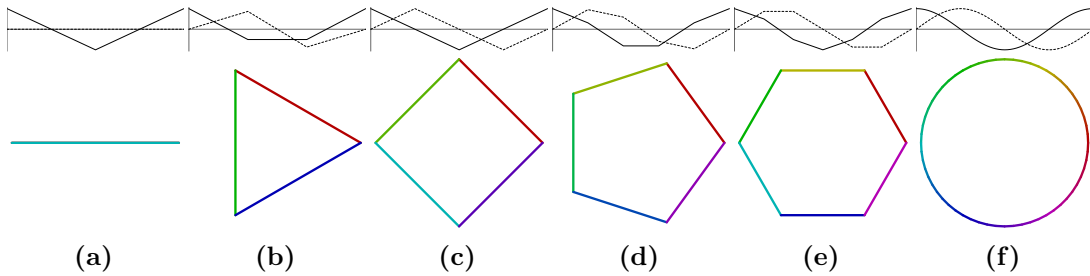
### 5.1.1 Constant

A constant is a sequence comprised of a repeating value. Its harmonic pattern function is  $\alpha_n = A\{0, \theta\}$ . Sonically, this correlates to a non-audible DC offset and thus is somewhat irrelevant to sound synthesis. However, a single complex number can describe the position of a sound in space granted it lies on a plane. Graphically, this sequence produces a collection of points located at the same position  $(x, y) = (A \cos 2\pi\theta, A \sin 2\pi\theta)$  on the complex plane. In mathematics, a

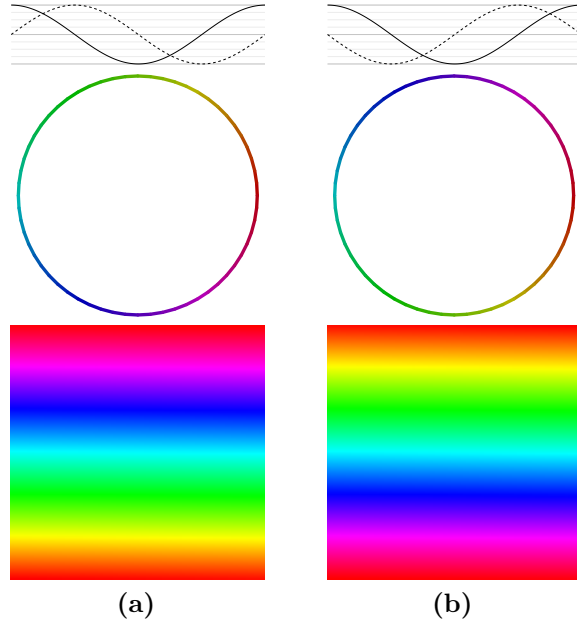
multiplicity is an occurrence where multiple solutions of an equation have the same value. The term multiplicity is used in this context to describe a geometric structure comprised of several points having the same value. While graphically, a multiplicity appears identical to a point, behaviorally, the two are quite different. This difference in behavior is analyzed more in depth in the next section when two harmonic shapes are discussed.

### 5.1.2 Regular Polygon

For  $|\ell| = 1$ , we obtain the vertices of all  $N$ -sided regular polygons (Fig. 5.1.1). For low  $N$ , we get the family of  $N$ -gons and as  $N \rightarrow \infty$ , we approach a circle. When  $m = -1$ , we obtain the same polygon for the case with  $\ell = 1$  and equivalent  $N$ , but with opposite winding direction. In general, when  $\ell > 0$ , the polygons wind in the counter-clockwise direction and when  $\ell < 0$ , the polygons wind in the clockwise direction (Fig. 5.1.2).



**Figure 5.1.1:** Regular polygons constructed from  $\alpha_n = \{1\}$  for (a-e)  $N = 2, 3, \dots, 6$  and (f)  $N = 60$ .

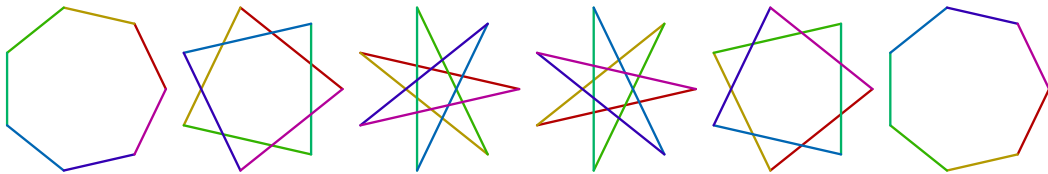


**Figure 5.1.2:** Negating frequency results in an opposite winding direction. Shown for (a)  $\alpha_n = \{1\}$  and (b)  $\alpha_n = \{-1\}$ .

The raster plots of  $\alpha_n = \{\pm 1\}$  that are shown in Fig. 5.1.2 display a small amount of tilt sloping downwards from the left side to the right side. The tilt arises due to the fact that the underlying topology of the domain of the raster plot is a toroidal helix. Although the tilt is not visually objectionable within a single raster plot, it becomes a noticeable problem when attempting to tile multiple plots. Tiling in the vertical direction is seamless, however, in the horizontal direction there is a one pixel offset. In order to obtain a smooth tiling horizontally, the raster plot data must be accessed using a fractional offset in the vertical direction to compensate for the tilting. Given a texture coordinate  $(r, s)$  where  $(0, 0)$  is the bottom-left corner and  $(1, 1)$  is the top-right corner, the corrected  $s$  coordinate is  $s' = s + r/\sqrt{N}$ .

### 5.1.3 Regular Star Polygon

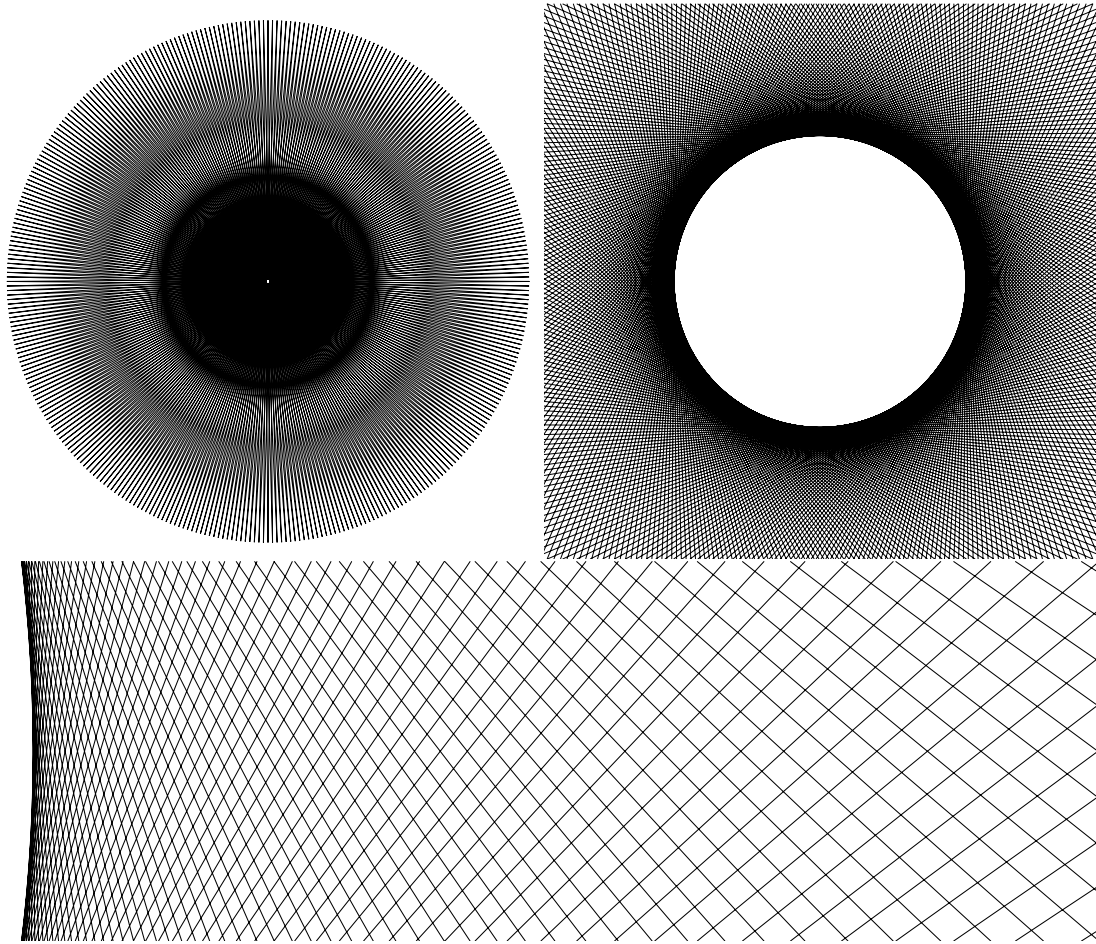
For  $|\ell| > 1, N \geq 5$ , we obtain the set of regular star polygons with Schläfli symbol  $\{N/\ell\}$ . The number of vertices of the star is  $a$  where  $a/b = N/\ell$  and  $a$  and  $b$  are coprime. The multiplicity of the star, i.e., the multiplicity of each vertex, is  $N/a$ . If  $N$  is prime, then all star polygons for  $|\ell| > 1$  have a multiplicity of 1. We also observe that for  $\ell$  and  $N$  coprime,  $\ell \in [1, N/2)$ , we obtain the  $(\ell - 1)^{th}$  stellation of a regular  $N$ -gon. The number of intersections of a non-degenerate star polygon  $\{N/\ell\}$  is  $N \cdot (\ell - 1)$ . The set of all regular star polygons  $\ell \in [0, N)$  form the basis functions of the complex discrete Fourier transform [35].



**Figure 5.1.3:** Regular star polygons produced from  $\alpha_n = \{\ell\}$  for  $N = 7$  and  $\ell = 1, 2, \dots, 6$  (left to right).

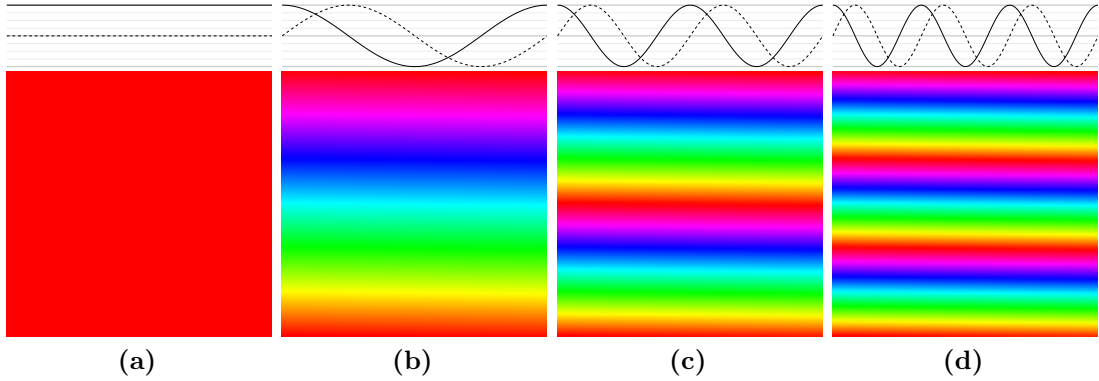
When  $\ell = \lceil \frac{N}{2} - 1 \rceil$ , the star polygon has the highest possible density. Visually, these types of star polygons produce the most complex patterns as they contain the maximum number of intersections for a star polygon with  $N$  vertices,  $N(\lceil \frac{N}{2} - 1 \rceil - 1)$ . Fig. 5.1.4 shows the densest star polygon with  $N = 360$  having a total of  $360 \cdot 178 = 64080$  intersections.





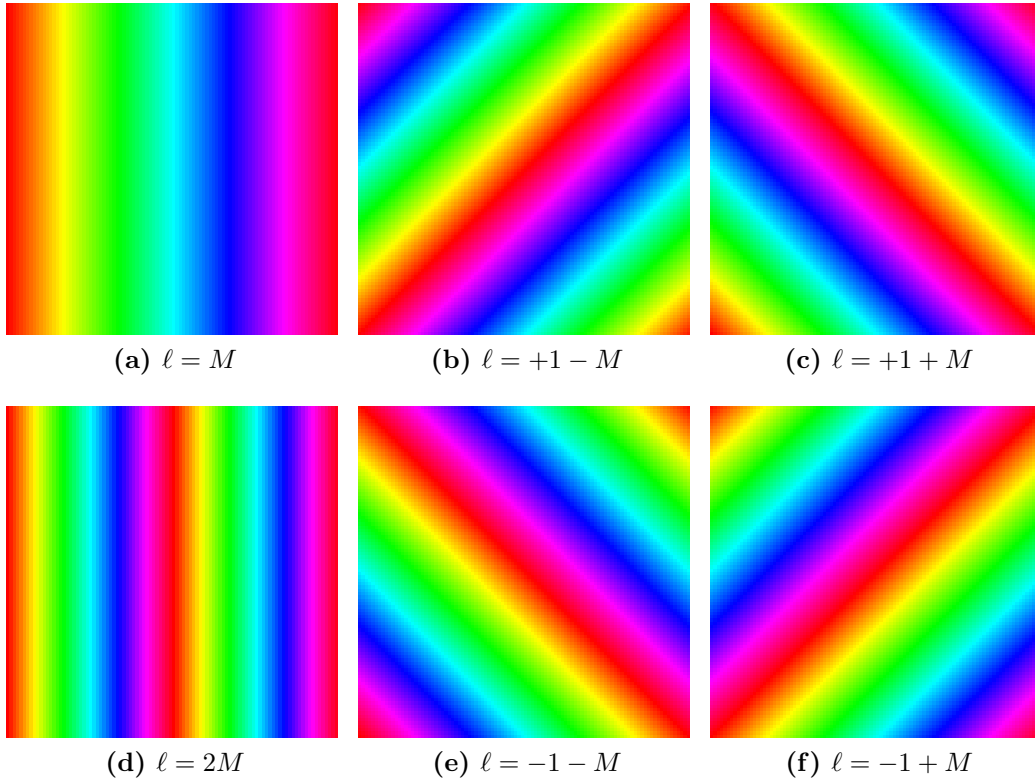
**Figure 5.1.4:** Densest  $N = 360$  star polygon at  $1\times$  magnification (top-left),  $64\times$  magnification (top-right) and  $1024\times$  magnification (bottom).

For large  $N$  and small  $\ell$ ,  $|\ell| > 2$ , the curve plot approaches a multiply wound circle. The component and raster plots reveal the signal to be the various harmonics of a complex sinusoid. The raster plot in particular reveals a family of approximate plane waves in the  $+y$  direction.



**Figure 5.1.5:** Component and raster plots of complex sinusoids for  $N = 100^2$  and  $\ell = 0, 1, 2, 3$  (a-d). Raster plots reveal approximate plane waves in the  $+y$  direction.

When  $N = M^2$  and  $\ell = M$ , the raster plot reveals a peculiar characteristic. We obtain exact plane waves in the  $+x$  direction. The entire set of plane waves in the  $x$  direction are produced from  $\ell = mM, m \in [0, M)$ . Furthermore, the basis functions of the the two-dimensional DFT,  $e^{i2\pi(\ell_x n_x + \ell_y n_y)/M}$ , can be approximated by  $\ell = \ell_x + \ell_y M$ . In principle, this technique can be extended to an  $n$ -dimensional raster plot approximating an  $n$ -dimensional DFT.



**Figure 5.1.6:** Raster plots displaying how one-dimensional complex sinusoids can approximate plane waves. The plots show various harmonic numbers,  $\ell$ , for  $M = 100$ .

### 5.1.4 Interleaved Harmonic

We define an *interleaved harmonic* as a pattern whose sequence is comprised of alternating subsequences of complex sinusoids having the same frequency and amplitude, but different phases. The subsequences form cosets of the original sequence so that given  $P$  subsequences the first subsequence consists of the elements  $n = 0, P, 2P, \dots$ , the second  $n = 1, P + 1, 2P + 1$ , the third  $n = 2, P + 2, 2P + 2$ , and so on. The harmonic pattern function of  $P$  interleaved harmonics is

$$\alpha_n = \left\{ p \frac{N}{P} + \ell \right\} \quad (5.1.1)$$

where  $p \in \mathbf{Z}$  is a permutation parameter. We can determine the formula for each subsequence by expanding Eq. 5.1.1 into complex sinusoidal form

$$\alpha_n = e^{i(2\pi n/N)(pN/P+\ell)}$$

then making the substitution  $n \rightarrow Pn + j$  to obtain the  $j^{\text{th}}$  subsequence

$$\alpha_{Pn+j} = e^{i(2\pi(Pn+j)/N)(pN/P+\ell)}$$

where  $n$  now lies in the interval  $[0, \frac{N}{P})$ . Simplifying, we get

$$\begin{aligned} \alpha_{Pn+j} &= e^{i(2\pi(Pn+j)/N)(pN/P+\ell)} \\ &= e^{i2\pi[(Pn/N)(pN/P+\ell)+(j/N)(pN/P+\ell)]} \\ &= e^{i(2\pi n/N)(pN+\ell P)} e^{i2\pi j(p/P+\ell/N)} \\ &= e^{i(2\pi n/N)\ell P} e^{i2\pi j(p/P+\ell/N)} \end{aligned}$$

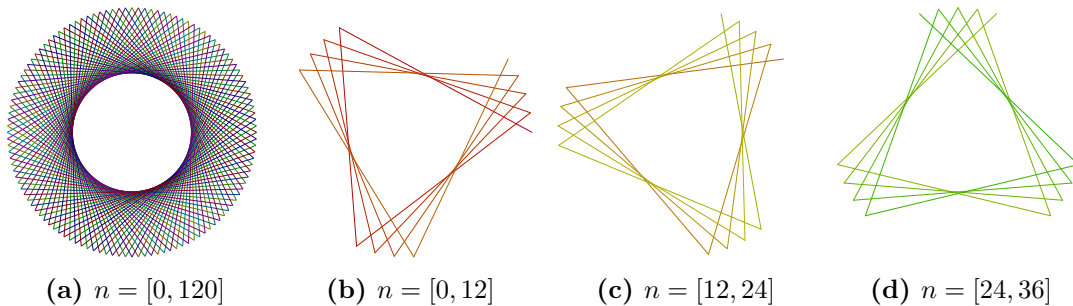
which translates to the harmonic pattern function

$$\alpha_{Pn+j} = \left\{ \ell P, j \left( \frac{p}{P} + \frac{\ell}{N} \right) \right\} \quad (5.1.2)$$

The harmonic subsequences thus have the same frequency that is  $P$  times the frequency of the original sequence, but different phases that depend in a complex way on several variables. The parameter  $p$  has the effect of rotating the  $j^{\text{th}}$  subsequence by  $jp(2\pi/P)$  radians. Additionally, each subsequence is rotated by a smaller increment  $j\ell(2\pi/N)$  radians as a consequence of being interleaved.

### 5.1.5 Simple Motion

We will use the term motion to mean a gradual change in shape, size, position, and/or orientation of an object over time. With a single harmonic, the only kind of mobile object that is expressible is a star polygon (including a point) rotating around the origin with uniform angular velocity. This is accomplished by taking subsequences of the sequence  $\alpha_n$  as a temporal succession of spatial snapshots. For example, taking the star polygon given by  $\alpha_n = \{41\}$  with  $N = 120$  (Fig. 5.1.7a), we can take every successive subsequence of 12 samples as representing a path in space. On each iteration of time, the next subsequence of 12 samples is plotted. The first three subsequences shown in Fig. 5.1.7b, Fig. 5.1.7c, and Fig. 5.1.7d illustrate how a rotating triangle is embedded within the entire space-time star polygon.

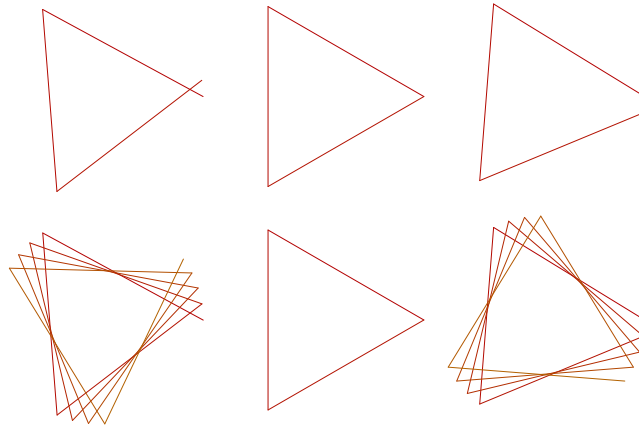


**Figure 5.1.7:** A single harmonic producing a rotating triangle. Figure (a) shows the entire space-time shape specified by  $\alpha_n = \{41\}$  with  $N = 120$  and (b-d) show a succession of length 12 subsequences.

The manner in which the entire sequence is divided into subsequences determines characteristics of how both the object and its motion are perceived. First, we define  $N_s$  as the number of elements in our spatial subsequences and  $N_t$  as the total number of spatial subsequences so that  $N = N_s N_t$ . Since we want to isolate the effects of  $N_s$  and  $N_t$  we will say that  $N$  is very large. When  $N_s = 1$ , we get a

single point rotating around the origin with a uniform angular velocity. On the other extreme, when  $N_s = N$ , we obtain a stationary star polygon. Thus, when  $N_s \ll N_t$  we get more finely-resolved and/or complex motion with reduced object complexity, while when  $N_s \gg N_t$ , the converse is true.

The most geometrically accurate and slowest (possibly stationary) rotating star polygon is obtained by choosing  $N_t = N/m$  rounded to the nearest integer where  $m$  is the number of vertices of the polygon. If  $N/m \in \mathbf{N}$ , then the polygon is stationary, otherwise it rotates by  $\pm 2\pi/N$  radians every  $N_s = m$  elements depending on whether  $N/m - \lfloor N/m \rfloor \gtrless \frac{1}{2}$ . If  $N/m \in \mathbf{N}$ , then we can add  $\pm 1$  to  $N_t$  to obtain motion in the counter-clockwise or clockwise direction. The top row of Fig. 5.1.8 shows the first four elements of the sequences  $\{41\}$ ,  $\{40\}$ , and  $\{39\}$  with  $N = 120$ . With  $\{41\}$  the last triangle vertex *overshoots* the first vertex while with  $\{39\}$  the last vertex *undershoots* the first vertex. With  $\{40\}$ , the first and last triangle vertices coincide (hence no motion). The bottom row of Fig. 5.1.8 shows a few more time steps of each sequence.



**Figure 5.1.8:** Top row, left to right: The first four elements of  $\{41\}$ ,  $\{40\}$ , and  $\{39\}$  with  $N = 120$ . Bottom row, left to right: The first twelve elements of  $\{41\}$ ,  $\{40\}$ , and  $\{39\}$  with  $N = 120$ .

Normally, a traveling wave in one-dimension is described by  $u(x, t) = Ae^{i(kx - \omega t + \theta)}$

where  $A$  is the amplitude,  $k$  and  $\omega$  are the spatial and temporal frequencies,  $\theta$  is the phase, and  $x$  and  $t$  represent spatial and temporal position. Rewriting  $u(x, t)$  as  $Ae^{i\theta}e^{ikx}e^{-i\omega t}$ , we see that it is the product of three independent components—a complex amplitude ( $Ae^{i\theta}$ ), a spatial unit complex sinusoid ( $e^{ikx}$ ), and a temporal unit complex sinusoid ( $e^{-i\omega t}$ ). The temporal component rotates the spatial component by a uniform amount at each instant of time. The complex amplitude component rotates and scales the wave by a fixed amount for all space and time positions. The harmonic pattern function can exhibit its own brand of traveling waves, where instead of having independent spatial and temporal complex sinusoid components as in  $u(x, t)$ , it fuses them into a single space-time complex sinusoid.

## 5.2 Order 2

The step from one harmonic to two harmonics is substantial in terms of the amount of new shapes, sounds, and patterns that can be constructed. This is due largely in part to the power of superposition that permits an immense variety of compound motions to be constructed from simpler circular motions. The increase in variety is also due to the fact that geometric inversion leads to new types of shapes—those generally classified as hyperbolic. Unlike single harmonic curves, two harmonic curves can lack discrete dihedral symmetry. However, when  $N \rightarrow \infty$ , the curves always exhibit continuous dihedral symmetry. All two harmonic curves are variations of a bicircloid curve—a curve traced by a point rigidly attached to a circle that rolls without slipping along another circle.

Two harmonic patterns have the general forms

$$\alpha_n = A_1\{k_1, \theta_1\} + A_2\{k_2, \theta_2\} \quad (5.2.1)$$

and

$$\alpha_n = \frac{1}{A_1\{k_1, \theta_1\} + A_2\{k_2, \theta_2\}}. \quad (5.2.2)$$

The order 2 patterns therefore consist of all sums of two harmonics and their complex inversions. All forms of Eq. 5.2.1 can be interpreted as frequency scaled and shifted transformations of a base kernel  $A_1\{0, \theta_1\} + A_2\{1, \theta_2\}$ . This is shown by rewriting Eq. 5.2.1 as

$$\alpha_n = A_1\{\ell, \theta_1\} + A_2\{m + \ell, \theta_2\}$$

where  $m$  and  $\ell$  are the frequency-scaling and -shifting amounts, respectively. In terms of frequency-domain transformations, this becomes

$$\alpha_n = f_{shift, \ell}(f_{scale, m}(A_1\{0, \theta_1\} + A_2\{1, \theta_2\}))$$

, a frequency scaling followed by a frequency shifting of a base kernel. This base kernel, discussed next, has the shape of an eccentric polygon.

### 5.2.1 Eccentric Polygon

The eccentric polygon lies at the core of all order 2 patterns and thus it is appropriate to consider it first. An eccentric regular polygon is given by the harmonic pattern function

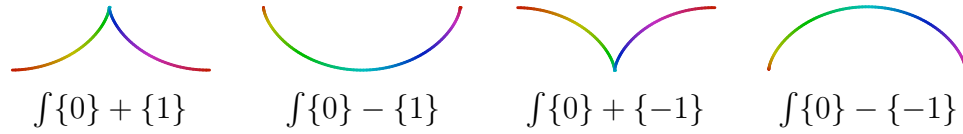
$$\alpha_n = a\{0\} + b\{\pm 1\} \quad (5.2.3)$$

where  $a$  is the eccentricity and  $b$  the radius of the polygon. There is not much to discuss about eccentric polygon patterns that was not covered in the discussion



of regular polygon patterns in 5.1.2. The only new characteristic is that these patterns are offset by a constant amount from the origin. The offset does, however, introduce novel patterns when Eq. 5.2.3 is integrated.

If we integrate Eq. 5.2.3, we obtain a single cycle of a trochoid curve. The trochoid is defined by a combination of a constant and circular differential. Because of the constant differential, the integrated curve will not be closed. When  $|a| = |b|$ , the trochoid is an ordinary cycloid, when  $|a| > |b|$  it is a curtate cycloid and when  $|a| < |b|$  it is a prolate cycloid.



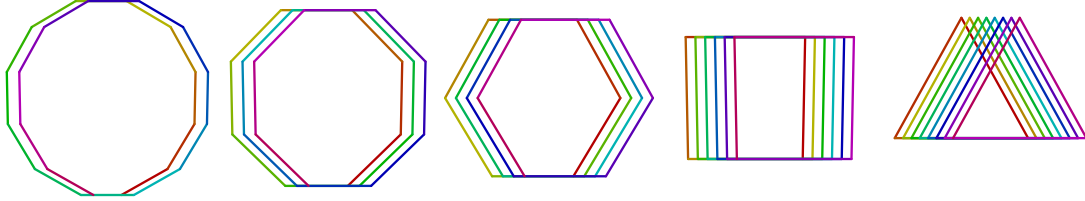
**Figure 5.2.1:** Ordinary cycloids produced through discrete integration of eccentric polygons.

A *moving polygon* is produced from

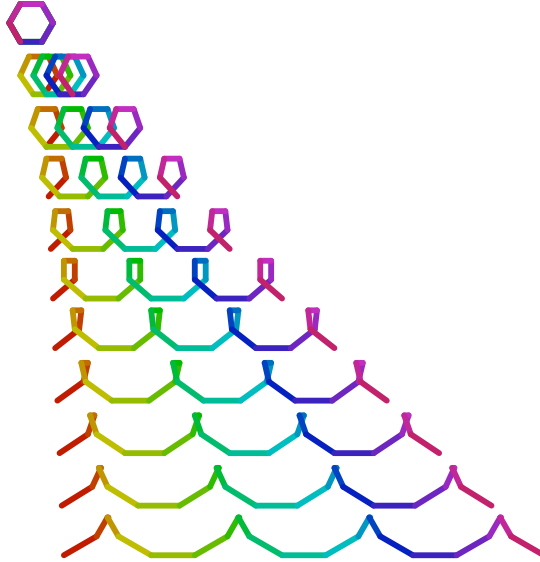
$$\alpha_n = \int a\{0\} + \left\{ \frac{N}{m} \right\}$$

where  $a$  is the velocity,  $m$  is the degree of the polygon,  $\frac{N}{m}$  is the number of cycles of the polygon and  $\frac{N}{m} \in \mathbf{Z}$ . Fig. 5.2.2 shows several moving polygons based on  $N = 24$ . The parameter  $a$  determines the linear velocity by which the polygon moves and the larger its value, the more the polygon is distorted along the direction of motion. As the polygon unfolds, it undergoes contractions and expansions depending on whether the path is moving against or along, respectively, the direction of motion. As  $a \rightarrow 1$ , the contractions and expansions become more exaggerated until the polygon unloops completely and the curve becomes an ordinary (cusped) cycloid (Fig. 5.2.3). When  $a = 0$ , the moving polygon degenerates into a static multiply-

wound polygon. This shows that there is an inherent trade-off between the velocity and the accuracy of shape of the polygon. For optimal results,  $a$  should be non-zero and small in order to exhibit motion with a minimal amount of distortion.



**Figure 5.2.2:** Moving regular polygons for  $N = 24$ ,  $a = 0.02$ , and  $m = 12, 8, 6, 4, 3$  (left to right).



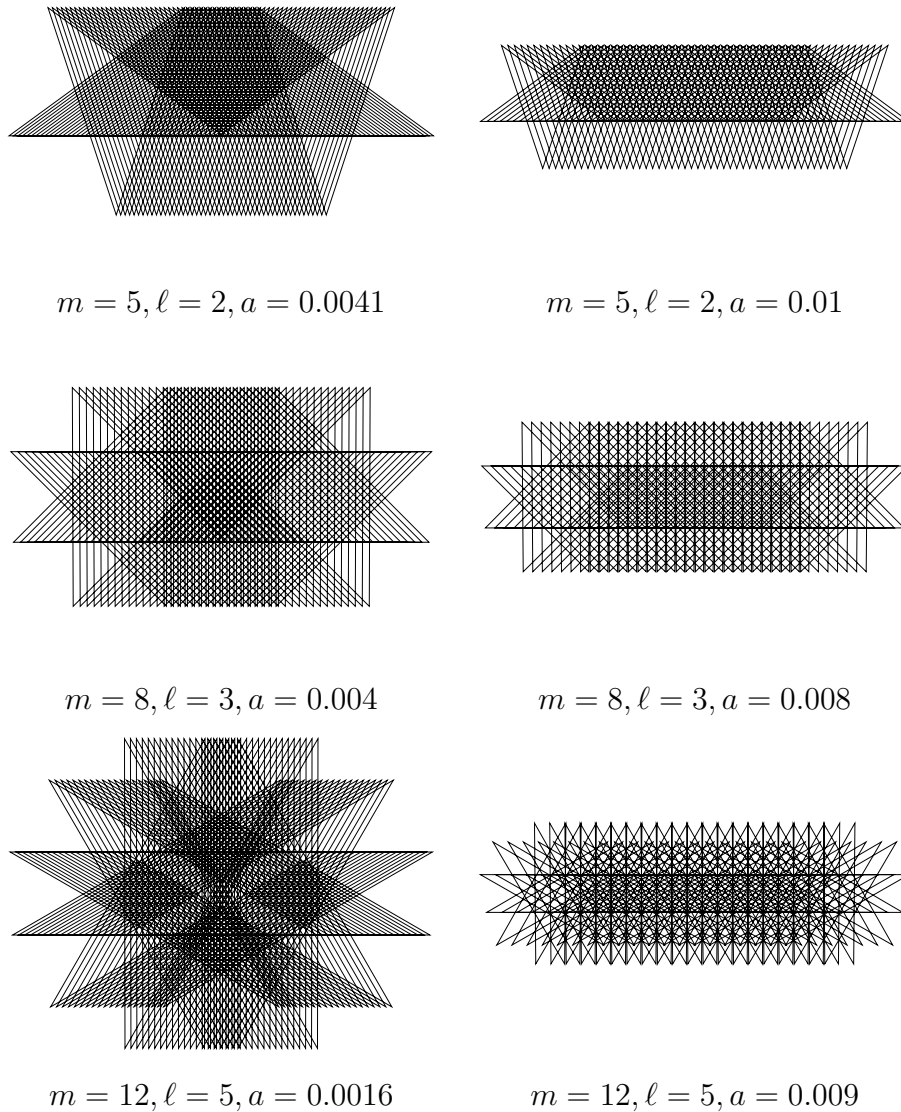
**Figure 5.2.3:** Progression from static polygon (top) to cycloid (bottom). The velocity parameter  $a$  is varied from from 0 to 1 in increments of 0.1 (top to bottom).

A moving polygon can be generalized further to a *moving star polygon* with the equation

$$\alpha_n = \int a\{0\} + \left\{ \ell \frac{N}{m} \right\}$$

which produces  $N/m$  star polygons with Schläfli symbol  $\{m/\ell\}$ . The moving star polygon shares the same trade-offs between velocity and shape accuracy as the

moving regular polygon. Through proper choice of parameters it is possible to construct elaborate interference patterns of lines that exhibit a high degree of structure but at the same time are slightly imperfect. Some examples are shown in Fig. 5.2.4.



**Figure 5.2.4:** Examples of moving star polygon patterns with  $N = 240$ .

The eccentric polygon has some important applications for audio. The eccentric

polygon and its inverse form the basis of comb filters commonly used for effect design. The sequence

$$\alpha_n = \{0\} + b\{m\} \quad (5.2.4)$$

is the frequency response of an all-zero comb filter with  $m$  notches while the inverse

$$\alpha_n = \frac{1}{\{0\} + b\{m\}} \quad (5.2.5)$$

is the frequency response of an all-pole comb filter with  $m$  resonances. Granted  $m > 0$ , the filters will be causal. For the case  $m = 1$ , we obtain the family of one-pole or one-zero filters with either low- or high-pass characteristic depending on the sign of  $b$ . We can generalize Eq. 5.2.4 and Eq. 5.2.5 to

$$\alpha_n = \{0\} + b\{m, \phi\} \quad (5.2.6)$$

and

$$\alpha_n = \frac{1}{\{0\} + b\{m, \phi\}} \quad (5.2.7)$$

to obtain more interesting filters whose frequency responses can be shifted in the frequency domain by the amount  $\phi$ . The caveat to using these filters is that the processed signal must be complex rather than real. Aside from this, the complex filters have the benefit of unifying low-pass, high-pass, band-pass, and notch filters into a single conceptual framework. Low- and high-pass type filters result when  $\phi$  is 0 or  $\frac{1}{2}$  and band-pass and notch filter types result for all other values of  $\phi$ . Eq. 5.2.5 is also useful for waveform synthesis as its spectrum is a complex exponential derived through series expansion

$$\frac{1}{\{0\} + b\{m\}} = \sum_{k=0}^{\infty} b^k \{mk\}$$

where  $m$  is now understood to control the pitch of the waveform. If the signal is processed further with a frequency shift, then more useful harmonic and inharmonic tones without a DC component can be obtained. The frequency-shifted harmonic pattern function is

$$\frac{\{\ell\}}{\{0\} + b\{m\}} = \sum_{k=0}^{\infty} b^k \{mk + \ell\}$$

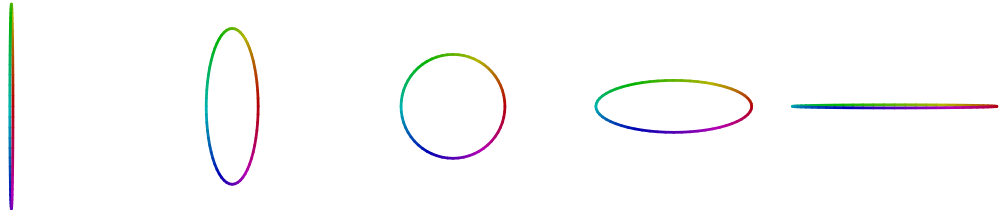
where  $\ell$  is the frequency-shifting amount.

### 5.2.2 Ellipse

In this context, an ellipse can be thought of as a regular polygon that is scaled differently along one axis passing through its center. The shape of the ellipse ranges anywhere from a circle to a lineal projection. An ellipse is given by

$$\alpha_n = b\{-1\} + \{1\}$$

where  $1 - b$  is the minor radius and  $1 + b$  is the major radius. When  $b = 1$ , the ellipse degenerates into  $2 \operatorname{Re}\{1\}$  which is a projection of a complex sinusoid on the real axis. Similarly, when  $b = -1$ , the ellipse degenerates into  $2 \operatorname{Im}\{1\}$  which is a projection of a complex sinusoid on the imaginary axis. The curve plots of  $\operatorname{Re}\{1\}$  and  $\operatorname{Im}\{1\}$  are a type of curve known as a *Tusi couple* [53], the simplest type of linear motion that can be produced from two circular motions.

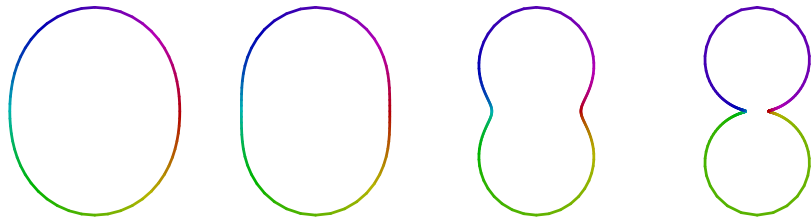


**Figure 5.2.5:** Ellipses resulting from  $b = -0.97, -0.5, 0, 0.5, 0.97$  (left to right).

The inverse of an ellipse is

$$\alpha_n = \frac{1}{b\{-1\} + \{1\}}. \quad (5.2.8)$$

The inverse ellipse ranges in shape from circle to stadium to peanut to joined circles. Unlike an ellipse, the inverse ellipse can have a concave shape. The distance between the two concave sections is  $\frac{1}{1+|b|}$  while the distance between the orthogonal bulbous sections is  $\frac{1}{1-|b|}$ .



**Figure 5.2.6:** Inverse ellipse curves for  $b = \frac{1}{10}, \frac{1}{6}, \frac{2}{5}, \frac{4}{5}$  (left to right).

Eq. 5.2.8 has the equivalent series

$$\frac{1}{b\{-1\} + \{1\}} = \sum_{k=0}^{\infty} (-b)^k \{-2k - 1\}$$

which can also be written

$$\frac{1}{\{-1\} + b\{1\}} = \sum_{k=0}^{\infty} (-b)^k \{2k + 1\}$$

to make all frequencies positive. An inverse ellipse therefore consists of odd harmonics whose amplitudes fall-off as a geometric progression. Integration of Eq. 5.2.8 results in

$$\int \frac{1}{b\{-1\} + \{1\}} = -i \sum_{k=0}^{\infty} \frac{(-b)^k}{-2k-1} \{-2k-1\}$$

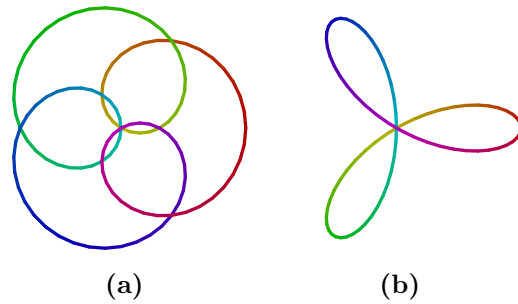
which approaches a square wave and log-cotangent wave as  $|b| \rightarrow 1$ .

### 5.2.3 Rose Curve

A rose curve is any curve constructed from the sum of two equiamplitude complex sinusoids. A rose curve has the equation

$$\alpha_n = \{k_1\} + \{k_2\}. \quad (5.2.9)$$

The number of petals on the rose is equal to  $|k_1 - k_2|$ . When  $k_1$  and  $k_2$  are not coprime, then a multiply wound rose results with  $|k_1 - k_2| / \text{gcd}(k_1, k_2)$  petals wound  $\text{gcd}(k_1, k_2)$  times. Rose curves can be classified into two main varieties— inward looping and outward looping. With inward looping roses, the tips of the loops intersect at the middle of the rose (Fig. 5.2.7a). With outward looping roses, the tips of the loops lie on a circle circumscribing the rose (Fig. 5.2.7b). There is a very simple condition that determines whether the loops are inward or outward. If  $k_1$  and  $k_2$  have the same sign, then the loops are inward; if  $k_1$  and  $k_2$  have opposite sign, then the loops are outward.



**Figure 5.2.7:** Roses with (a) inward and (b) outward pointing petals.

Considering the amount of inward versus outward looping roses with a given number of petals, it is important to note that there exist far fewer inward looping roses than outward looping roses. Fig. 5.2 shows a chart of all rose curves consisting of one to eight petals that are unique up to similarity and have only one winding. The columns are ordered by harmonic frequency  $k$  while the rows are ordered by a positive integer  $m$  designating cyclic symmetry class  $C_m$ . The rose equation for each cell is thus  $\alpha_n = \{k\} + \{k + m\}$ . In the table, the curves with  $k < 0$  are outward looping while the curves with  $k > 0$  are inward looping. All unique outward looping curves are shown for roses having up to eight petals, however, only a miniscule number of inward looping varieties are shown. In fact, there are an infinite number of inward looping roses within each symmetry group  $k$ . The set of all inward looping roses is the infinite set  $\{k : k \leq -m, 0 \leq k\}$  while the set of all outward looping roses is the complement finite set  $\{k : -m < k < 0\}$ .

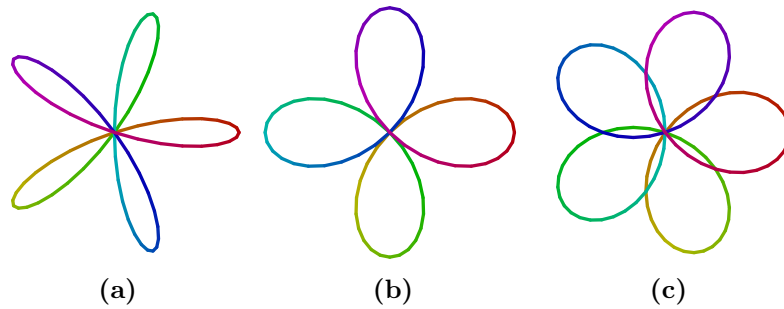
For outward looping roses, there are additional conditions that determine the



relationship between petals. These are

$$\begin{cases} \|k_1| - |k_2|| = 1 & \text{non-touching petals} \\ \|k_1| - |k_2|| = 2 & \text{touching petals} \\ \|k_1| - |k_2|| \geq 3 & \text{intersecting petals} \end{cases} \quad (5.2.10)$$

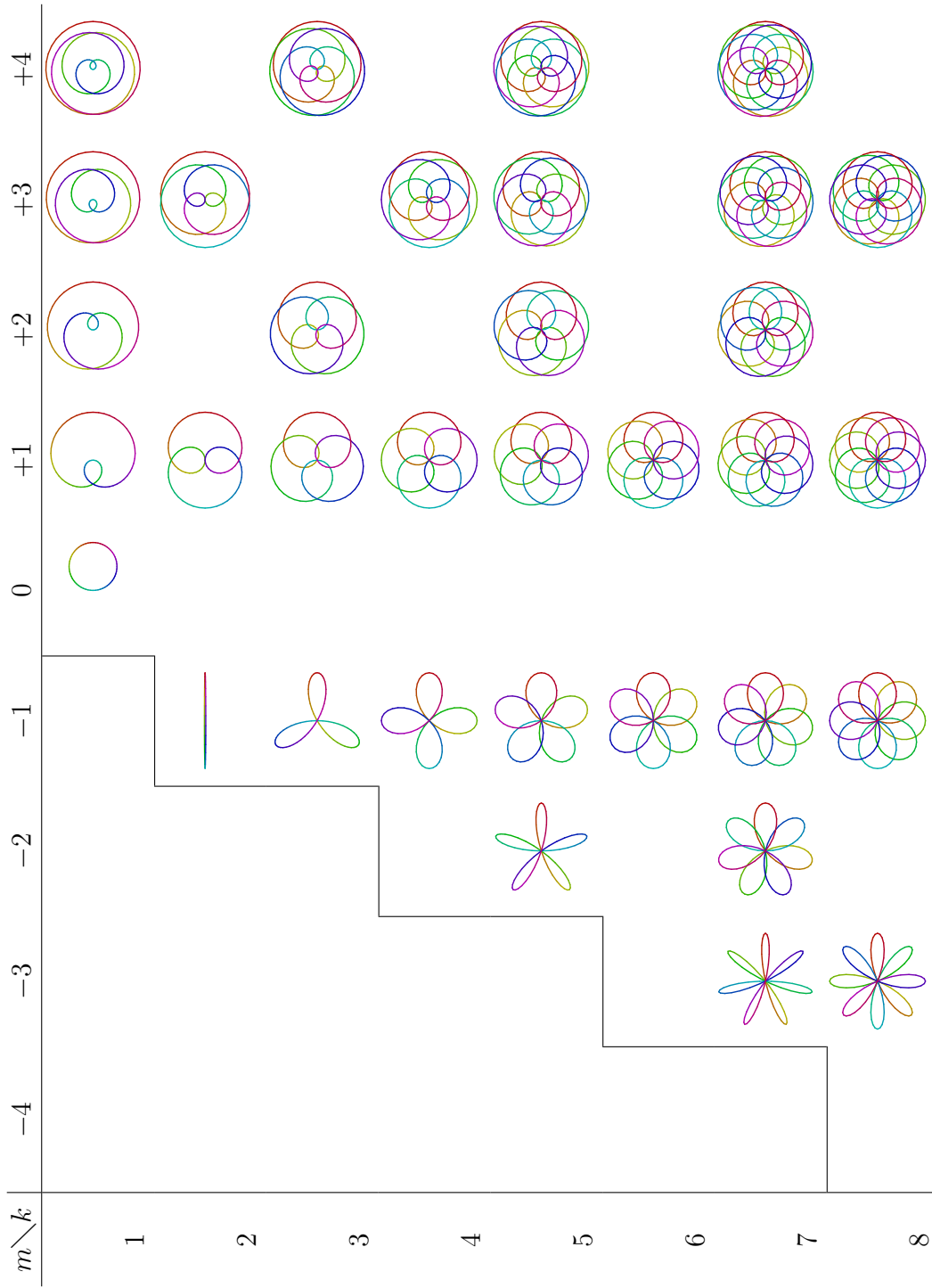
Curve plots illustrating these three petal conditions are shown in Fig. 5.2.8.



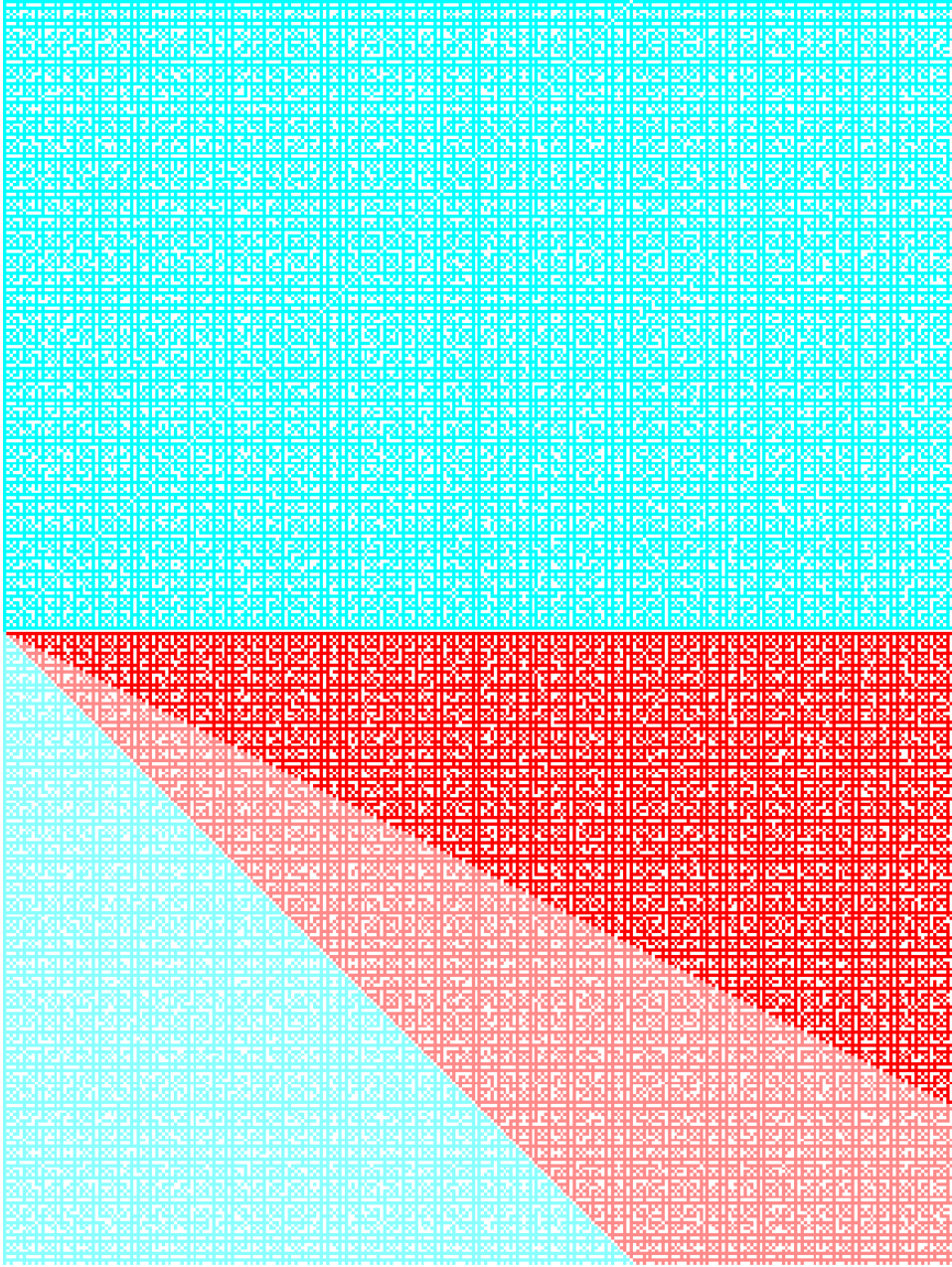
**Figure 5.2.8:** Outward looping roses with the three different petal intersection conditions: (a) non-touching, (b) touching, and (c) intersecting.

We notice as a consequence of Eq. 5.2.10, that only those rose curves with even symmetry  $m$  can have touching petals. The two other cases, non-touching and intersecting, are possible with any value of  $m$ .

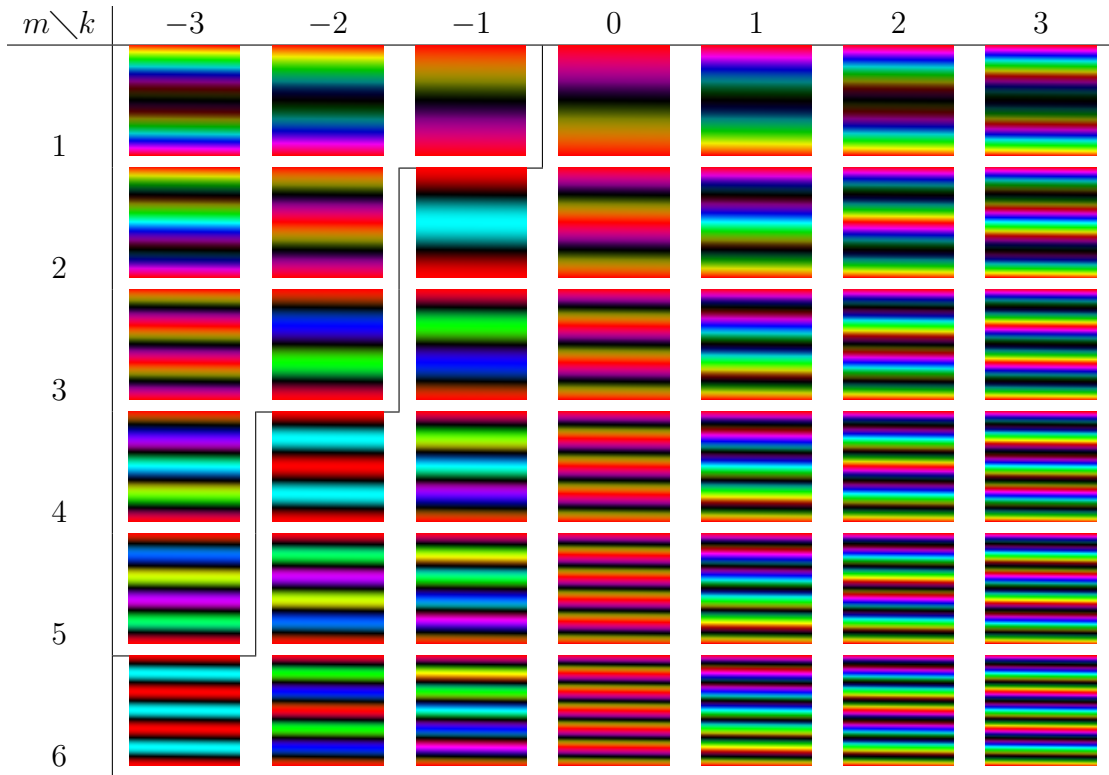
Next, we will consider raster plots of rose curves (Table 5.3).



**Table 5.2:** Singly-wound rose curves from one to eight petals that are unique up to similarity. The curves are given by  $\alpha_n = \{k\} + \{k + m\}$ . The solid line running through the table demarcates where the patterns reverse sequence.



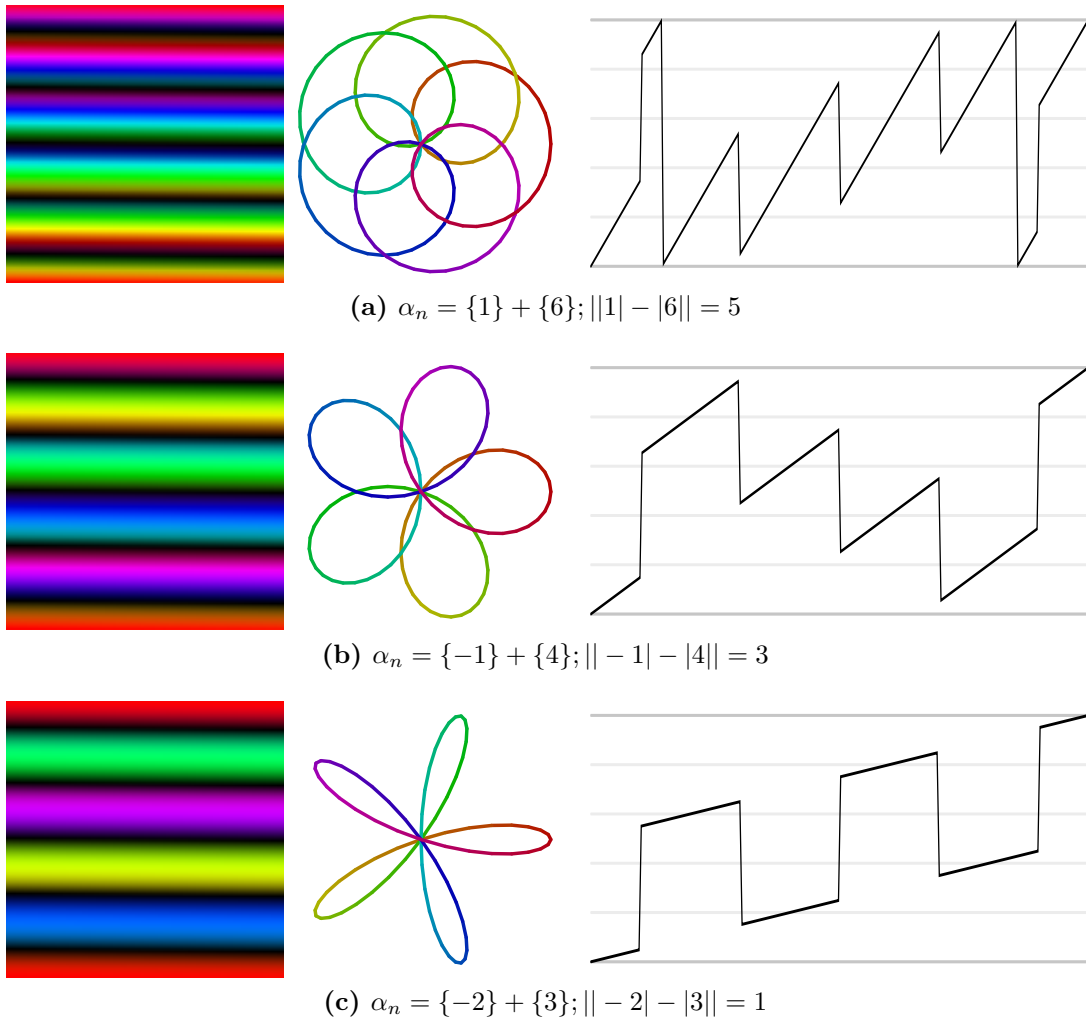
**Figure 5.2.9:** Visualization of similar roses. Columns are  $k \in [-200, 200]$  going left to right and rows are  $m \in [1, 300]$  going top to bottom. Red indicates outward roses while cyan indicates inward roses. The lighter colors indicate the conjugates (reverse windings) of the darker colors.



**Table 5.3:** Complex plane wave superpositions derived from  $\alpha_n = \{k\} + \{k + m\}$ ,  $N = 100^2$ . The solid line running through the table demarcates where the patterns reverse sequence.

As with curve plots of rose curves, raster plots of outward loopings roses tend to have more identifiable features than inward looping roses. While in the curve plot these features are a number of distinct petals circling around the origin, with the raster plot we see well-defined bands of nearly constant hue. The smaller the quantity  $||k_1| - |k_2||$ , the less the hue varies within any given band. The variation in hue follows analogous principles of overlapping, touching, and non-touching petals in the curve plots. Non-touching petals are the thinnest having the least amount of variation in angular excursion while in all other cases the petals are wider having a greater amount of angular excursion. Mathematically, these features (invariant hue and thin petals) are a consequence of the phase component of the complex

sequence holding a relatively constant value over a certain subinterval of samples. In Fig. 5.2.10, raster, curve, and phase plots of  $\alpha_n = \{k\} + \{k + 5\}$  are compared for decreasing values of  $\|k - |k + m|\|$ . As  $\|k - |k + m|\|$  decreases, there is a corresponding decrease in the local slopes of the phase function. The slope of the phase function is directly related to the curvature of the curve as it passes through the origin. Curves having less curvature at the origin (in the extreme case approaching a line) correspondingly exhibit less change in phase and appear more line-like overall. The steps in the phase function are a result of the curve flipping direction as it passes through the origin. In all cases, the phase stepping amount is approximately equal to  $\pi$  since the curve approaches a line passing through the origin on an infinitesimal scale.



**Figure 5.2.10:** Comparison of raster plot (left) and curve plot (middle) with phase plot (right) of the complex sequence  $\alpha_n = \{k\} + \{k + 5\}$ .

Through integration of Eq. 5.2.9, two additional families of curves are generated. Integrating once leads to the “cuspid” family of curves of which the deltoid and astroid are members. Integrating twice produces a family of curves having regularly spaced regions that are nearly a straight line. Since integration becomes an operator on the complex amplitudes in the frequency domain, both of these families of curves have simple closed forms in the frequency domain. These two derived families of curves are discussed in the next sections.

## 5.2.4 Cuspoid

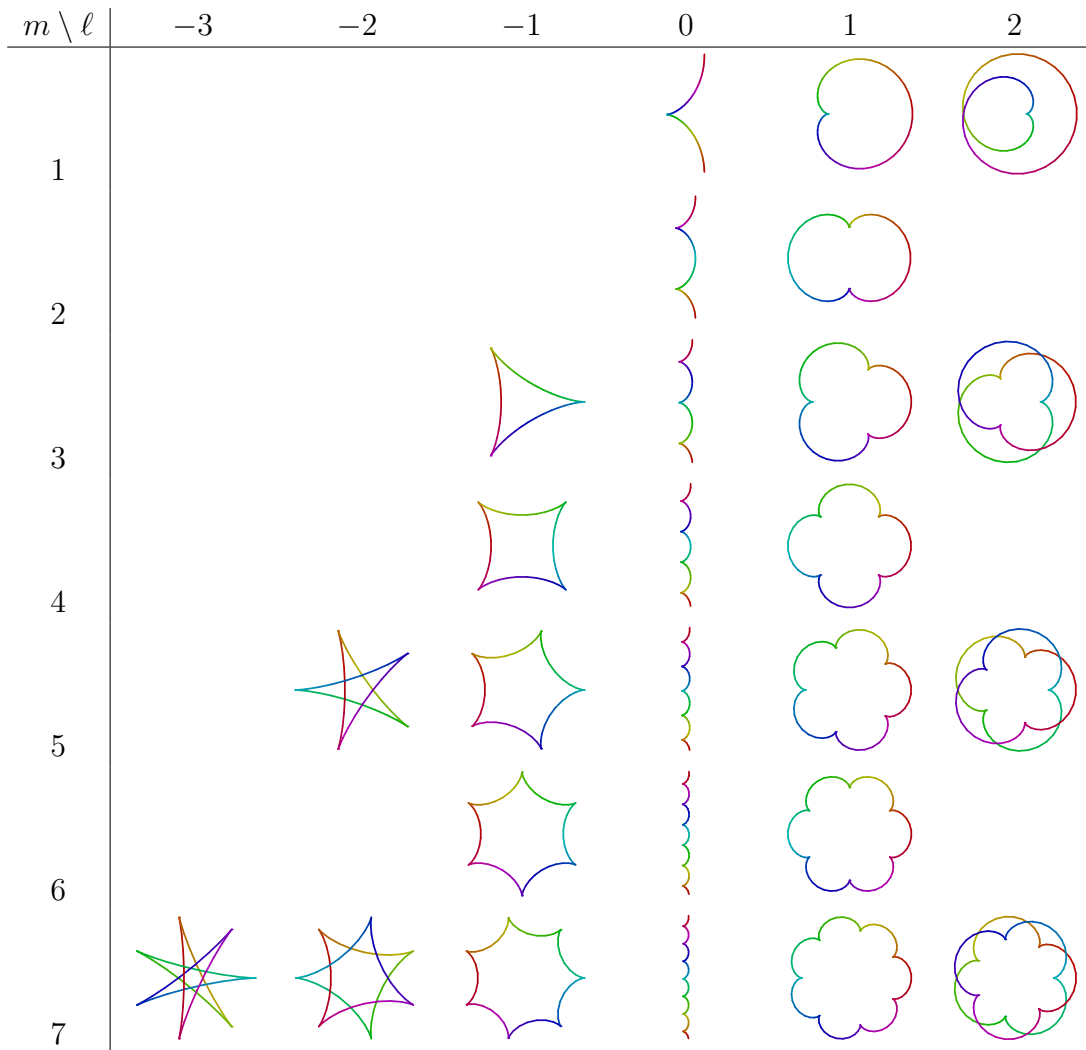
We define a *cuspoid* as an integrated rose curve. These curves are categorized as constant interpolation pattern (Section 4.4). Cuspoids resemble regular (star) polygons with cusps at the vertices and curved paths connecting the vertices. The harmonic pattern function of a cuspoid is

$$\alpha_n = i \int \{\ell\} + \{\ell + m\}$$

or in closed-form as

$$\alpha_n = \frac{1}{\ell} \{\ell\} + \frac{1}{\ell + m} \{\ell + m\}.$$

The cuspoid family of curves includes several well-known curves: the deltoid ( $\ell = -1, m = 3$ ), the astroid ( $\ell = -1, m = 4$ ), the cardioid ( $\ell = 1, m = 1$ ), the nephroid ( $\ell = 1, m = 2$ ), and the cycloid ( $\ell = 0$ ). Cuspoids share all the same behaviors as rose curves with respect to  $\ell$  and  $m$ , namely degeneracy and symmetry patterns, but have cusps instead of loops. Table 5.4 presents several low-frequency cuspoids up to similarity. When  $\ell < 0$ , the curves between cusps bend inward while for  $\ell > 0$ , the curves bend outwards. When  $\ell = 0$ , the curves are cycloids.



**Table 5.4:** Low-frequency, non-similar cuspidoids given by  $\alpha_n = i f\{\ell\} + \{\ell + m\}$ .

### 5.2.5 Smooth Star Polygon

When adding harmonics whose amplitudes are the inverse square of their frequencies, we obtain curves having segments that approach lines [11]. The linear portions are explained through the notion of a linear interpolation pattern (Section 4.4). When only two harmonics meeting this criteria are summed, we obtain a family of curves that are simply low order (two component) Fourier star polygons [89]. The



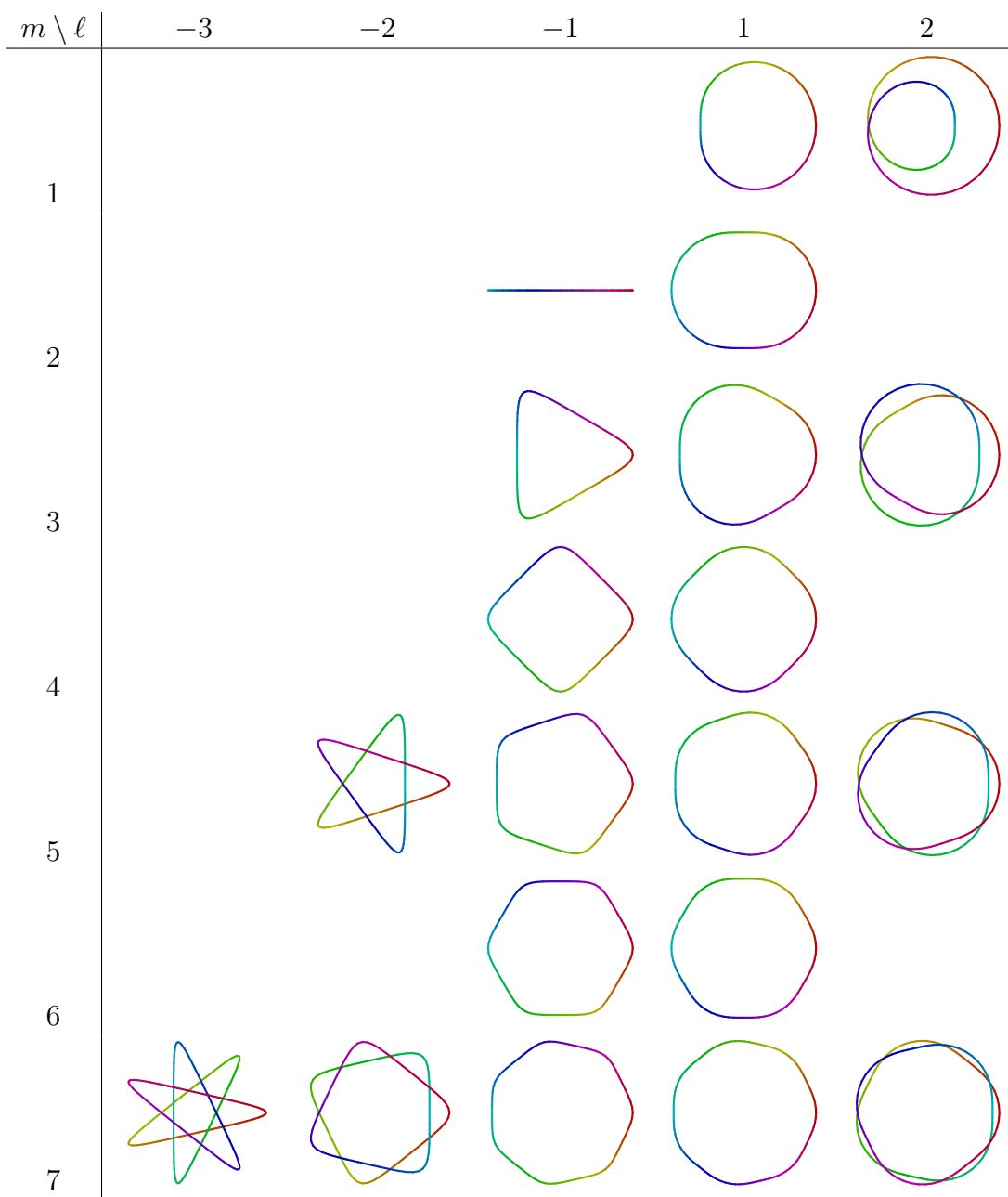
equation of smooth star polygons is

$$\alpha_n = - \iint \{\ell\} + \{\ell + m\}$$

or, in closed-form,

$$\alpha_n = \frac{1}{\ell^2} \{\ell\} + \frac{1}{(\ell + m)^2} \{\ell + m\}.$$

Like with rose curves, the quantity  $\lambda = |\ell + \ell + m|$  plays an important role in local curvature along of the curve. The smaller  $\lambda$ , the more the curve will “double back” on itself having longer linear portions punctuated by sharper bends. In the extreme case  $\lambda = 0$ , the curve collapses into a line. Table 5.5 presents several low-frequency smooth star polygons up to similarity. Curves for  $\ell = 0$  are not shown because there are an infinite amount of them. Integrating the constant term  $\{0\}$  twice produces a linear polynomial term with arbitrary coefficients.



**Table 5.5:** Low-frequency, non-similar smooth star polygons given by  $\alpha_n = \frac{1}{\ell^2}\{\ell\} + \frac{1}{(\ell+m)^2}\{\ell+m\}$ .

### 5.2.6 Low $N$ Rose Curve

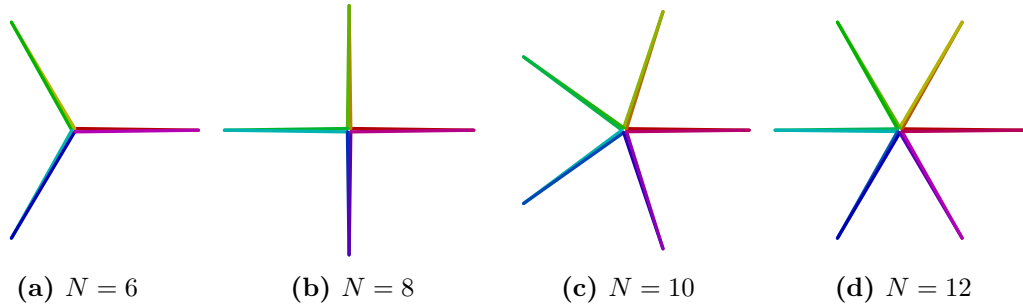
For small values of  $N$ , rose curves produce a variety of rectilinear and polygonal shapes. Since these patterns come in a seemingly endless variety, only some of the more interesting shapes are discussed. A spoke-like pattern with  $\frac{N}{2}$  spokes is constructed from

$$\alpha_n = \{1\} + \left\{ \frac{N}{2} + 1 \right\}$$

where  $N = 2, 4, 6, \dots$ . The sequence is an alternation between the vertices of a regular  $\frac{N}{2}$ -gon and points at the origin. The actual complex sequence is

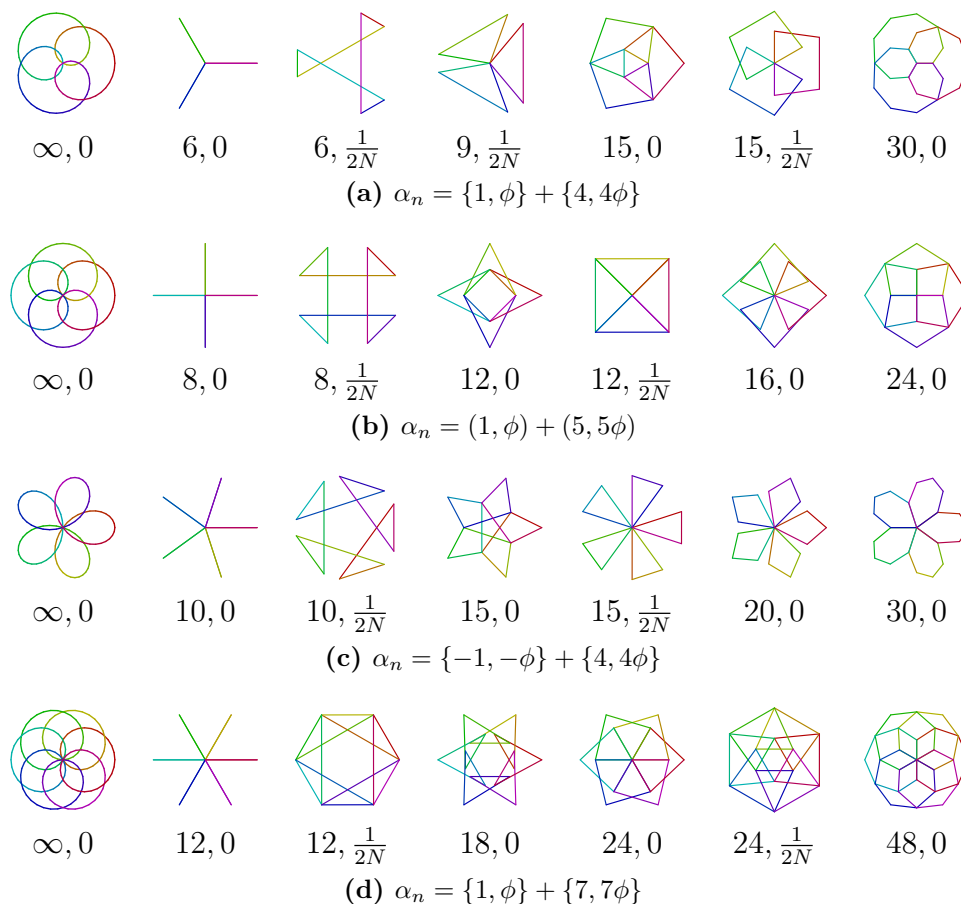
$$1, 0, e^{i(1 \cdot 2\pi/(N/2))}, 0, e^{i(2 \cdot 2\pi/(N/2))}, 0, \dots, e^{i((N/2-1) \cdot 2\pi/(N/2))}, 0.$$

When successive points are connected by lines, a spoke pattern emerges (Fig. 5.2.11).



**Figure 5.2.11:** Spoke shapes given by  $\alpha_n = \{1\} + \left\{ \frac{N}{2} + 1 \right\}$ .

Fig. 5.2.12 presents an assortment of low  $N$  rose curves having interesting symmetrical properties such as meeting vertices and overlapping edges.



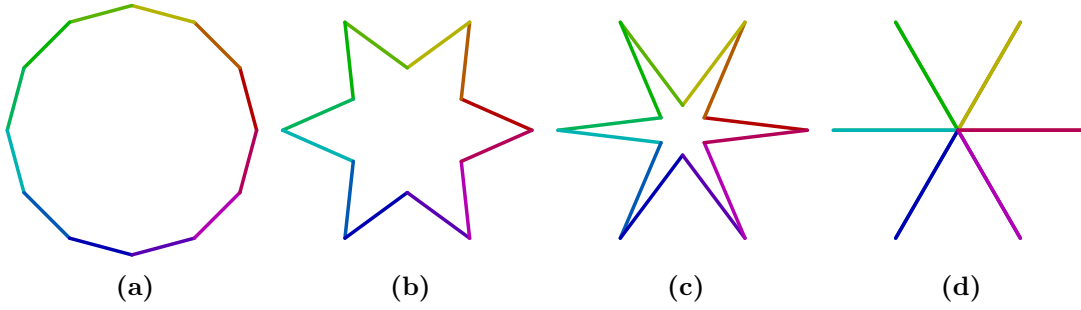
**Figure 5.2.12:** A sampling of low  $N$  rose curves. The leftmost column displays the continuous rose curve shape ( $N \rightarrow \infty$ ). The numbers under each figure are  $N, \phi$ .

## 5.2.7 Star

A star [119] is produced from

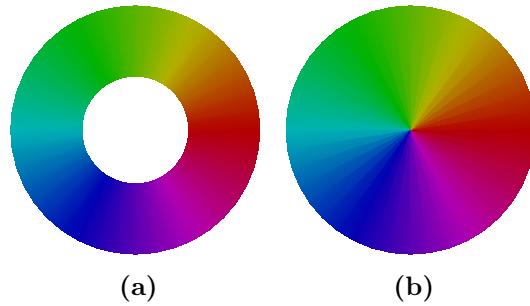
$$\alpha_n = \{1\} + b \left\{ \frac{N}{2} + 1 \right\} \quad (5.2.11)$$

where  $N = 2, 4, 6, \dots$  and  $b \in [0, 1]$  is a “brightness” factor determining how pointed the star is. When  $b = 0$ , a regular  $N$ -gon results and when  $b = 1$  we get a spoke as discussed above. Fig. 5.2.13 shows the effect of varying the parameter  $b$  from 0 to 1.



**Figure 5.2.13:** Star shapes given by  $\alpha_n = \{1\} + b \left\{ \frac{N}{2} + 1 \right\}$  for  $N = 12$  and  $b = 0, \frac{1}{3}, \frac{2}{3}, 1$  (a-d). The shapes progress from a regular polygon to a spoke.

As  $N \rightarrow \infty$ , the star can be used to construct an annulus or a disc by drawing a triangle strip between successive points.



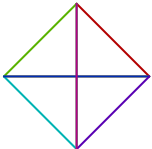
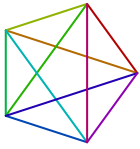
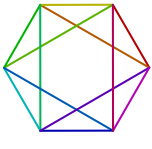
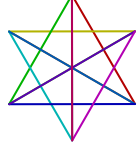

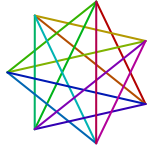





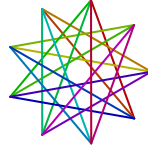




**Figure 5.2.14:** Connecting star points with a triangle strip creates (a) an annulus ( $b < 1$ ) or (b) a disc ( $b = 1$ ).

## 5.2.8 Polygon Star Wrapping

A *polygon star wrapping* is a curve comprised of the superimposition of two or more regular star polygons from the same symmetry group. These curves are a generalization of the star (Eq. 5.2.11) and are given by

$$\alpha_n = a \left\{ 1, \frac{1}{2N} \right\} + b \left\{ m + 1, \frac{m + 1}{2N} \right\}$$

where  $N = 2, 4, 6, \dots$ ,  $m = \frac{N}{2}$  and  $a, b \in [0, 1]$ . Table 5.6 shows a selection of these patterns that were empirically tuned to make vertices coincide. Each vertex has at most four edges. Exact formulas for the amplitudes were not investigated, although they would most likely involve relatively simple trigonometric relations.

$m = 4$				
	$\sqrt{2} - 1, 1$			
$m = 5$				
	$0.7265, 1$			
$m = 6$				
	$1, 1$	$0.2680, 1$		
$m = 7$				
	$1, 0.7975$	$0.4816, 1$		
$m = 8$				
	$1, 0.6682$	$0.6682, 1$	$0.1989, 1$	
$m = 9$				
	$1, 0.5774$	$0.8391, 1$	$0.3640, 1$	
$m = 10$				
	$1, 0.5095$	$1, 1$	$0.5095, 1$	$0.1584, 1$

**Table 5.6:** Polygon star wrappings. The numbers under each figure are the harmonic amplitudes  $a, b$ .

## 5.2.9 Interleaved Bicircloid

We define an *interleaved bicircloid* as a pattern produced from the sum of two interleaved harmonics (5.1.4). Like an interleaved harmonic, it consists of  $P$  alternating subsequences, but instead of the subsequences being star polygons, they are bicircloids. Interleaved bicircloids are important patterns since they provide a fundamental way of producing multiple superimposed (overlapping) curves. The harmonic pattern function of  $P$  interleaved bicircloids is

$$\alpha_n = a \left\{ p \frac{N}{P} + k \right\} + b \left\{ q \frac{N}{P} + k + m \right\}$$

where  $\frac{N}{P} \in \mathbf{N}$ . Using Eq. 5.1.2, we determine the equations of the subsequences to be

$$\alpha_{Pn+j} = a \left\{ kP, j \left( \frac{p}{P} + \frac{k}{N} \right) \right\} + b \left\{ (k+m)P, j \left( \frac{q}{P} + \frac{k+m}{N} \right) \right\}. \quad (5.2.12)$$

Eq. 5.2.12 shows that each bicircloid subsequence is unique up to phase only; the frequencies do not depend on  $j$ . Since the only difference between bicircloids is a phase rotation and position shift, the shapes of all bicircloids are the same. Some specific instances of interleaved bicircloids are presented next.

An *interleaved eccentric regular polygon* consists of a circular ring of regular polygons. The equation of  $P$  interleaved eccentric regular polygons is given by

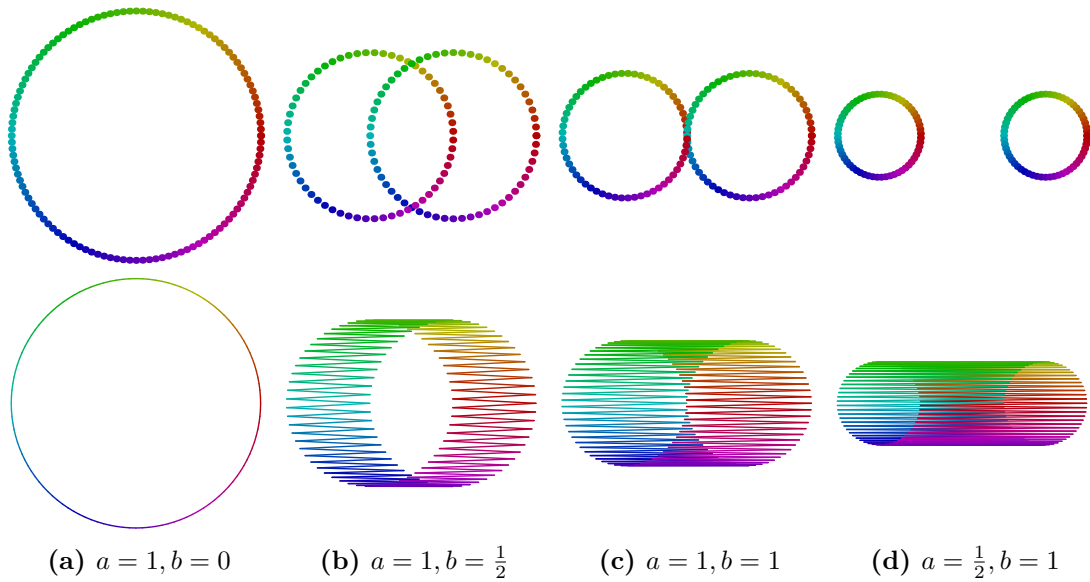
$$\alpha_n = a\{1\} + b \left\{ \frac{N}{P} \right\}$$



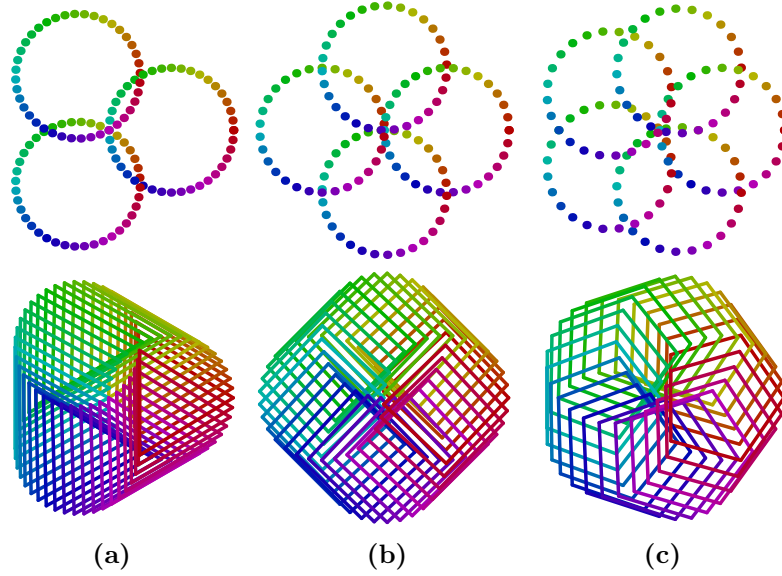
where the  $j^{\text{th}}$  subsequence is

$$\alpha_{Pn+j} = a \left\{ P, \frac{j}{N} \right\} + b \left\{ 0, \frac{j}{P} \right\}.$$

When  $b > a$ , this partitioning becomes more apparent as the figures no longer overlap with one another (Fig. 5.2.15). Fig. 5.2.15 shows curve plots of interleaved eccentric regular polygons for  $P = 2$  while Fig. 5.2.16 shows plots for  $P = 3, 4, 5$ .



**Figure 5.2.15:** A 120-gon progressively split into two 60-gons by variation of parameters  $a$  and  $b$  of  $\alpha_n = a\{1\} + b\{\frac{120}{2}\}$ . The top figures show the vertices and the bottom figures show the edges.



**Figure 5.2.16:** Equiamplitude ( $a = b$ ) interleaved eccentric polygons (a)  $\alpha_n = \{1\} + \{\frac{120}{3}\}$ , (b)  $\alpha_n = \{1\} + \{\frac{120}{4}\}$ , (c)  $\alpha_n = \{1\} + \{\frac{120}{5}\}$ . The top figures show the vertices and the bottom figures show the edges.

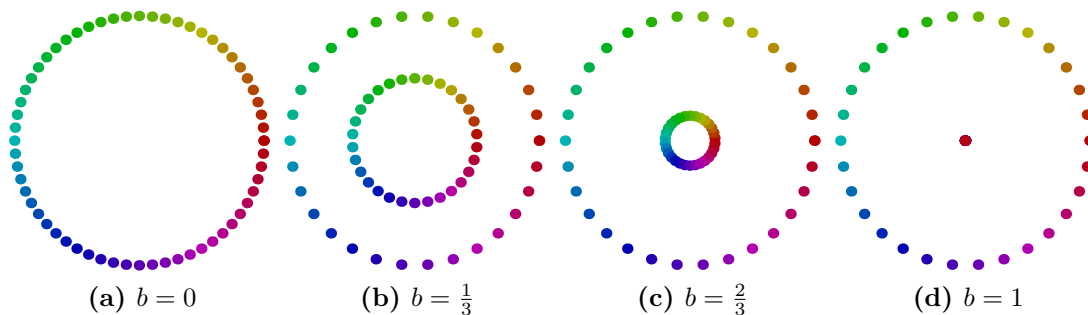
Revisiting the star defined as  $\alpha_n = \{1\} + b \left\{ \frac{N}{2} + 1 \right\}$  we can show that it is in fact two interleaved regular  $\frac{N}{2}$ -gons that differ in phase by  $\frac{1}{N}$ . From Eq. 5.2.12, we determine its  $j^{\text{th}}$  subsequence to be

$$\alpha_{2n+j} = \left\{ 2, \frac{j}{N} \right\} + b \left\{ 2, \frac{j}{2} + \frac{j}{N} \right\}$$

and therefore its two subsequences to be

$$\begin{aligned} \alpha_{2n+0} &= \{2\} + b \{2\} \\ &= (1+b)\{2\} \\ \alpha_{2n+1} &= \left\{ 2, \frac{1}{N} \right\} + b \left\{ 2, \frac{1}{2} + \frac{1}{N} \right\} \\ &= (1-b) \left\{ 2, \frac{1}{N} \right\}. \end{aligned}$$

For  $j = 0$ , we obtain a polygon with amplitude  $1 + b$ , while for  $j = 1$  we get a polygon with amplitude  $1 - b$ . Fig. 5.2.17 shows vertex curve plots for increasing  $b$ . As  $b \rightarrow 1$ , the  $j = 1$  interleaved polygon collapses to a point at the origin.



**Figure 5.2.17:** Interleaved 30-gons constructed from  $\alpha_n = \{1\} + b \left\{ \frac{60}{2} + 1 \right\}$ : (a) regular 60-gon, (b) and (c) star figures, and (d) spoke.

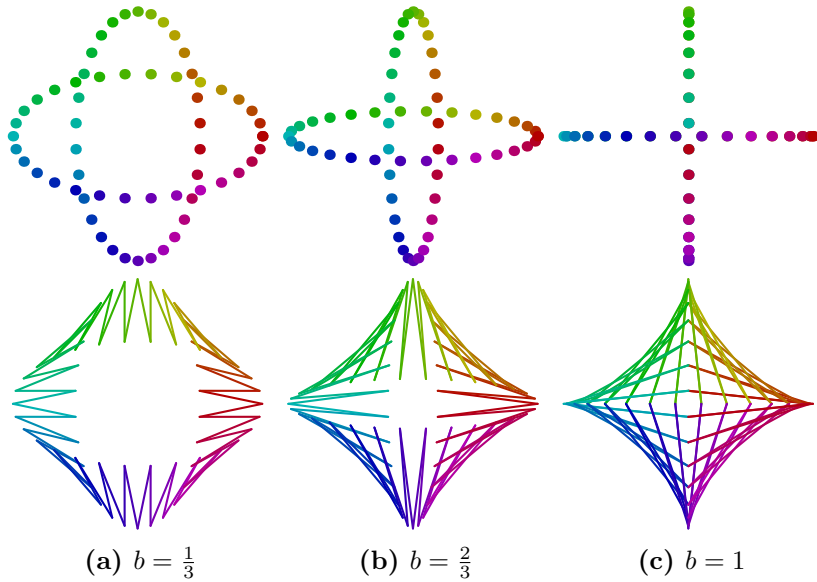
If the star figure formula is modified slightly to

$$\alpha_n = \{1\} + b \left\{ \frac{N}{P} - 1 \right\}$$

we obtain *interleaved ellipses* whose  $j^{\text{th}}$  subsequence is

$$\alpha_{Pn+j} = \left\{ P, \frac{j}{N} \right\} + b \left\{ -P, \frac{j}{P} - \frac{j}{N} \right\}.$$

Fig. 5.2.18 shows vertex and edge curve plots for several values of  $b$  with  $m = 2$ .



**Figure 5.2.18:** Interleaved ellipses given by  $\alpha_n = \{1\} + b \left\{ \frac{60}{2} - 1 \right\}$  for increasing  $b$ .

The last specialization of an interleaved bicircloid considered is a *simple interleaved bicircloid* defined by

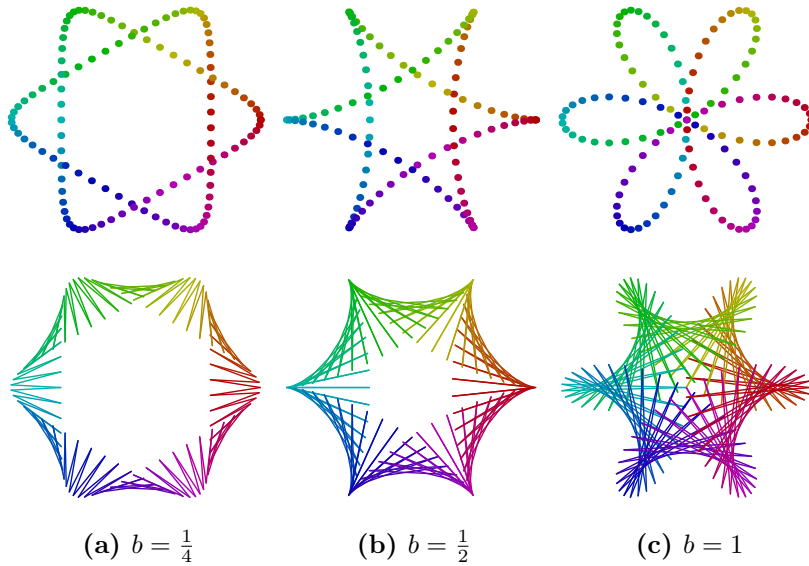
$$\alpha_n = \{k\} + b \left\{ \frac{N}{P} + k + m \right\}$$

with  $j^{\text{th}}$  subsequence given by

$$\alpha_{Pn+j} = \left\{ kP, \frac{j}{P} + \frac{jk}{N} \right\} + b \left\{ (k+m)P, \frac{j}{P} + \frac{j(k+m)}{N} \right\}.$$


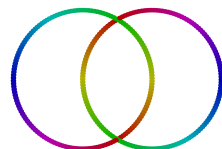

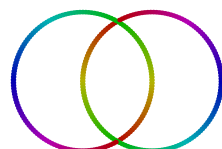

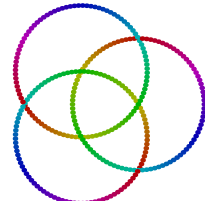
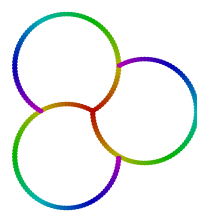
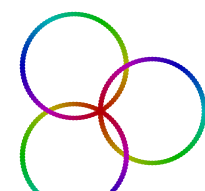
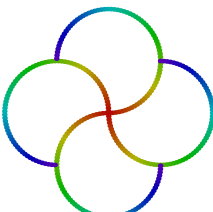
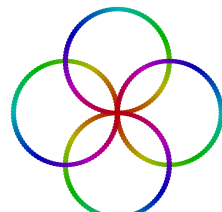
When  $b = 1$ , we obtain an *interleaved rose curve*. In Fig. 5.2.19, several curve plots are shown for  $P = 2$ ,  $k = -1$ ,  $m = 3$  and varying  $b$ . Of special importance is the figure when  $b = 1$ ; this is a *hexafolium*, a rose curve with  $D_6$  symmetry having non-overlapping petals. It is made of two superimposed  $D_3$  rose curves in reflection around the imaginary axis. We cannot obtain a similar rose curve using  $\alpha_n = \{2\} + \{-4\}$  (Eq. 5.2.9, Eq. 5.2.10) since 2 and  $-4$  are not coprime and as

such cause the curve to degenerate into a doubly-wound curve  $\alpha_n = \{1\} + \{-2\}$ .



**Figure 5.2.19:** Interleaved bicircloids given by  $\alpha_n = \{1\} + b \left\{ \frac{120}{2} - 2 \right\}$  and various  $b$ .

By taking subsequences of interleaved bicircloids, many new types of curves can be constructed, some of them well-known (Fig. 5.2.20).

Name / Equation	Subsequence	Full Sequence
Vesica Piscis $\alpha_n = \frac{1}{2} \left\{ \frac{N}{2} \right\} + \left\{ \frac{N}{2} + 1, \frac{1}{3} \right\}$	 $n = [0, \frac{N}{3}]$	 $n = [0, N]$
Double Link $\alpha_n = \frac{1}{2} \left\{ \frac{N}{2} \right\} + \left\{ \frac{N}{2} + 1, \frac{1}{3} \right\}$	 $n = [\delta, N - \delta]$	 $n = [0, N]$
Triquetra $\alpha_n = \frac{1}{2 \sin(\pi/3)} \left\{ \frac{N}{3} \right\} + \left\{ \frac{N}{3} + 1, \frac{1}{4} \right\}$	 $n = [0, \frac{N}{2}]$	 $n = [0, N]$
3 Overlapping Discs $\alpha_n = \left\{ \frac{N}{3} \right\} - \left\{ \frac{N}{3} + 1 \right\}$	 $n = [0, \frac{5}{6}N]$	 $n = [0, N]$
4 Overlapping Discs $\alpha_n = \left\{ \frac{N}{4} \right\} - \left\{ \frac{N}{4} + 1 \right\}$	 $n = [0, \frac{3}{4}N]$	 $n = [0, N]$

**Figure 5.2.20:** Some patterns produced from subsequences of interleaved bicircloids.

### 5.2.10 Simple Beat

A simple beat pattern is a special case of a rose curve whose harmonic frequencies are within close proximity to one another. The general form of a simple beat is given by

$$\alpha_n = \frac{1}{2}(\{k + m\} \pm \{k\})$$

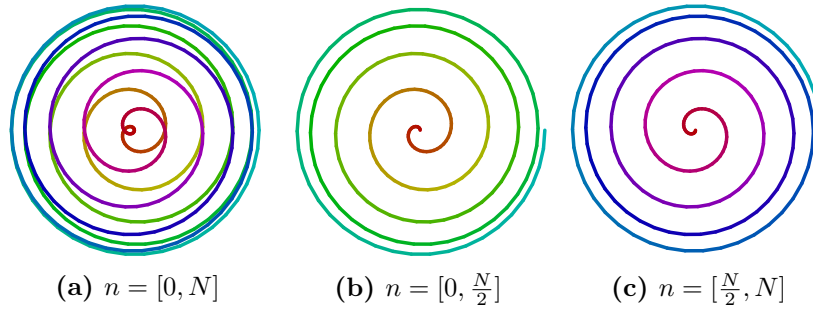
where  $m$  is the number of beats and  $m \ll k$ . The addition or subtraction of the complex sinusoids determines whether the beat is a *falling beat* or a *rising beat*, respectively. A falling beat begins and ends at unit amplitude while a rising beat begins and ends at zero amplitude.

The equivalent factored form of a falling beat is  $\alpha_n = \{k + \frac{m}{2}\} \cdot \text{Re}\{\frac{m}{2}\}$ . This form more clearly reveals a falling beat to consist of a complex sinusoid,  $\{k + \frac{m}{2}\}$ , multiplied by a cosine envelope,  $\text{Re}\{\frac{m}{2}\}$ . The equivalency between the two forms is simple to show

$$\begin{aligned} \alpha_n &= \frac{1}{2}(\{k + m\} + \{k\}) \\ &= \left\{k + \frac{m}{2}\right\} \frac{1}{2} \left( \left\{\frac{m}{2}\right\} + \left\{-\frac{m}{2}\right\} \right) \\ &= \left\{k + \frac{m}{2}\right\} \text{Re}\left\{\frac{m}{2}\right\} \end{aligned} \quad (5.2.13)$$

Similarly, a rising beat has a factored form given by  $\alpha_n = \{k + \frac{m}{2}\} \cdot \text{Im}\{\frac{m}{2}\}$  showing it to consist of a complex sinusoid,  $\{k + \frac{m}{2}\}$ , multiplied by a sine envelope,  $\text{Im}\{\frac{m}{2}\}$ . Again, the equivalency between the two forms is shown as follows:

$$\begin{aligned} \alpha_n &= \frac{1}{2}(\{k + m\} - \{k\}) \\ &= \left\{k + \frac{m}{2}\right\} \frac{1}{2} \left( \left\{\frac{m}{2}\right\} - \left\{-\frac{m}{2}\right\} \right) \\ &= \left\{k + \frac{m}{2}\right\} \text{Im}\left\{\frac{m}{2}\right\} \end{aligned} \quad (5.2.14)$$



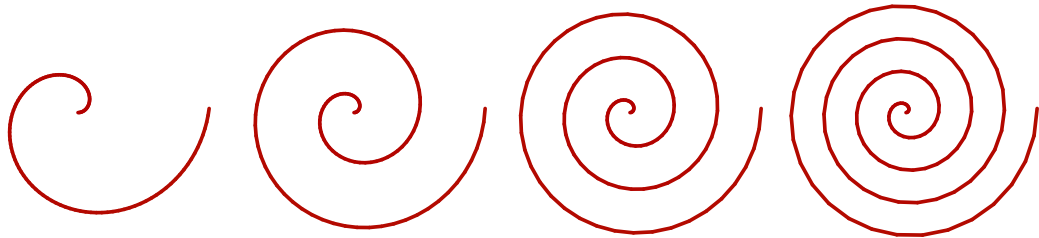
**Figure 5.2.21:** Anatomy of a rising beat  $\alpha_n = \frac{1}{2}(\{10\} - \{9\})$ . Figure (a) shows the entire beat while (b) and (c) show the first and second half-sequences, respectively.

### 5.2.11 Archimedes' Spiral

An Archimedes' (or linear) spiral is derived from the initial subsequence of a rising beat as described above. A spiral with  $k$  windings is given to good approximation by the subsequence

$$\alpha_{[0,M)} = i \left( \left\{ \left\{ \frac{N}{M}k \right\} \right\} - \left\{ \left\{ \frac{N}{M}k + 1 \right\} \right\} \right)$$

where  $k \ll M \ll N$  and  $\frac{N}{M} \in \mathbf{N}$ . The close fit to linear growth of the spiral stems from the fact that  $\sin(\theta) \approx \theta$  for small  $\theta$ . For  $\theta < 0.4$ , the difference between the curves,  $\theta - \sin \theta$ , is given approximately by  $(0.549\theta)^3$ .



**Figure 5.2.22:** Linear spirals with  $k = 1, 2, 3, 4$  winding(s) (left to right). The parameters are  $N = 16000, M = 160$ .

John Whitney's example of a radial differential motion pattern, where 60



radially equidistant points move with an angular velocity proportional to their distance from the origin, displays a succession of Archimedes' spirals with winding number increasing from 0 to 1 in increments of  $\frac{1}{8}$  [126]. Fig. 5.2.23 shows his example frames reproduced using the harmonic pattern function

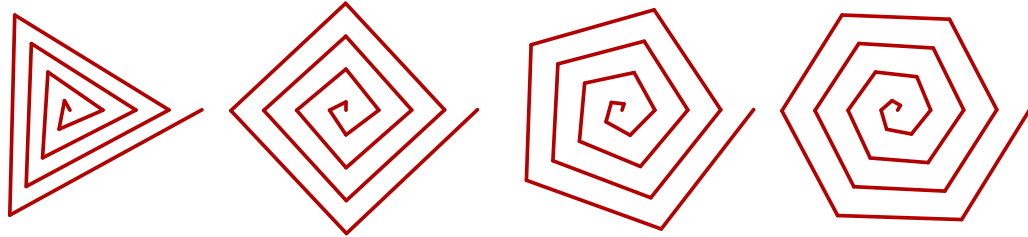
$$\alpha_{[0,60]} = -i \left( \left\{ -\frac{12000}{25}m \right\} - \left\{ -\frac{12000}{25}m - 1 \right\} \right)$$

for  $m = 0, 1, 2, \dots, 8$ .



**Figure 5.2.23:** John Whitney's example of a radial differential motion pattern.

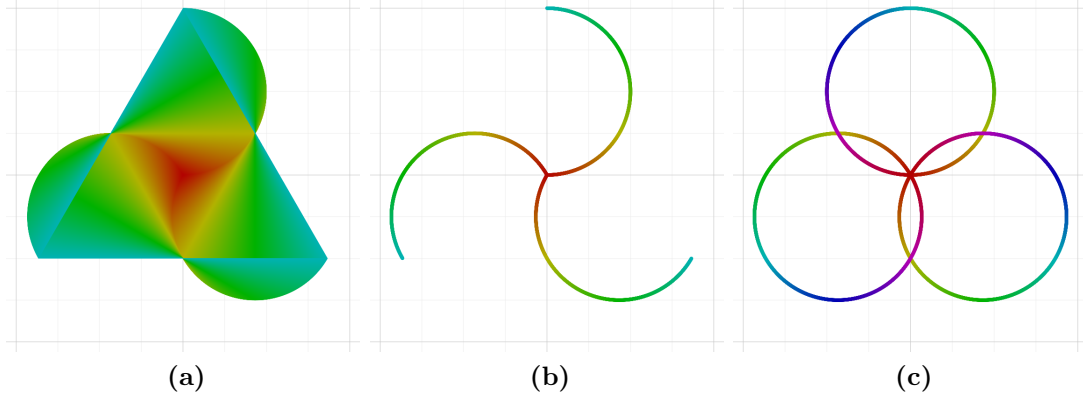
A regular  $m$ -gon linear spiral (also called a spirangle [128]) with  $k$  windings is obtained from the subsequence  $\alpha_{[0,km]} = i(\{\frac{N}{m}\} - \{\frac{N}{m} + 1\})$  where  $\frac{N}{m} \in \mathbf{N}$ .



**Figure 5.2.24:** Regular polygon linear spirals with  $m = 3, 4, 5, 6$  polygon vertices (left to right) and  $k = 4$  windings.

If we extend the  $m$ -gon linear spiral subsequence to the half-sequence  $\alpha_{[0,N/2]}$ , we observe that the successive vertices of the extended spiral lie on  $m$  half-circle arcs. Fig. 5.2.25a shows the extended spiral with vertices connected with lines and Fig. 5.2.25b shows the vertices as points. In the line-connected figure, it is evident that the spiral undergoes a  $90^\circ$  counter-clockwise rotation. Fig. 5.2.25c is

the entire sequence of the 3-gon linear spiral and clearly shows the vertices to lie on three circles intersecting at the origin. These figures are interleaved bicircloids (5.2.9).



**Figure 5.2.25:** Extrapolation of triangular linear spiral approximation to (a), (b) half and (c) full sequences. The curve begins as a triangular spiral and evolves into three intersecting circles. The curve is given by  $\alpha_n = i(\{\frac{N}{3}\} - \{\frac{N}{3} + 1\})$ .

### 5.2.12 Inverse Beat

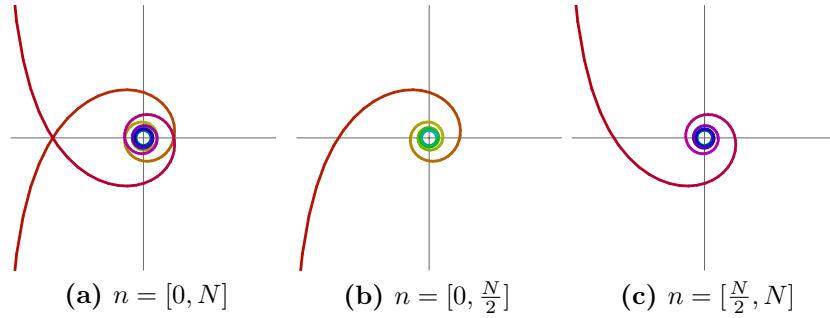
The general form of an inverse beat is

$$\alpha_n = \frac{2}{\{k + m\} \pm \{k\}}$$

where  $m$  is the number of beats and  $m \ll k$ . If we decompose the harmonic pattern function in factors

$$\begin{aligned} \alpha_n &= \frac{2}{\{k + m\} \pm \{k\}} \\ &= \frac{2}{\{k + \frac{m}{2}\}(\{\frac{m}{2}\} \pm \{-\frac{m}{2}\})} \\ &= \left\{-k - \frac{m}{2}\right\} \frac{1}{\frac{1}{2}(\{\frac{m}{2}\} \pm \{-\frac{m}{2}\})} \\ &= \left\{-k - \frac{m}{2}\right\} \sec\left(\pi \frac{n}{N} m - \frac{\pi}{4} \pm \frac{\pi}{4}\right) \end{aligned}$$

we see that it is composed of a complex sinusoid multiplied by a secant or cosecant envelope.



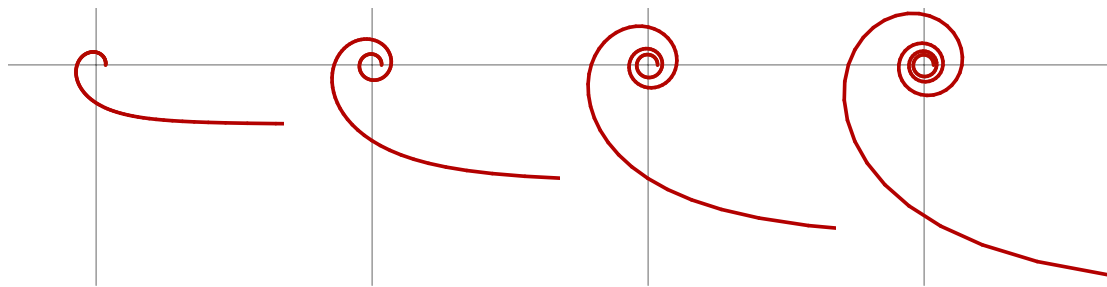
**Figure 5.2.26:** Anatomy of an inverse rising beat  $\alpha_n = \frac{1}{2}(\{10\} - \{9\})$ . Figure (a) shows the entire beat while (b) and (c) show the first and second half-sequences, respectively.

### 5.2.13 Hyperbolic Spiral

A hyperbolic spiral is the inverse curve of an Archimedes' spiral (5.2.11). It can be approximated by the subsequence

$$\alpha_{[0,M)} = \frac{1}{i(\{\frac{N}{M}k\} - \{\frac{N}{M}k + 1\})}$$

where  $k \ll M \ll N$  and  $\frac{N}{M} \in \mathbf{N}$ .



**Figure 5.2.27:** Hyperbolic spirals with  $m = 1, 2, 3, 4$  winding(s) (left to right).

### 5.2.14 Trochoid

In 5.2.1, it was discussed how trochoids could be produced by integrating an eccentric polygon. It is also possible to generate the trochoid as a subinterval of a bicircloid having a rolling circle with some finite radius and fixed circle with an infinite radius. Based on this perspective, a trochoid with  $k$  cycles can be approximated by the harmonic pattern function

$$\alpha_{[0,M)} = a \left\{ \frac{N}{M} k \right\} + \{1\}$$

where  $k \ll M \ll N$  and  $\frac{N}{M} \in \mathbf{N}$ . In order to keep the curve near unit scale, we choose a unit rather than infinite radius for the fixed circle and a relatively small radius for the rolling circle. This means that the trochoid extends along a small arc of a unit circle from  $\theta = 0$  to  $\frac{2\pi M}{N}$ . Given  $f = \frac{N}{M}k$ , the amplitude  $a$  determines whether we obtain a prolate ( $a > \frac{1}{f}$ ), curtate ( $a < \frac{1}{f}$ ), or cusped ( $a = \frac{1}{f}$ ) cycloid.

### 5.2.15 Standing Waves

As is well known in physics, a standing wave results from the sum of two sinusoidal waves propagating with equal velocity in opposite directions (J. d'Alembert, 1747). A standing wave in one dimension is described mathematically as

$$B(x, t) = A(x + vt) + A(x - vt)$$

where  $x$  designates position,  $t$  is time,  $A$  is a sinusoidal traveling wave with velocity  $v$ , and  $B$  is the resultant standing wave. If  $A$  is taken to be a complex sinusoid,

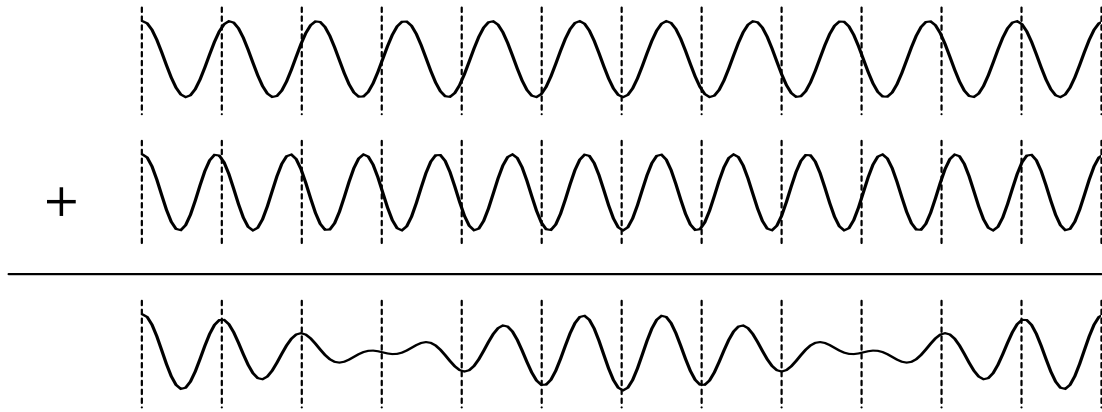
then  $B$  can be decomposed into independent spatial and temporal components as

$$\begin{aligned}
 B(x, t) &= e^{i(x+vt)} + e^{i(x-vt)} \\
 &= e^{ix}(e^{ivt} + e^{-ivt}) \\
 &= e^{ix}2 \operatorname{Re}(e^{ivt}).
 \end{aligned}$$

In this formulation, it becomes clear that the standing wave's amplitude modulates with angular frequency  $v$  radians/sec. We classify this type of standing wave as a *discontinuous space-time pattern*, as defined above, since the space and time components behave independently of one another. We can approximate a standing wave as a continuous *space-time pattern* with the harmonic pattern function

$$\alpha_n = \{k - 1\} + \{k + 1\}$$

where  $N_t = k$  is the number of time frames and  $N_s = N/N_t$  is the number of samples per time frame. As Fig. 5.2.28 illustrates, a standing wave given in terms of the harmonic pattern function is a single cycle of a beat spanning across space and time. The vertical dashed lines in the figure demarcate the spatial periods of  $N_s$  samples while time advances from left to right over  $N_t$  frames.



**Figure 5.2.28:** Illustration of standing wave given by space-time curve  $\alpha_n = \{11\} + \{13\}$  where  $N_t = 12$ .

### 5.2.16 Inverse Bicircloid

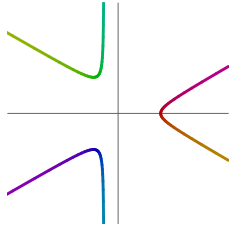
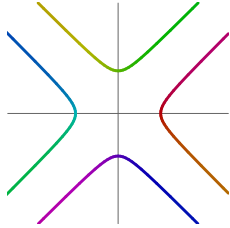
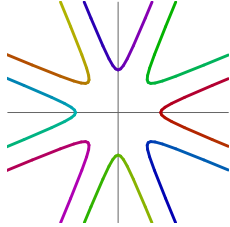
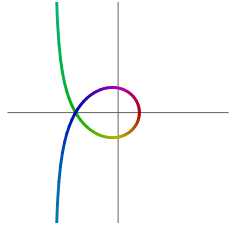
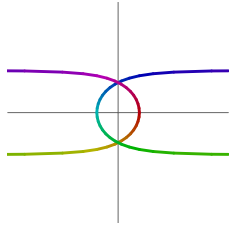
An inverse bicircloid is the complex inversion of a bicircloid and has the harmonic pattern function

$$\alpha_n = \frac{1}{b_1\{k_1\} + b_2\{k_2\}}. \quad (5.2.15)$$

A particularly important class of inverse bicircloids are the *inverse rose curves*. These have the harmonic pattern function

$$\alpha_n = \frac{1}{\{k\} + \{k + m\}}.$$

Inverse rose curves describe many well-known planar curves, such as the epispiral, trisectrix of Maclaurin, and trisectrix of Delange (Table 5.7).

Curve Plot	Name	$\alpha_n$	Inverse
	Epispiral	$\frac{1}{\{-1\}+\{2\}}$	Trifolium
	Epispiral (cross curve)	$\frac{1}{\{-1\}+\{3\}}$	Quadrifolium
	Epispiral	$\frac{1}{\{-3\}+\{5\}}$	
	Trisectrix of Maclaurin	$\frac{1}{\{1\}+\{2\}}$	Limaçon
	Trisectrix of Delange	$\frac{1}{\{1\}+\{3\}}$	Dürer Folium

**Table 5.7:** Inverse Rose Curves

The inverse bicircloid sequence is especially pertinent to sound synthesis as it produces waveforms whose spectrum is a complex exponential. We can obtain more

insight into the sonic characteristics of these waveforms by factoring Eq. 5.2.15 as

$$\begin{aligned}\alpha_n &= \frac{1}{b_1} \cdot \frac{\{-k_1\}}{\{0\} + \frac{b_2}{b_1}\{k_2 - k_1\}} \\ &= \frac{1}{b_1}\{\ell\} \cdot \frac{\{0\}}{\{0\} - b\{m\}}\end{aligned}\tag{5.2.16}$$

where  $b = -\frac{b_2}{b_1}$ ,  $\ell = -k_1$ , and  $m = k_2 - k_1$ . The factor  $\frac{1}{b_1}\{\ell\}$  is an amplitude scaling and frequency shift by  $\ell$ . Now if we let

$$\hat{\alpha}_n = \frac{\{0\}}{\{0\} - b\{m\}}$$

then

$$\mathcal{F}(\hat{\alpha}_n) = \sum_{k=0}^{\infty} b^k e^{i2\pi mk/N}$$

which is a sequence of harmonics whose non-zero amplitudes follow a geometric sequence with factor  $b$  spaced  $m$  harmonics apart. Thus,  $\alpha_n$  is simply an amplitude-scaled and frequency-shifted version of  $\hat{\alpha}_n$ . Subsequently, the spectrum of Eq. 5.2.16 is

$$\mathcal{F}(\alpha_n) = \frac{1}{b_1} \sum_{k=0}^{\infty} b^k e^{i2\pi(mk+\ell)/N}.$$

We now present three harmonic pattern functions that are capable of producing myriad “smooth” waveforms for sound synthesis:

$$\begin{aligned}\frac{\{\ell\}}{\{0\} - b\{m\}} & \quad \text{smooth delta} \\ \int i \frac{\{\ell\}}{\{0\} - b\{m\}} & \quad \text{smooth constant} \\ \iint - \frac{\{\ell\}}{\{0\} - b\{m\}} & \quad \text{smooth linear}\end{aligned}$$

The inverse bicircloid is capable of producing a certain class of smooth classical



waveforms for use in sound synthesis. We can obtain a log-sine (real part) and saw (imaginary part) waveform from

$$\int i \frac{\{1\}}{\{0\} - b\{1\}}$$

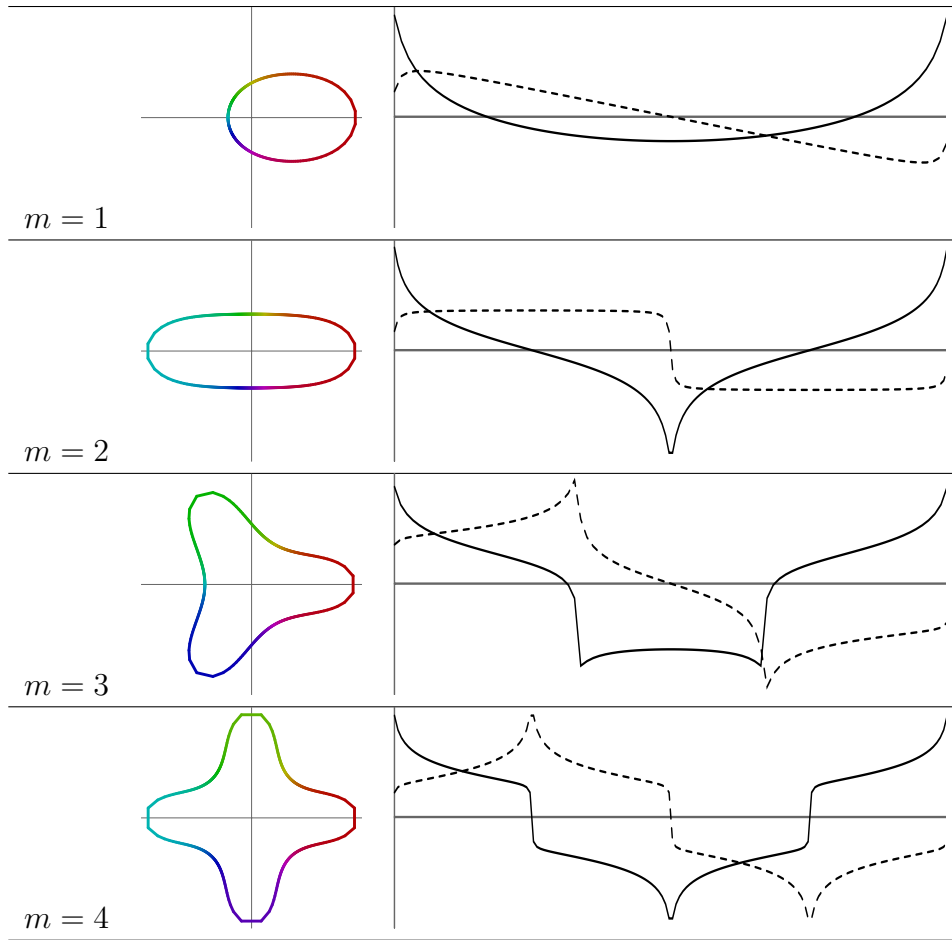
and a log-cotangent (real part) and square (imaginary part) waveform from

$$\int i \frac{\{1\}}{\{0\} - b\{2\}}$$

where the parameter  $b \leq 1$  controls the brightness of the waveforms. In general, an entire family of waveforms with harmonic spacing  $m$  and whose harmonic amplitudes vary as the reciprocal of their frequency are produced via

$$\alpha_n = \int i \frac{\{1\}}{\{0\} - b\{m\}}. \quad (5.2.17)$$

Curve and (waveform) component plots of Eq. 5.2.17 for various  $m$  are shown in Fig. 5.2.29. Besides having the ability to control the amplitude of upper harmonics, an immediate benefit of using Eq. 5.2.17 to produce classical waveforms is that it automatically produces quadrature signals that are naturally fit for frequency shifting transformations. One caveat is that these waveforms are not band-limited and thus the parameter  $b$  must be controlled accordingly to avoid aliasing artifacts.



**Figure 5.2.29:** Smooth saw ( $m = 1$ ) and square ( $m = 2$ ) waveforms along higher symmetry extrapolations ( $m = 3, 4$ ).

In addition to the once-integrated waveforms produced from Eq. 5.2.17, we can also obtain a family of twice-integrated waveforms with the harmonic pattern function

$$\alpha_n = \iint -\frac{\{1\}}{\{0\} - b\{m\}}. \quad (5.2.18)$$

Some special cases of twice-integrated waveforms include the parabolic waveform (real part)

$$\iint -\frac{\{1\}}{\{0\} - b\{1\}}$$

the triangle waveform

$$\iint -\frac{\{1\}}{\{0\} - b\{2\}}$$

and the quadrature triangle waveform

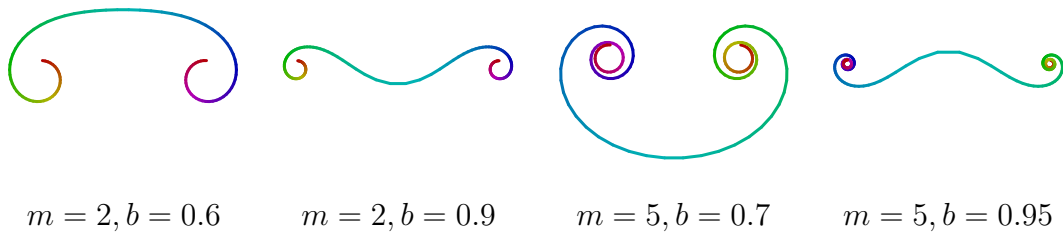
$$\iint -\frac{\{1\}}{\{0\} - b\{4\}}.$$

### 5.2.17 Volute Curve

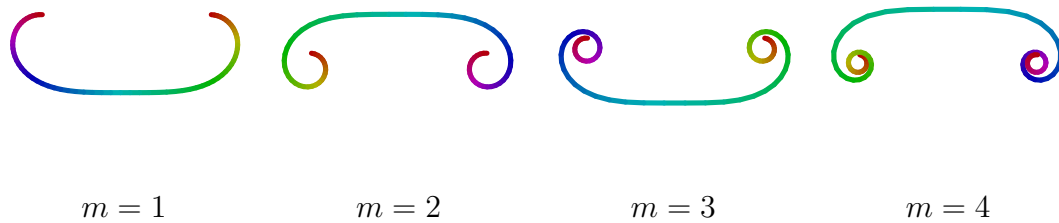
We define a *volute curve* as a special case of a polynomial spiral [23, 118] whose curvature is a function of the square of its arc length plus some constant. It is given by the harmonic pattern function

$$\alpha_n = \int \frac{1}{\{m\} + b\{m+1\}}$$

where the number of windings on each spiral is  $\frac{m}{2}$ . The parameter  $b$  controls the bend of the curve connecting the two spiral ends. Some example curves are shown in Fig. 5.2.30. When  $b = \frac{m}{m+1}$ , the segment connecting the two spirals is linear (Fig. 5.2.31). This stems from the fact that non-integrated curve has a cusp at  $n = N/2$ . These non-integrated curves are inverse curves of cuspsoids (5.2.4).



**Figure 5.2.30:** Various volute curves.



**Figure 5.2.31:** Volute curves with linear middle segment. The parameter  $b$  is  $\frac{m}{m+1}$ .

### 5.3 Order 3

While the number of new types of patterns introduced going from one harmonic to two harmonics is dramatic, there is an even bigger leap going to three harmonics. However, granted this, many three harmonic patterns involve the modulation of a wavy sinusoidal curve. These sinusoidal curves are constructed from the sum of two harmonics having equal amplitudes and frequencies that are equal or close in magnitude, but opposite in sign. Some examples are the Tusi couple and the class of narrow-lobe rose curves. Sinusoidal curves tend to produce interesting patterns since they create envelope curves at their tips and dense sheets of parallel lines intersecting at various angles.

Like order 2 patterns, there are only two unique order 3 harmonic pattern functions:

$$\alpha_n = A_1\{k_1, \theta_1\} + A_2\{k_2, \theta_2\} + A_3\{k_3, \theta_3\}$$

and its inversion

$$\alpha_n = \frac{1}{A_1\{k_1, \theta_1\} + A_2\{k_2, \theta_2\} + A_3\{k_3, \theta_3\}}.$$

### 5.3.1 Eccentric Tusi Couple

While an eccentric Tusi couple alone is not interesting from the standpoint of planar figures, when we integrate it we obtain a (real) sinusoidal curve. The *integrated eccentric Tusi couple* is given by

$$\alpha_n = \int a\{0\} - \{m, \phi\} + \{-m, -\phi\}$$

which produces a cosine curve along the real axis with  $m$  periods and a phase of  $2\pi\phi$  radians.



**Figure 5.3.1:** Integrated eccentric Tusi couples with  $\phi = 0$ ,  $m = 1$  (left) and  $m = 5$  (right).

### 5.3.2 Botanic Curve

A botanic curve [116] has the harmonic pattern function

$$\alpha_n = \{1\} + a(\{1 - m\} + \{1 + m\}). \quad (5.3.1)$$

The equivalent formula in polar coordinates is  $r = 1 + 2a \cos(2\pi mn/N)$ . Some of the curves obtained by Young and Wheatstone (Fig. 2.1.1 and Fig. 2.1.3) are instances of botanic curves. The botanic curve can also be seen as the projection

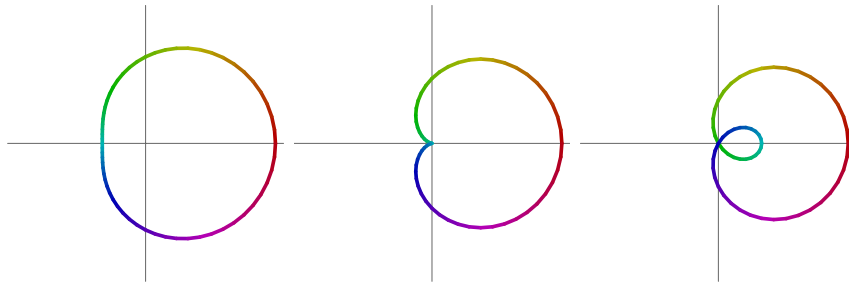
on the  $xy$  plane of a helical torus given by the parametric equation

$$x = \cos(\theta)(1 + a \cdot \cos(m\theta))$$

$$y = \sin(\theta)(1 + a \cdot \cos(m\theta))$$

$$z = a \cdot \sin(m\theta).$$

When  $m = 1$ , the botanic curve is the limaçon of Pascal.



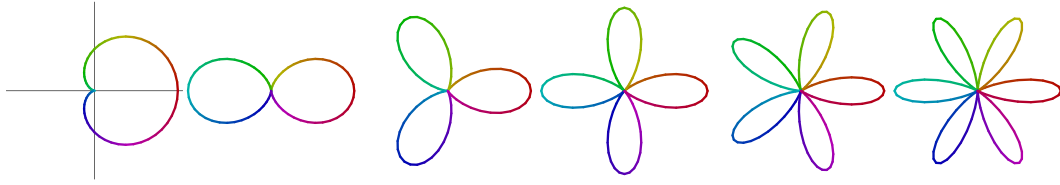
**Figure 5.3.2:** Botanic curves with  $m = 1$  and  $a = \frac{1}{4}$ ,  $a = \frac{1}{2}$  (eccentric cardioid), and  $a = 1$  (limaçon trisectrix) shown left to right.

### 5.3.3 Petal Curve

We define a *petal curve* as a special case of a botanic curve given by

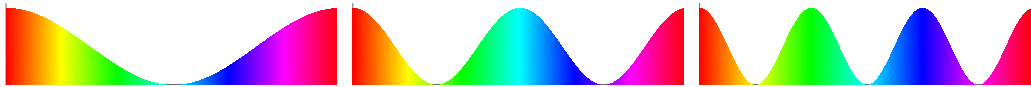
$$\alpha_n = \{1\} + \frac{1}{2}(\{1 - m\} + \{1 + m\})$$

where  $m$  is the order of dihedral symmetry. In polar coordinates, it is  $r = 1 + \cos(2\pi mn/N)$ . A petal curve has a similar shape as a rose curve, but differs in that there are no degenerate symmetry orders and it does not intersect itself, but rather has cusps that touch at the origin. For  $m = 2$ , the curve is also called a double egg [117].



**Figure 5.3.3:** Petal curves with  $m = 1, 2, 3, 4, 5, 6$  (left to right).

The complex sequence of this curve has two unique properties: the magnitude is a versed cosine function and the phase is linear and monotonic (the same phase profile as a single-cycle complex sinusoid).



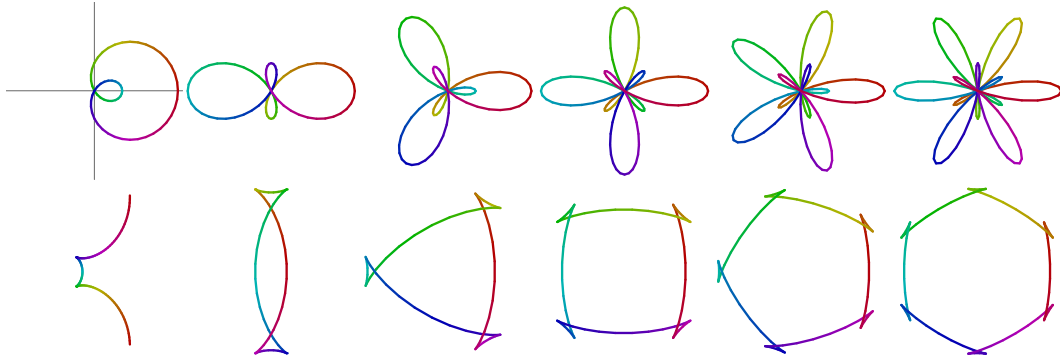
**Figure 5.3.4:** Magnitude/phase plots of petal curves for  $m = 1, 2, 3$  (left to right).

### 5.3.4 Double Rose Curve

We define a *double rose curve* as an extension of a rose curve through the addition of one harmonic. It is given by

$$\alpha_n = \{\ell\} + \{\ell - m\} + \{\ell + m\} \quad (5.3.2)$$

where  $m$  determines the number of petals. When  $m$  and  $\ell$  are odd, the smaller petals are centered within the larger petals, otherwise, the smaller and larger petals alternate. For  $\ell = 1$  and all  $m$ , odd or even, the curve only intersects itself at the origin. The double rose curve subsumes three well-known planar curves—the limaçon trisectrix ( $\ell = 1, m = 1$ ), the cycloid of Ceva ( $\ell = 1, m = 2$ ), and Freeth's nephroid ( $\ell = 2, m = 1$ ).



**Figure 5.3.5:** Double rose curves with  $\ell = 1$  and  $m = 1, 2, 3, 4, 5, 6$  (top row, left to right). Once-integrated curves are displayed in the bottom row.

The double rose is categorized as a delta interpolation pattern Section 4.4. It is also a special case of the more general Fourier polygon which is presented in greater detail in 5.4.5. This relationship is more obvious if we integrate Eq. 5.3.2. As shown in Fig. 5.3.5, the resulting curves become constant interpolation patterns and begin to resemble polygons with  $m$  vertices.

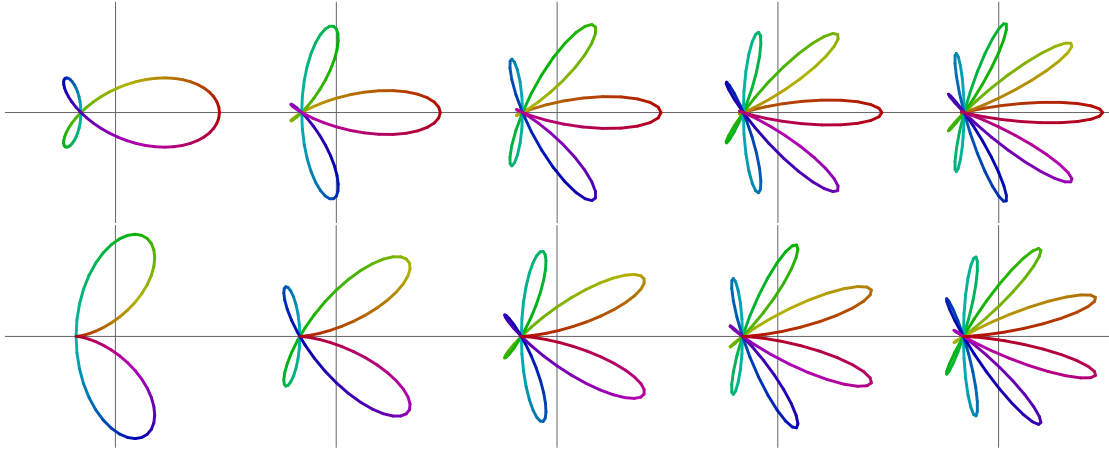
### 5.3.5 Fanned Rose

We define a *fanned rose curve* as the curve given by

$$\alpha_n = \{1\} + \{1 + m, \phi\} + \{-m, \phi\}$$

where  $\phi = 0$  or  $\frac{1}{2}$  and the number of lobes is  $2m + 1 - 2\phi$ . When  $\phi = 0$  there are an odd number of lobes and when  $\phi = \frac{1}{2}$  the number is even. When  $m = 1$ , this equation produces two well-known plane curves— the trefoil curve ( $\phi = 0$ ) and the bifolium curve ( $\phi = \frac{1}{2}$ ). A variety of fanned rose curves are shown in Fig. 5.3.6.





**Figure 5.3.6:** Fanned rose curves for  $\phi = 0, m = 1, 2, 3, 4, 5$  (top row, left to right) and  $\phi = \frac{1}{2}, m = 1, 2, 3, 4, 5$  (bottom row, left to right).

One of the main differences of the even- from the odd-lobed curves is that the even-lobed curves contain a cusp between the two largest lobes whereas the odd-lobed curves contains no cusps. Technically speaking, the cusp lies exactly at the boundary between a prolate (non-looping) and curtate (looping) curve. Furthermore, the subcomponents  $\{1 + m, \phi\} + \{-m, \phi\}$  describe a rose curve with  $2m + 1$  loops which is always odd. Therefore, the even loop curves can be seen as an odd loop curve where one loop lies at the boundary of becoming unlooped (a cusp).

As  $m$  increases, it becomes more apparent that the curve is enclosed in an envelope with the shape of a cardioid. This can be shown by factoring the harmonic components containing  $m$  so that

$$\begin{aligned} \alpha_n &= \{1\} + \left\{\frac{1}{2}\right\} \left( \left\{\frac{1}{2} + m, \phi\right\} + \left\{-\frac{1}{2} - m, \phi\right\} \right) \\ &= \{1\} + 2 \left\{\frac{1}{2}\right\} \operatorname{Re} \left\{\frac{1}{2} + m, \phi\right\}. \end{aligned}$$

If we consider only the maxima and minima of  $\operatorname{Re} \left\{\frac{1}{2} + m, \phi\right\}$ , 1 and  $-1$ , respec-

tively, it becomes clear that the tips of the loops of the curve form two envelopes  $\{1\} \pm 2\{\frac{1}{2}\}$  which are the upper and lower half-plane portions of a cardioid, respectively. Together, these envelopes form the envelope of the entire curve, a complete cardioid. This observation leads to a more general type of curve which will be called an *envelope bicircloid*.

### 5.3.6 Envelope Bicircloid

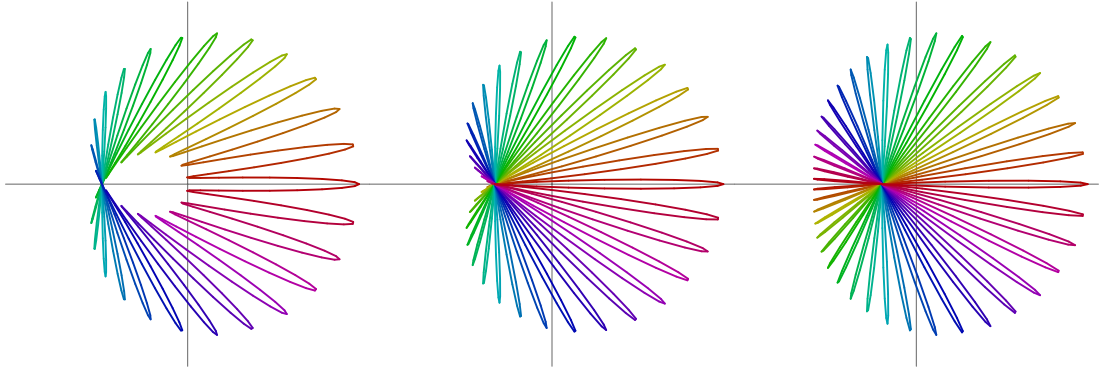
An *envelope bicircloid* generalizes several seemingly disparate curves into one family of curves. These curves, loosely speaking, consist of a sinusoidal curve whose minima and maxima, typically  $-1$  and  $1$ , trace out two independent bicircloid curves. The harmonic pattern function of an envelope bicircloid is

$$\alpha_n = \{p\} + \frac{b}{2}(\{q + m\} + \{q - m\}) \quad (5.3.3)$$

where  $m \gg p, q$ . The equations of the envelopes are found by factoring Eq. 5.3.3

$$\begin{aligned} \alpha_n &= \{p\} + \frac{b}{2}(\{q + m\} + \{q - m\}) \\ &= \{p\} + b\{q\}\frac{1}{2}(\{m\} + \{-m\}) \\ &= \{p\} + b\{q\} \operatorname{Re}\{m\} \end{aligned}$$

revealing the two envelopes  $\{p\} \pm b\{q\}$ . The parameters  $q$  and  $m$  can take on half-integer values, but only if both of them are half-integers since the sum or difference of any two half-integers is an integer. When  $q$  and  $m$  are both half-integer, then the envelope is a single bicircloid formed from the union of two bicircloid halves produced by the extrema of  $\operatorname{Re}\{m\}$  (Fig. 5.3.7).



**Figure 5.3.7:** Envelope bicircloids given by  $p = 1$ ,  $q = \frac{1}{2}$ ,  $m = 20\frac{1}{2}$ ,  $b = 1, \frac{1}{2}, \frac{1}{4}$  (left to right).

### 5.3.7 Conic Sections

A conic section is the curve of intersection between a double-cone and a plane.

The standard parameterization of a conic section is

$$f(\phi) = \frac{e^{i\phi}}{1 + b \cos(\phi)}$$

where  $\phi \in [0, 2\pi)$  and  $b \in [0, 2]$ . The standard parameterization directly maps into the harmonic pattern function

$$\alpha_n = \frac{\{1\}}{\{0\} + b \operatorname{Re}\{1\}} \quad (5.3.4)$$

where  $\phi \rightarrow 2\pi n/N$ . The parameter  $b$  determines the shape of the curve as follows:

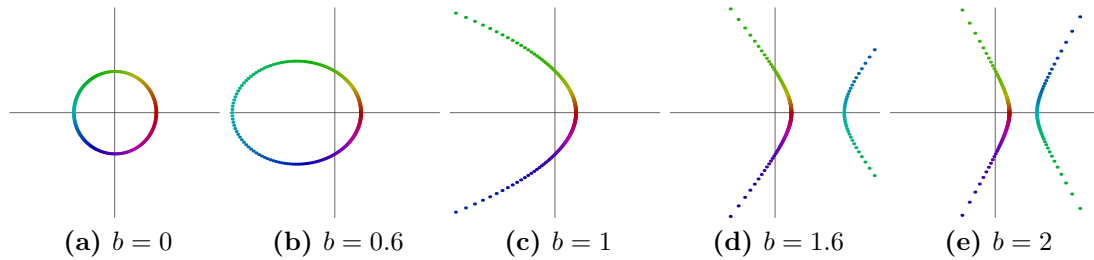
$$\left\{ \begin{array}{ll} b = 0 & \text{circle} \\ b \in (0, 1) & \text{ellipse} \\ b = 1 & \text{parabola} \\ b \in (1, 2] & \text{hyperbola} \end{array} \right.$$

The ellipse and hyperbola curves resulting from a conic section do *not* exhibit velocity symmetry around their vertical reflection axis as do the curves given in 5.2.2 and 5.4.1, respectively. If the sign of  $b$  is negative, the figure opens up to the right rather than to the left as  $|b|$  increases.

We can write Eq. 5.3.4 in the alternate form

$$\alpha_n = \frac{1}{\{-1\} + \frac{b}{2}(\{-2\} + \{0\})}$$

by reduction where it becomes clear that a conic section is the inverse curve of the limaçon of Pascal and, furthermore, a special case within the family of inverse botanic curves.



**Figure 5.3.8:** Conic sections circle, ellipse, parabola, and hyperbola.

We can generalize the symmetry of a conic section through definition of an inverse botanic curve given by

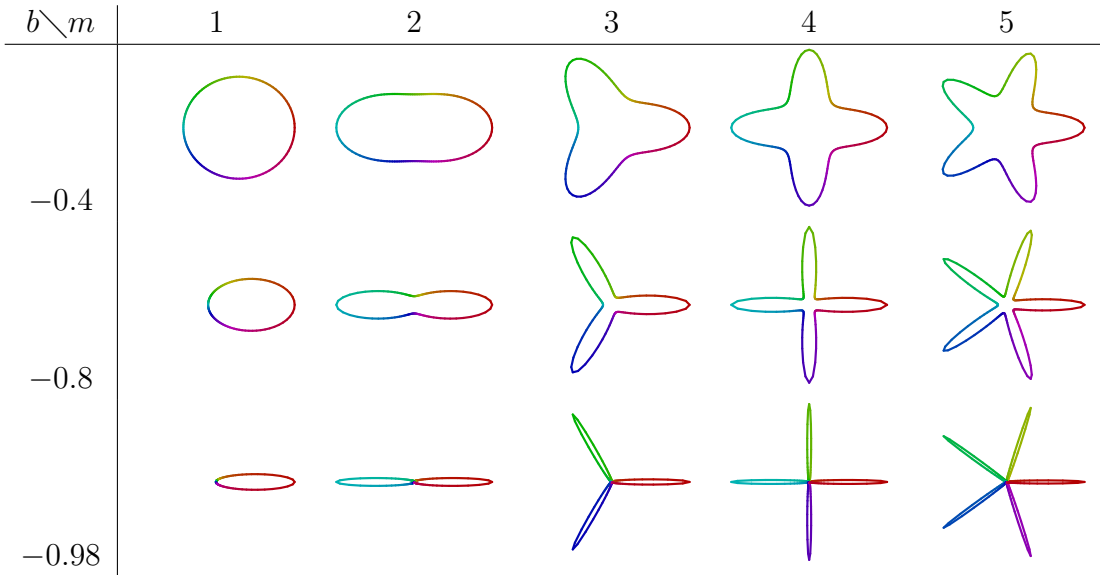
$$\alpha_n = \frac{\{1\}}{\{0\} + b \operatorname{Re}\{m\}}$$

or equivalently

$$\alpha_n = \frac{1}{\{-1\} + \frac{b}{2}(\{-m-1\} + \{m-1\})}$$

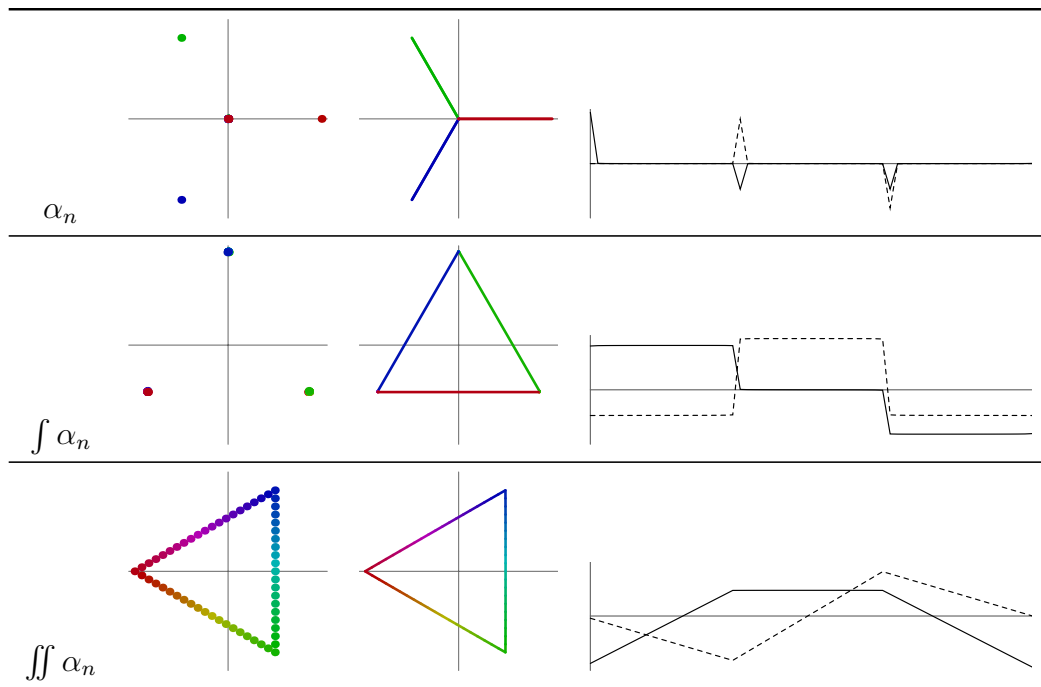
where the amplitude  $b$  acts as a sharpness parameter. Curves plots for various  $m$  and  $b$  are shown in Table 5.8. As  $|b| \rightarrow 1^-$ , the curves become more spoke-like and

the vertices get more concentrated near the origin. They can therefore be classified as delta interpolation patterns. In the case where  $m = 1$ , the curve approaches a delta function.

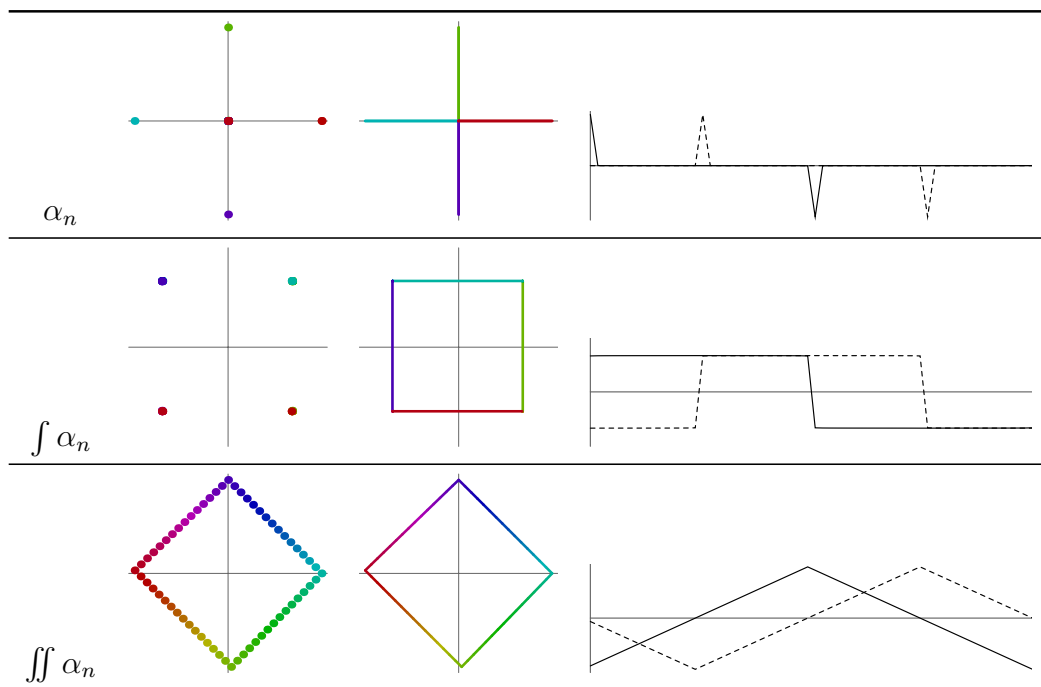


**Table 5.8:** Inverse botanic curves for various  $m$  and  $b$ . When  $m = 1$ , the curves are conic sections.

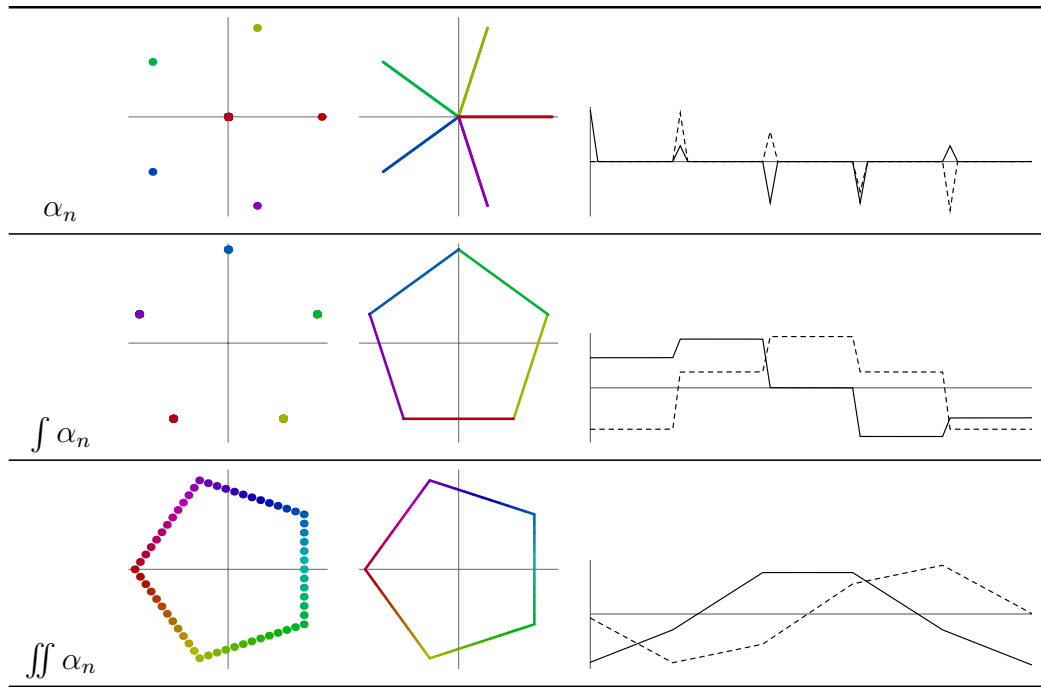
An interesting case presents itself when  $|b| \rightarrow 1^-$  and  $N/m \in \mathbf{N}$ . Here we get spoke-like curves whose tips result from inverting the cusps near the origin of the inverse petal curve. Because  $N$  is an integer multiple of  $m$ , the  $m$  points closest to the origin of the inverse petal curve are all the same distance from the origin. This means that when they are inverted, they again lie at the same distance from the origin. What makes this interesting, is that when the curve is integrated, the result will be in the form of a regular polygon. When integrated once, the points stack up on the vertices of the polygon and when integrated twice, the points are distributed uniformly along the edges. Tables 5.9, 5.10, and 5.11 show vertex/edge curve plots and component plots of integrations of inverse botanic curves with  $b = 0.9999$ ,  $N = 60$ , and  $m = 3, 4, 5$ , respectively.



**Table 5.9:** Integrations of an inverse botanic curve with  $b = 0.9999$ ,  $N = 60$ , and  $m = 3$ .



**Table 5.10:** Integrations of an inverse botanic curve with  $b = 0.9999$ ,  $N = 60$ , and  $m = 4$ .



**Table 5.11:** Integrations of an inverse botanic curve with  $b = 0.9999$ ,  $N = 60$ , and  $m = 5$ .

### 5.3.8 Double-sided Spectral Exponential

A complex sequence whose spectrum is an asymmetric double-sideband exponential is given by

$$\alpha_n = \frac{1}{1 - a\{-m\} - b\{m\}} \quad (5.3.5)$$

where  $a$  and  $b$  control the fall-off of the negative and positive frequency exponentials, respectively. To obtain well-behaved spectra,  $a + b$  must be less than 1. This pattern is the same as an inverse botanic curve (5.3.7) when frequency shifted up one harmonic  $\{1\}$ . To show that the spectrum is indeed a double-sided exponential,

we start with a product of two single-sided spectral exponentials and then simplify

$$\begin{aligned}
\alpha_n &= \left( \frac{1}{1 - a'\{-m\}} \right) \left( \frac{1}{1 - b'\{m\}} \right) & (5.3.6) \\
&= \frac{1}{(1 + a'b') - a'\{-m\} - b'\{m\}} \\
&= \frac{1}{1 - \frac{a'}{1+a'b'}\{-m\} - \frac{b'}{1+a'b'}\{m\}}.
\end{aligned}$$

The final result is equivalent to Eq. 5.3.5 with  $a$  and  $b$  in terms of  $a'$  and  $b'$ . Since

$$\frac{1}{1 - a\{m\}} = \sum_{k=0}^{\infty} a^k \{mk\}$$

we determine the spectrum of Eq. 5.3.5 to be a product of two exponential functions

$$\left( \sum_{k=0}^{\infty} a'^k \{mk\} \right) \left( \sum_{k=0}^{\infty} b'^k \{-mk\} \right).$$

### 5.3.9 Moving Bicircloid

Like the moving polygon discussed in 5.2.1, a moving bicircloid is a uniformly spaced repetition of bicircloid curves along a line of motion. Its harmonic pattern function is

$$\alpha_n = \int a + A_1 k_1 \{mk_1\} + A_2 k_2 \{mk_2\}$$

where  $a \in \mathbf{C}$  determines the direction and speed of motion of  $m$  bicircloids given by  $A_1 \{k_1\} + A_2 \{k_2\}$ . When  $A_1 = A_2$ , we obtain a moving rose curve, when  $A_1 = \frac{1}{k_1}$  and  $A_2 = \frac{1}{k_2}$ , we obtain a moving cuspid, and when  $A_1 = \frac{1}{k_1^2}$  and  $A_2 = \frac{1}{k_2^2}$ , we obtain a moving smooth star polygon.

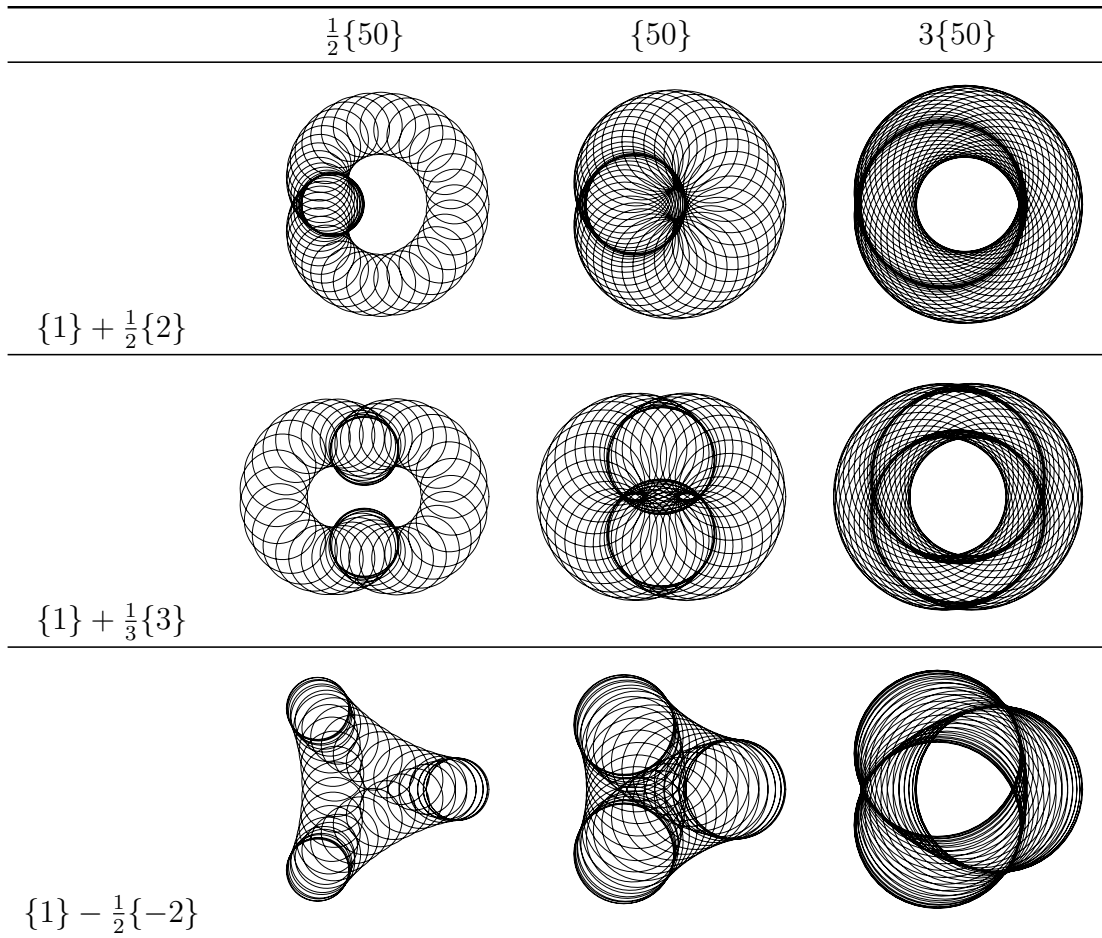


### 5.3.10 Circle Cuspoid

We define a *circle cuspoid* as a curve comprised of a cuspoid (5.2.4) base curve and a higher-frequency circular curve. In the resulting curve, there appear circles wherever a cusp is present in the base curve. The reason the circles appear at the cusps is because the velocity there momentarily becomes zero. At other points along the curve, the circular curve gets stretched out resembling something like a trochoid. This type of pattern is seen in some phonautograph images (Fig. 2.1.4c). The circle cuspoid is given by

$$\alpha_n = \frac{1}{k_1}\{k_1\} + \frac{1}{k_2}\{k_2\} + a\{p\}$$

where  $p \gg k_1, k_2$ . Some examples of circle cuspoids are shown in Fig. 5.3.9. Regardless of the amplitude of the circular curve, the circles remain clearly visible at the cusp points of the base cuspoid. The circle cuspoid can be generalized to use any constant interpolation pattern as a base curve and any other high-frequency curve as the duplicated curve.



**Figure 5.3.9:** Circle cuspsoids. The rows are different base cuspid curves, a cardioid, a nephroid, and a deltoid going top to bottom, and the columns are circular curves with different amplitudes.

### 5.3.11 Circle Chain

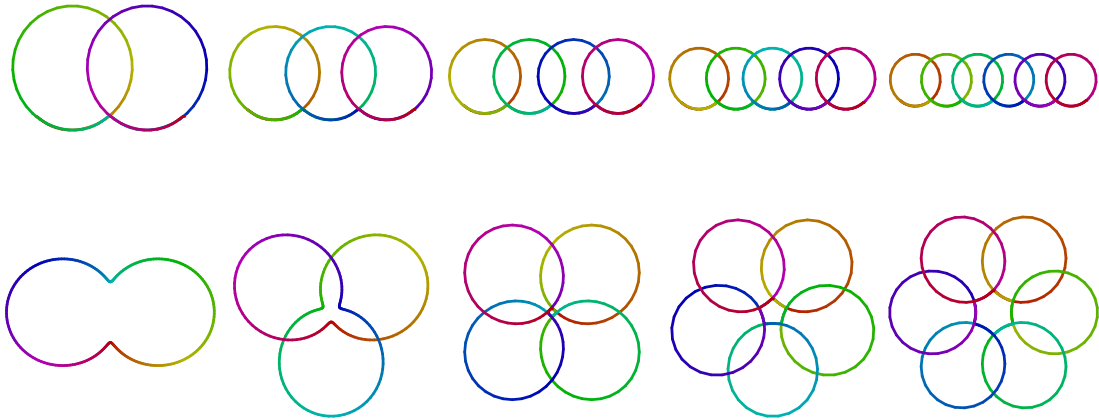
We define a *circle chain* as the curve given by

$$\alpha_n = \int a\{\ell\} + \{\ell + m\} - \{\ell + 2m\}$$

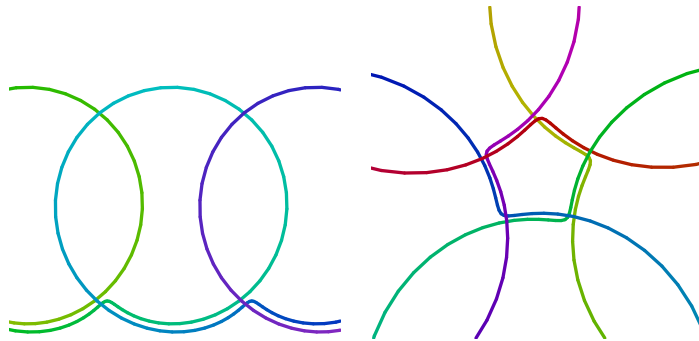
where  $m$  is the number of circles,  $\ell \in [-1, 0]$  is the winding amount, and  $a \approx 0.215$ .

A circle chain is a unicursal curve that appears like a chain of multiple circles.

Examples of this curve were first given by Bazley [11]. Fig. 5.3.10 shows some examples of curves for the parameter  $\ell$  and  $m \in [2, 6]$ . When  $\ell = -1$  and  $m \leq 3$ , the circles lose the appearance of being individual curves. Fig. 5.3.11 shows details at the center of the circle chains with  $m = 5$  revealing how the curve almost perfectly coincides with itself at intersection points at the bottom for  $\ell = 0$  and center for  $\ell = -1$ . The phase of the  $\{\ell + m\}$  component is adjusted slightly to make the curve's path more visible.



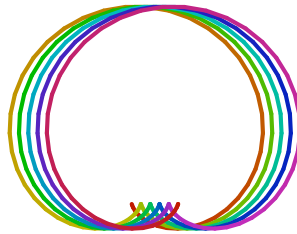
**Figure 5.3.10:** Circle chain curves. The symmetry parameter  $m$  ranges from 2 to 6 going left to right. The top row curves have  $\ell = 0$  and the bottom row curves have  $\ell = -1$ .



**Figure 5.3.11:** Details at center of circle chain curves for  $m = 5$  and  $\ell = 0$  (left) and  $\ell = -1$  (right). The curves are skewed slightly to make the path more visible.

We can understand more about the circle chain curve if we set  $b$  to some small

amount. Fig. 5.3.12 shows the resulting curve when  $m = 5$ ,  $\ell = 0$ , and  $a = 0.015$ . It is clearly a type of moving cardioid curve similar to the moving polygons discussed in 5.2.1. Therefore, a circle chain curve with  $\ell = 0$  is a rather unique case of a moving cardioid.



**Figure 5.3.12:** A circle chain curve is a special case of a moving cardioid curve.

## 5.4 Higher Order

In this section, some harmonic pattern functions with an order greater than 3 are presented. Clearly, this can in no way be comprehensive, so only some more important or well-known patterns are discussed in relation to the harmonic pattern function.

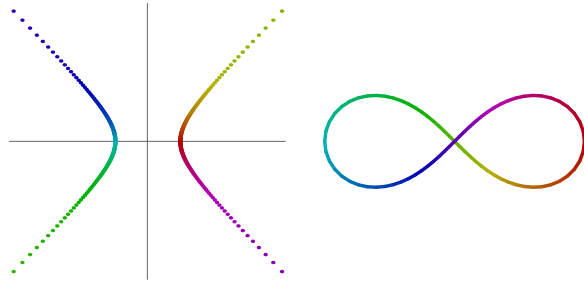
### 5.4.1 Rectangular Hyperbola

The rectangular hyperbola discussed here is different from the hyperbola produced from a conic section in 5.3.7. Unlike the conic section hyperbola, the rectangular hyperbola is centered at the origin and its speed is symmetrical between both branches (Fig. 5.4.1). The harmonic pattern function of a rectangular hyperbola is

$$\alpha_n = \frac{a\{0\} + b\text{Im}\{1\}}{\text{Re}\{1\}}$$

where  $a$  is its horizontal scaling and  $b$  is its vertical scaling. The lemniscate of Bernoulli (Fig. 5.4.1) is the inverse curve of a rectangular hyperbola. Accordingly, its harmonic pattern function is

$$\alpha_n = \frac{\operatorname{Re}\{1\}}{\{0\} + \operatorname{Im}\{1\}}.$$



**Figure 5.4.1:** Rectangular hyperbola (left) and its inverse curve, the lemniscate of Bernoulli (right).

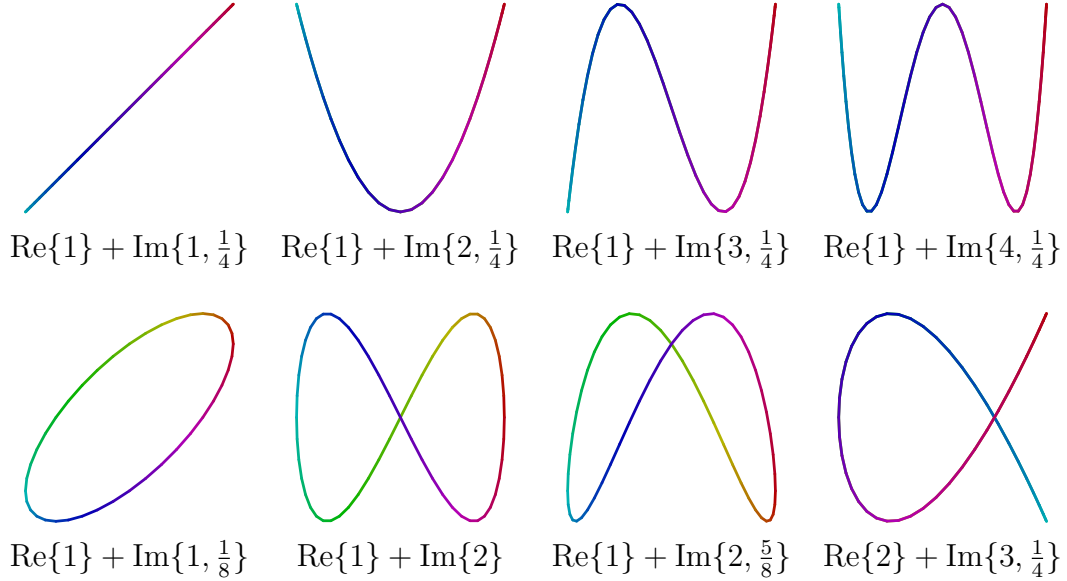
## 5.4.2 Bowditch Curves

A Bowditch curve is the locus of two independent simple harmonic motions along two orthogonal axes. Its harmonic pattern function is a sum of two harmonic projections on the real and imaginary axes given by

$$\begin{aligned} \alpha_n &= \frac{\{k_0, \phi_0\} + \{-k_0, \phi_0\} + \{k_1, \phi_1\} - \{-k_1, \phi_1\}}{2} \\ &= \operatorname{Re}\{k_0, \phi_0\} + \operatorname{Im}\{k_1, \phi_1\}. \end{aligned} \quad (5.4.1)$$

A Bowditch curve is degenerate (loops back on itself) when either  $k_0$  is even and  $\sin \delta = 0$  or  $k_0$  is odd and  $\cos \delta = 0$  where  $\delta = 2\pi(k_0\phi_1 - k_1\phi_0)$  [65]. Some well-known algebraic curves that are also Bowditch curves include the circle, line, ellipse, lemniscate of Gerono, Chebyshev polynomials, Tschirnhausen cubic, saddlebag

[65], and besace curve [115]. Table 5.12 displays several of these algebraic curves with their corresponding harmonic pattern function beneath.



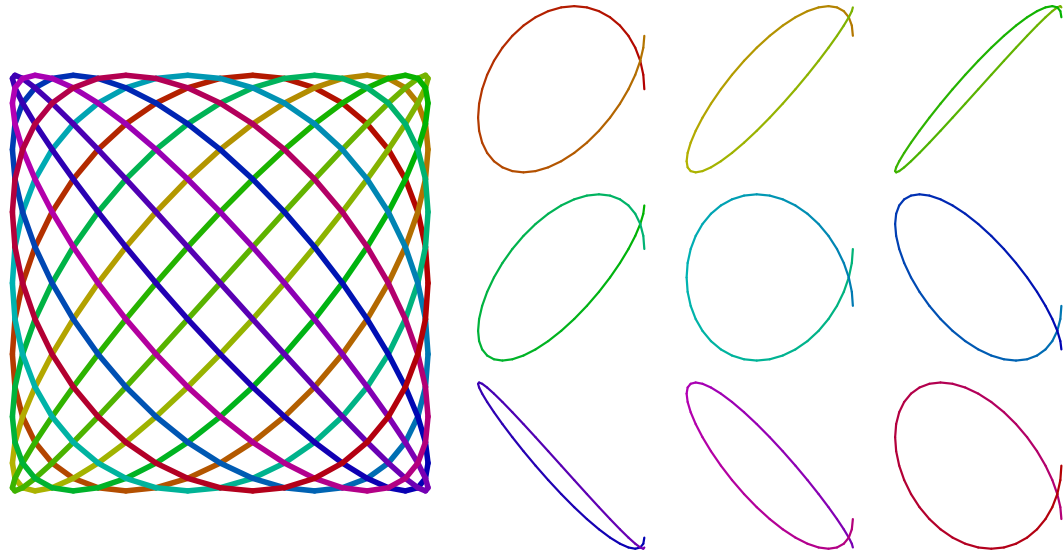
**Table 5.12:** Well-known algebraic curves that are also Bowditch curves. On the top row going left to right are the Chebyshev polynomials of degree 1 (a line), degree 2 (a parabola), degree 3, and degree 4. On the bottom row going left to right are an ellipse, lemniscate of Geronon, saddlebag, and Tschirnhausen cubic.

When  $k_0$  is odd and  $k_1 = k_0 \pm 1$ , the Bowditch curve forms a crosshatched sinusoidal pattern with a square envelope. The harmonic pattern function is defined as

$$\alpha_n = \text{Re}\{\ell\} + \text{Im}\{\ell \pm 1\}$$

where  $\ell$  is odd. If partitioned into  $\ell$  contiguous subsequences so that the  $j^{\text{th}}$  subsequence has indices  $n \in [\frac{N}{\ell}j, \frac{N}{\ell}(j+1))$ , this pattern captures a continuous motion from circle to ellipse to line and back. However, since the entire pattern is unicursal, the intermediate circles and ellipses are not closed. This development was also observed by Rigge [87] who stated, in reference to a similar pattern, “. . . because the transition is continuous, there is in reality never a true ellipse, nor

straight line, nor a circle, since not one of those drawn is a closed curve.” The term  $\text{Im}\{\ell \pm 1\}$  determines whether the curve associated with each subsequence overshoots or undershoots its starting point. Fig. 5.4.2 shows a curve plot of  $\text{Re}\{9\} + \text{Im}\{10\}$  along with 9 successive subsequences that show its evolution from circle to line and back. If we let  $N_t = \ell$  be the number of temporal frames of motion and  $N \rightarrow \infty$ , then as we increase  $N_t$  we obtain both higher temporal and shape resolutions. That is, as  $N_t$  increases, the subsequence curves more closely approximate ideal (closed) ellipses. In addition, as  $N_t$  increases, the curve of the entire sequence forms a denser crosshatched pattern.



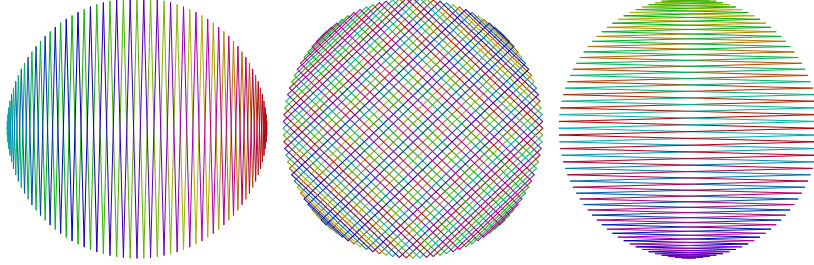
**Figure 5.4.2:** The larger curve on the left is the entire curve plot of  $\text{Re}\{9\} + \text{Im}\{10\}$ . The grid of curves on the right shows 9 successive subsequences of the entire curve, in order, going from top to bottom, then left to right.

A family of unit-circle patterns in the shape of a crosshatched disc is given by

$$\alpha_n = \text{Re}\{\ell\} + \text{Im}\left\{\frac{N}{2} + \ell\right\}$$

where  $\ell$  determines the obliqueness of the crosshatch. When  $\ell = \pm 1$  the crosshatch

is vertical, when  $\ell = \frac{N}{2} \pm 1$  it is horizontal, and when  $\ell = \frac{N}{4} \pm 1$  it is right-angled (Fig. 5.4.3). For other values of  $\ell$ , the angle of the crosshatch falls between these extremes.



**Figure 5.4.3:** Crosshatched disc patterns for  $\ell = 1, \frac{N}{4} + 1, \frac{N}{2} + 1$  (left to right).  $N = 120$ .

As a final note, integration of Bowditch curves does not lead to any novel patterns. Integrating Eq. 5.4.1 (ignoring phase terms for simplicity), we obtain

$$\begin{aligned}
 \alpha_n &= \int \operatorname{Re}\{k_0\} + \operatorname{Im}\{k_1\} \\
 &= \int \{k_0\} + \{-k_0\} + \{k_1\} - \{-k_1\} \\
 &= \frac{1}{ik_0} \{k_0\} + \frac{1}{-ik_0} \{-k_0\} + \frac{1}{ik_1} \{k_1\} - \frac{1}{-ik_1} \{-k_1\} \\
 &= -i \left[ \frac{1}{k_0} (\{k_0\} - \{-k_0\}) + \frac{1}{k_1} (\{k_1\} + \{-k_1\}) \right] \\
 &= -i \left( \frac{1}{k_0} \operatorname{Im}\{k_0\} + \frac{1}{k_1} \operatorname{Re}\{k_1\} \right) \\
 &= \frac{1}{k_0} \operatorname{Im} \left\{ k_0, -\frac{1}{4} \right\} + \frac{1}{k_1} \operatorname{Re} \left\{ k_1, -\frac{1}{4} \right\}
 \end{aligned}$$

which is another Bowditch curve whose sinusoidal components are swapped and scaled by the reciprocal of their frequency. One unique case is when  $k_0 = 0$  where we obtain a (real) sinusoidal curve on the Argand plane. This, however, is a special case of the integrated eccentric Tusi couple discussed in 5.3.1.



### 5.4.3 Comb Filters

A general comb filter transfer function is generated by

$$\alpha_n = \frac{a_0 + a_m \{m\}}{1 - b_m \{m\}} \quad (5.4.2)$$

which is a discrete sampling of the continuous function

$$H(z) = \frac{a_0 + a_m z^m}{1 - b_m z^m}$$

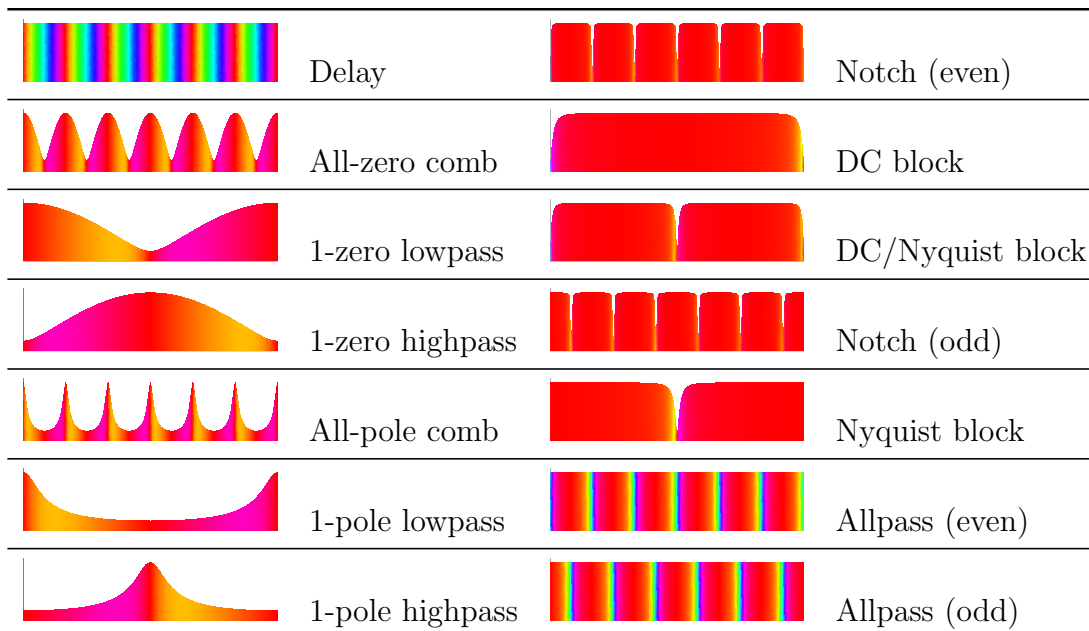
with difference equation

$$y[n] = a_0 x[n] + a_m x[n - m] + b_m y[n - m].$$

For the filter to be stable,  $|b_m| < 1$ . By appropriate selection of the parameters  $a_0$ ,  $a_m$ ,  $b_m$ , and  $m$ , a wide variety of filter transfer functions can be produced. These are summarized in Table 5.13. The parameter  $m$  determines the number of “distortions” that repeat at regular intervals (precisely  $N/m$  samples) along the sequence. A distortion is simply a deviation from uniform magnitude and/or zero phase.

Name	$m$	$a_0$	$a_m$	$b_m$	$c$
Delay	$> 0$	0	1	0	1
All-zero	$> 0$	1	$[-1, 1]$	0	$\frac{1}{1+ a_m }$
1-zero lowpass	1		$[0, 1]$		
Averager			1		
1-zero highpass			$[-1, 0]$		
Differencer			-1		
All-pole	$> 0$	1	0	$(-1, 1)$	$1 -  b_m $
1-pole lowpass	1			$[0, 1)$	
Leaky integrator				$[0.99, 1)$	
Integrator				1	
1-pole highpass				$(-1, 0]$	
Notch (even)	$> 0$	1	-1	$[0, 1)$	$\frac{1+ b_m }{2}$
DC blocker	1				
DC/Nyquist blocker	2				
Notch (odd)	$> 0$	1	1	$(-1, 0]$	
Nyquist blocker	1				
Allpass (even)	$> 0$	$-b_m$	-1	$[0, 1)$	1
Allpass (odd)	$> 0$	$b_m$	1	$(-1, 0]$	

**Table 5.13:** Parametric descriptions of comb filters.



**Table 5.14:** Magnitude/phase frequency responses of the general comb filter types. Frequencies run from 0 on the left to  $N - 1$  on the right. The height of the graph is  $|z|$  while the hue corresponds to  $\arg z$  where  $0, \frac{1}{3}2\pi, \frac{2}{3}2\pi \rightarrow$  red, green, blue.

We can extend Eq. 5.4.2 to permit shifting of the sequence by adding a single phase variable. This *shiftable comb filter* has the harmonic pattern function

$$\alpha_n = \frac{a_0 + a_m \{m, \phi\}}{1 - b_m \{m, \phi\}}$$

where  $\phi$  is a shift amount in  $(0, 1)$ . The difference equation of the shiftable comb filter is

$$y[n] = a_0 x[n] + (a_m x[n - m] + b_m y[n - m]) e^{i2\pi\phi}.$$

When  $m = 1$ ,  $\phi$  operates like a center frequency parameter that shifts the single pole/zero in the frequency spectrum thus creating a resonant/notch filter. For a one-pole filter, what is typically called the cut-off frequency is really the bandwidth of the resonant peak. For  $m > 1$ , continuous linear increment of  $\phi$  results in a barber-pole phasing effect [14]. For the shiftable comb filter to operate correctly,

the input signal must be complex-valued. If only a real-valued signal is available, then it can be sufficiently complexified by passing it through a Hilbert filter.

#### 5.4.4 Truncated Spectral Exponential

A truncated spectral exponential is a complex sequence whose spectrum has the shape of a truncated exponential function. It is the difference of two (infinite) spectral exponentials (Eq. 5.2.16). Its harmonic pattern function is

$$\alpha_n = \frac{\{0\} - b^K \{mK\}}{\{0\} - b\{m\}} \quad (5.4.3)$$

where  $m$  is the harmonic spacing or degree of symmetry,  $K$  is the total number of harmonics, and  $b$  is the decay factor. Setting  $b = 1$  produces a series of equiamplitude harmonics. Numerical problems can be avoided by setting  $b$  to a value slightly less than 1. A frequency-shift factor of  $\{\ell\}$  can be applied to avoid the DC term or to create inharmonic spectra. Eq. 5.4.3 can be expanded into the series

$$\alpha_n = \sum_{k=0}^{K-1} b^k e^{-i(2\pi n/N)mk}.$$

The series expansion is derived by separating terms in Eq. 5.4.3

$$\alpha_n = \frac{\{0\}}{\{0\} - b\{m\}} - \frac{b^K \{mK\}}{\{0\} - b\{m\}}$$

then expanding each term and simplifying

$$\begin{aligned}
\alpha_n &= \sum_{k=0}^{\infty} b^k e^{-i(2\pi n/N)mk} - \sum_{k=0}^{\infty} b^{k+K} e^{-i(2\pi n/N)(m[k+K])} \\
&= \sum_{k=0}^{\infty} b^k e^{-i(2\pi n/N)mk} - \sum_{k=K}^{\infty} b^k e^{-i(2\pi n/N)mk} \\
&= \sum_{k=0}^{K-1} b^k e^{-i(2\pi n/N)mk}.
\end{aligned}$$

The truncation of the series is due to the fact that  $b^{k+K} = b^K b^k$ , i.e., the function  $b^k$  remains similar under a shift in position  $k$ .

All order 1 (Section 5.1) and order 2 (Section 5.2) patterns are generalized by Eq. 5.4.3, however, this is a somewhat trivial result as direct synthesis/summation of harmonics is more straightforward. When  $b = 1$ , a truncated spectral exponential generalizes all patterns comprised of a finite number of harmonics with equal amplitude and equally-spaced frequencies. These include double rose curves (5.3.4) and delta Fourier polygons (5.4.5).

### 5.4.5 Fourier Polygons

The Fourier polygons discussed here are the discrete version of continuous polygons constructed from Fourier series [89]. Fourier polygons are “overcomplete” polygons in that they are constructed from a relatively larger number of points than their symmetry class. They should not be confused with the geometrically exact  $N$ -gons discussed in 5.1.2 and 5.1.3 made from only a single harmonic. These single harmonic polygons are also referred to as “Fourier polygons” elsewhere [35], however, we do not adopt the same terminology as Fourier series generally involve functions constructed from a superposition of *many* harmonics, not just one. The single

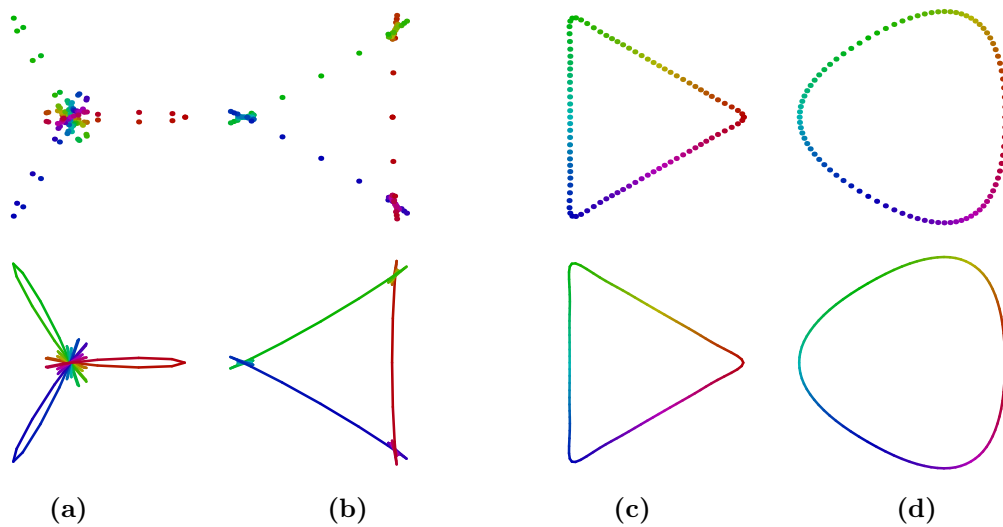
harmonic polygons could be termed *finite circles* as they are simply complex roots of unity described by the cyclic group,  $\mathbf{Z}/n\mathbf{Z}$  [106].

We define regular Fourier polygons as

$$\alpha_n = \sum_{k=\ell(m)} \frac{\{k\}}{k^p} \quad (5.4.4)$$

where  $p$  determines the smoothness  $C^p$  of the curves [101],  $m \in \mathbf{N}$  is the symmetry class of the polygon and  $\ell(m)$  is equivalent to  $(\dots, \ell-2m, \ell-m, \ell, \ell+m, \ell+2m, \dots)$ . Computing Eq. 5.4.4 with a finite number of harmonics can either be done through direct summation or through integrations of a truncated spectral exponential (Eq. 5.4.3) with  $b = 1$ .

For  $p = 1$  and  $p = 2$  two types of regular polygons emerge—*constant* and *linear*, respectively. The distinction between constant and linear polygons is related to the distance between successive points along the curve. For the constant variety, the curve makes relatively small orbits around the (ideal) polygon vertices before jumping rapidly to the next polygon vertex (Fig. 5.4.4b). There are generally far more points at the polygon’s vertices than along its edges. For the linear variety, successive points along the curve are at approximately the same distance from one another (Fig. 5.4.4c). Thus, there are more points along the edges of the polygon than at the vertices.



**Figure 5.4.4:** Curve plots of (a) delta ( $p = 0$ ), (b) constant ( $p = 1$ ), (c) linear ( $p = 2$ ), and (d) quadratic ( $p = 3$ ) Fourier 3-gons made with 8 harmonics and  $N = 90$  points.

For the case of  $p = 0$ , the resulting curves are not regular polygons, but rather spoke-like curves. We refer to these as *delta* Fourier polygons, a third variety along with constant and linear. Delta polygons have the characteristic of making small orbits around the origin while periodically making a rapid excursion outwards towards a polygon vertex and then back to the origin (Fig. 5.4.4a). Thus, overall, points are concentrated near the origin. As  $p \rightarrow -\infty$ , the curve approaches a circle.

Fourier polygons have a strong relationship with the classical waveforms discussed in 2.3.2. Many of the classical waveforms can be obtained from Fourier polygons with  $m = 1, 2$  (Table 5.15). For  $m = 1$  we obtain all (or even) harmonic waveforms and for  $m = 2$  we get odd harmonic waveforms. The all harmonic

classical waveforms are

$$\begin{aligned} impulse_n &= \operatorname{Re} \sum_{k=1(1)} \frac{\{k\}}{k^0} \\ saw_n &= \operatorname{Im} \sum_{k=1(1)} \frac{\{k\}}{k^1} \\ parabola_n &= \operatorname{Re} \sum_{k=1(1)} \frac{\{k\}}{k^2} \end{aligned}$$

and the odd harmonic classical waveforms are

$$\begin{aligned} alternatingImpulse_n &= \operatorname{Re} \sum_{k=1(2)} \frac{\{k\}}{k^0} \\ square_n &= \operatorname{Im} \sum_{k=1(2)} \frac{\{k\}}{k^1} \\ triangle_n &= \operatorname{Re} \sum_{k=1(2)} \frac{\{k\}}{k^2} \end{aligned}$$

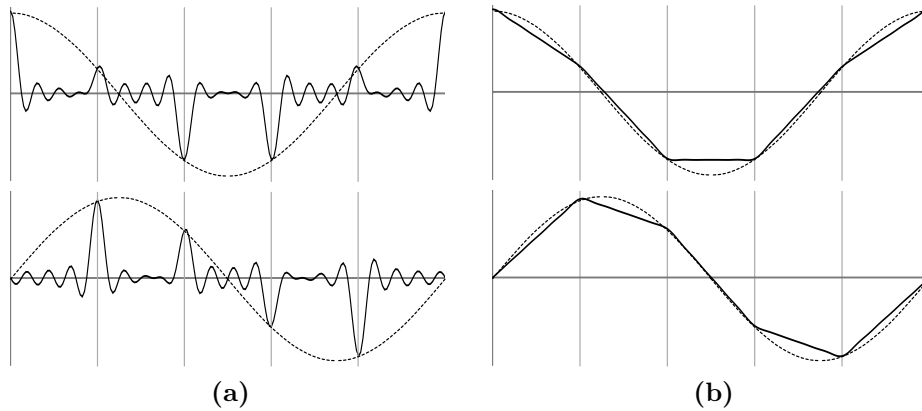
For  $saw_n$  and  $parabola_n$ , we either assert  $k \neq 0$  or live with the fact that they are centered at the point  $(\infty, 0)$  on the extended complex plane.

Fourier polygons are a particular class of interpolation patterns as described in Section 4.4. Fourier polygons approximate a discrete sampling of a complex sinusoid along with a particular interpolation policy between the sample points. The number of samples taken is  $m$  (the symmetry degree) while the smoothness of the path taken between samples is  $C^p$ . Table 5.15 shows plots for different values of  $m$  and  $p$  for comparison (for  $m = 1$ , the infinite offset caused by the component  $\{0\}/0$  is removed). For the delta Fourier polygons ( $p = 0$ ), the path between samples is  $C^0$  smooth and consists of complex sinusoid values at sample points and zero elsewhere. The constant Fourier polygons ( $p = 1$ ) approximate a truncating interpolation algorithm between sample points while the linear Fourier polygons



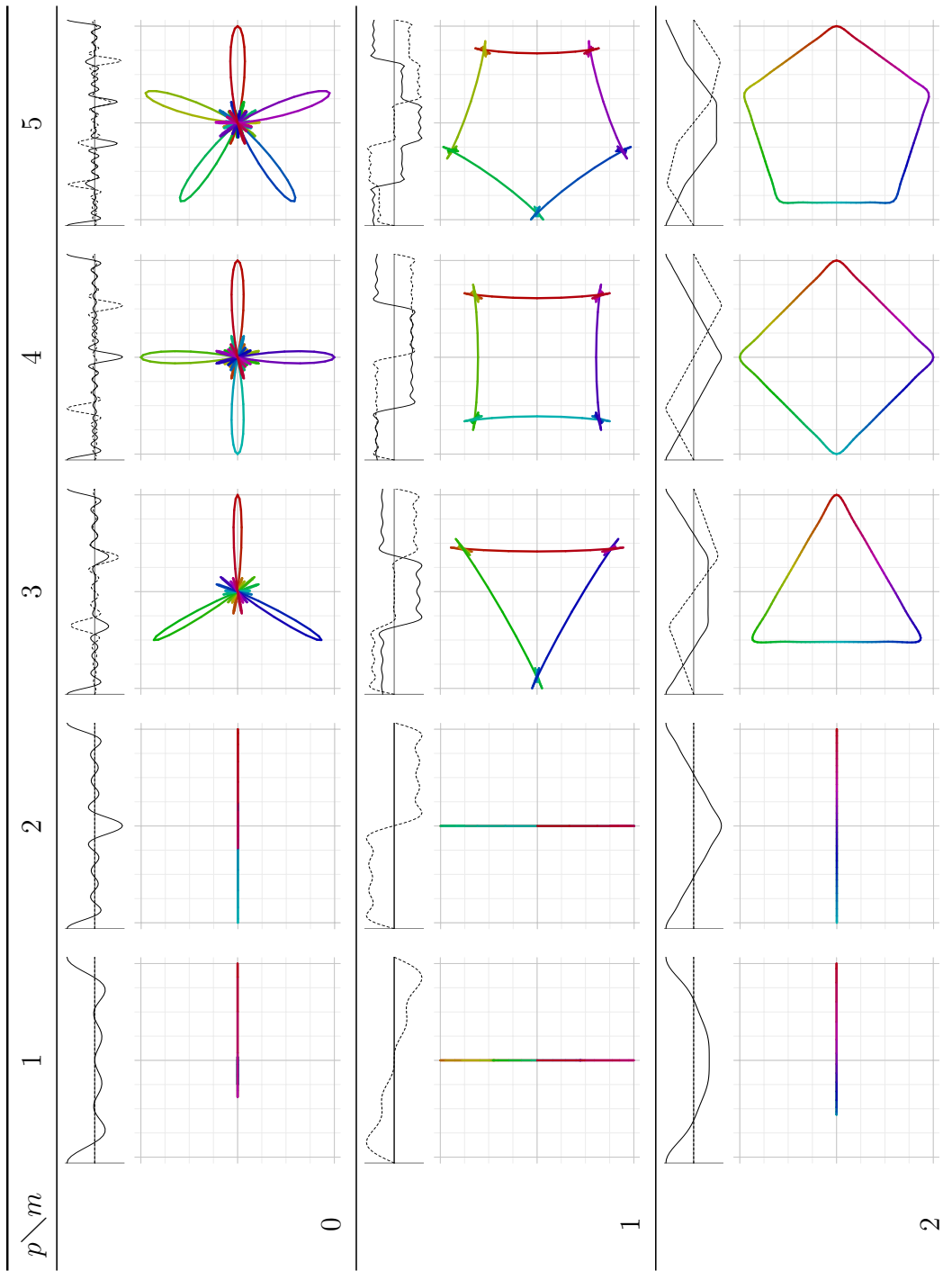
( $p = 2$ ) approximate a linear interpolation algorithm between sample points. This interpolation becomes more evident when  $m \geq 5$ . For  $m = 2$ , the classical square and triangle waves can be interpreted as being constructed from truncating and linear interpolation, respectively, between the two points of a digon. For  $m = 4$ , we obtain, again, both square and triangle waves by the two interpolation methods between the points of a square. This time, however, the waveforms are complex (quadrature) signals rather than the purely real (or imaginary) waveforms obtained with  $m = 2$ . We could even go so far as to say that the complex waveform obtained with  $m = 4$  is the most genuine square wave since its curve plot is also a square!

If we take a closer look at the plots in Table 5.15, we notice a small discrepancy in the interpolation paths between the cases  $p = 1$  and  $p = 0, 2$ . This is more easily revealed by the real and imaginary component plots. For delta and linear Fourier polygons, the real and imaginary projections approximate a discrete sampling and interpolation of a cosine and sine function, respectively (Fig. 5.4.5).



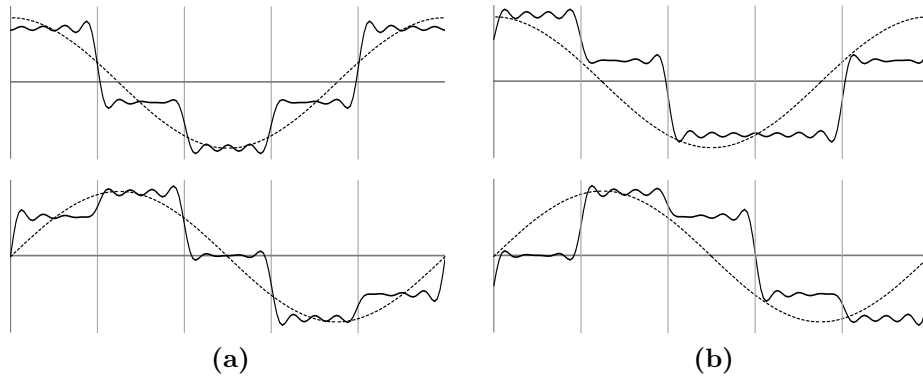
**Figure 5.4.5:** Real and imaginary projections of Fourier polygons with (a)  $p = 0$  and (b)  $p = -2$ . Vertical lines show sample boundaries.

However, for constant Fourier polygons, we see upon closer inspection that the sampling occurs exactly halfway between sample boundaries (Fig. 5.4.6a). We can



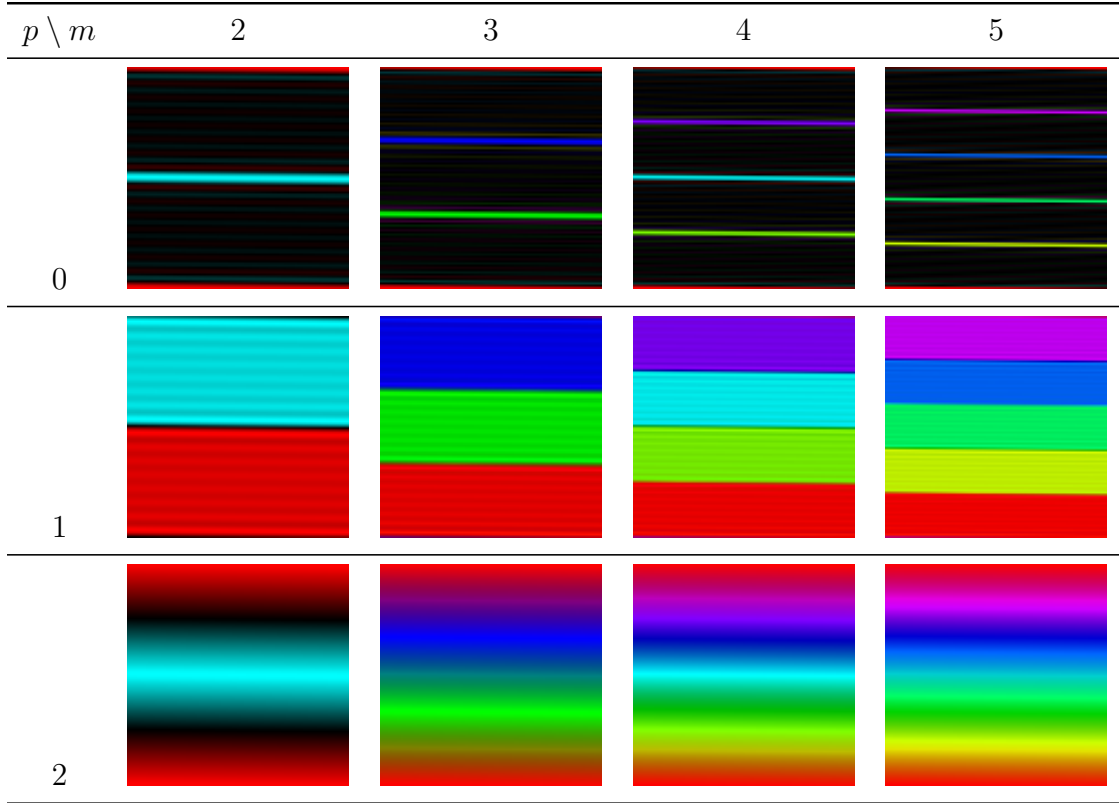
**Table 5.15:** Regular polygon families constructed from  $\alpha = \sum_{k=1}^{m-1} \{k\} / k^p$ .

correct this, so sampling occurs on the sample boundaries, by applying a global rotation factor of  $e^{-i\pi/m}$  to the complex sequence (Fig. 5.4.6b).



**Figure 5.4.6:** Real and imaginary projections of Fourier polygons with  $p = 1$ . Figure (a) is a constant polygon with  $m = 5$  and (b) is the same curve rotated by  $-\pi/5$ . Vertical lines show sample boundaries.

Raster plots of several Fourier polygons are shown in Table 5.16. When  $p = 0$ , the patterns are evenly-spaced horizontal lines. When  $p = 1$ , the patterns become a series of horizontal filled-in bars. When  $p = 2$ , the patterns resemble plane waves (5.1.3) propagating vertically, although the actual functions are piece-wise linear rather than sinusoidal.



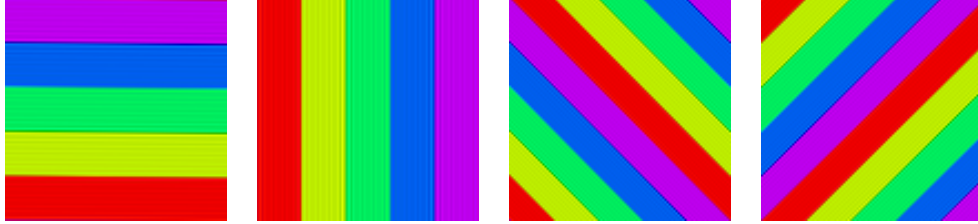
**Table 5.16:** Raster plots of  $\alpha_n = \sum_{k=1(m), |k| < 8m} \{k\} / k^p$ . For  $p = 1$ ,  $\alpha_n$  is multiplied by the phase correction factor  $e^{-i\pi/m}$ .

Through a simple frequency-scaling transformation, we can obtain raster patterns at different angles. The frequency-scaled Fourier polygon is given by

$$\alpha_n = \sum_{k=\ell(m)} \frac{\{sk\}}{k^p}$$

where  $s \in \mathbf{Z}$  is the frequency scaling factor and  $\ell$ ,  $m$ , and  $p$  are the same as in Eq. 5.4.4. In the position domain, the frequency scaling operation can be performed by rescanning the complex sequence generated from Eq. 5.4.4 by the factor  $s$ , i.e. changing its pitch. Some frequency-scaled Fourier polygon raster plots are shown in Fig. 5.4.7. It is apparent that these patterns have a similar structure as sinusoidal plane waves in that  $s$  controls the direction of propagation, but differ

in that the waveform itself is non-sinusoidal. In this way, these patterns could be used as basis functions for more complex “self-similar” patterns.



**Figure 5.4.7:** Raster plots of frequency-scaled Fourier polygons by the amounts  $s = 0, M, M + 1, M - 1$  (left to right) where  $M = \sqrt{N}$ ,  $m = 5$ ,  $\ell = 1$ , and  $p = 1$ .

As a final note, one of the strengths of many-harmonic Fourier polygons over single-harmonic polygons (5.1.2) and star polygons (5.1.3) is that they do not depend strongly on  $N$  as long as  $N$  is large. In the case of single-harmonic polygons, the number of vertices of the polygon is exactly equal to  $N$ . With Fourier polygons, the number of vertices of the polygon depends only on the frequency interval between harmonics and thus more than one polygon order (symmetry) can be constructed using the same  $N$ .

## Conclusion

This chapter has systematically looked at specific instances of harmonic patterns arising from (combinations of) one, two, three, and many harmonics. Many well-known waveform functions (e.g., sine, square, saw, and triangle waves) and curves (e.g., star polygon, circle, ellipse, parabola, hyperbola, and spirals) are producible from simple harmonic pattern functions. Single harmonic patterns always consist of points spaced uniformly along the circumference of a circle. Viewing a succession of subsequences of certain regular star polygons over time can give the appearance of another regular star polygon rotating at a constant

speed. Two harmonic patterns have an annular envelope consisting of an inner and an outer circular envelope. Conglomerates of several interleaved patterns can be produced by using certain high-frequency components. Three harmonic patterns bring forth a new level of complexity, but generally abide by combinations of rules from one and two harmonic patterns. For example, the circle cuspid (5.3.10) is a circle that moves continuously along the path of a cuspid. More generally, all three harmonic patterns can be seen to consist of a two-harmonic base pattern on which a one-harmonic pattern moves. The many harmonic patterns looked at are simple extrapolations and combinations of lower harmonic patterns.

The harmonics that comprise a sequence have particular effects on the resulting sound waveforms or visual patterns. Some harmonic combinations lead to patterns that are interesting both visually and sonically and other combinations lead to interesting visual results, but not sonic, and vice-versa. First, we discuss the visual and aural differences. The presence of high-frequency components in a sequence leads to more complicated patterns visually, but aurally, the resulting waveforms are often too bright or inaudible. Such sounds can be made more pleasing by pitch- or frequency-shifting them down into a lower frequency range, although this is not always straightforward since some sequences may contain both low- and high-frequency components. DC and Nyquist components are visually salient, yet sonically inaudible. Phase is also more visually salient than sonically. Rotating the phase of a harmonic component can produce a new curve with little resemblance to the original, however, sonically, this effect is not heard. The effect of combining negative and positive frequencies is difficult to distinguish sonically, yet visually is quite dramatic. A trifolium ( $\{-1\} + \{2\}$ ) and limaçon ( $\{1\} + \{2\}$ ) are visually quite distinct, yet aurally similar. Now, we discuss attributes that are salient both visually and aurally. Amplitude modulation (or beating) leads to interesting

patterns both visually and sonically. Curves comprised of beating sinusoids have a sheet-like appearance displaying complicated intersection patterns. Waveforms with beats sound more lively as they convey long-term temporal development. Constant interpolation patterns are both visually and sonically interesting. These patterns exhibit a peculiar unity between extreme stasis and change. The patterns are identified by long periods of positional invariance or local orbiting demarcated by sudden jumps in position.

## 6. Future Research Directions

---

This dissertation provided a solid theoretical foundation for the combined synthesis of sonic and visual patterns in two dimensions. Most of the patterns analyzed were relatively simple since the focus of this work was to systematically investigate what were believed to be the most fundamental principles. A natural question to posit is how the harmonic pattern function can either be applied directly or extended to produce other types of patterns based on the results of this dissertation work. Some open research paths in this direction are now briefly discussed.

### 6.1 Three-dimensional Patterns

How can the results of this dissertation be carried into three dimensions? Raster plots in three dimensions are a simple extension of the two-dimensional case presented. The only modification that needs to be made is for the raster motion to sweep out the area of a cuboid rather than a rectangle. The harmonic pattern function inherently provides a basis for generating patterns using a three-dimensional inverse discrete Fourier transform. Generating three-dimensional curves is a less trivial research question. There are at least four different paths to consider in moving to three dimensions—quaternions, coordinate frames, stereoscopic phasing, and the Riemann sphere. These are briefly discussed in turn.



On first thought, it seems logical to use quaternions to generate three-dimensional curves as they are the next higher-dimension (four-dimensional) division algebra after the complex numbers. Quaternions are like complex numbers in all respects except that they form a division ring rather than a division field meaning that commutativity does not hold. Lack of commutativity, however, does not seem to be a large disadvantage. The problem with quaternions begins to surface when considering how they can be used as basic generators akin to complex sinusoids. We can use two complex numbers, one defining a phase and amplitude and the other defining a frequency, to generate regular (star) polygons on a plane through recursive multiplication. It would be natural to think that doing the same with quaternions would generate regular polyhedra, but this is not the case. Recursive multiplication of a quaternion by another unit quaternion (the frequency component) generates a regular (star) polygon on a hyperplane. Thus, a quaternionic sinusoid is still a planar curve, albeit embedded in four dimensions. In terms of generating simple patterns, we gain very little going from complex numbers to quaternions. A quaternionic sinusoid could more easily be constructed by starting with a complex sinusoid and rotating it into four dimensions. In short, quaternions are not naturally capable of generating basic patterns of higher dimension; they still only generate two-dimensional patterns albeit embedded in four dimensions.

The coordinate frame approach extends the work of Abelson and diSessa [3] in steering a turtle in three dimensions. A coordinate frame in three dimensions consists of 3 orthonormal 3-vectors that encode the orientation of an object (its local coordinate system). The tip of at least one of these basis vectors can be used to define the position of a point in space that traces a curve. In order to parameterize the coordinate frame, Euler angles can be used. Euler angles describe how to successively rotate a coordinate frame along the planes formed by its basis

vectors. In three dimensions, at least three Euler angles are required to describe an orientation. If each of these Euler angles are the phase component of a complex sinusoid, then we have a description of a curve on a unit sphere. An *Euler harmonic* would thus consist of three complex sinusoids with independent frequencies and phases. If the frequencies are identical, then the curve is constrained to a great circle on a unit sphere similarly to a quaternionic sinusoid. Since Euler rotations in three dimensions do not commute (like quaternions), there are several flavors of Euler harmonics based on the planes that are rotated and the order they are rotated in. A common Euler rotation convention is ZXZ which rotates the coordinate frame around its local Z, X, and Z axes in succession. More investigation would be required to determine if there are any advantages to using one rotation convention over another as well as the effects of using more than three combined Euler rotations.

*Stereoscopic phasing* is the term we give to the process of simulating separate images for each eye by generating two two-dimensional curves with identical parameters except for slightly differing phases. This method is described in detail by Rigge [85]. The advantage of this approach is that the harmonic pattern function can be used directly with only the addition of one or more phase differencing parameters. One potential liability of stereoscopic phasing is its reliance on stereoscopic viewing techniques in order to perceive the three-dimensional curves. This means that the curve does not have an immediate three-dimension description. To do so would require mapping the horizontal difference between the points of each eye's curve into a depth value.

A mathematically well-established technique for generating three-dimensional curves from two-dimensional curves is stereographic projection of the complex plane onto the Riemann sphere. Through this mapping, the entire complex plane

including infinity (the extended complex plane  $\mathbf{C}^\infty$ ) is mapped onto a unit sphere. The north pole of the sphere is infinity while the south pole is zero. Stereographic projection is an attractive option since it is a parameter-free mapping from the complex plane into three dimensions and thus the harmonic pattern function can be used without any modification. Additionally, many transformations on the complex plane have simple corresponding effects on the Riemann sphere. Inverting a curve reflects its image around the equator of the Riemann sphere. The inversion symmetric patterns discussed in Section 4.6 are therefore entirely symmetric around the equator. Basic motions on the sphere correlate with simple scale, rotation, and translation operations of complex numbers which are generalizable through the Möbius transformation [74]. In order to construct curves off of the unit sphere, multiple sphere curves can be summed together. Each unit sphere curve would have its own unique harmonic pattern function description so that when the sphere points are added together they interfere to create a three-dimensional curve. An open research problem is how to best parameterize this additive sphere model.

## 6.2 Self-similar Patterns

While the harmonic pattern function uses complex sinusoids as basis functions, there is no reason why other functions could not be used. One of the problems with using sinusoids as a basis function is that highly-localized features, such as impulses and steps, require the sum of many sinusoids. This problem is partially circumvented through use of a rational function of complex sinusoids, however, it can still be useful conceptually and pragmatically to start with a more harmonically-rich basis function, i.e., an arbitrary *complex waveform*. One example in sound synthesis is generation of pulse waveforms through the subtraction of two saw

waveforms with different phases. While a complex sinusoid is fully parameterized by a frequency, amplitude, and phase, a complex waveform will have at least one additional frequency and phase parameter. If we designate the complex sinusoid's frequency and phase parameters as a frequency shift and phase shift, respectively, then a complex waveform could have in addition to these, frequency scale (or pitch) and phase rotation parameters. The reason these parameters are not used with complex sinusoids is because they are redundant. For a complex sinusoid, a frequency shift and frequency scale can be conflated into a single transformation. The same is true for a phase shift and phase rotation.

The Fourier polygons discussed in 5.4.5 are a good starting point for investigating alternative basis functions. Fourier polygons are not only geometrically intuitive as they are isomorphic to star polygons, but they are closely connected to many of the fundamental waveform shapes used in sound synthesis such as the saw, square, and triangle waveforms. Fourier polygons of the constant interpolation variety could be particularly useful for constructing patterns fixed to some underlying lattice structure. Triangle and square Fourier polygons could be used to generate patterns based on Eisenstein and Gaussian integers, respectively. In particular, the artistic practices of Hindu kolam and ni-Vanuata sand drawing are based on unicursal patterns drawn over a regular lattice of points. Fourier polygons could assist in the study and classification of such patterns. Additionally, it is possible that certain self-similar fractal curves, such as the dragon, Gosper, Hilbert, and Lévy C curves, can be fully parameterized using superpositions of Fourier polygons.

### 6.3 Level Set Patterns

While the harmonic pattern function is capable of generating n-dimensional textures through an approximation of Fourier synthesis, this potential was not fully explored in this dissertation. There is still much to be investigated in the vibration patterns of rectangular plates and three-dimensional cuboidal volumes. Through use of level sets, new types of disconnected planar curves and three-dimensional surfaces can be generated. These new curves and surface would be defined in terms of a harmonic pattern function potentially with a single isolevel amount, if not zero. For example, a Chladni pattern on a square plate is defined by the level set

$$0 = \cos nx \cos my - \cos mx \cos ny$$

where  $x, y \in [-\pi, \pi]$  and  $n, m \in \mathbf{N}$ . Rewriting this as a complex Fourier series, we obtain

$$\begin{aligned} 0 &= \cos nx \cos my - \cos mx \cos ny \\ &= \frac{1}{2}[\cos(nx - my) + \cos(nx + my) - \cos(mx - ny) - \cos(mx + ny)] \\ &= \operatorname{Re}(e^{i(nx-my)} + e^{i(nx+my)} - e^{i(mx-ny)} - e^{i(mx+ny)}) \end{aligned}$$

which is the real part of the sum of four diagonal plane waves. The associated harmonic pattern function of this system is

$$0 = \operatorname{Re}(\{n - mM, \phi_1\} + \{n + mM, \phi_2\} - \{m - nM, \phi_3\} - \{m + nM, \phi_4\})$$

where  $\phi_1 = \frac{n-mM}{2}$ ,  $\phi_2 = \frac{n+mM}{2}$ ,  $\phi_3 = \frac{m-nM}{2}$ , and  $\phi_4 = \frac{m+nM}{2}$ . Mapping this to a raster plot with equal dimensions of  $M = \sqrt{N}$  gives a discretized version of

the rectangular Chladni pattern. To visualize the nodal lines, the pattern can be colored brighter where the magnitude of complex values approach zero.

## 7. Conclusion

---

This dissertation presented the harmonic pattern function, a rational function of inverse discrete Fourier transforms, that integrates synthesis of sound waveforms, graphical patterns, and spatiotemporal trajectories. The significance of this dissertation is not only in recognizing a simple mathematical function capable of efficiently describing many known sound waveforms and visual patterns, but also in showing them to be special cases of more general families of patterns. Such generalizations permit meaningful relationships to be made between more specific patterns within and across modalities. Additionally, through generalization comes the ability to extrapolate—find diversity in unity.

Here are the findings of this dissertation along with a discussion of their significance:

1. *The frequencies and phases of the complex harmonics comprising a complex sequence determine the cyclic and dihedral symmetries of its corresponding curve plot.*

The fact that harmonic amplitudes and phases are continuous parameters means that it is possible to smoothly morph between various degrees and types of planar symmetry, including asymmetry. At the core of these symmetrical curves is a regular star polygon and a particular path between vertices that makes up a more complex curve. The underlying regular star polygon is

a function of frequency only while the path between vertices depends on amplitude and phase. Certain paths, such as delta functions, constants, and lines, completely describe the curves of regular polygons going beyond a simple group theoretic classification.

2. *The harmonic pattern function efficiently—with very few harmonics—describes a large variety of planar curves, raster-based patterns, and sound waveforms.* Specific examples of well-known audio/visual patterns and some novel extensions and extrapolations of these patterns demonstrated the suitability of the harmonic pattern function as a model for multimodal pattern generation. Chapter 5 presented a systematic investigation of patterns consisting of one, two, and three harmonics and a selection of important patterns consisting of more harmonics. Many well-known patterns are described using a small number of harmonics. Additionally, simple transformations can naturally extend these patterns to other similar patterns.
3. *Patterns that would otherwise be disconnected or be defined explicitly across multiple dimensions can be approximated from smooth one-dimensional signals.*

Section 5.1.3 showed how single complex sinusoids can, to good approximation, produce complex-valued plane waves, the basis functions of the two-dimensional (discrete) Fourier transform. The same principle can be extended to three or more dimensions. This is significant since it means that the calculation of a particular complex sequence can be independent from its representation as pattern on an  $n$ -dimensional torus. In 5.1.5 and 5.2.15, it was shown how one and two harmonic patterns can approximate moving and standing sinusoidal waves, respectively. Interleaved patterns



are constructed using frequencies that are large factors of the length,  $N$ , of the complex sequence. These were investigated for a single harmonic (5.1.4) and for two harmonics (5.2.9). Interleaved patterns permit the production of multiple disconnected curves from a single complex sequence. Therefore, the harmonic pattern function encodes patterns based not only harmonic superpositions, but also on superimpositions. In 5.3.11, it was shown how a chain of apparently disconnected, overlapping circles can be produced from a unicursal curve. Unlike interleaved patterns, this curve attains its disconnected nature by tracing over itself while each subcurve intersects at least one other subcurve of the entire curve.

4. *Inversion-symmetric patterns, including unit circle patterns, are producible from any complex sequence using a series of simple transformations.*

Unit circle patterns (Section 4.5) are attained through the operation of conjugate division, element-wise division of a complex sequence by its complex conjugate. More general inversion-symmetric patterns (Section 4.6) are produced by position shifting the divisor by a variable amount before conjugate division. Inversion-symmetric patterns can be extended through frequency shifting.

While the harmonic pattern function compactly describes myriad known audio/visual patterns and indicates a strong potential for describing many more, it is still uncertain to what its role is in the larger picture of pattern generation. One of its most important attributes is that it provides a direct and complete way of describing the formal symmetries of patterns. Symmetry is important since it permits any number of identical motifs to be constructed at once; this brings a sense of coherence to a pattern. Explicit symmetry breaking is an important

supplement if such motifs are to be made distinguishable from one another; this brings a desirable sense of diversity from unity to a pattern. Too much diversity or too much regularity lead to boring patterns. Slight breaks from symmetry tend to produce the most engaging patterns [37, 8].

The world around us is an arena of sounds, shapes, and patterns. Through evolution, we have acquired the ability to directly perceive some of these phenomena giving us a picture of the world that is comprehensible, but necessarily incomplete. To help fill in these gaps of our understanding, we can develop mathematical models to extrapolate from what we know. The harmonic pattern function is such a mathematical model that not only serves both art and science, but helps reconcile them. It provides a common language for describing the patterns found both in nature and in human artifacts. In the context of digital arts and design, the harmonic pattern function can provide a starting point for and bring cohesion to the underlying structure of abstract audio/visual works. It provides a fertile ground for artists searching for both new and archetypical shapes, sounds, and patterns. In the realm of science, it provides a unified description of many recurring patterns found in nature, such as spirals, cardioids, cycloids, conic sections, beats, plane waves, and moving/standing waves. Without a shared understanding, art and science will continue to remain separate human endeavors missing a potential opportunity to benefit from one another and coevolve. The harmonic pattern function was arrived at by making such a consideration, and, while not claimed to be a universal solution, is seen as the right step in this direction.

# Bibliography

- [1] Adriano Abbado. Perceptual correspondences of abstract animation and synthetic sound. *Leonardo. Supplemental Issue*, 1:3–5, 1988.
- [2] Adriano Abbado. Perceptual correspondences of animation and synthetic sound. Master’s thesis, MIT Media Laboratory, 1988.
- [3] Harold Abelson and Andrea A. diSessa. *Turtle Geometry: The Computer as a Medium for Exploring Mathematics*. MIT Press, 1980.
- [4] George Adams. Of the geometric pen. In *Geometrical and Graphical Essays*, pages 151–154. C. Baldwin, London, 1813.
- [5] Hubert Airy. Pendulum autographs i. *Nature*, 4:310–313, August 1871.
- [6] Bill Alves. Digital harmony of sound and light. *Computer Music Journal*, 29(4):45–54, 2005.
- [7] Frederick J. Ampel and Ted Uzzle. The history of audio and sound measurement. In *Proceedings of the 94th AES Convention*, Berlin, 1993.
- [8] Anthony Ashton. *Harmonograph: A Visual Guide to the Mathematics of Music*. Walker Publishing Company, Inc., New York, 2003.
- [9] Jeff Babb and James Currie. The brachistochrone problem: Mathematics for a broad audience via a large context problem. *The Montana Mathematics Enthusiast*, 5(2 & 3):169–184, 2008.
- [10] Alan H. Barr. Superquadrics and angle-preserving transformations. *IEEE Computer Graphics and Applications*, 1(1):11–23, 1981.
- [11] Thomas Sebastian Bazley. *Index to the Geometric Chuck: A Treatise Upon the Description, In the Lathe, of Simple and Compound Epitrochoidal or “Geometric” Curves*. Waterlow and Sons, London, 1875.
- [12] A. Bell and C. Macfarquhar. Geometric pen. In Colin Macfarquhar and George Gleig, editors, *Encyclopædia britannica: or, A dictionary of arts, sciences, and miscellaneous literature*, volume 14. 1797.

- [13] Salomon Bochner. *The Dictionary of the History of Ideas: Studies of Selected Pivotal Ideas*, volume 4, chapter Symmetry and Asymmetry, pages 346–53. Charles Scribner’s Sons, New York, 1973.
- [14] Harald Bode and Robert Moog. A high-accuracy frequency shifter for professional audio applications. *Journal of the Audio Engineering Society*, 20(6):453–458, 1970.
- [15] Suzanne Boll. Visions and views in multimedia. *IEEE Multimedia*, 13(2):15–17, 2006.
- [16] Nathaniel Bowditch. On the motion of a pendulum suspended from two points. *Memoirs of the American Academy of Arts and Sciences*, 3:413–436, 1815.
- [17] Cameron Browne. Harmonograms. *Computers and Graphics*, 31:292–300, 2007.
- [18] John H. Conway, Heidi Burgiel, and Chaim Goodman-Strauss. *The Symmetries of Things*. A K Peters, Ltd., 2008.
- [19] R. L. Cosgriff. Identification of shape. Technical Report 820-11 ASTIA (AD 254 792), Ohio State University Research Foundation, Columbus, 1960.
- [20] Roger Dannenburg. Sound synthesis from real-time video images. In *Proceedings of the 2003 International Computer Music Conference*, 2003.
- [21] James Dean. Motions of the earth as seen from the moon. *Memoirs of the American Academy of Arts and Sciences*, 3:241, 1815.
- [22] Frank Dietrich. Visual intelligence: The first decade of computer art (1965-1975). *Leonardo*, 19(2):159–169, 1986.
- [23] F. Dillen. The classification of hypersurfaces of a euclidean space with parallel higher fundamental form. *Mathematische Zeitschrift*, 203(1):635–643, 1990.
- [24] Charles Dodge and Thomas A. Jerse. *Computer Music: Synthesis, Composition, and Performance*. Schirmer, second edition, 1997.
- [25] John Edwards. Ornamental turning lathes and their accessories. <http://www.the-sot.com/craft.html>, 2006.
- [26] Sir Howard Warburton Elphinstone. *Patterns For Turning: Comprising Elliptical and Other Figures Cut on the Lathe Without the Use of any Ornamental Chuck*. Bradbury, Evans, and Co., London, 1872.

- [27] Patrick Feaster, editor. *The Phonautographic Manuscripts of Édouard-Léon Scott de Martinville*. FirstSounds.org, 2009.
- [28] Joseph Fourier. *The Analytical Theory of Heat*. Cambridge University Press, 1878.
- [29] Herbert W. Franke. *Computer Graphics - Computer Art*. Springer-Verlag, second, revised and enlarged edition, 1985.
- [30] Wm. Randolph Franklin and Alan H. Barr. Faster calculation of superquadric shapes. *IEEE Computer Graphics and Applications*, 1(3):41–47, 1981.
- [31] Michael Gasperi. Michael Gasperi’s Grey Walter machina speculatrix page. <http://www.extremenxt.com/walter.htm>, 2010.
- [32] Johan Gielis. A generic geometric transformation that unifies a wide range of natural abstract shapes. *American Journal of Botany*, 90(3):333–338, 2003.
- [33] Johan Gielis. *Inventing the Circle*. Geniaal bvba, Antwerpen Nederlands, 2003.
- [34] Andrew S. Glassner. A shape synthesizer. *IEEE Computer Graphics and Applications*, 17(3):40–51, 1997.
- [35] Andrew S. Glassner. Fourier polygons. *IEEE Computer Graphics and Applications*, 19(1):84–91, 1999.
- [36] Chris Godsil and Gordon F. Royle. *Algebraic Graph Theory*. Springer-Verlag, New York, 2001.
- [37] Joseph Goold, Charles E. Benham, Richard Kerr, and L. R. Wilberforce. *Harmonic Vibrations and Harmonic Figures*. Newton and Co., London, 1909.
- [38] Guido Grandi. *Flores Geometrici Ex Rhodonearum Et Cloeliarum Curvarum Descriptionibus Resultantes*. Kessinger Publishing, LLC, 1728.
- [39] István Hargittai and Magdolna Hargittai. *Symmetry: A Unifying Concept*. Shelter Publications, Bolinas, California, 1994.
- [40] Esq. Henry Perigal, Junior. *Experimental Researches in Kinematics; Designed to Exemplify and Elucidate The Laws of Motion, By The Organical Development of Their Representative, Or Characteristic Curves, The Resultants of Combinations of Movements*. London, 1838.

- [41] Christopher S. Henshilwood, Francesco d’Errico, Royden Yates, Zenobia Jacobs, Chantal Tribolo, Geoff A. T. Duller, Norbert Mercier, Judith C. Sealy, Helene Valladas, Ian Watts, and Ann G. Wintle. Emergence of modern human behavior: Middle stone age engravings from South Africa. *Science*, 295:1278–1280, 2002.
- [42] John Jacob Holtzapffel. *The Principles and Practice of Ornamental Or Complex Turning*. Dover Publications, Inc., 1973.
- [43] Margaret Watts Hughes. Visible sound. i. voice figures. *The Century*, 42:37–40, 1891.
- [44] John Holt Ibbetson. *Specimens In Eccentric Circular Turning*. Longman, Orme, Brown, Green and Longman, London, third edition, 1800.
- [45] John Holt Ibbetson. Description of the geometric chuck. *Mechanics’ Magazine*, 6:552–553, 1827.
- [46] John Holt Ibbetson and Bern Dibner. *A Brief Account of Ibbetson’s Geometric Chuck, Manufactured by Holtzapffel and Co.: With a Selection of Specimens Illustrative of Some of Its Powers*. A. Hancock, London, 1833.
- [47] Alejandro Jaimes, Nicu Sebe, and Daniel Gatica-Perez. Human-centered computing: A multimedia perspective. In *Proceedings of the 14th Annual ACM International Conference on Multimedia*, pages 855–864, 2006.
- [48] Ramesh Jain. Are we doing multimedia? *IEEE Multimedia*, 10(4):112–111, 2003.
- [49] Aleš Jaklič, Aleš Leonardis, and Franc Solina. *Segmentation and Recovery of Superquadrics*. Kluwer Academic Publishers, Dordrecht, The Netherlands, 2000.
- [50] Hans Jenny. *Cymatics*. Basel: Basilius Presse AG, 1963.
- [51] L. B. W. Jolley. *Summation of Series*. Dover Publications, Inc., 1961.
- [52] M. I. Kargapolov and Yu. I. Merzlyakov. Group. In Michiel Hazewinkel, editor, *Encyclopaedia of Mathematics*. Kluwer Academic Publishers, 2001.
- [53] E. S. Kennedy. Late medieval planetary theory. *Isis*, 57:365–378, 1966.
- [54] Ben Laposky. Electronic abstraction: A new approach to design. Exhibition Catalogue, Sanford Museum, Cherokee, Iowa, 1953.
- [55] Ben Laposky. Oscillons: Electronic abstractions. *Leonardo*, 2(4):345–354, 1969.

- [56] Ben Laposky. *Artist and Computer*, chapter Oscillons: Electronic Abstractions, pages 21–22. Harmony Books, 1975.
- [57] J. Dennis Lawrence. *A Catalog of Special Plane Curves*. Dover Publications, Inc., New York, 1972.
- [58] Michael Leyton. Group theory in architecture 2: Why symmetry? why asymmetry? *Visual Mathematics*, 1(4), 1999.
- [59] Michael Leyton. *A Generative Theory of Shape*. Springer-Verlag Berlin Heidelberg, 2001.
- [60] Jules Antoine Lissajous. Mémoire sur l'étude optique des mouvements vibratoires. *Annales de Chimie et de Physique*, 51:147–231, 1857.
- [61] E. H. Lockwood. *A Book Of Curves*. Cambridge University Press, 1961.
- [62] Gareth Loy. Composing with computers- a survey of some compositional formalisms and music programming languages. In *Current Directions in Computer Music Research*, pages 292–396. MIT Press, Cambridge, Massachusetts, 1989.
- [63] Max Mathews. *The Technology of Computer Music*. The M.I.T. Press, Boston, 1969.
- [64] Max V. Mathews. An acoustic compiler for music and psychological stimuli. *The Bell System Technical Journal*, 40(3):677–694, May 1961.
- [65] Julio Castineira Merino. Lissajous figures and chebyshev polynomials. *The College Mathematics Journal*, 34(2):122–127, 2003.
- [66] Pierre Mertz and Frank Gray. A theory of scanning and its relation to the characteristics of the transmitted signal in telephotography and television. *Bell System Technical Journal*, 13:464–515, July 1934.
- [67] Gordon Monro and Jeff Pressing. Sound visualization using embedding: The art and science of auditory autocorrelation. *Computer Music Journal*, 22(2):20–34, 1998.
- [68] F. Richard Moore. *Elements of Computer Music*. Prentice Hall, New Jersey, 1990.
- [69] James A. Moorer. The synthesis of complex audio spectra by means of discrete summation formulas. *Journal of the Audio Engineering Society*, 24(9):717–727, 1976.

- [70] James A. Moorer. Signal processing aspects of computer music: A survey. *Proceedings of the IEEE*, 65(8):1108–1137, 1977.
- [71] R. E. Moritz. On the construction of certain curves given in polar coordinates. *The American Mathematical Monthly*, 24(5):213–220, 1917.
- [72] William Moritz. Mary Ellen Bute: Seeing sound. *Animation World Network*, 1(2), 1996.
- [73] Janet H. Murray. *Hamlet on the Holodeck*. MIT Press, 1998.
- [74] Tristan Needham. *Visual Complex Analysis*. Oxford University Press, USA, 1999.
- [75] Georg Nees. *Generative Computergraphik*. Siemens AG, Berlin-Munich, 1969.
- [76] Erich Neuwirth. Designing a pleasing sound mathematically. *Mathematics Magazine*, 74(2):91–98, 2001.
- [77] W. Henry Northcott. *A Treatise on Lathes And Turning, Simple, Mechanical, And Ornamental*. Longmans, Green, and Company, London, 1868.
- [78] Alan V. Oppenheim and Ronald W. Schaffer. *Discrete-time Signal Processing*. Prentice Hall, New Jersey, second edition, 1999.
- [79] Randall Packer and Ken Jordan, editors. *Multimedia: From Wagner to Virtual Reality, Expanded Edition*. W.W. Norton and Company, Inc., New York, 2001.
- [80] Roger Penrose. *The Road to Reality*. Alfred A. Knopf, New York, 2004.
- [81] Henry Perigal. Revolution and rotation. *The Astronomical Register*, 2(24):309–316, December 1864.
- [82] John Perry and W. E. Ayrton. On the music of colour and visible motion. *Proceedings of the Physical Society London*, 3(18):18–28, 1879.
- [83] Chris Pike and Jeremy J. Wells. Two-dimensional fourier processing of rasterised audio. In *Proceedings of the 12th International Conference on Digital Audio Effects (DAFx-09)*, pages 271–278, 2009.
- [84] Richard A. Proctor. *A Treatise on the Cycloid and All Forms of Cycloidal Curves and On the Use of Such Curves in Dealing with the Motions of Planets, Comets, etc. and of Matter Projected From the Sun*. Longmans, Green, and Company, 1878.
- [85] William F. Rigge. Stereoscopic harmonic curves. *School Science and Mathematics*, 24(1):29–36, 1924.



- [86] William Francis Rigge. Cuspidal envelope rosettes. *The American Mathematical Monthly*, 29(1):6–8, 1922.
- [87] William Francis Rigge. *Harmonic Curves*. Loyola University Press, Chicago, Illinois, 1926.
- [88] Curtis Roads. *The Computer Music Tutorial*. MIT Press, 1996.
- [89] Alain Robert. Fourier series of polygons. *The American Mathematical Monthly*, 101(5):420–428, 1994.
- [90] John W. Rutter. *Geometry of Curves*. Chapman & Hall/CRC, 2000.
- [91] Remko Scha. *Exploding Aesthetics. L & B Series of Philosophy of Art and Art Theory*, volume 16, chapter Readymades, Artificial Art, New Media. Rodopi, 2001.
- [92] Asok K. Sen. A product-delay algorithm for graphic design. *Computers and Graphics*, 22(6):759–764, 1998.
- [93] Asok K. Sen. The product-delay algorithm: Graphic design with amplitude- and frequency-modulated waveforms. *Computers and Graphics*, 23:169–174, 1999.
- [94] Asok K. Sen. Mathematics, computers and visual arts: Some applications of the product-delay algorithm. *Leonardo*, 33(3):203–205, 2000.
- [95] A. V. Shubnikov and V. A. Koptsik. *Symmetry in Science and Art*. Plenum Press, New York, 1974.
- [96] Charles S. Slichter. Harmonic curves of three frequencies. *Trans. Wisc. Acad. Sci.*, 11:449–451, 1896.
- [97] Julius O. Smith. *Mathematics of the Discrete Fourier Transform (DFT) with Audio Applications*. W3K Publishing, 2007.
- [98] D. D. Sokolov. Lamé curve. In Michiel Hazewinkel, editor, *Encyclopaedia of Mathematics*. Kluwer Academic Publishers, 2001.
- [99] D. D. Sokolov. Rose (curves). In Michiel Hazewinkel, editor, *Encyclopaedia of Mathematics*. Kluwer Academic Publishers, 2001.
- [100] Tim Stilson and Julius O. Smith. Alias-free digital synthesis of classic analog waveforms. In *Proceedings of the 1996 International Computer Music Conference*, Hong Kong, 1996.
- [101] Gilbert Strang. *Computational Science and Engineering*. Wellesley-Cambridge, 2007.

- [102] Giovan Battista Suardi. *Nuovi istromenti per la descrizione di diverse curve antiche e moderne e di molte altre, che servir possono alla speculazione de' Geometrici, ed all'uso de' Practici*. 1752.
- [103] Ivan Sutherland. Sketchpad: A man-machine graphical communication system. Technical Report 574, University of Cambridge Computer Laboratory, 1963.
- [104] Ivan Sutherland. Sketchpad: A man-machine graphical communication system. In *Proceedings of AFIPS Conference*, volume 23, 1963.
- [105] Wladyslaw Tatarkiewicz. The great theory of beauty and its decline. *The Journal of Aesthetics and Art Criticism*, 31(2):165–180, 1972.
- [106] Audrey Terras. *Fourier Analysis on Finite Groups and Applications*. Cambridge University Press, 1999.
- [107] Jr. Thomas B. Greenslade. The kaleidophone. *The Physics Teacher*, 30:38–39, 1992.
- [108] Joseph Tierney, Charles M. Rader, and Bernard Gold. A digital frequency generator. *IEEE Transactions on Audio and Electroacoustics*, AU-19(1):48–57, March 1971.
- [109] W. T. Tutte. *Graph Theory*. Cambridge University Press, 2001.
- [110] Alexandre Vitkine. Photographic and electronically generated images. *Leonardo*, 19(4):305–309, 1986.
- [111] Mary D. Waller. *Chladni Figures: A Study in Symmetry*. G. Bell and Sons LTD, London, 1961.
- [112] William Grey Walter. An imitation of life. *Scientific American*, pages 42–45, May 1950.
- [113] William Grey Walter. A machine that learns. *Scientific American*, pages 60–63, August 1951.
- [114] Scott Wardle. A hilbert-transformer frequency shifter for audio. In *Proceedings of the DAFX98 Workshop on Digital Audio Effects*, 1998.
- [115] Jan Wassenaar. besace. <http://www.2dcurves.com/quartic/quarticbs.html>, 2010.
- [116] Jan Wassenaar. botanic curve. <http://www.2dcurves.com/roulette/rouletteb.html>, 2010.

- [117] Jan Wassenaar. (extended) Ceva's trisectrix. <http://www.2dcurves.com/sextic/sextict.html>, 2010.
- [118] Jan Wassenaar. polynomial spiral. <http://www.2dcurves.com/spiral/spiralps.html>, 2010.
- [119] Jan Wassenaar. (simple) star. <http://www.2dcurves.com/line/linest.html>, 2010.
- [120] Steven Weinberg. From BCS to the LHC. *AAPPS Bulletin*, 18(2):30–35, 2008.
- [121] Eric W. Weisstein. Dissymmetric. In *MathWorld—A Wolfram Web Resource*. <http://mathworld.wolfram.com/Dissymmetric.html>, 2011.
- [122] Hermann Weyl. *Symmetry*. Princeton University Press, Princeton, New Jersey, 1952.
- [123] Charles Wheatstone. Description of the kaleidophone, or phonic kaleidoscope; a new philosophical toy, for the illustration of several interesting and amusing acoustical and optical phenomena. *The Quarterly Journal of Science, Literature and Art*, 23:344–351, 1827.
- [124] Robert J. Whitaker. Harmonographs. i. pendulum design. *American Journal of Physics*, 69(2):162–173, 2001.
- [125] Robert J. Whitaker. Harmonographs. ii. circular design. *American Journal of Physics*, 69(2):174–183, 2001.
- [126] John Whitney. *Digital Harmony: On the Complementarity of Music and Visual Art*. Kingsport Press, 1980.
- [127] John Whitney. To paint on water: The audiovisual duet of complementarity. *Computer Music Journal*, 18(3):45–52, 1994.
- [128] Wikipedia. Spirangle - Wikipedia, the free encyclopedia. <http://en.wikipedia.org/wiki/Spirangle>, 2010.
- [129] Godfrey Winham and Kenneth Steiglitz. Input generators for digital sound synthesis. *The Journal of the Acoustical Society of America*, 47(2):665–666, 1969.
- [130] Robert C. Yates. *Curves And Their Properties*. Robert C. Yates, 1952.
- [131] Woon Seung Yeo and Jonathan Berger. A framework for designing image sonification methods. In *Proceedings of ICAD 05-Eleventh Meeting of the International Conference on Auditory Display*, Limerick, Ireland, 2005.

- [132] Woon Seung Yeo and Jonathan Berger. Raster scanning: A new approach to image sonification, sound visualization, sound analysis and synthesis. In *Proceedings of the 2006 International Computer Music Conference*, pages 34–41, New Orleans, LA, 2006.
- [133] Thomas Young. Outlines of experiments and inquiries respecting sound and light. *Philosophical Transactions of the Royal Society of London*, 90:106–150, 1800.
- [134] Charles Zahn and Ralph Roskies. Fourier descriptors for plane closed curves. *IEEE Transactions on Computers*, 21(3):269–281, 1972.
- [135] Anthony Zee. *Fearful Symmetry*. Princeton University Press, 1986.